#9

~~CONFIDENTIAL~~

AD 325 247

Reproduced
by the

ARMED SERVICES TECHNICAL INFORMATION AGENCY
ARLINGTON HALL STATION
ARLINGTON 12, VIRGINIA

K-2

~~CONFIDENTIAL~~

NOTICE: When government or other drawings, specifications or other data are used for any purpose other than in connection with a definitely related government procurement operation, the U. S. Government thereby incurs no responsibility, nor any obligation whatsoever; and the fact that the Government may have formulated, furnished, or in any way supplied the said drawings, specifications, or other data is not to be regarded by implication or otherwise as in any manner licensing the holder or any other person or corporation, or conveying any rights or permission to manufacture, use or sell any patented invention that may in any way be related thereto.

CONFIDENTIAL

THE GENERAL MILLS ELECTRONICS GROUP
RESEARCH DEPARTMENT
2003 East Hennepin Avenue
Minneapolis 13, Minnesota

This document consists of 225 pages and is number 5 of 13 copies, series B, and the following — attachments.

FOURTH QUARTERLY PROGRESS REPORT ON DISSEMINATION OF SOLID AND LIQUID BW AGENTS (Unclassified Title)

For Period 4 March - 4 June, 1961

Contract No. DA-18-064-CML-2745

Prepared for
U. S. Army Biological Warfare Laboratories
Fort Detrick
Frederick, Maryland

Submitted by: J E Upton
J. E. Upton for
G. R. Whitnah
Project Manager

Approved by: S. P. Jones
S. P. Jones, Manager
Materials & Mechanics Research

Report No. 2216
Project No. 82408
Date - August 10, 1961

CONFIDENTIAL

FOREWORD

Staff members of the Research and Development Departments who have participated in directing and conducting the investigations and preparing the discussions presented in this report include Mr. S. P. Jones, Jr., Mr. G. Whitnah, Mr. A. Anderson, Dr. J. Baumstark, Dr. J. Park, Mr. J. Upton, Mr. W. L. Torgeson, Mr. J. Nash, Mr. C. Hagberg, Mr. F. Stroom, Mr. G. Morfitt, Mr. L. Graf, Mr. R. Griffith, Mr. I. Hall, Mr. J. Pilney, Mr. R. Dahlberg, Mr. J. Ungs and Miss M. Johnson.

ABSTRACT

This Fourth Quarterly Progress Report presents the research on dissemination of solid and liquid agents. The research on this project is directed toward the development of weapon systems for line-source dissemination from high-speed, low-flying aircraft.

It has been found that the viability of Sm subjected to air streams simulating a jet engine exhaust is radically affected. Compaction tests on Sm showed some viability reduction.

Measurements were made of the coefficient of friction and the bulk density of various powders.

A theoretical analysis of the force required to lift a disk embedded in a dilatant material was conducted. Theoretical results were in good agreement with experimental data.

Thermal conductivity and viscosity measurements of egg slurries were carried out. Rheological properties of Sm slurries were investigated and data are presented.

Boundary layer studies are reported which indicate that wind tunnel tests on deagglomeration are slightly conservative as compared to actual flight conditions.

High-speed motion pictures presented in this report give an insight into the breakup of Sm agglomerates. Deagglomeration to primary particles of Sm has been observed.

A mathematical model of a line dissemination system was studied. Computed data of infection probability as a function of downwind distance are also given in this report.

An investigation of the store-carrying capacities of an unmanned aircraft and a preliminary design of a liquid disseminating unit is included in the Appendices.

TABLE OF CONTENTS

TABLE OF CONTENTS (Continued)

LIST OF ILLUSTRATIONS

LIST OF ILLUSTRATIONS (Continued)

LIST OF ILLUSTRATIONS (Continued)

LIST OF TABLES

1. INTRODUCTION

This is the Fourth Quarterly Progress Report on the program of research on dissemination of solid and liquid BW agents, being conducted under Contract No. DA-18-064-CML-2745. This research is directed toward the development of disseminating stores to be carried externally on high-performance delivery aircraft.

The three-month period covered by this report is a part of Phase II, which was started in December 1960. The objective of Phase II, in the field of solid agent dissemination, is to advance the state of knowledge in the areas of characterization, delivery, metering, dissemination and deagglomeration of finely-divided solid materials, to provide data for design of a research prototype disseminator. In the field of liquid agent dissemination, Phase II includes the design of a research prototype disseminator and the fabrication of one unit.

This report presents progress in several investigations currently being conducted to meet these objectives. Because of the large scope of this project, a number of relatively independent studies are required. Most of the subjects discussed in this report were introduced in our Third Quarterly Progress Report [1.1], to which the reader is referred for additional background information.

1.1 General Mills, Inc. Report No. 2200, Dissemination of Solid and Liquid BW Agents, (unclassified title) May 15, 1961 (Confidential).

2. EFFECT OF ELEVATED AIR STREAM TEMPERATURES ON THE VIABILITY OF SERRATIA MARCESCENS AEROSOLIZED FROM LIQUID SUSPENSION

Killing of airborne bacteria by means of disinfectants in aerosol form or by gases, ultraviolet radiation and incineration has been and continues to be an important area of interest in the field of microbiology. It is recognized that incineration brings about complete sterilization of contaminated air. However, to the author's knowledge, information on the effect of exposing biological aerosols for short periods of time to temperatures below that of incineration is nonexistent.

The purpose of the experiments reported here was to obtain data which will enable prediction of the effect of mixing a viable biological aerosol with the hot exhaust gases of a jet engine. The present report explores the possibility of viability loss in an aerosol composed of Serratia marcescens (Sm) when the organisms are exposed for a period of 1.7 seconds to various temperatures. The 1.7 second exposure time used in these experiments was chosen from an analysis of the jet plume of the North American F-100, as presented in North American Aircraft Report NA-60-1403. An exposure time as large as 1.7 seconds was considered necessary in order to account for turbulent mixing effects which exist at the point of interception of the aerosol streamlines with the plume. It is planned to continue this work by studying the effect of shorter exposure times at various temperatures.

2.1 Experimental

Cell suspensions of Sm which were used in these aerosol studies were prepared from pellets of the organism furnished by Fort Detrick. The apparatus used in these experiments is shown schematically in Figure 2.1.1. A five gallon

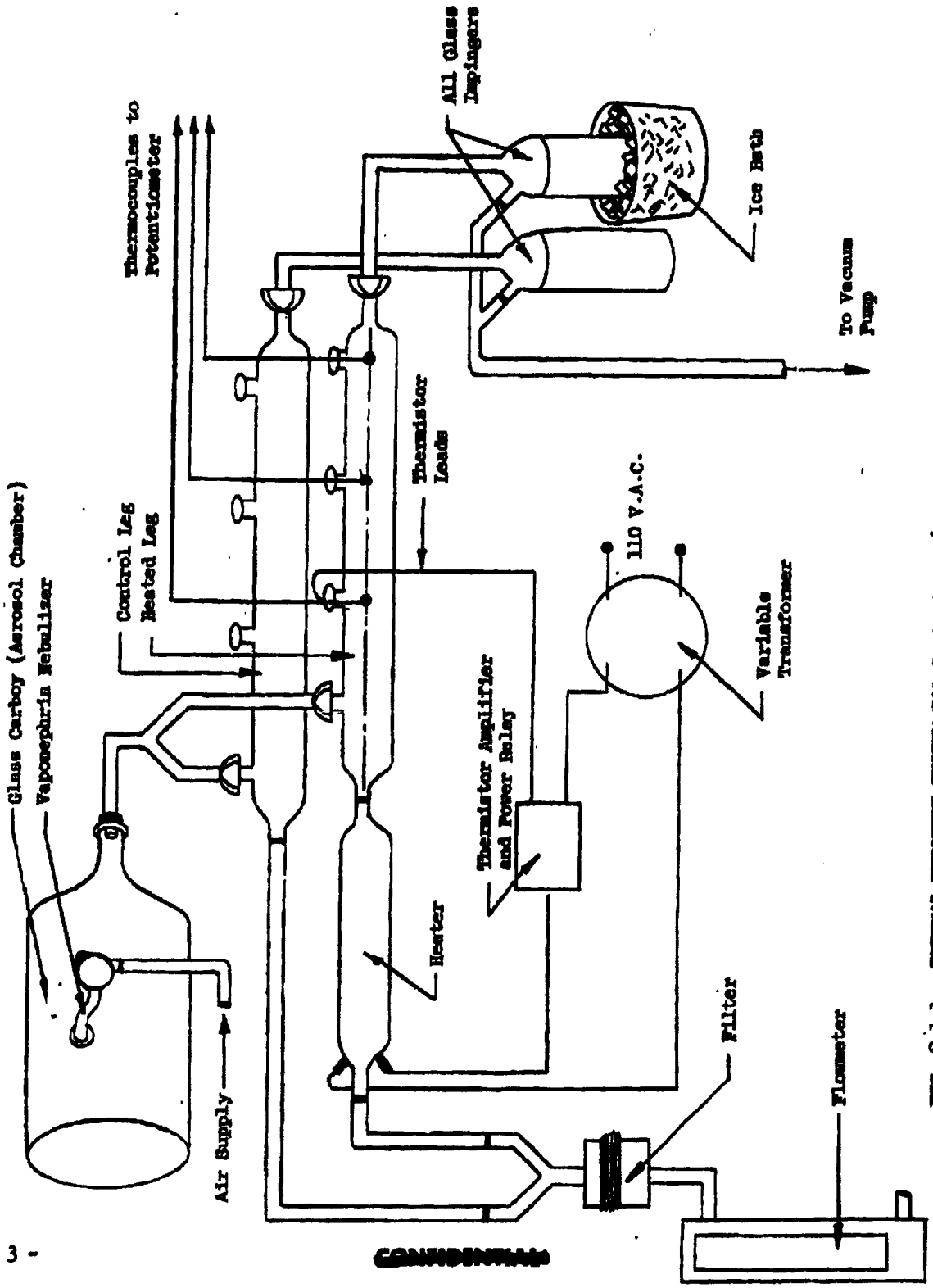

FIG. 2.1.1 THERMAL EXPOSURE SYSTEM FOR Sn AEROSOLS (SHOWN WITH INSULATION REMOVED)

glass carboy, which serves as the aerosol chamber, is connected to two identical 91.5 x 2.5 cm glass tubes by means of a "Y" tube. Heated air is mixed with aerosol in one of the tubes while room air is mixed with the other half of the aerosol. The unheated aerosol, which receives room air, serves as the control sample. During the course of experiments in which both legs of the apparatus received unheated air it was found that the control leg of the apparatus received approximately 1.3 times as much aerosol as the heated leg. If the aerosol chamber with "Y" tube was turned through 180°, then with both legs unheated it was found that the control leg received only 1/1.3 times as much aerosol as the heated leg. Therefore, unequal flow through the two legs was caused by the "Y" tube flow-splitter. Consequently, all percent recovery data from heated runs were multiplied by the factor 0.76.

Aerosols were generated using a modified Vaponephrin nebulizer charged with six ml of the cell suspension.

2.1.1 Sampling of Aerosols

Aerosols were sampled simultaneously from both the heated leg of the apparatus and the unheated control leg using All Glass impingers. The flow rate in all cases was 12.5 liters per minute with all runs having a duration of 15 minutes. An individual particle or organism was exposed for a period of 1.7 seconds to the heated air stream. This was true for all runs to be discussed. Approximately 10^{10} viable organisms were collected in the control impinger during a 15 minute run. The collecting fluid was 10 ml of sterile tryptose saline diluent (composition described below) plus two drops of sterile olive oil to reduce foaming. After the 15 minute

sampling period had elapsed, the impingers were removed from the apparatus and cooled in an ice bath. After cooling, the contents were quantitatively transferred to 50 ml volumetric flasks and diluted to volume with tryptose saline diluent. After thorough mixing, the contents of the volumetric flasks were serially diluted for viability determinations.

2.1.2 Viability Determinations

The medium used in viability determinations was composed of the following:

Wilson's peptone	2.0 g
Cerelose	0.5 g
NaCl	0.5 g
Agar	2.5 g
Distilled water to 100 ml	
pH adjusted to 6.8	

Serial dilutions were made in tryptose saline diluent of the following composition:

Tryptose	0.1 g
NaCl	0.5 g
Distilled water to 100 ml	

All viability determinations were made using sterile plastic petri dishes. After the plates were poured, they were placed in a 37°C incubator for a period of two hours prior to plating. This treatment removed any excess moisture which might interfere with subsequent development of colonies. Samples of 0.1 ml from the final dilution were streaked on the surface of the

agar plates with sterile glass streaking rods. The plates were then incubated at a temperature of 37°C.

2.2 Results and Discussion

The effect of heated air streams on the viability of Sm in aerosol form is presented in Table 2.2.1. These data represent the average percent recoveries determined from at least six separate tests at each temperature. Each determination was based on the aerosolization and collection of approximately 10^{10} viable organisms. The same results showing the mean percent recovery and the deviation of the mean are presented in Figure 2.2.1. The decrease in viability at 50°C amounted to about 51%, at 75°C 72%, at 100°C 92%, and at the maximum temperature of 125°C, a decrease of 99% From these results it is readily apparent that aerosols of Sm are significantly affected by heated air.

Since it is generally known that aerosols of vegetative organisms exhibit an appreciable decay rate even under optimum conditions, the results obtained in these experiments were not unexpected. As in other types of experiments where bacteria in aerosol form are subjected to lethal agents, e.g., UV radiation, the susceptibility of the organisms is usually a function of the medium in which the organisms are grown, the phase in the growth cycle at which the organisms are harvested, the matrix surrounding the organism(s) after the water surrounding the nebulized droplet has evaporated, and the conditions of the experiment.

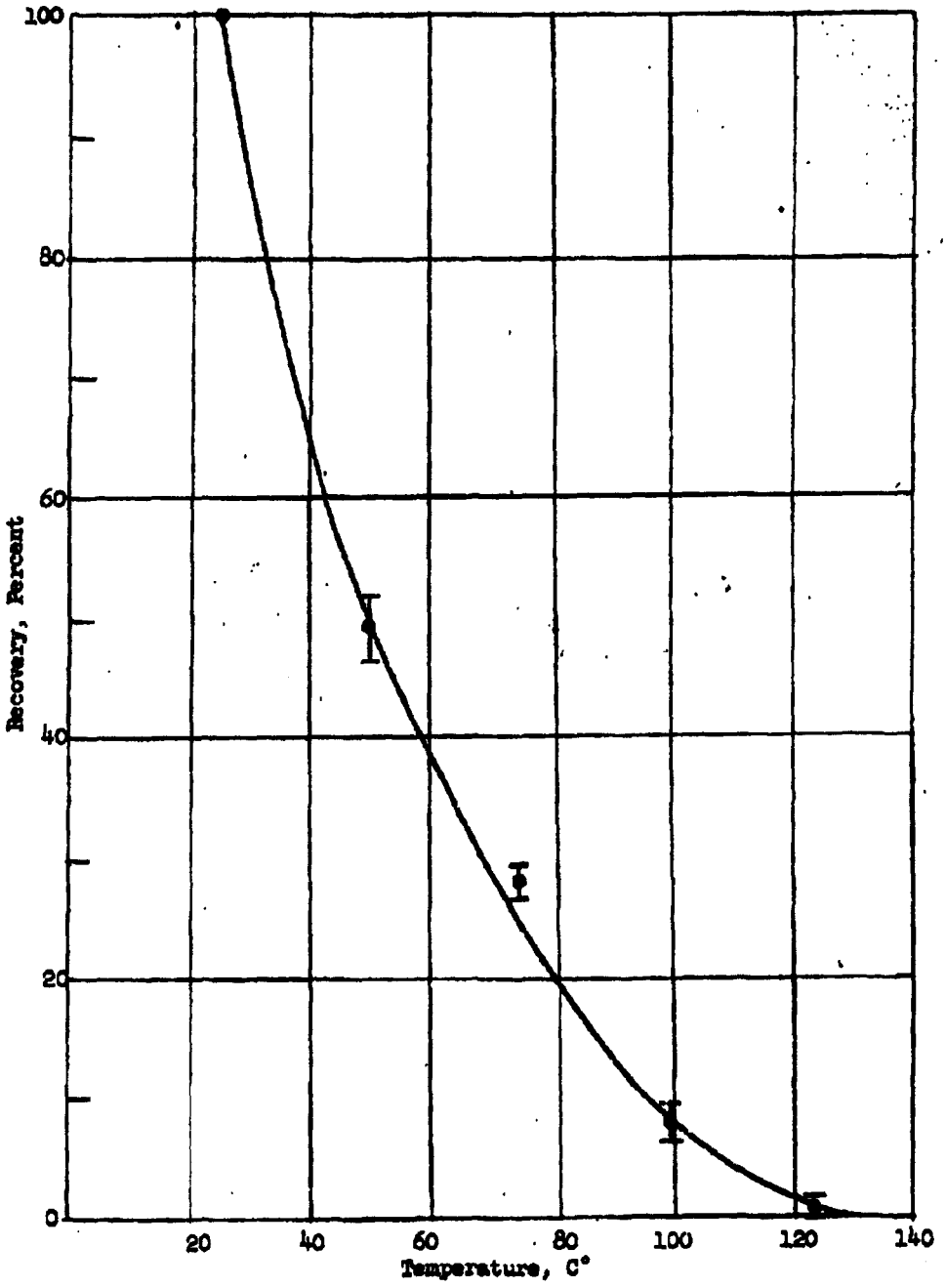

FIGURE 2.2.1 EFFECT OF HEATED AIR STREAMS ON THE VIABILITY OF AEROSOLS OF S. MARCESCENS

TABLE 2.2.1

EFFECT OF ELEVATED AIR STREAM TEMPERATURES ON THE VIABILITY OF SERRATIA MARCESCENS AEROSOLIZED FROM LIQUID SUSPENSION

Temperature, °C	Recovery, Percent*	Mean Deviation
25	100	---
50	49	2.8
75	28	1.5
100	8	1.6
125	0.8	0.5

Duration of all runs was 15 minutes.

*Average of six determinations

It was previously stated that the incubation temperature was 37°C. Since this temperature would be considered by some investigators to be slightly higher than optimum for S. marcescens, the possibility existed that somewhat different results might be found if the organisms were incubated at a lower temperature. Such a possibility exists because of the results of Anderson[2.1.1] who found that Escherichia coli B, following irradiation with ultraviolet light, produced significantly more colonies when incubated at 40°C rather than the customary 30°C. In order to determine whether or not the results of these experiments were influenced by the 37°C incubation temperature, two additional determinations were made at an air stream temperature of 75°C. From each run, 12 plates were prepared from the control leg and 12 plates from the heated

2.1.1 Anderson, E. H., Heat Reactivation of Ultraviolet-inactivated Bacteria. J. Bacteriol. 61, 389 (1951).

sample. Six control plates and six plates from the heated sample were placed in the 37°C incubator. The remaining six plates from each of the samples were incubated at room temperature. The results of this experiment are presented in Table 2.2.2.

TABLE 2.2.2

EFFECT OF INCUBATION TEMPERATURE ON THE RECOVERY OF AEROSOLS OF SERRATIA MARCESCENS EXPOSED TO AN AIR STREAM TEMPERATURE OF 75°C

	Recovery, Percent	
Run Numbers	37°C (Incubation Temp.)	25°C (Incubation Temp.)
1	32	31
2	30	28

From these results it can be seen that a lower temperature of incubation produces fewer colonies of the organisms from the heated sample. Whether these results are statistically significant or not must await further experimentation. However, it does appear that the 37°C incubation temperature is not deleterious to optimum growth of the organism.

Since the results of these experiments indicate an appreciable decrease in the viability of the organisms even at fairly low temperatures, the proximity of the disseminating device to the jet engine will be a significant parameter in the design of a BW delivery system.

3. EXPERIMENTS ON THE CHARACTERISTICS OF POWDERS

In order to determine those fundamental properties of finely-divided dry powders which affect their feeding and handling characteristics, information is being obtained on the coefficient of friction of powders sliding against various materials, the bulk density of powders as a function of compressive load, and the shear strength of powder beds. Correlation will then be sought between these characteristics and the output and energy required to operate feeding devices such as pistons and screw feeders.

3.1 Frictional Forces Between Powders and Channel Walls

In a previous report,[3.1.1] results were given for the frictional forces between talc powder and a glass cylinder. The experimental technique was described and a theoretical relationship derived for the forces involved. This relationship is:

$$\frac{F_A}{F_R} = e^{\frac{4\mu C_1}{D} L} \qquad (3.1)$$

where: F_A = force applied at one end of a plug of powder confined in a cylinder

F_R = resistive force at the other end of the plug of powder

μ = coefficient of friction between powder and cylinder wall

C_1 = constant

D = diameter of confining cylinder

L = length of compressed plug of powder.

According to this equation, a plot of the logarithm of F_A/F_R vs L/D should be a straight line.

3.1.1 General Mills, Inc. Report No. 2200, Third Quarterly Progress Report on Dissemination of Solid and Liquid BW Agents (Unclassified Title) May 15, 1961, pp. 5-16 (Confidential).

The term $C_1 \mu$ can be calculated from the slope of the line. The exact value of the coefficient of friction μ cannot be determined because C_1 is not known. C_1 is the ratio of the forces within the powder bed which are perpendicular and parallel to the applied force (i.e., $C_1 = \frac{F_\perp}{F_\parallel}$).

During the period covered by this report, tests were performed in cylinders of various materials using talc powder and finely ground Sm. The results of these tests are shown in Figures 3.1.1 and 3.1.2 (in the form of the best straight line through the data points for a given cylinder material). The cylinders used were not all the same length or diameter. The physical dimensions of the various cylinders are presented in Table 3.1.1.

TABLE 3.1.1

PHYSICAL DIMENSIONS OF CYLINDERS AND PISTONS USED IN FRICTION MEASUREMENTS

Cylinder Material	Length (in)	I.D. (in)	O.D. (in)	Piston Diameter (in)
Glass	7	1.185	1.37	1.182
Aluminum	18	1.500	1.90	1.486
Teflon	12	0.895	1.50	0.891
Stainless Steel	18	1.500	1.90	1.486

The values for the term $C_1 \mu$ were calculated from the slopes of the lines in Figures 3.1.1 and 3.1.2 and are given in Table 3.1.2.

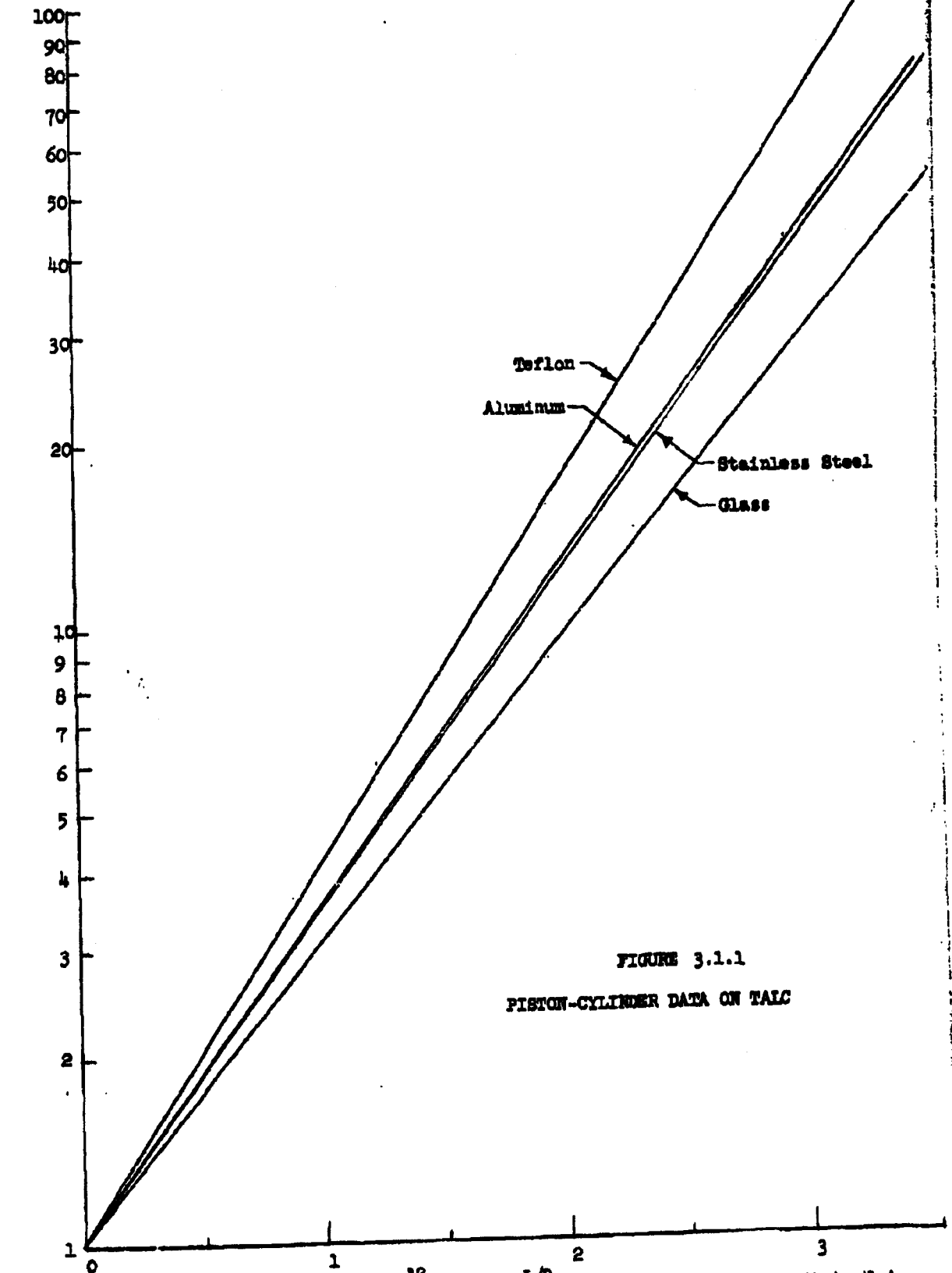

FIGURE 3.1.1

PISTON-CYLINDER DATA ON TALC

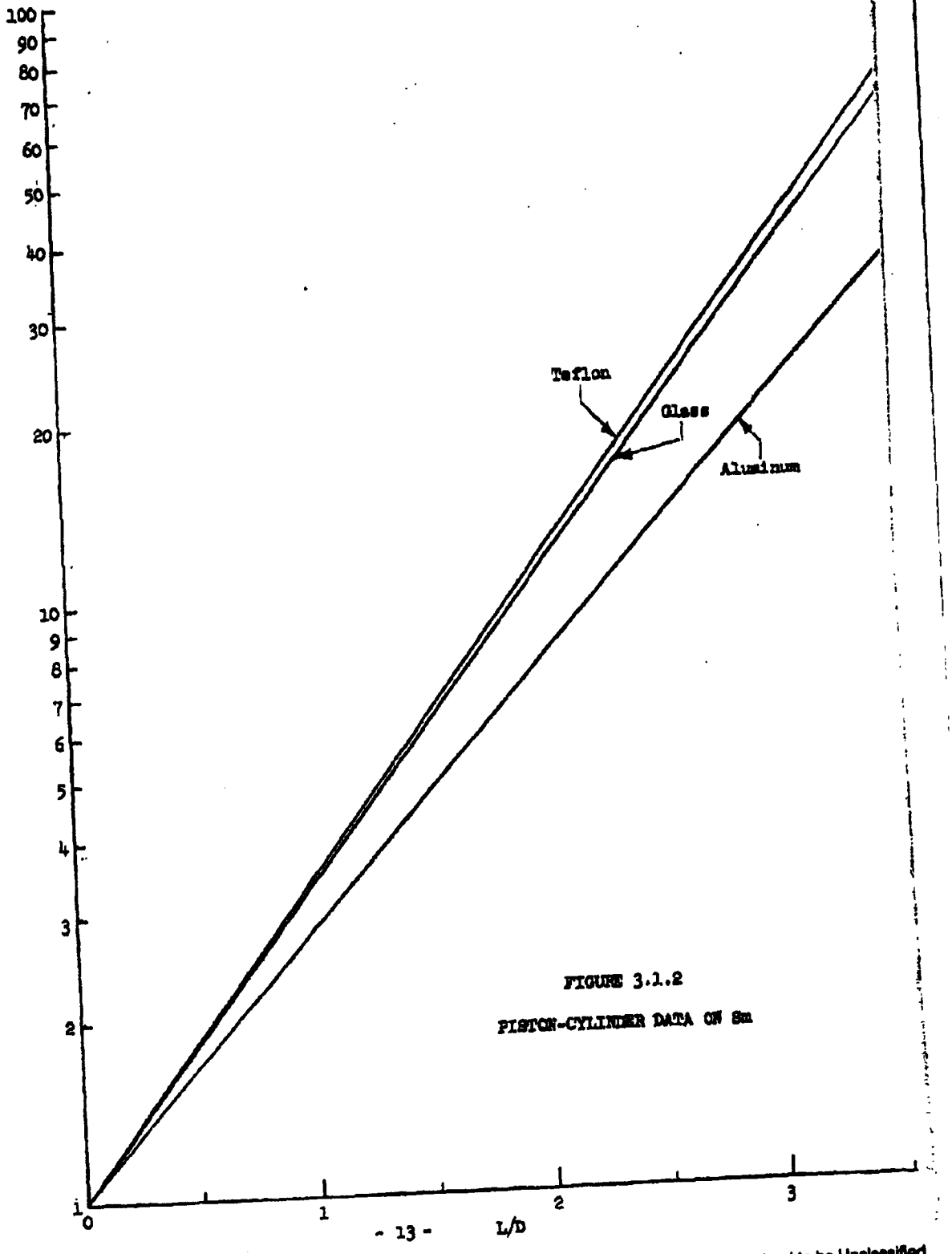

FIGURE 3.1.2

PISTON-CYLINDER DATA ON Sm

TABLE 3.1.2

VALUES OF THE TERM $C_1\mu$ FOR TALC POWDER AND Sm FOR VARIOUS CYLINDER MATERIALS

Powder	Cylinder	$C_1\mu$
Talc	Glass	0.279
Talc	Aluminum	0.319
Talc	Teflon	0.358
Talc	Stainless Steel	0.315
Sm	Glass	0.301
Sm	Aluminum	0.256
Sm	Teflon	0.306

In all of the tests at least four different values of F_R were tested. These values for the different cylinders are:

Glass	35.0, 84.2, 134.1, and 183.3 gm
Aluminum	77, 170, 357, and 450 gm
Teflon	21.7, 49.5, 76.7, and 104.5 gm
Stainless Steel	77, 170, 357, and 450 gm

There was some question as to what effect the surface roughness of the cylinder material had on the friction measurements. To study this effect, an aluminum cylinder of similar dimension to the one previously used was polished on the inside and a series of tests were made with talc powder. The data obtained are shown in Figure 3.1.3, indicating that the surface roughness, as encountered in these tests with aluminum, is not an influencing factor. The surface roughness of the inside of all the cylinders was measured with the

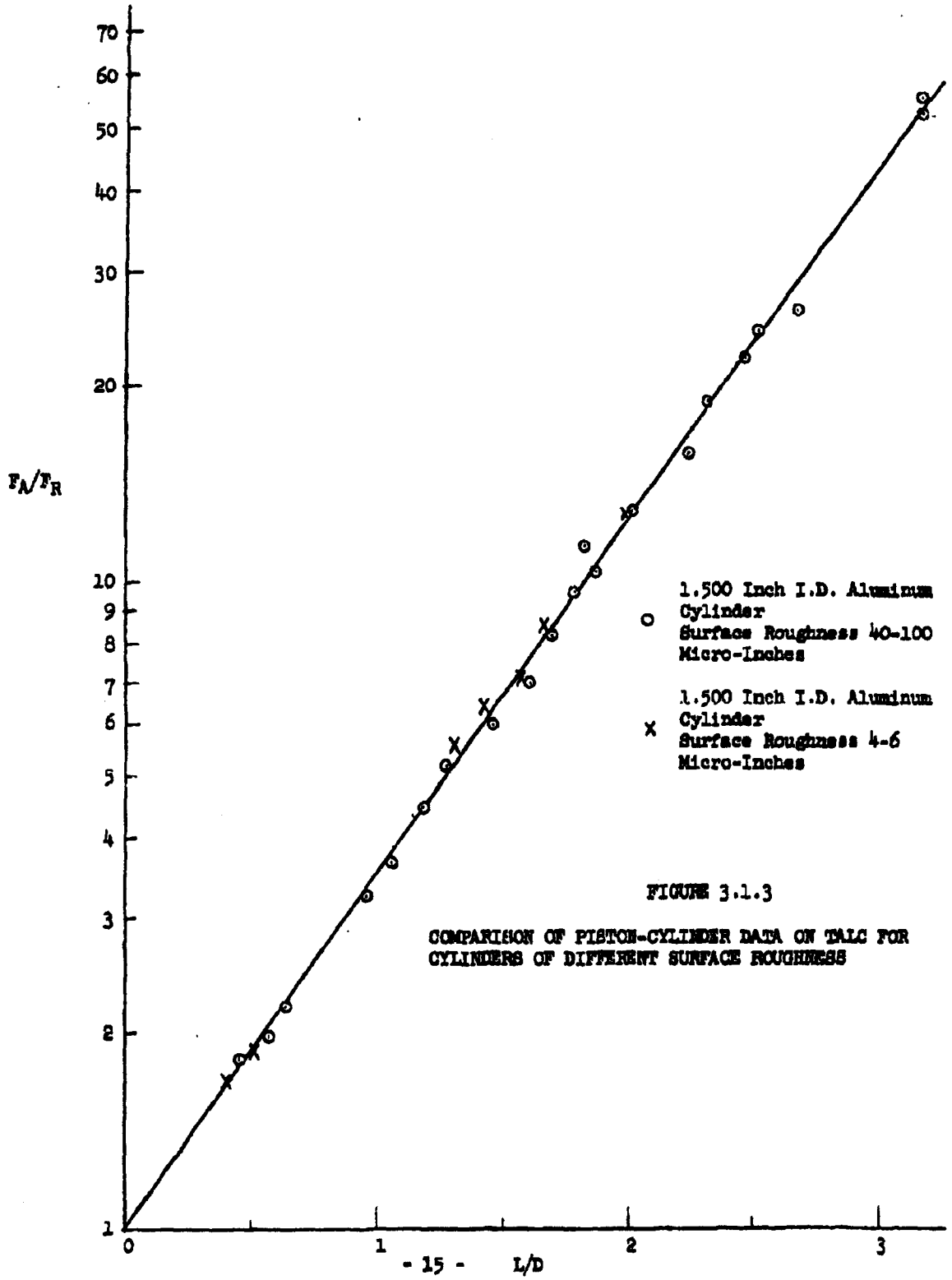

FIGURE 3.1.3

COMPARISON OF PISTON-CYLINDER DATA ON TALC FOR CYLINDERS OF DIFFERENT SURFACE ROUGHNESS

Surfindicator Model BL-110;[3.1.2] which measures "the arithmetical average deviation from the mean line" in micro-inches. Table 3.1.3 shows the surface roughness of the cylinders.

TABLE 3.1.3

AVERAGE SURFACE ROUGHNESS OF THE INSIDE OF VARIOUS CYLINDERS USED IN EXPERIMENTS

Cylinder Material	Surface Roughness of Inside of Cylinder
Glass	2.5 - 4 micro-inches
Aluminum	40 - 100 micro-inches
Teflon	75 - 150 micro-inches*
Stainless Steel	10 - 15 micro-inches
Polished Aluminum	4 - 6 micro-inches

* Estimated. Teflon is too soft to be measured with the instrument.

A test was also conducted to determine what effect the inside diameter of the cylinder had on the results. According to the theory developed, for any given powder and cylinder material, all points of the plot of log F_A/F_R vs L/D should be on the same straight line regardless of the cylinder diameter. Another aluminum cylinder was obtained which was 12 inches long by 0.825 inches inside diameter, and had an average surface roughness on the inside of 20-25 micro-inches. The cylinder was tested with talc powder and the results are compared with those of the 1.500 inches inside diameter aluminum tube in Figure 3.1.4. As can be seen, all the points can be adequately represented by the same straight line, indicating that cylinder diameter has no effect on the results.

3.1.2 Manufactured by Brush Electronics Company, Cleveland, Ohio.

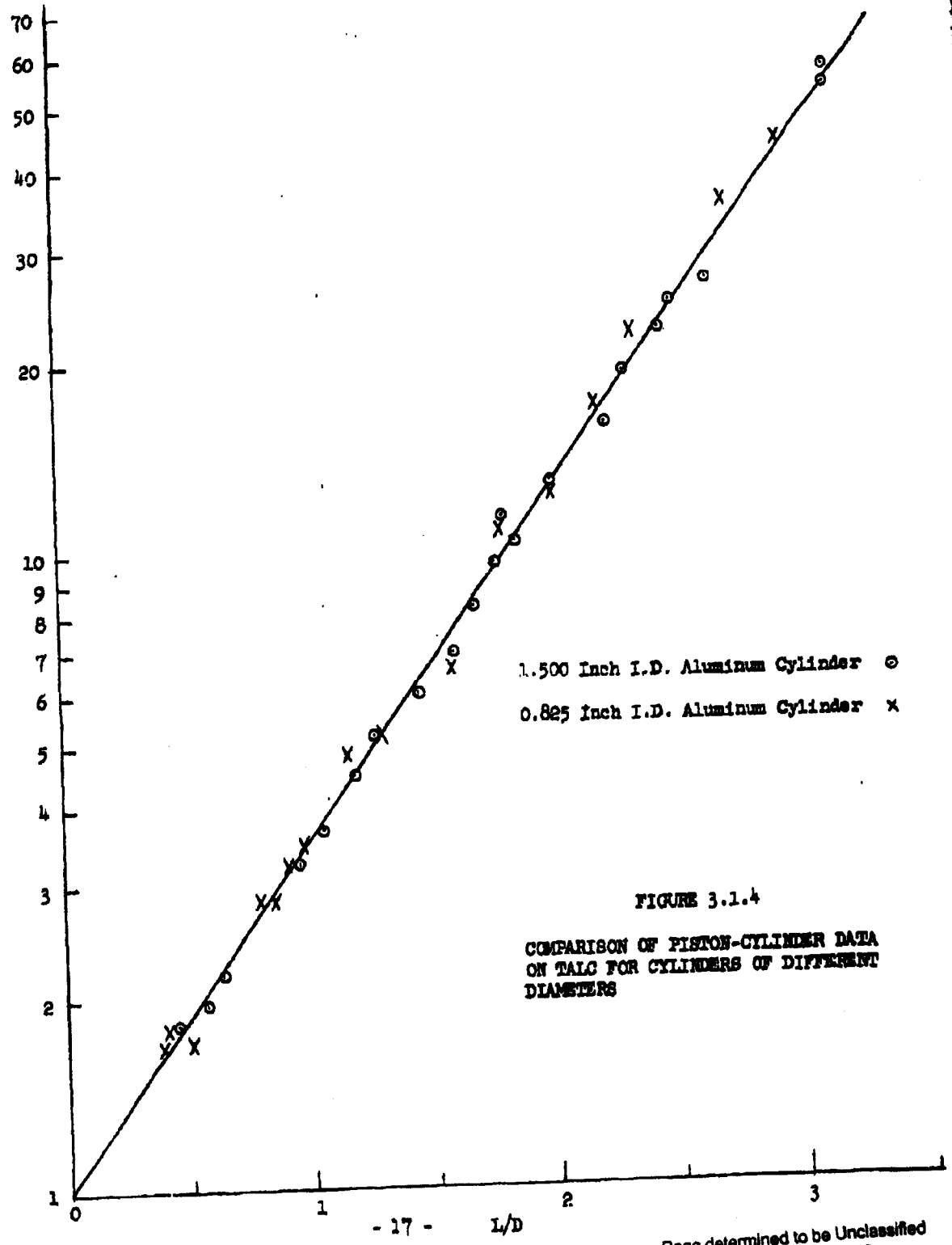

FIGURE 3.1.4

COMPARISON OF PISTON-CYLINDER DATA ON TALC FOR CYLINDERS OF DIFFERENT DIAMETERS

3.2 Coefficient of Friction Between Powders and Various Materials

A method of determining the coefficient of friction directly between powders and various materials is described by Cremer et al.[3.2.1] In this method a plate of the material to be tested is sprinkled with powder and tilted until the mass of powder slides off. Figure 3.2.1 shows the force diagram.

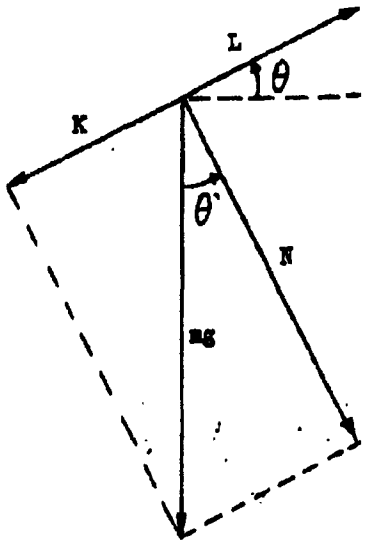

FIGURE 3.2.1

If the static friction is based on the conventional theory of Coulomb, then K = the frictional force L and:

$$L = \mu N = \mu mg \cos\theta \qquad (3.2)$$

3.2.1 Cremer, M., F. Conrad and T. Kraus. "Die Haftfähigkeit von Pulvern und ihre Anwendung zur Bestimmung von Korngrössen," Angewandte Chemie, Vol. 64, 1952, pp. 10-11.

where: μ = coefficient of friction

m = mass of the powder

g = acceleration of gravity.

From Figure 3.2.1 it can be seen that:

$$K = mg \sin \theta. \tag{3.3}$$

Substituting for K and L we have:

$$mg \sin \theta = \mu mg \cos \theta \tag{3.4}$$

or

$$\mu = \tan \theta. \tag{3.5}$$

An attempt was made to measure the coefficient of friction of talc and Sm by this manner with very little success. The difficulties encountered were:

1. For small masses of powder, there was no angle at which the mass would slide (up to 90°).

2. For larger masses, the powder would break away from the mass in varying amounts and slide off. The entire mass of powder would seldom slide off at the same time. It was also difficult to maintain uniform thickness of the mass of powder.

In order to solve these problems, it was decided to compress a plug of powder in a hydraulic press and then use this plug of powder to determine the coefficient of friction by noting the angle at which it slides. A steel cylinder was obtained which had the dimensions: length 9", I.D. 1.60", O.D. 2.37". The powder was sifted into this cylinder, compressed in the hydraulic press using a piston 1.57" in diameter, placed on a tilting table,[3.2.2] and the angle of slide measured. The angle of slide was measured by placing the plug

3.2.2 Manufactured by The Angle Computer Co., Glendale, California.

of powder on a clean, dry surface, and also by dusting the surface first with the powder under test. In either case, the angle of slide was the same, indicating that the coefficient of friction of the actual powder was being measured.

No measurement of the compressive force was made for the measurements with talc powder. However, it is estimated that the force used was about 1.7×10^7 dynes/cm^2. For Sm, the force was varied from 1.7×10^6 to 1.0×10^8 dynes/cm^2, with no appreciable variation in the angle of slide. Thereafter, a force of 1.7×10^7 dynes/cm^2 was used for the tests. In Table 3.2.1 are the results of these tests. At least 10 measurements on the angle of slide were made on each material and the value given is the average of these measurements.

TABLE 3.2.1

COEFFICIENT OF FRICTION OF TALC POWDER AND Sm FROM TILTING TABLE METHOD.

Material	Average Angle of Slide	Deviation	Coefficient of Friction
Talc Powder			
Aluminum	33.6°	2.4°	0.664
Glass	30.7	4.8	0.594
Teflon	36.2	1.2	0.732
Stainless Steel	33.0	3.5	0.649
Sm			
Aluminum	33.2	8.8°	0.654
Glass	35.2	5.8	0.705
Teflon	35.9	4.1	0.724

From the results of these experiments and the results of the piston cylinder experiments, the value of the constant C_1 (defined below) can be calculated. Table 3.2.2 gives the values determined for C_1.

TABLE 3.2.2

VALUES OF THE CONSTANT C_1

Material	Coefficient of Friction (μ)	C_1/μ	C_1
Talc			
Aluminum	0.664	0.319	0.481
Glass	0.594	0.286	0.482
Teflon	0.732	0.358	0.489
Stainless Steel	0.649	0.315	0.486
Sm			
Aluminum	0.654	0.256	0.392
Glass	0.705	0.301	0.427
Teflon	0.724	0.306	0.483

The average value of C_1 for talc powder is 0.484 and for Sm is 0.414. The variation of the value of C_1 for talc is much less than for Sm, indicating that the values for the coefficient of friction for talc and the various materials is probably more reliable (compare deviations in angle of slide, Table 3.2.1).

These values for the constant, C_1, indicate that with both talc and Sm stress transmission in the powder bed is such that a force slightly less than one half of the applied force is created in a direction perpendicular to that of the applied force.

3.3 Average Bulk Density of Talc Powder and Sm Under Various Compressive Forces

In these tests the bulk density of the powder was determined as a function of the compressed length of the plug of powder under various loads. The apparatus used was an 18 inch length of aluminum pipe of 1.500 inch I.D., a 1.486 inch diameter piston, and various weights.

The procedure was to sift a known weight of powder into the cylinder, place the piston on top of the powder, and measure the length of the compressed powder. Then additional weights were added and the length of the compressed powder plug was again measured. The compressed plug was removed from the cylinder and the process repeated with a different quantity of powder. Knowing the weight of the powder and the dimensions of the powder plug, the bulk density can be computed. This is the average bulk density since the density will vary along the entire length, being highest at a cross section next to the piston.

A plot of the logarithm of bulk density (ρ) vs the length of the compressed plug (L) was made for each compressive force, resulting in a curve which could be represented by the relationship:

$$\rho = \alpha + \beta \epsilon^{-k L^n} \qquad (3.6)$$

where α, β, and k are constants. If α is assumed to be the bulk density of the loose, uncompressed powder (ρ_o), then the equation can be written:

$$\rho - \rho_o = \beta \epsilon^{-k L^n} \qquad (3.7)$$

A plot of log $(\rho - \rho_o)$ vs L^n should be a straight line with intercept β and slope k.

The loose bulk density of talc was found to be 0.153 gm/cm^3 and that of Sm to be 0.285 gm/cm^3. A plot of log $(\rho - \rho_0)$ vs $L^{1/3}$ gave a straight line, indicating that the average bulk density of these powders under compression is:

$$\rho = \rho_0 + \beta \epsilon^{-k L^{1/3}} \qquad (3.8)$$

Figure 3.3.1 is a typical plot of log ρ vs L for a specified compressive load, and Figure 3.3.2 is a plot of log $(\rho - \rho_0)$ vs $L^{1/3}$ for the same compressive load. Figure 3.3.3 is a plot of the average bulk density of talc versus the length of compressed plug of powder under various compressive forces.

Figure 3.3.4 is the same type of plot for Sm. Table 3.3.1 gives the values of the constants β and k for the various compressive forces for both talc powder and Sm. The value of $\rho_{(L=0)}$ is also given. This quantity is defined as the bulk density of the powder at a cross section next to the piston or compressive force. It is determined by adding the value of the loose bulk density of the powder (ρ_0) to the value of the intercept β.

The value of the term k seems to be fairly constant for talc powder with an average value of 0.464. This is not true for Sm. There is a definite decrease in k with increasing compressive force. Figure 3.3.5 is a plot of the values of k, β, and $\rho_{(L=0)}$ for talc powder, and Figure 3.3.6 is a similar plot for Sm.

In the future, it is planned to make tests on polyvinyl alcohol powder using the piston-cylinder and tilting table methods to measure the frictional properties, and also determine the bulk density under various compressive forces. It is also planned to measure the shear strength of talc powder, Sm,

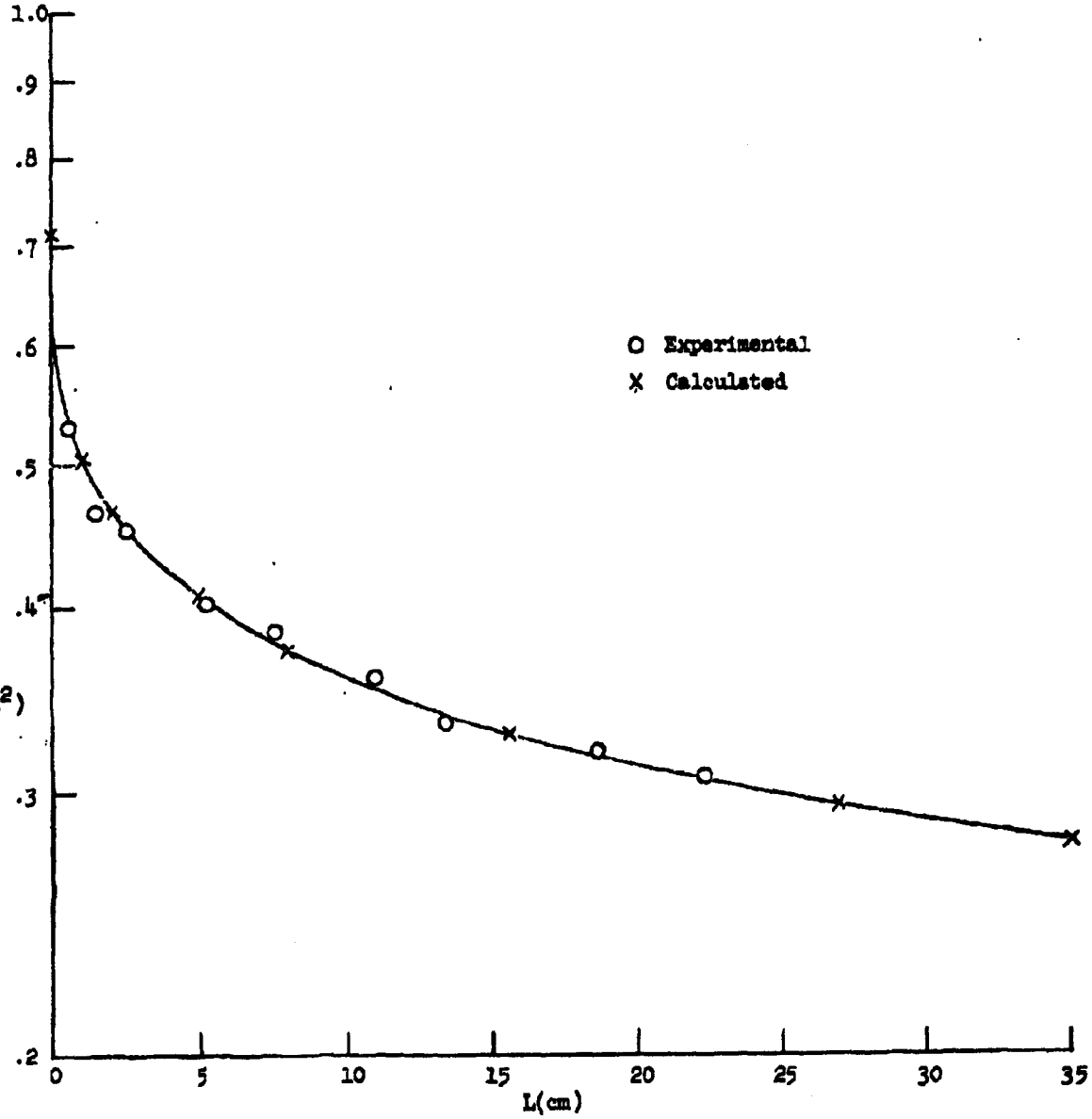

FIGURE 3.3.1 AVERAGE BULK DENSITY (ρ) OF TALC AS A FUNCTION OF PLUG LENGTH (L) UNDER A COMPRESSIVE FORCE OF 3.72×10^5 Dynes/cm^2

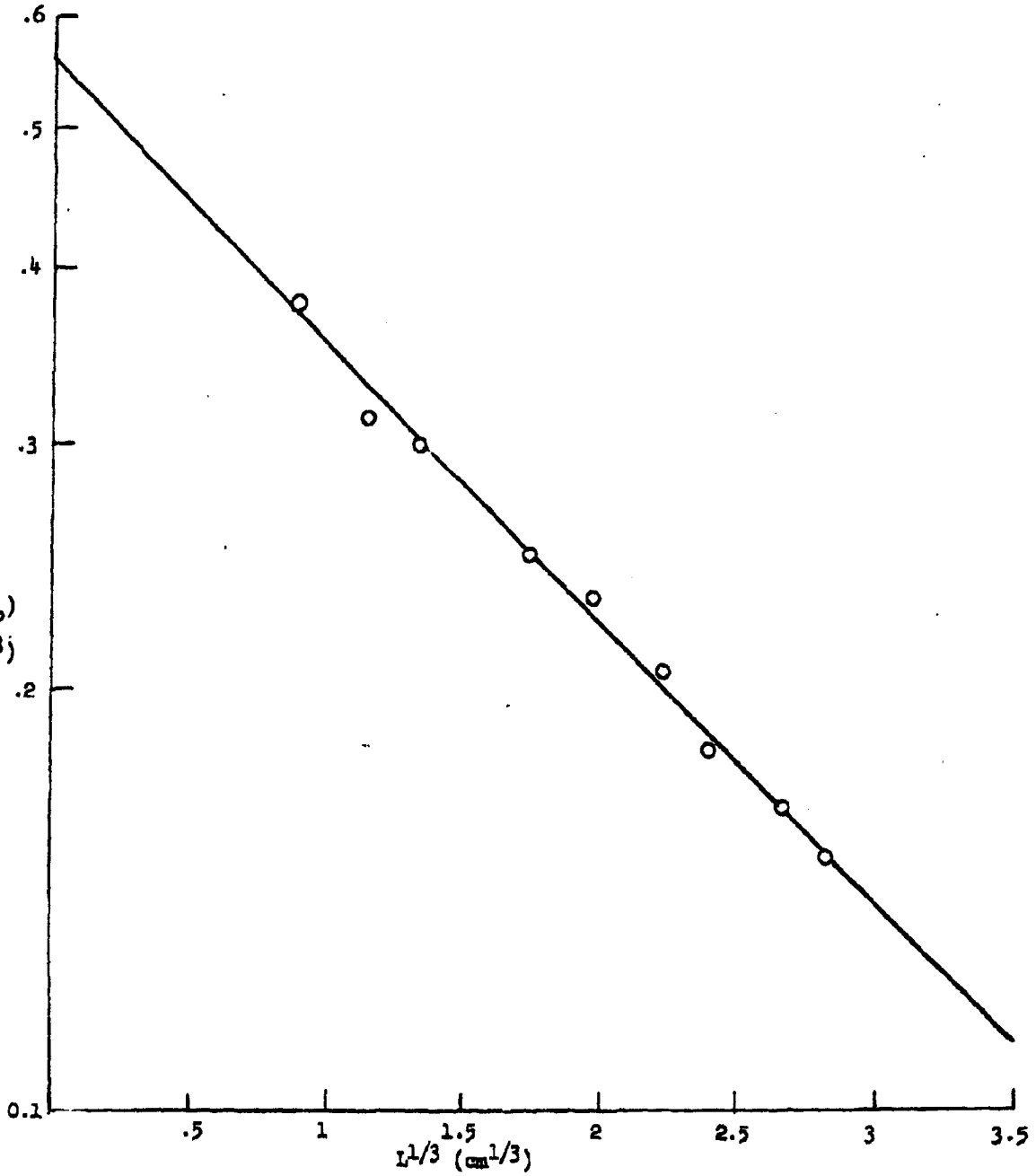

FIGURE 3.3.2 A PLOT OF $(\rho - \rho_o)$ VS $L^{1/3}$ FOR TALC UNDER A COMPRESSIVE FORCE OF 3.72×10^5 Dynes/cm^2

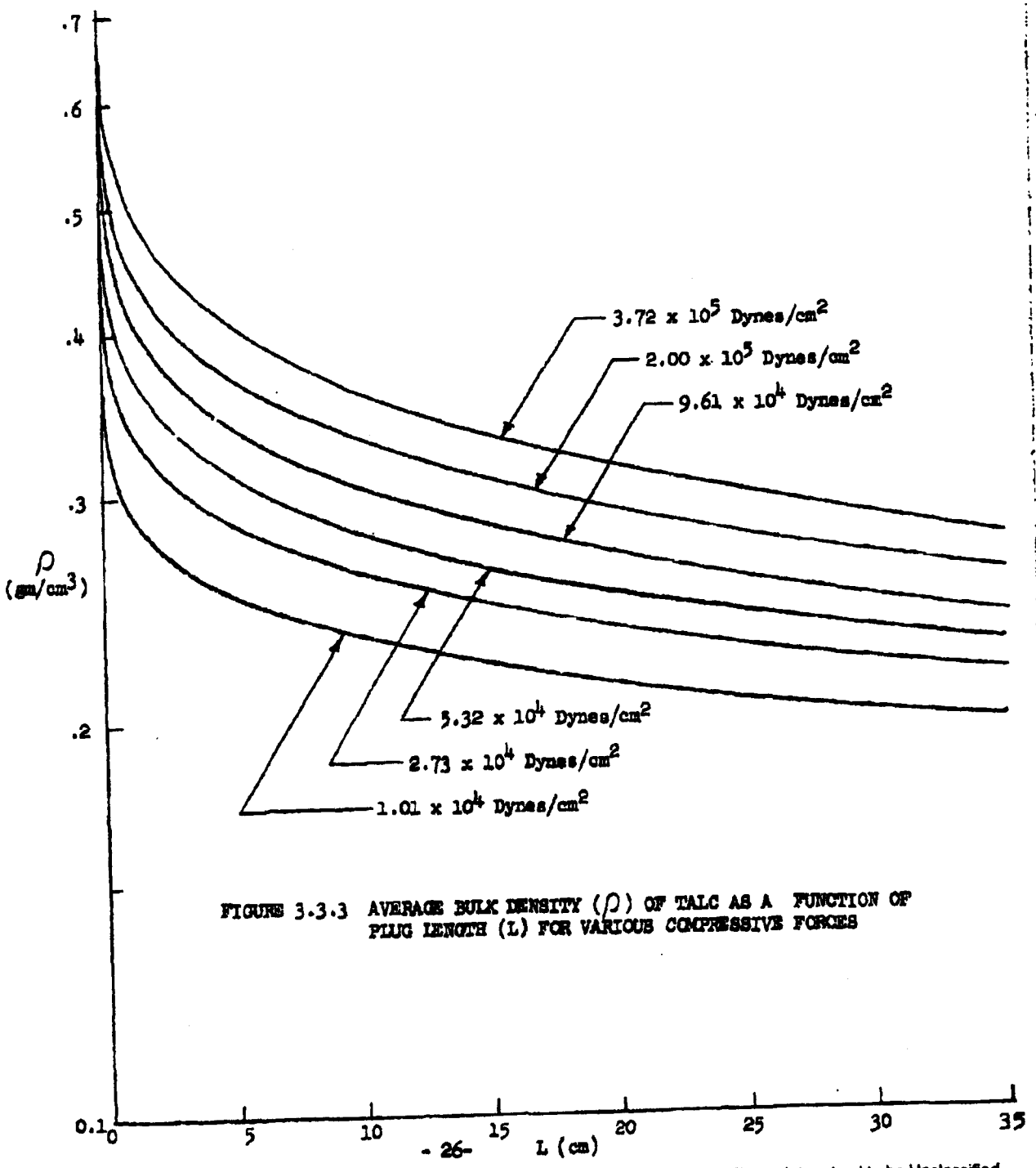

FIGURE 3.3.3 AVERAGE BULK DENSITY (ρ) OF TALC AS A FUNCTION OF PLUG LENGTH (L) FOR VARIOUS COMPRESSIVE FORCES

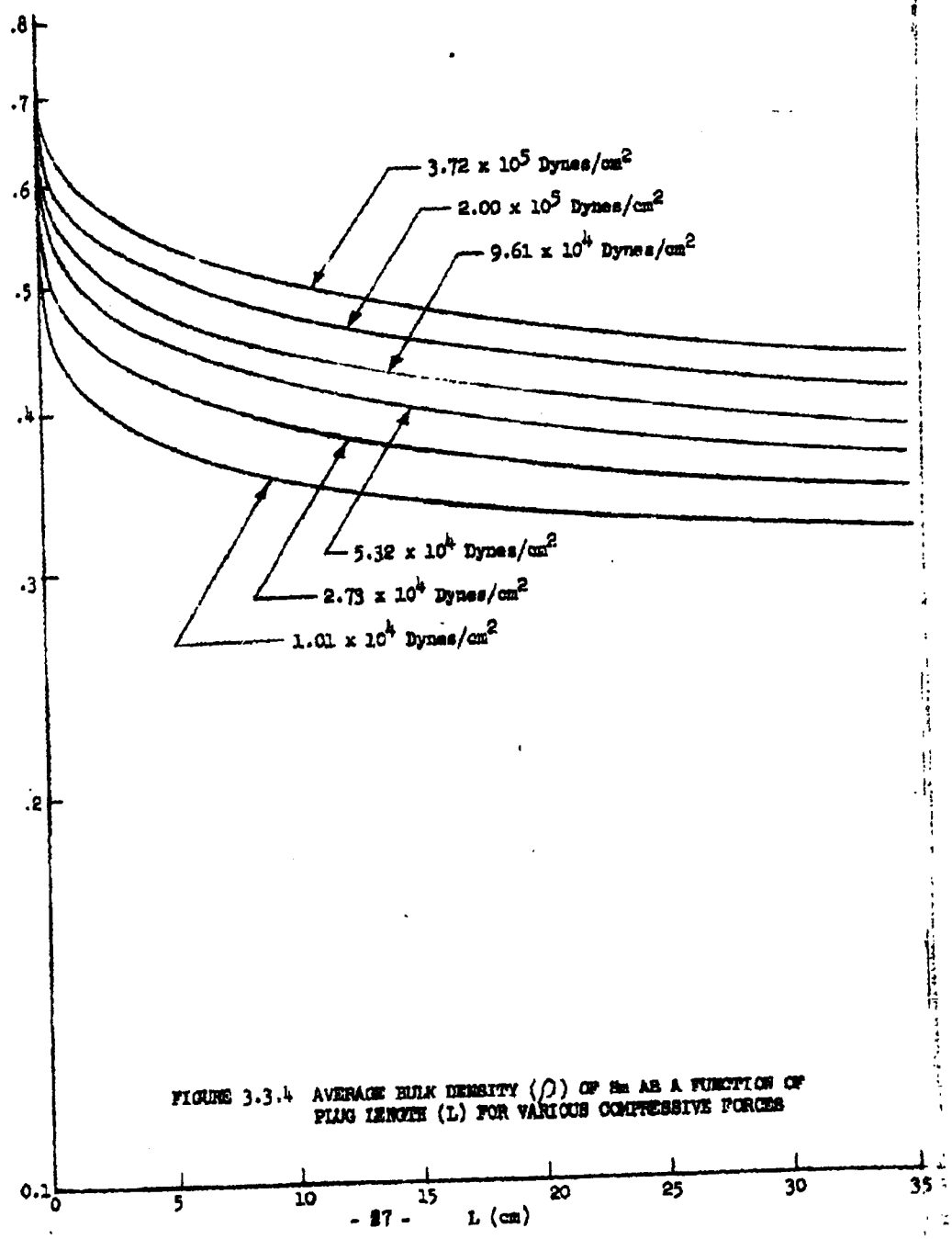

FIGURE 3.3.4 AVERAGE BULK DENSITY (ρ) OF Sn AS A FUNCTION OF PLUG LENGTH (L) FOR VARIOUS COMPRESSIVE FORCES

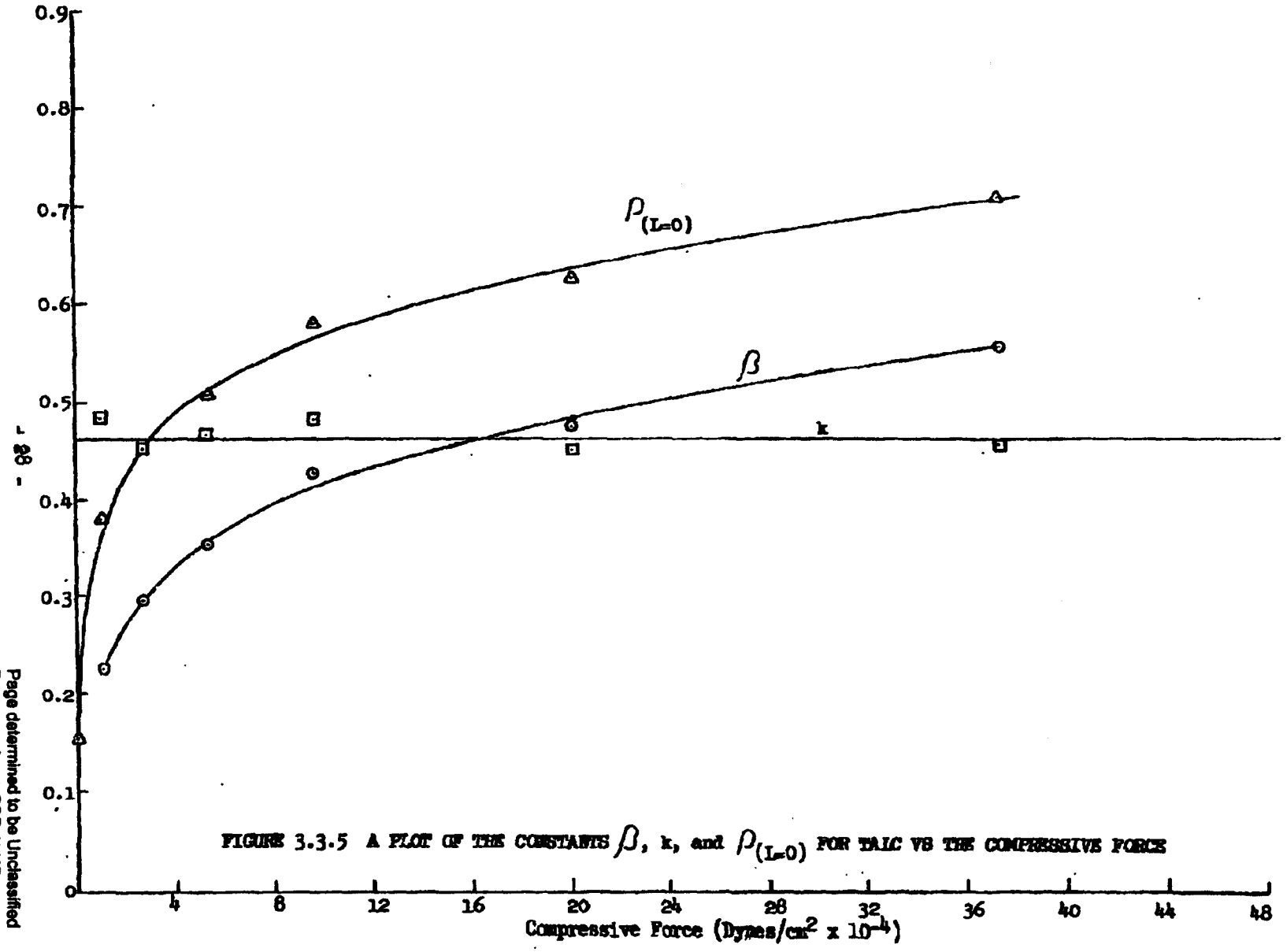

FIGURE 3.3.5 A PLOT OF THE CONSTANTS β, k, and $\rho_{(L=0)}$ FOR TALC VS THE COMPRESSIVE FORCE

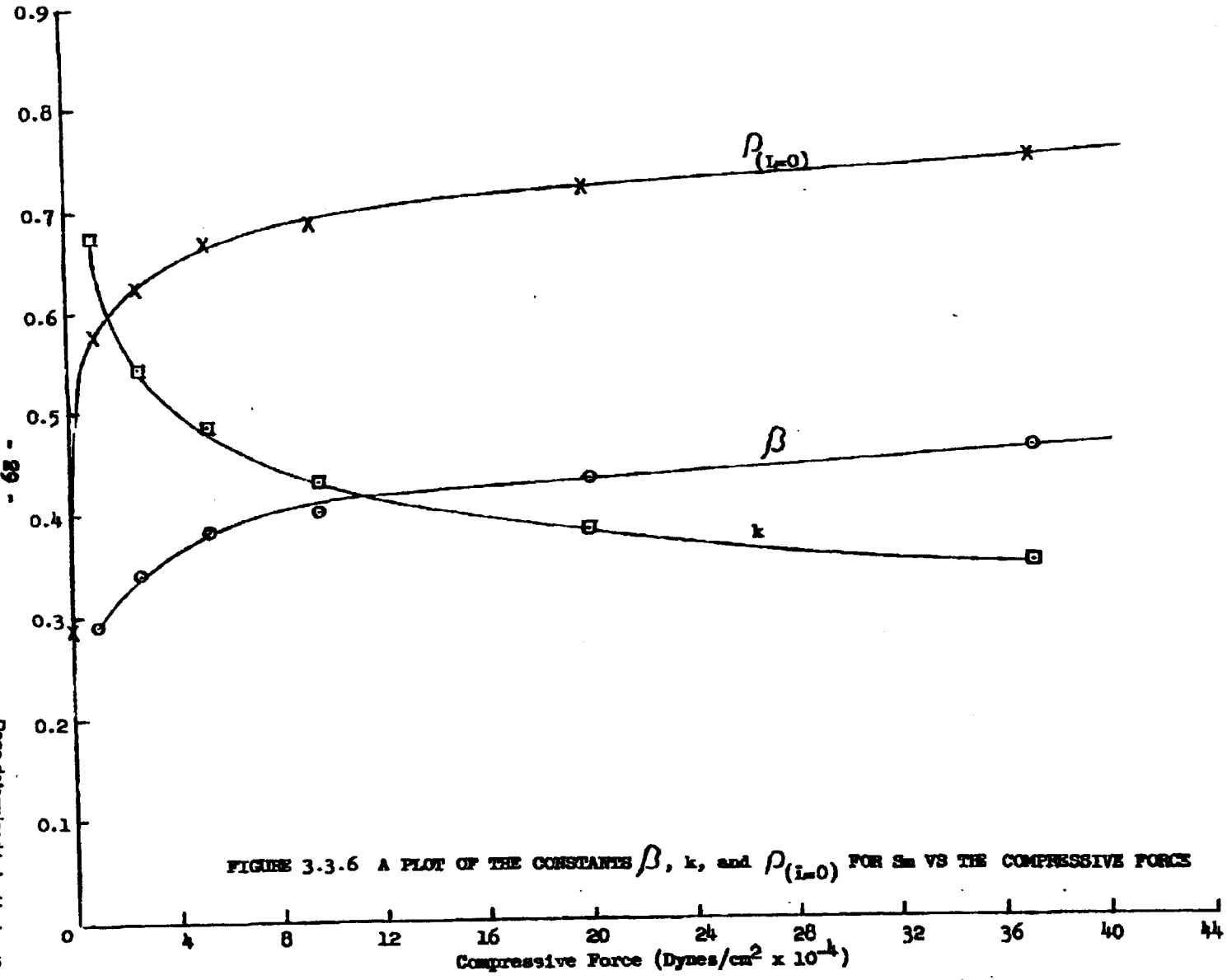

FIGURE 3.3.6 A PLOT OF THE CONSTANTS β, k, and $\rho_{(L=0)}$ FOR Sm VS THE COMPRESSIVE FORCE

and P.V.A. An attempt will be made to correlate these properties of the three powders to the feed rate of a screw feeder as reported previously[3.3.1] and with the torque required to operate the screw feeder.

TABLE 3.3.1

VALUES OF THE CONSTANTS β, k, AND $\rho_{(L=0)}$ FOR TALC POWDER AND Sm UNDER VARIOUS COMPRESSIVE FORCES

Compressive Force	β	k	$\rho_{(L=0)}$
Talc Powder			
1.01×10^4 dynes/cm^2	0.227	0.483	0.380
2.73×10^4 dynes/cm^2	0.297	0.451	0.450
5.32×10^4 dynes/cm^2	0.354	0.467	0.507
9.61×10^4 dynes/cm^2	0.426	0.481	0.579
2.00×10^5 dynes/cm^2	0.473	0.449	0.626
3.72×10^5 dynes/cm^2	0.557	0.456	0.710
Sm			
1.01×10^4 dynes/cm^2	0.291	0.676	0.576
2.73×10^4 dynes/cm^2	0.339	0.542	0.624
5.32×10^4 dynes/cm^2	0.382	0.486	0.667
9.61×10^4 dynes/cm^2	0.401	0.432	0.686
2.00×10^5 dynes/cm^2	0.432	0.381	0.717
3.72×10^5 dynes/cm^2	0.458	0.346	0.743

3.3.1 General Mills, Inc. Report No. 2161, Second Quarterly Progress Report on Dissemination of Solid and Liquid BW Agents (Unclassified Title) Feb. 13, 1961, pp. 2-13 (Confidential).

4. THEORETICAL STUDY OF POWDER MECHANICS

In previous reports two basic approaches for studying the mechanical behavior of particulate materials have been examined. The first was based upon interactions among individual particles,[4.1] while the second dealt with bulk properties of powders.[4.2] During the current report period, additional theoretical and experimental work has been carried out along the lines of the second approach.

A theoretical study has been made of the force required to lift a disk imbedded in material having dilatant properties. The results were found to agree well with experiments conducted with glass beads. These theoretical developments and possibilities for further research along theoretical lines are discussed herein.

4.1 Analysis of the Force Required to Lift a Long Cylindrical Rod from a Granular Bed

Consider a long cylindrical rod imbedded in an elastic granular bed at a depth y_o which is large compared with the diameter of the rod. The axis of the rod is parallel with the bed surface; also, the granular material is assumed to have a shear strength characteristic of the form:[4.2]

$$\tau = \sigma \tan \phi \qquad (4.1)$$

The force required per unit length to lift the rod from the bed may be determined as follows. For a line load of magnitude P grams/cm, applied to an

4.1 General Mills, Inc. Report No. 2161, Second Quarterly Progress Report on Dissemination of Solid and Liquid BW Agents (Unclassified Title), Feb. 13, 1961, pp. 46-55. (CONFIDENTIAL).

4.2 General Mills, Inc. Report No. 2200, Third Quarterly Progress Report on Dissemination of Solid and Liquid BW Agents (Unclassified Title), May 15, 1961, pp. 22-38 (CONFIDENTIAL).

elastic medium as shown in Figure 4.1.1, the stress at a point defined by the polar coordinates (r, θ) is in the radial direction and defined by the equations:[4.2]

$$\sigma_r = \frac{2P}{\pi} \frac{\cos\theta}{r} \; ; \; \sigma_\theta = t_{r\theta} = 0 \tag{4.2}$$

The local condition for shear failure within the bed is defined by the expression:[4.2]

$$\sin\phi = \frac{\sigma_1 - \sigma_2}{\sigma_1 - \sigma_2} \tag{4.3}$$

where σ_1 and σ_2 are major and minor principal stresses at a point within the granular bed (see Figure 4.1.1). If it is assumed that the initial stress distribution in the bed due to its weight is hydrostatic, the slip condition from Equations (4.2) and (4.3) becomes:

$$\sin\theta = \frac{1}{1 + \frac{\pi\gamma y_0^2}{P} \left(\frac{r}{y_0}\right) \frac{\left(1 - \frac{y}{y_0}\right)}{\cos\theta}} \tag{4.4}$$

where γ is the density of the material.

From an analysis of Equation (4.4) it is found that, for a given load P, there exists a region of nearly circular cross-section within which the material is in a state of shear failure, and an external region which is in statical equilibrium under the load P. The shape of the surface separating these regions is defined by the equation:

$$\frac{r}{y_1} = \sqrt{\left(\frac{y}{y_1}\right) \left(\frac{1 - y_1}{1 - y}\right)} \tag{4.5}$$

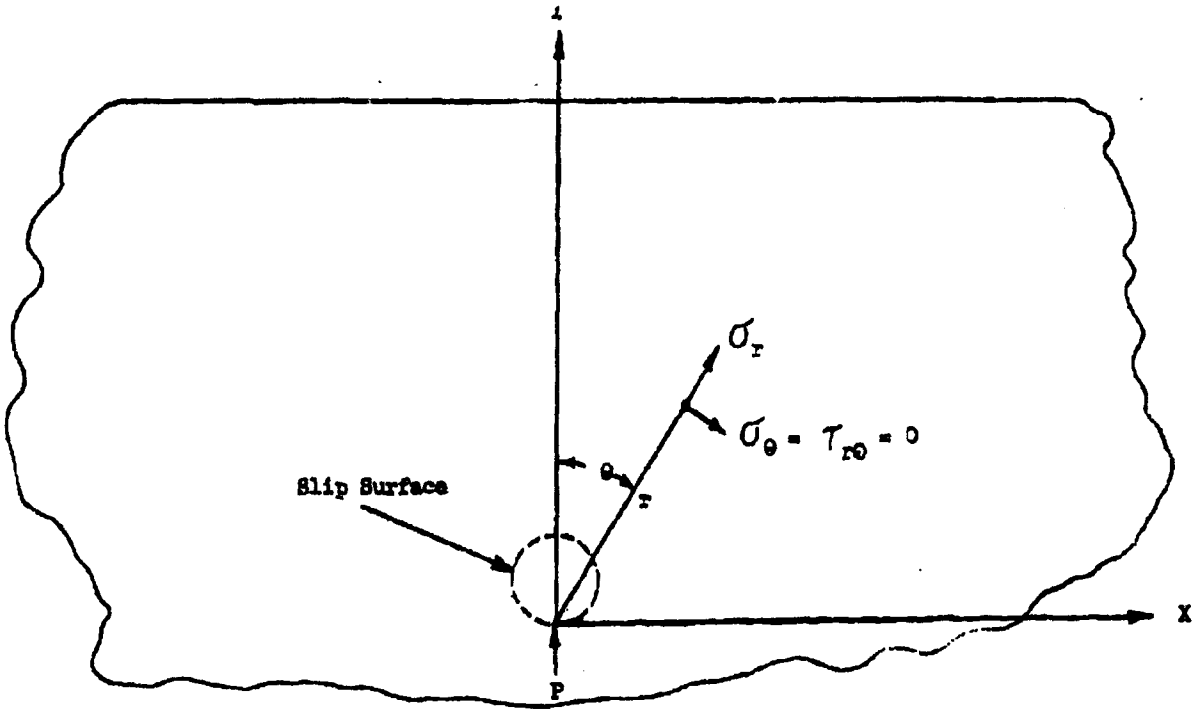

FIGURE 4.1.1 NOMENCLATURE FOR ANALYSIS OF STRESSES IN A GRANULAR BED - TWO DIMENSIONAL LOADING P g/cm

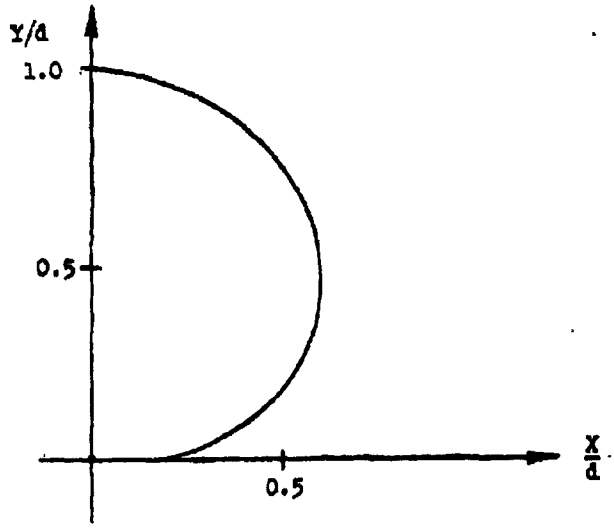

FIGURE 4.1.2 THEORETICAL TWO-DIMENSIONAL SLIP SURFACE; $\phi = 30°$, $P/\pi d^2 = 5$

where y^1 is obtained by solving the quadratic:

$$y^1 (1 - y^1) = \frac{P}{\gamma \pi y_o^2} \frac{1 - \sin \phi}{\sin \phi} . \qquad (4.6)$$

For $\phi = 30°$ and $\frac{P}{\gamma \pi y_o^2} = 5$, the shape of the slip boundary is as shown in Figure 4.1.2. The force per unit length required to lift a smooth rod having a cross-sectional shape defined by the slip surface (Equation 4.5) is, from Equation (4.4):

$$P = \pi \gamma y_o d \left(1 - \frac{d}{y_o}\right) \frac{\sin \phi}{1 - \sin \phi} \qquad (4.7)$$

where $d = y^1$ defines the "diameter" of the nearly-circular rod.

This equation is valid only for very small values of d/y_o, since the boundary conditions at the surface of the bed are not satisfied by the approximate solution given above. This defect can be removed by applying an image load $P' = P$ at the point $y = 2 y_o$ as shown in Figure 4.1.3. With this loading, the stresses at the surface $y = y_o$ vanish as required at the free surface. Carrying out an analysis similar to that given above, it is found that the required load per unit length is:

$$P = \pi \gamma y_o d \left(1 - \frac{d}{2y_o}\right) \frac{\sin \phi}{1 - \sin \phi}. \qquad (4.8)$$

These results are particularly interesting in that the load P varies linearly with the depth of immersion y_o.

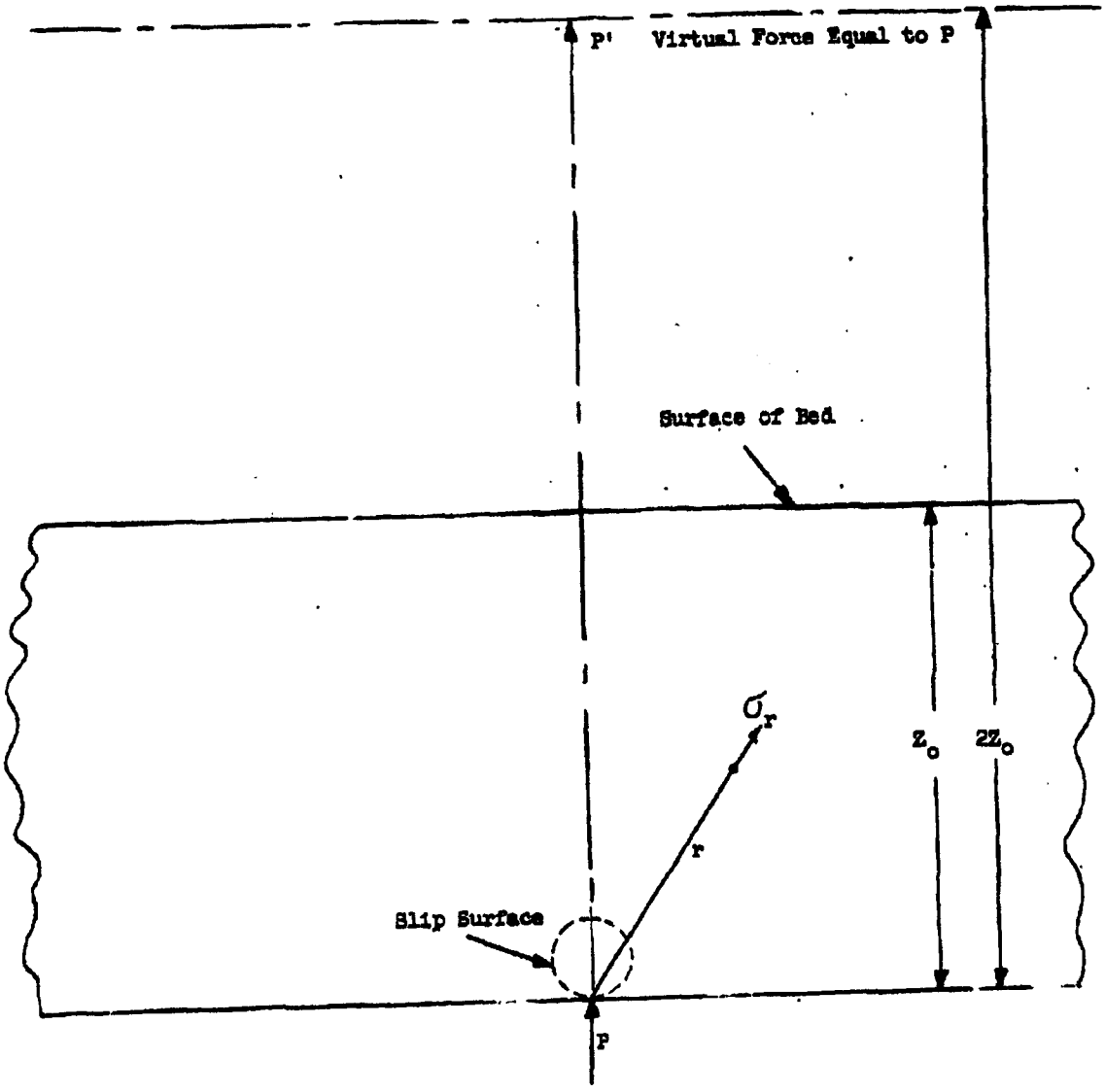

FIGURE 4.1.3 POINT LOAD IN A TWO DIMENSIONAL BED OF POWDER WITH A VIRTUAL FORCE TO CORRECT FOR BOUNDARY CONDITIONS ON THE SURFACE OF THE BED

4.2 Analysis of the Force Required to Lift an Imbedded Disk from a Granular Bed

An approximate analysis of the force required to lift an imbedded disk from a bed composed of elastic granules can be carried out along the lines of the above two-dimensional analysis. For a point load applied normal to the surface of a semi-infinite elastic solid, Boussinesq[4.3] obtained the stress components:

$$\sigma_r = \frac{3P}{2\pi} \frac{r^2 z}{(z^2 + r^2)^{5/2}},$$

$$\sigma_z = \frac{3P}{2\pi} \frac{z^3}{(z^2 + r^2)^{5/2}},$$

$$\tau_{rz} = \frac{3P}{2\pi} \frac{rz^2}{(z^2 + r^2)^{5/2}}, \qquad (4.9)$$

where r and z are cylindrical coordinates (see Figure 4.2.1).

Taking the origin at a point at depth z_o from the surface of the bed, the requirement that the stresses be zero at the bed surface may be satisfied, as in the two-dimensional case, by considering a fictitious load $P' = P$ to act at the point $z = 2z_o$. The stress distribution is then obtained by superposition using Equation (4.9).

The slip condition is again given by Equation (4.2), on the assumption of a linear shear strength characteristic as expressed by Equation (4.1).

Carrying out an analysis similar to those previously described, it was found that the force needed to lift an approximately spherical object of

4.3 Timoshenko, S. and J. N. Goodier. Theory of Elasticity, 2nd Edition, McGraw-Hill (1951), p. 85.

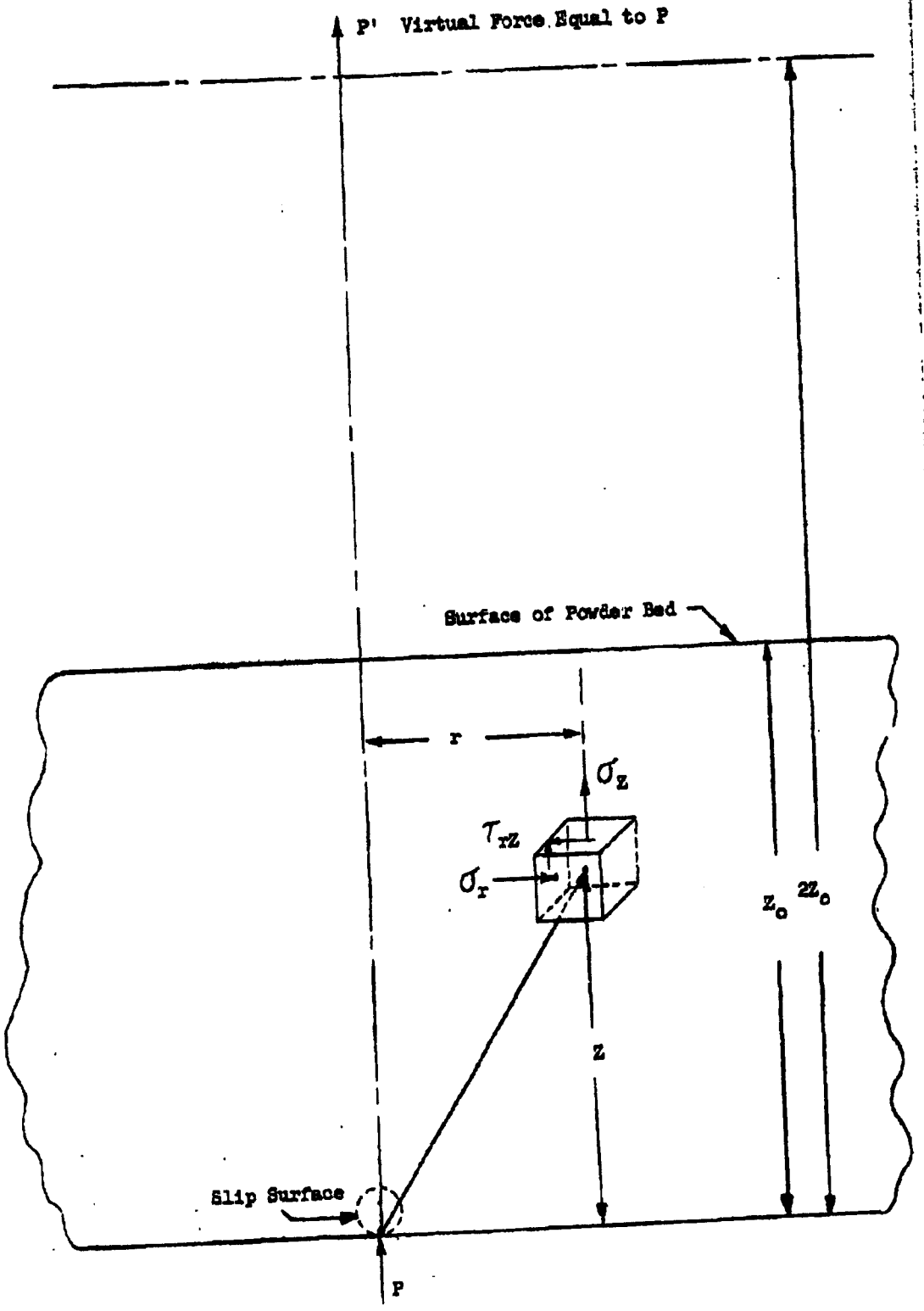

FIGURE 4.2.1 POINT LOAD IN A THREE DIMENSIONAL BED OF POWDER

diameter d, imbedded to a depth z_o in a granular bed, is:

$$P = \frac{2\pi\gamma d^3}{3} \frac{\sin\phi}{1-\sin\phi} f\left(\frac{2z_o}{d}\right) . \qquad (4.10)$$

The function $f = \left(\frac{2z_o}{d}\right)\left(1 + \frac{d}{2z_o}\right)^2$ is plotted in Figure 4.2.2, indicating the way in which P varies with the depth z_o.

Although the load approaches a linear dependence on depth for large values of z_o/d in the axisymmetric case, it is apparent that a considerable departure from linearity occurs for small values of z_o/d. In the range $1.1 < z_o/d < 8.0$, the theoretical load is represented quite accurately by the power law: $Q \sim d^{1.625} \cdot z_o^{1.375}$.

4.3 Discussion of the Theory and Comparison with Experiment

The analytical results presented above conflict somewhat with earlier disk-lifting experiments[4.2] which indicated that the force required to lift an imbedded disk from finely-divided materials such as talc, saccharin, etc., varies approximately as the 3/2 power of the depth.

In order to check the validity of the theoretical conclusions for dilatant materials, disk-lifting experiments were conducted using glass beads of diameter 100 and 200 microns, respectively. The apparatus and technique employed in these tests are described in an earlier report[4.1]. The results are shown in Figure 4.3.1. Within the range covered by the experiments, the agreement between theory and experiment is very good.

The shear strength characteristic employed in the theory (Equation 4.1) was also checked experimentally for the 200 micron glass beads using the apparatus shown in Figure 4.3.2. The results of these tests are shown in Figure 4.3.3. The shear angle obtained from the test data is $\phi = 26.8°$.

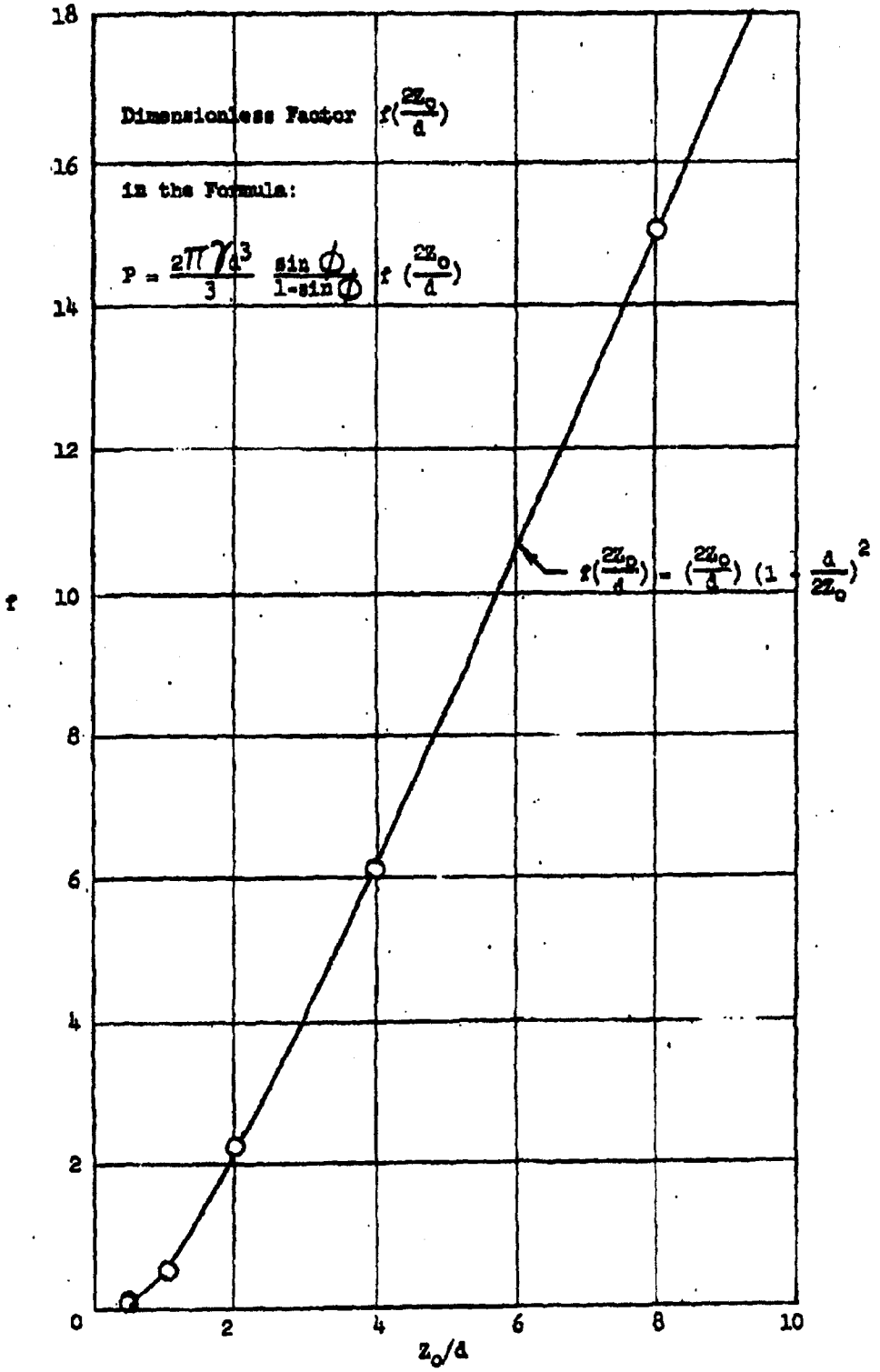

FIGURE 4.2.2 GRAPH OF f vs z_o/d

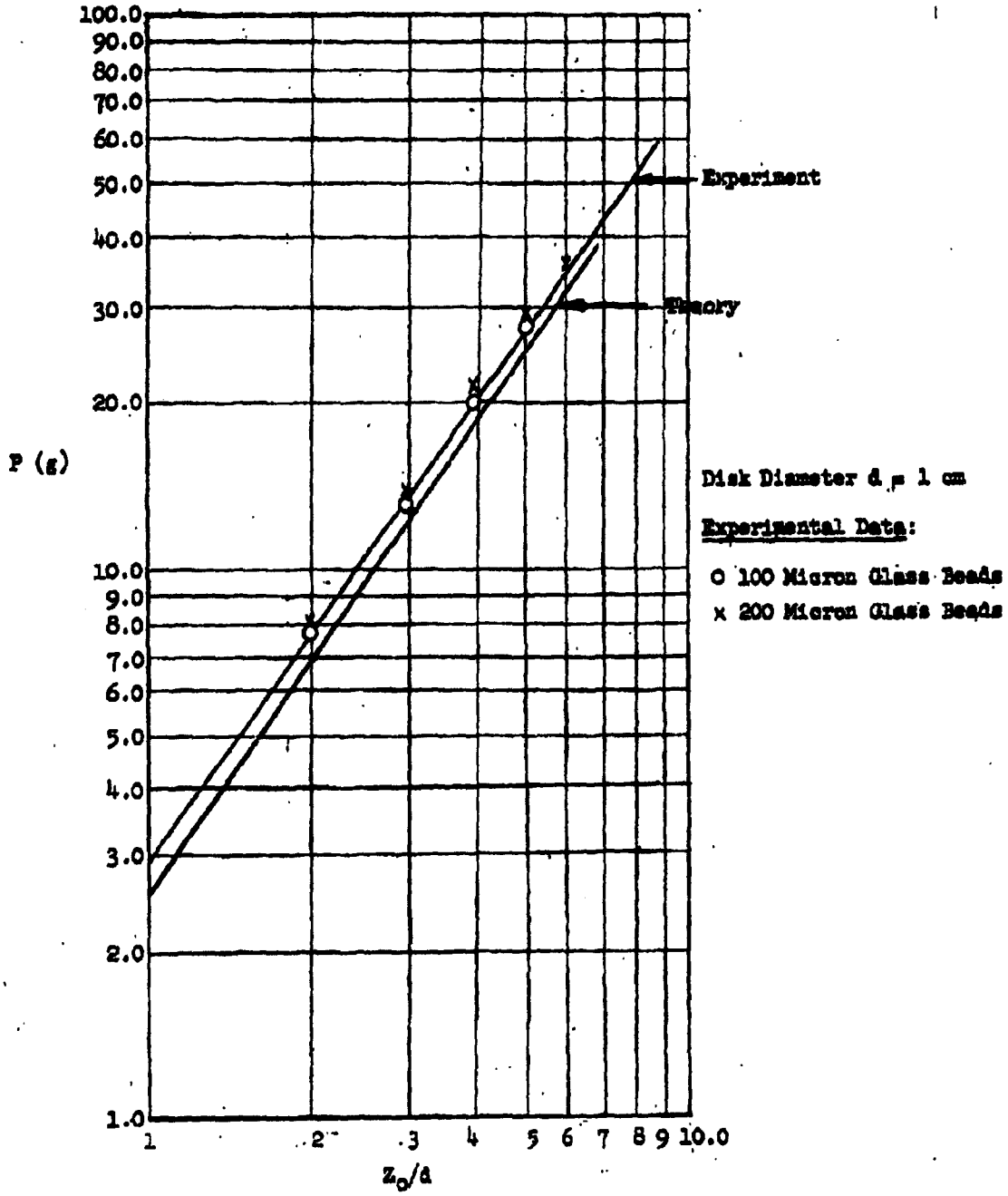

FIGURE 4.3.1 FORCE REQUIRED TO LIFT AN IMBEDDED DISK FROM GRANULAR BED vs Z_o/d

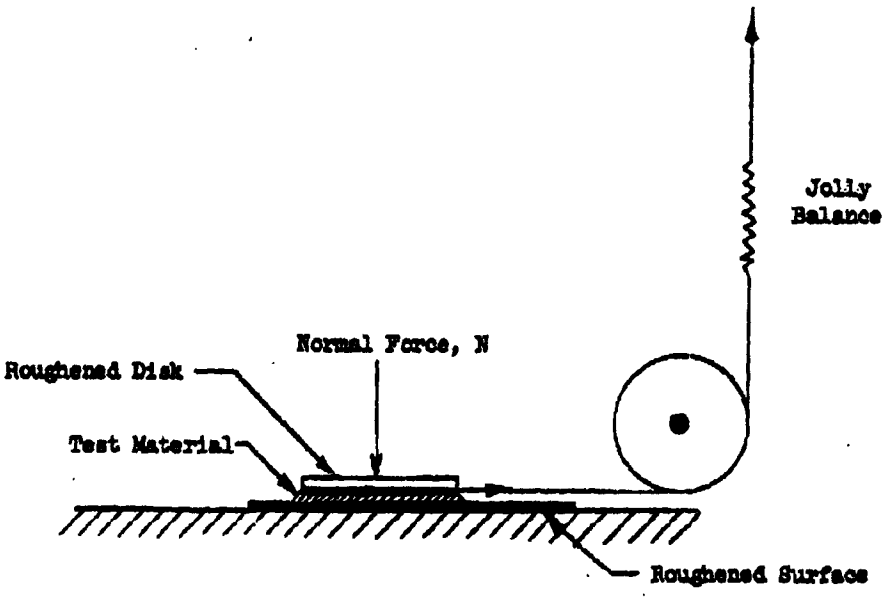

FIGURE 4.3.2 DIRECT SHEAR TEST APPARATUS

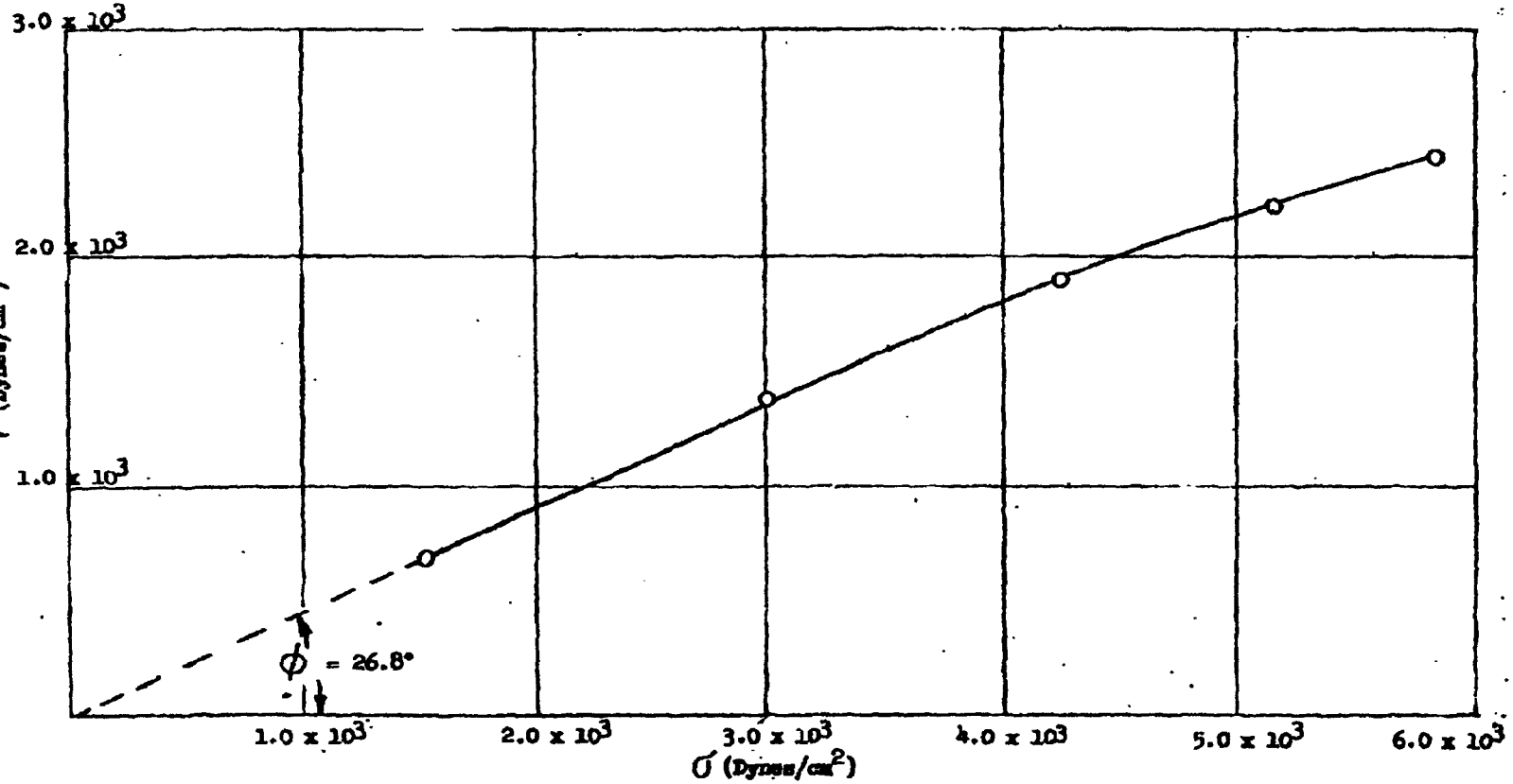

FIGURE 4.3.3. SHEAR STRENGTH CHARACTERISTIC FOR 200 MICRON GLASS BEADS

Some caution is necessary in interpreting these shear strength measurements because of possible limitations in the experimental technique. It appears that a direct shear test of this type, in which a tangential shear stress is applied to a thin layer of the material under test, as indicated in Figure 4.3.2, may constrain the material so as to prevent natural shear failure. Another difficulty with this type of test is that since the state of stress in the horizontal plane is not defined, the natural shear angle cannot be inferred from the test results. In spite of these possible shortcomings, direct shear tests should be satisfactory for measuring the relative shear strength of granular and particulate materials.

In comparing the behavior of dilatant materials composed of relatively large particles with that of finely-divided organic powders, it is observed that the dilatant materials tend to flow whereas the latter materials often exhibit a tendency to break up and form lumpy aggregates when displaced. This difference in handling qualities may be attributed, at least in part, to two fundamental factors: (1) compactibility and (2) interparticulate forces. The role played by interparticulate forces is difficult to isolate from other factors when dealing with finely-ground powders. However, it is entirely feasible to generate controlled interparticle forces among relatively large rigid particles such as glass beads or steel shot. Since these materials are dilatant, the influence of compaction is eliminated, thus enabling a study of the effects of interparticle forces on the behavior of particulate materials.

By conducting experiments with such materials, it is believed possible to gain considerable insight into factors responsible for the handling

characteristics of dry materials. Accordingly, tests of this nature are planned in future work. At the same time, an effort will be made to extend the theory described herein to include effects of interparticle forces.

5. INVESTIGATIONS OF PROPERTIES OF SLURRIES

During this reporting period, the viscosity and thermal conductivity of four egg slurry samples were determined. Additional information on the rheology and density of Sm slurries in a liquid fluorochemical was obtained.

5.1 Properties of Egg Slurries

The viscosity of four egg slurries (W.E.S. #1, #2, #3 and #4) was redetermined using a new shipment of frozen samples received from Fort Detrick. One of the egg slurries used for previously reported viscosity determinations[5.1.1] contained large solid particles which clogged the capillary viscometer, thereby preventing attainment of meaningful measurements. Current data on the other three samples are presented for comparison purposes.

The new egg slurry samples also were used in the determination of thermal conductivity as a function of temperature.

5.1.1 Viscosity of Egg Slurries

The egg slurry samples designated W.E.S. #1, #2, #3 and #4 were evaluated using an Ostwald capillary viscometer. The two most viscous slurries (W.E.S. #1 and #2) were also evaluated in a concentric cylinder rotational viscometer (modified Stormer viscometer).

Sample W.E.S. #1, when analyzed in the Stormer viscometer at 20°C, was found to be non-Newtonian in the shear rate range of 32 to 310 sec^{-1}. The apparent viscosities at different shear rates are presented in Table 5.1.1.

5.1.1 General Mills Report No. 2161, Second Quarterly Progress Report on Dissemination of Solid and Liquid BW Agents (Unclassified title) Feb. 13, 1961, p. 81 (Confidential).

TABLE 5.1.1

APPARENT VISCOSITY OF W.E.S. #1 VERSUS SHEAR RATE

Shear Rate (sec^{-1})	Apparent Viscosity (centipoise)
32	56.6
79	46.2
134	41.0
190	38.5
251	36.5
310	35.5

The apparent viscosity determined in the Ostwald viscometer was 43.1 centipoise.

Sample W.E.S. #2 also was found to exhibit non-Newtonian flow behavior in the Stormer viscometer at 20°C. Table 5.1.2 shows the variation in apparent viscosity with shear rate for this slurry.

TABLE 5.1.2

APPARENT VISCOSITY OF W.E.S. #2 VERSUS SHEAR RATE

Shear Rate (sec^{-1})	Apparent Viscosity (centipoise)
78	7.5
165	11.0
299	12.2
419	13.1

The apparent viscosity obtained in the Ostwald viscometer was 7.79 centipoise at 20°C.

Figure 5.1.1 is a plot of the shear rate versus shear stress data obtained from the Stormer viscometer on samples W.E.S. #1 and #2.

The viscosity of slurries W.E.S. #3 and #4 was too low to be accurately evaluated in the Stormer viscometer. At 20°C, values of 1.66 and 1.35 centi-

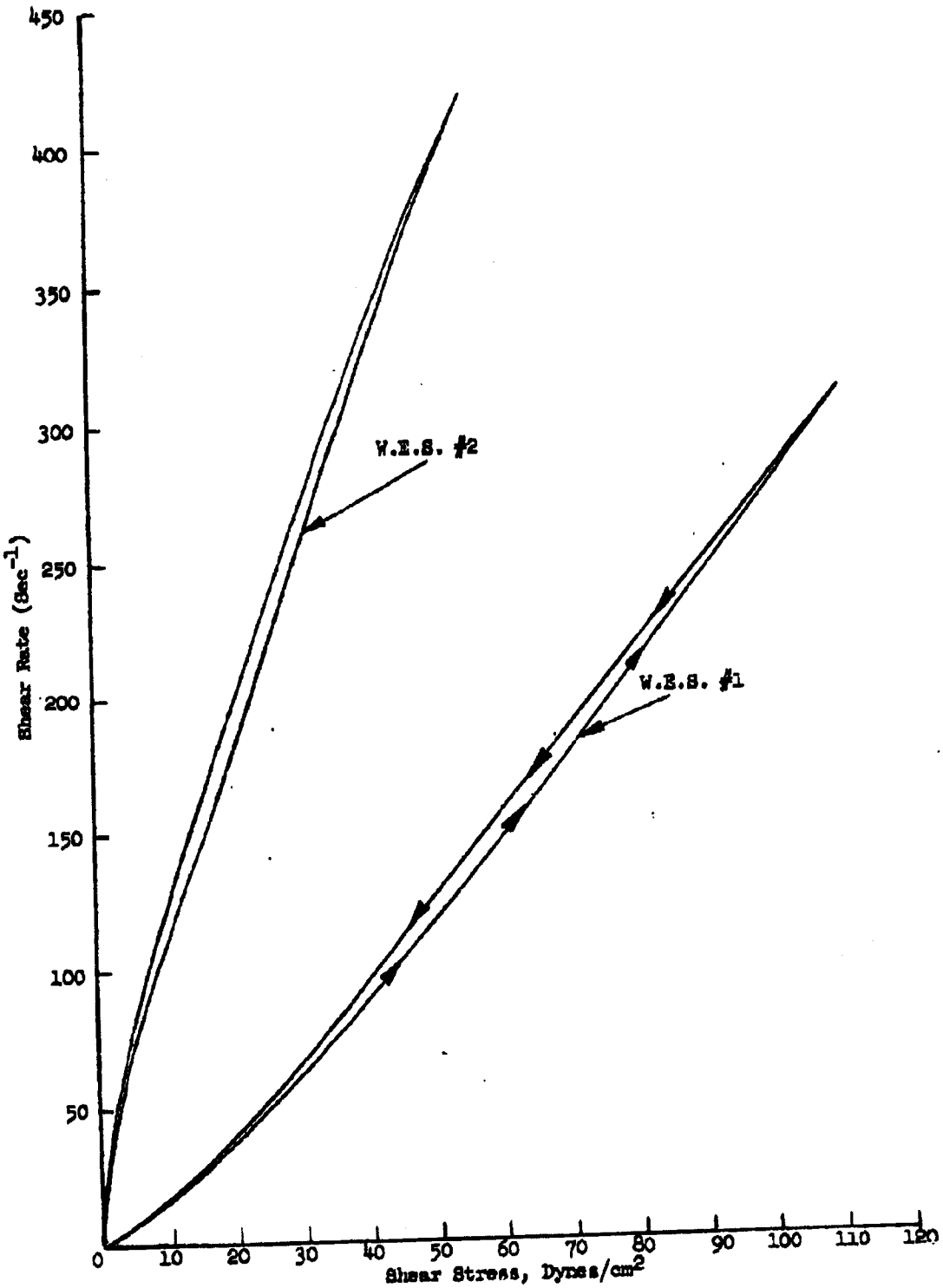

FIGURE 5.1.1 CONSISTENCY CURVES FOR W.E.S. #1 AND #2 AT 20°C

poise were determined in the Ostwald viscometer for the apparent viscosities of slurries W.E.S. #3 and #4 respectively.

5.1.2 Thermal Conductivity of Egg Slurries

The thermal conductivity of egg slurry samples W.E.S. #1, #2, #3 and #4 was determined using the experimental apparatus and technique described in an earlier report.[5.1.2] The thermal conductivity cell (Figure 5.1.2) contains two liquid canisters which are formed by three copper discs. The upper canister was filled with a reference liquid (water) and the lower canister with one of the four egg slurries under test. Water was chosen as a reference liquid because its thermal conductivity is well known, and its absolute value was believed to be close to that of the egg slurries. The upper solid line in Figure 5.1.3 is the average value for the thermal conductivity of water as reported in the literature, and the dotted lines represent the minimum and maximum values which have been found.[5.1.3]

By placing the cell on its side with the copper discs in a vertical position, the cell was easily filled without entrapping air bubbles. Liquid was slowly forced into the cell from the bottom until the canister overflowed. The canister openings were then sealed and the cell was inserted into a Styrofoam insulation sleeve. Constant temperature water from a large, constant temperature bath was circulated through the heat sink. Readings from the six thermocouples in the copper discs were checked periodically for about forty-five minutes. When no further change in temperature was noted, the temperature drops across the canisters were recorded.

5.1.2 General Mills Report No. 2200, Third Quarterly Progress Report on Dissemination of Solid and Liquid BW Agents (Unclassified title) May 15, 1961, pp. 56- 61 (Confidential).

5.1.3 International Critical Tables, Vol. 5, p. 227

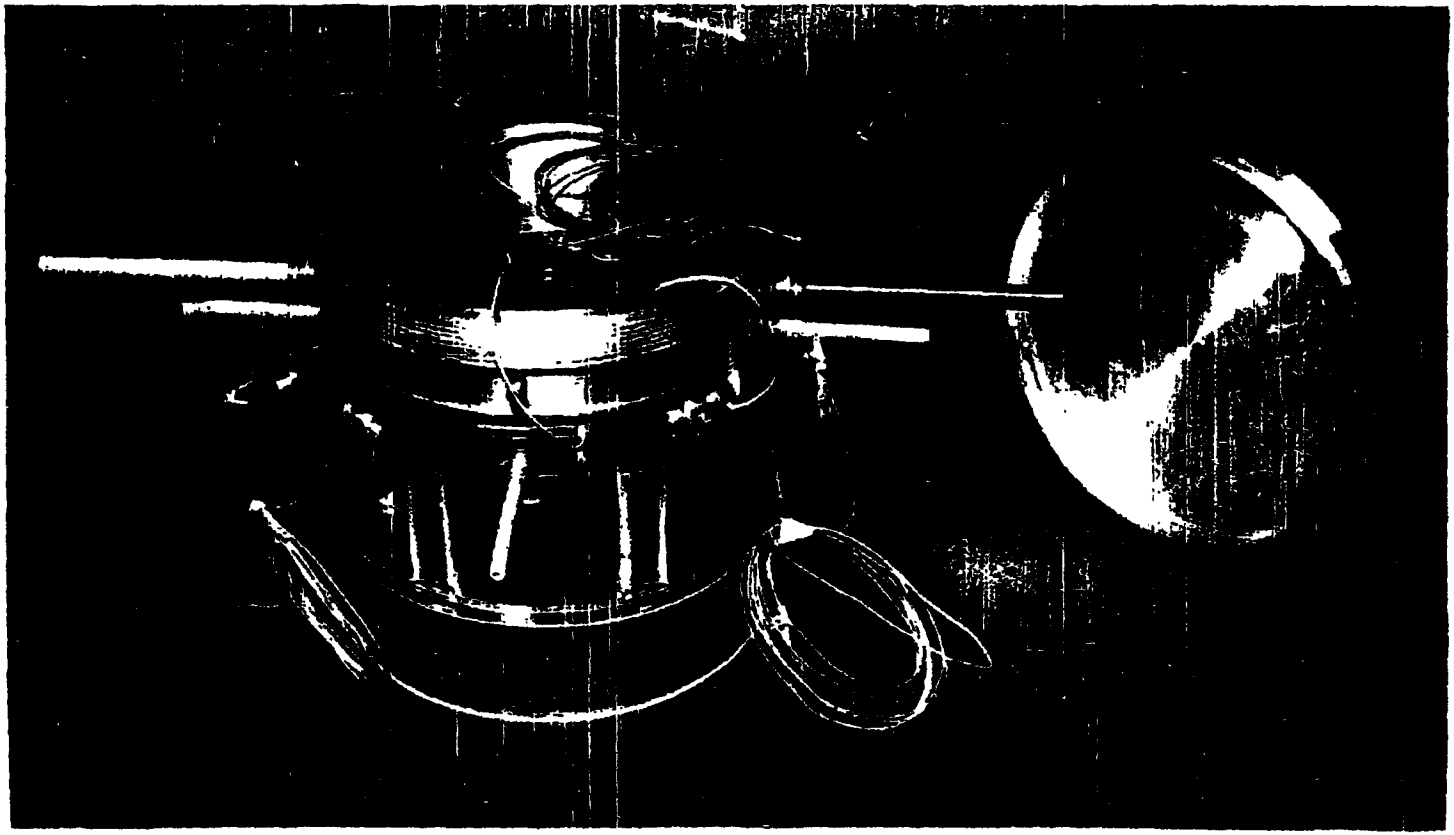

FIGURE 5.1.2 THERMAL CONDUCTIVITY CELL

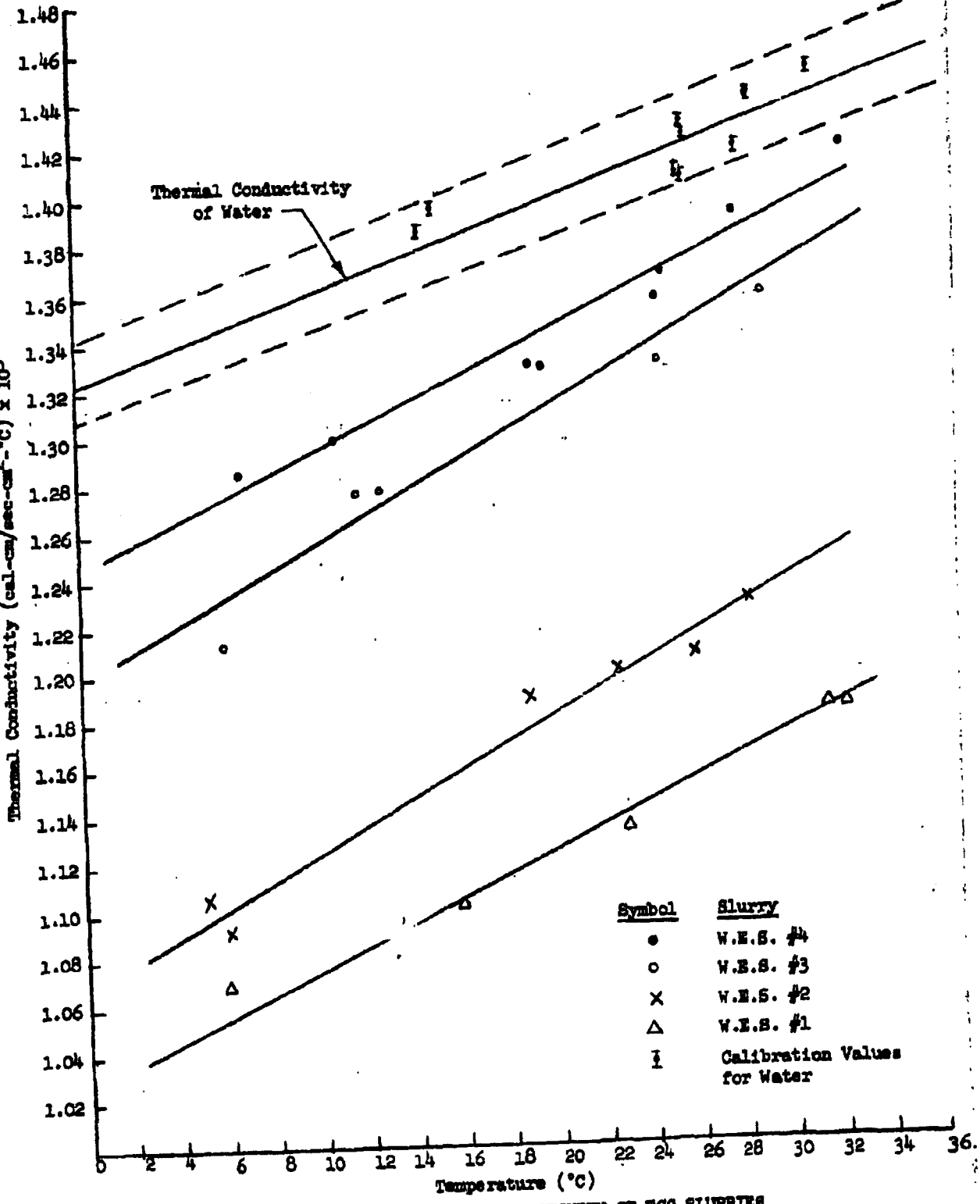

FIGURE 5.1.3 THERMAL CONDUCTIVITY OF EGG SLURRIES

The cell was calibrated by filling both canisters with double-distilled water. Results of the calibration revealed a 2 percent systemic error as calculated from the following relationships which were presented in an earlier report:[5.1.4]

$$q = K_w A \frac{\Delta T_w}{\Delta X} = K_s A \frac{\Delta T_s}{\Delta X} \qquad (5.1)$$

where: q = heat flux through the cell

K_w = thermal conductivity of water

K_s = thermal conductivity of slurry

ΔT_w = temperature drop across the water layer

ΔT_s = temperature drop across the slurry layer

A = area through which heat flows (equal for both liquids)

ΔX = distance between the discs (equal for both liquids).

Thus:
$$K_w \Delta T_w = K_s \Delta T_s \qquad (5.2)$$

and:
$$K_s = K_w \frac{\Delta T_w}{\Delta T_s} \qquad (5.3)$$

In calibrating with water in both canisters, $K_s = K_w$ and therefore it would be expected that $\Delta T_s = \Delta T_w$. However, a larger temperature drop was recorded across the upper canister for all runs regardless of whether the mean temperature of the water in either layer was above or below the ambient temperature. In each case, the error could be accounted for by applying a correction factor as follows:

$$K_s = K_w \frac{\Delta T_w}{\Delta T_s} (0.9786). \qquad (5.4)$$

5.1.4 General Mills, Inc. Report 2200, Third Quarterly Progress Report on Dissemination of Solid and Liquid BW Agents (Unclassified title) May 15, 1961, p. 59 (Confidential).

It has been calculated that if the distance between the disks of the upper layer exceeded the thickness of the lower water layer by 0.002 inch, this difference could account for the consistent error. Such a small variation in thickness is beyond the ability to measure once the cell is assembled. In view of the constancy of the error, Equation 5.4 was used in calculating the thermal conductivity of the egg slurry samples.

The thermal conductivity of egg slurry samples W.E.S. #1, #2, #3 and #4 are presented in Table 5.1.3.

TABLE 5.1.3

THERMAL CONDUCTIVITY OF EGG SLURRY SAMPLES

W.E.S. #1 Temp. (°C)	W.E.S. #1 $K_g \times 10^3$ (cal-cm/sec-cm^2-°C)	W.E.S. #2 Temp. (°C)	W.E.S. #2 $K_g \times 10^3$ (cal-cm/sec-cm^2-°C)
5.9	1.069	5.2	1.105
15.9	1.102	6.0	1.092
22.9	1.133	18.9	1.188
31.5	1.182	22.6	1.199
32.2	1.182	25.9	1.206
		28.2	1.228

W.E.S. #3 Temp. (°C)	W.E.S. #3 $K_g \times 10^3$ (cal-cm/sec-cm^2-°C)	W.E.S. #4 Temp. (°C)	W.E.S. #4 $K_g \times 10^3$ (cal-cm/sec-cm^2-°C)
6.0	1.213	6.8	1.285
11.8	1.277	10.9	1.299
12.7	1.277	19.1	1.329
19.6	1.328	24.5	1.355
24.5	1.329	24.9	1.367
29.0	1.357	27.9	1.391
		32.4	1.418

The data of Table 5.1.3 are presented in graphical form in Figure 5.1.3. The straight lines through the experimental points were calculated by the method of least squares and appear to be an adequate representation of the data.

All of the lines have approximately the same slope, and the thermal conductivity values of the egg slurry samples fall within a range between 78 and 97 percent of the value for water.

5.2 Rheological Behavior of Sm Slurries

Additional information on the flow characteristics of Sm slurries in a fluorochemical liquid have been determined. The density of these slurries has been measured, and an apparatus has been designed and is being built to study the flow behavior through capillary tubes.

5.2.1 Effect of Surface Active Agent on the Rheology of Sm Slurries

Previously reported results[5.2.1] on the flow behavior of Sm slurries were obtained with samples containing a surface active agent designated L-1161 and manufactured by Minnesota Mining and Manufacturing Company. This fact was inadvertently omitted from the discussion of experimental results. The surface active agent was especially compounded by 3M for use with their fluorochemical liquids. Samples have been sent to Fort Detrick for determination of compatibility of the agent with biological materials. One tenth of one percent by weight of the fluorochemical liquid, FC-75, was used in the preparation of slurries for the earlier rheological investigations. It was assumed at the start of those investigations that a surface active agent would be needed to prevent phase separation since a small amount of Sm added to FC-75 and blended thoroughly came out of suspension rapidly. Investigations conducted during this report period have been designed to determine the stability of thick Sm slurries without a surface active agent, and the change in rheological properties caused by the omission of this agent.

5.2.1 General Mills, Inc. Report No. 2200, Third Quarterly Progress Report on Dissemination of Solid and Liquid BW Agents (Unclassified title), May 15, 1961, pp. 62-75).

An attempt also was made to measure the viscosity of Sm slurries containing a concentration of solids greater than 25 percent by weight, the upper limit previously investigated.

The same technique was followed in preparing the slurries which has been reported previously, except that no surface active agent was added. Results indicated that the apparent viscosity of slurries without additive was strongly dependent upon mechanical history. Therefore, it was necessary to obtain initial consistency curves at increasing and decreasing shear stress as well as consistency curves after extended periods of shearing at a constant shear stress. The initial consistency curves indicated that thick slurries (25 percent by weight Sm), subjected to only a small amount of prior shearing, exhibit thixotropy, i.e., apparent viscosity decreases with shear. However, upon shearing these slurries for extended periods of time at a constant shear stress, the initial trend toward a decrease in apparent viscosity is reversed and the apparent viscosity begins to increase. This latter phenomenon is called rheopexy. According to the literature, rheopexy can be exhibited by suspensions which contain anisometric particles. The increase in apparent viscosity is believed to be caused by shear-induced orientation of anisometric particles. Rheopectic materials have been observed to retain this orientation for considerable periods of time following the removal of the shear stress.

Consistency curves for Sm slurries without a surface active agent and containing 16.7, 25.0 and 28.6 percent by weight Sm are presented in Figure 5.2.1. All data were obtained at a temperature of 20°C. The experimental

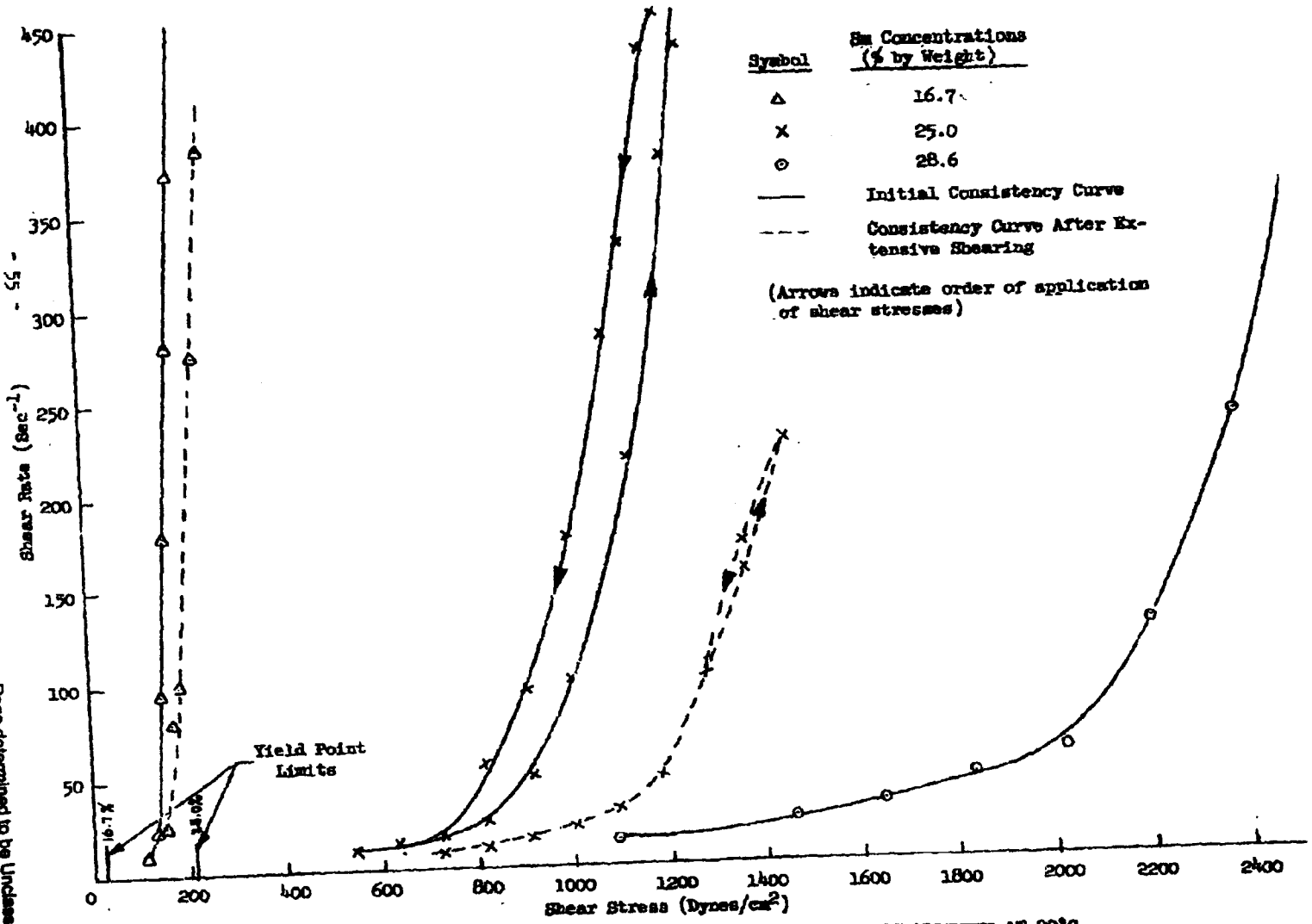

FIGURE 5.2.1 CONSISTENCY CURVES FOR Sm SLURRIES WITHOUT AN ADDITIVE AT 20°C

data which were obtained shortly after the slurry had reached the equilibrium temperature of the bath are represented by solid lines in Figure 5.2.1. The consistency curves obtained after extensive shearing are represented by broken lines.

It was found that slurries containing 16.7 percent by weight Sm have nearly the same consistency curve with or without the surface active agent. Furthermore, the consistency curves obtained at increasing and then decreasing shear stress agree quite well for both slurries, but with some slight evidence of thixotropy in the case of the slurry without additive. After shearing the slurry continuously for 3000 revolutions at a shear stress of about 200 dynes/cm^2, the curve was shifted toward higher apparent viscosity.

A slurry containing no additive and 25 percent by weight Sm initially exhibits considerable thixotropy as evidenced by the form of the consistency curves obtained at increasing and then decreasing shear stress. After shearing continuously for 3000 revolutions at a shear stress of about 1100 dynes/cm^2, the curve is shifted considerably toward higher apparent viscosities. Thus, the phenomenon of rheopexy becomes more prominent with increasing solids concentration.

The consistency curve obtained on a slurry containing no additive and 28.6 percent by weight Sm is also presented in Figure 5.2.1. This slurry was much too thick to handle in the coaxial cylinder viscometer. The apparent high yield point made it difficult to remove air trapped below the bob upon immersion and prevented the slurry from flowing over the top of the bob when it was lowered into the cup. The curve presented was obtained at increasing

shear stress and probably is only a crude representation of the true flow behavior. Attempts will be made in the future to obtain data on these thicker slurries using capillary viscometry.

Minimum yield points for Sm slurries containing 16.7 and 25 percent by weight of solids are indicated on the shear stress axis of Figure 5.2.1. These values were obtained by increasing the torque to the critical value which would induce rotation of the bob, even though rotation would subsequently cease.

The change in apparent viscosity with shearing for the 25 percent by weight Sm slurry is presented in Figure 5.2.2 in terms of change in shear rate with number of bob revolutions. As was stated previously, the sample was sheared for 3000 revolutions of the bob at a constant shear stress of about 1100 dynes/cm^2. Both the initial thixotropic behavior and subsequent rheopexy are evident from this figure.

Observation of the slurry samples after completion of the tests revealed no visual evidence of phase separation of the Sm and FC-75.

Upon discovering the rheopectic behavior of these concentrated Sm slurries without surface active agent, an investigation was made of the amount of FC-75 liquid which evaporated from the slurry during the experiment. The results showed that a change in slurry concentration from 25.0 to 25.2 percent could be expected during the time period of the experiment. Such a small change cannot account for the increase in apparent viscosity with time. Therefore, the phenomenon of rheopexy is a real characteristic of Sm slurries without additives. The initial yield point and thixotropic behavior of these

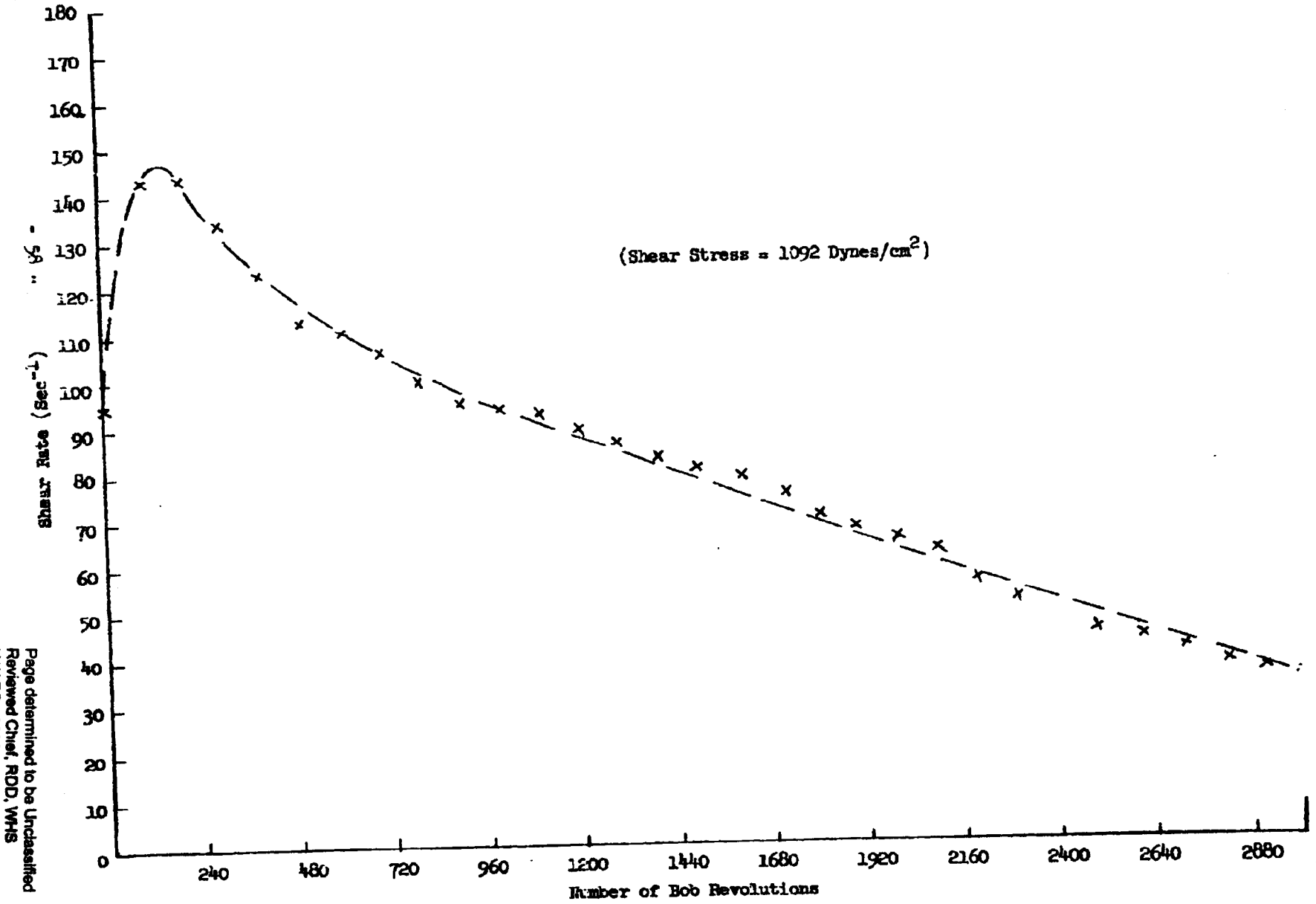

FIGURE 5.2.2 SHEAR RATE VERSUS NUMBER OF BOB REVOLUTIONS FOR 25% BY WEIGHT Sm SLURRY

slurries is probably due to the break-up of flocculated particles, and the subsequent rheopectic behavior to the orientation of aniasometric Sm particles upon additional shearing.

The complexity of the flow behavior of Sm slurries without surface active agent renders impossible the extrapolation of flow data obtained from experiments in the coaxial cylinder viscometer to flow behavior through tubes and orifi. Therefore, future experiments will be confined to investigating flow through capillary tubes.

5.2.2 Apparatus for Capillary Viscometry Studies

Capillary viscometry will be employed to extend the rheological investigation of Sm slurries to higher shear rates and greater solids concentration. Because Sm slurries are non-Newtonian fluids, a range of shear stresses must be used. This will be accomplished by varying the pressure drop across the capillary.

The viscometer that will be used is being constructed at the present time. It is reported[5.2.2] to be convenient, absolute and accurate and is capable of covering a wide range of shear stress in a single determination. The apparatus is shown schematically in Figure 5.2.3. A column of mercury forces the sample through the capillary tube. Measurement of the height of the mercury column as a function of time yields both the pressure drop and flow rate.

The relation between the shear stress τ and the shear rate $f(\tau)$ for this instrument is given by:

$$\frac{f(\tau)}{\tau} = -\frac{m}{B}\left[1 + \frac{1}{9.212\ m^2} \cdot \frac{dm}{dt}\right] \qquad (5.5)$$

5.2.2 Maron, S., J. Krieger and A. Sisko. J. Appl. Phys. 25: 971 (1954)

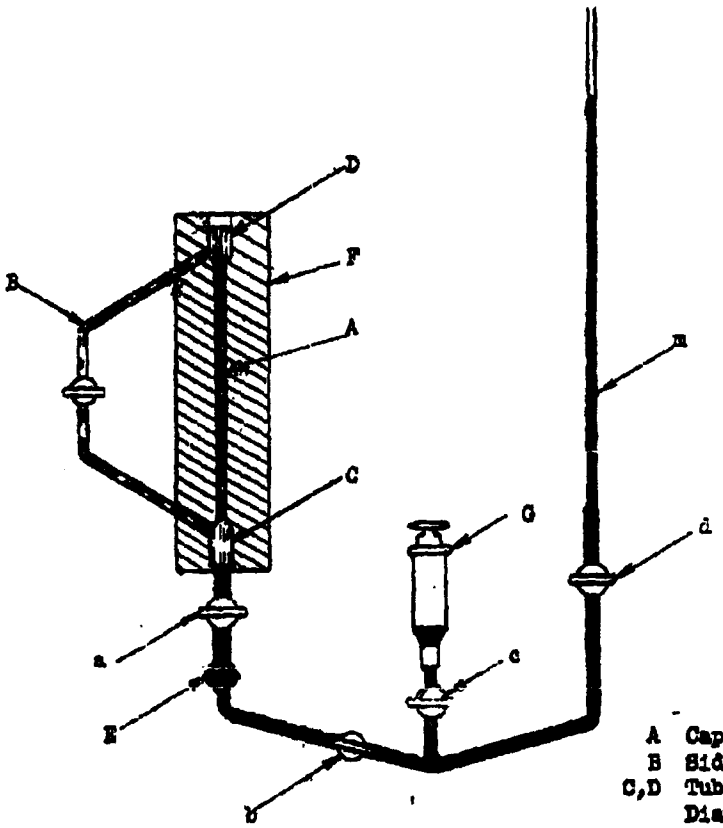

A Capillary
B Sidearm Tube
C,D Tubes of the Same Diameter
E Ball and Socket Joint
F Water Jacket
G Syringe
a,b,c,d Stopcocks
m Mercury Column

FIGURE 5.2.3 CAPILLARY VISCOMETER

where: $m = \frac{d \log h}{dt}$

h = height of mercury column

t = time

B = constant.

5.2.3 Densities of Sm Slurries

In order to permit calculation of the weight penalty involved in slurry systems as compared to dry powder stores, density measurements of Sm in FC-75 for various solids concentration have been made at 20.0°C. From this data the weight of biological material per unit volume can be calculated as a function of solids concentration.

The slurries were prepared by weighing the ingredients on an analytical balance and then mixing thoroughly with a perforated plate stirrer which was described in the previous quarterly report. The end of a pipette was inserted well below the surface of the slurry, and the pipette was filled by applying suction through the top. When full, the pipette was sealed at both ends and weighed. The densities obtained are recorded in Table 5.2.1.

TABLE 5.2.1

DENSITY OF Sm SLURRIES

Weight percent of Sm	Density at 20.0°C (gm/cm^3)
0	1.77 at 25°C
16.7	1.66
20.0	1.62
25.0	1.58

6. BOUNDARY LAYER STUDIES

Growth of the boundary layer on the disseminating store is of considerable interest in this program, because the performance of the disseminator may be substantially affected by the local flow conditions at the point of release of the agent. A knowledge of the boundary layer growth is useful in (a) selecting a suitable location for the discharge of the disseminating store, and (b) correlating the results of experiments in a wind tunnel with the performance of a full-size store under flight conditions.

In Section 6.1 below, calculations of boundary layer growth on an aircraft store are presented. In Section 6.2, calculations of boundary layer growth in the wind tunnel are given. This information is considered important in interpreting the results of the wind tunnel deagglomeration studies discussed in Section 7.

6.1 Boundary Layer on an Aircraft Store

The boundary layer thickness on an NACA series 65A store of fineness ratio 8.0 was calculated for a Mach number of 0.9 at sea level with air temperature of 80°F. The length selected for these illustrative calculations was 17 ft. Two methods were used, the first assumes the boundary layer is similar to that formed over a flat plate in one-dimensional incompressible flow with zero streamwise pressure gradient. For this case, the thickness of the boundary layer is given by the following relations:

$$\delta_L = \frac{4.64x}{Re_x} \quad \text{for laminar flow} \qquad (6.1)$$

and

$$\delta_t = \frac{.376x}{(Re_x)^{1/5}} - 2 \quad \text{for turbulent flow} \qquad (6.2)$$

where:

x = distance measure along store surface in flow direction

$Re_x = \frac{Vx}{\nu}$ = Reynolds' number based on x.

As the boundary layer develops from the stagnation point, it changes from laminar to turbulent at some location x_t depending on the stream turbulence, stream Mach number and the surface condition. The point of transition was determined by using a critical Reynolds' number of 8000 according to Reference 1. For this Reynolds' number, transition occurs at approximately 0.01 in. from the stagnation point; thus, for purposes of calculation the laminar regime was neglected. The boundary layer thickness, using only Equation 6.2 above, is shown in Fig. 6.1.1 as a function of distance along the store axis. Equation 6.2 does not represent the actual situation near the stagnation point and for this reason the curve starts at x = .20 ft. The boundary layer separates from the body at some point beyond the maximum body thickness. Location of the separation point can be estimated by examining surface pressure distribution data for the store. Such data was not available for this store, however, and the separation point was estimated by examining the pressure distribution data for prolate spheroids as given in Reference 2. By this method we find that the boundary layer should separate

1. Heaslet, M. and Nitzberg, G., The Calculation of Drag for Airfoil Sections and Bodies of Reduction at Subcritical Speeds, NACA RM A7B06, 1947.

2. Cole, R. I., Pressure Distributions on Bodies of Revolution at Subsonic and Transonic Speeds, NACA RM L52D30, 1952.

FIG. 6.1.1 BOUNDARY LAYER THICKNESS FOR NACA 65A STORE OF f = 8.0

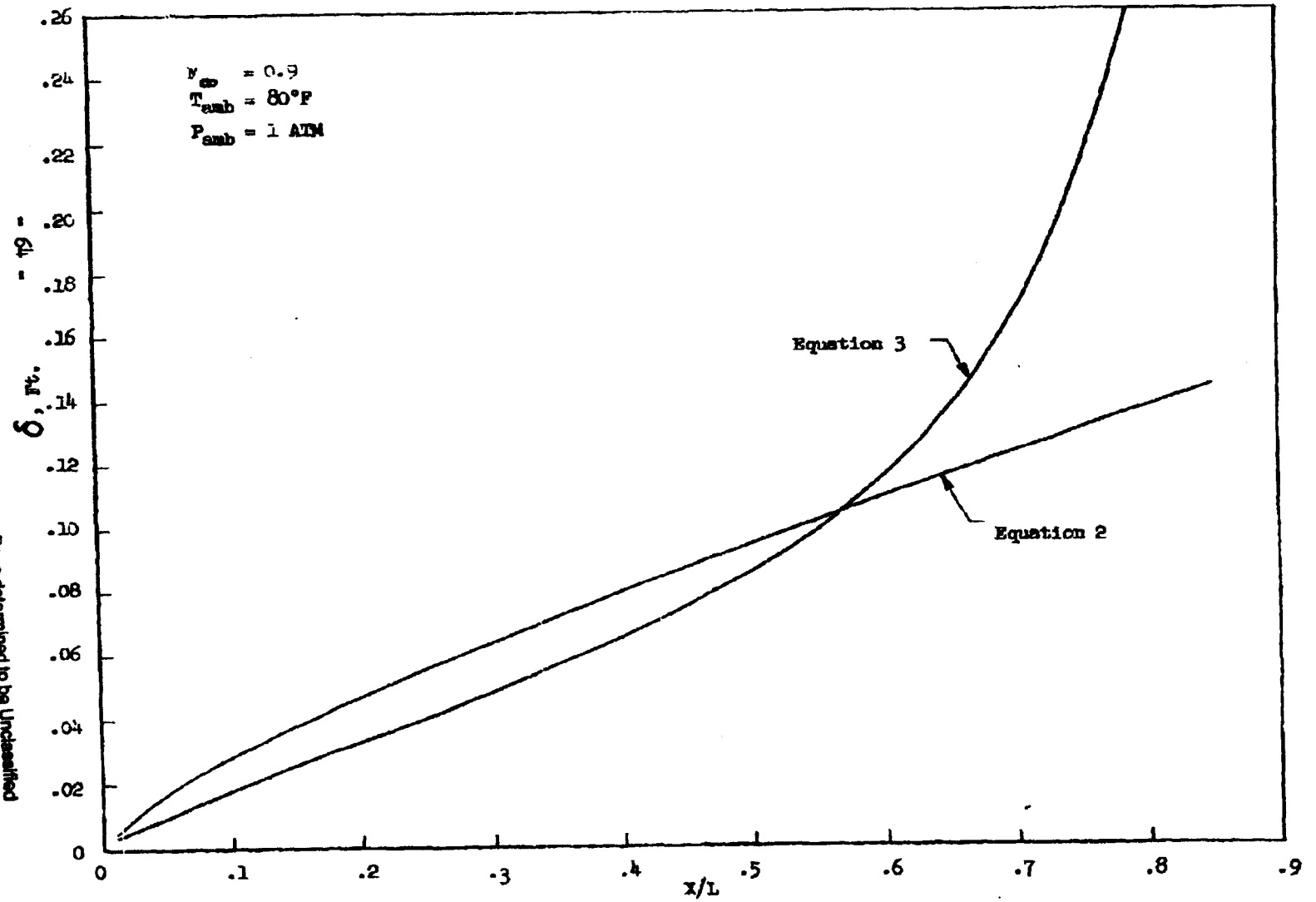

from the body at between 80 and 90 percent of the axial chord. By drawing the separated stream lines parallel to the store axis, the size of the turbulent wake can be approximated. Actually, the wake would converge slightly, because the static pressure in the wake is less than the free stream static pressure. The boundary layer is drawn to scale on the store shown in Fig. 6.1.2 for comparison of the relative sizes of the boundary layer thickness and the store. Effects of pylon boundary layer and aircraft wing down wash are neglected, because it is assumed that the boundary layer developing on the under side of the wing and on the pylon will not be think enough to affect the store boundary layer and also that the store will be mounted ahead of the wing down wash field.

The second method used to calculate the boundary layer thickness includes the compressibility and 3-dimensional effects that occur in the actual situation. The method was presented by Englert in Reference 3 as an extension of an earlier work by Truckenbrodt in Reference 4. In applying this method it was necessary to start with the pressure-distribution data and deduce the local Mach number and sonic velocity along the surface by assuming isentropic flow. Pressure distribution data were again taken from Reference 2. The thickness of the fully turbulent boundary layer is given by:

---

3. Englert, G. W., Estimation of Compressible Boundary Layer Growth over Insulated Surfaces with Pressure Gradient, NACA TN 4022, 1957.

4. Truckenbrodt, E., A Method of Quadrature for Calculation of the Laminar and Turbulent Boundary Layer in Case of Plane and Rotationally Symmetrical Flow, NACA TM 1379, 1955.

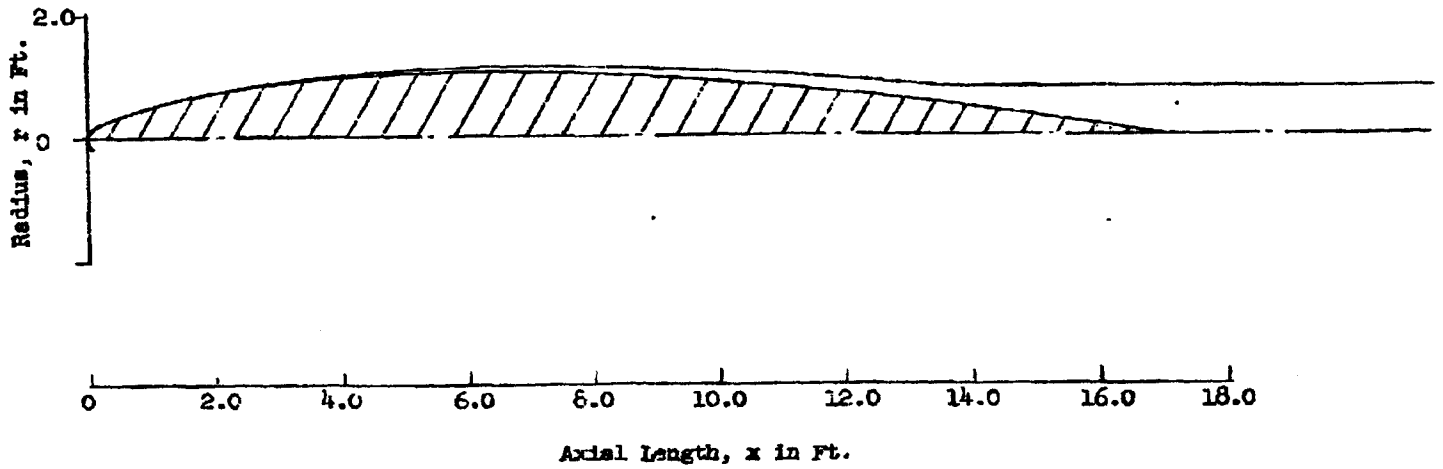

FIG. 6.1.2 BOUNDARY LAYER ON NACA 65A SERIES STORE OF f = 8.0

$$\delta_t = \frac{\pi}{7} \left[\frac{\eta^{6/7}}{\left(\frac{a_e}{a_o}\right)^{\left(\frac{+1}{-1}\right)} M_e 3_r} \right] \qquad (6.3)$$

where:

$$\eta = \frac{.0076}{\left(\frac{a_e}{a_o}\right)^{5/21}} \left(\frac{\nu_o}{a_o}\right)^{1/6} \int_o^x M_e^{10/3} r^{7/6} \left(\frac{a_e}{a_o}\right)^{\frac{3\gamma-1}{\gamma-1}} dx \qquad (6\ 4)$$

and:

a_e = local free stream sonic velocity

a_o = sonic velocity at stagnation

ν_o = kinematic viscosity at stagnation

x = distance along flow direction

r = body radius at x

M_e = local free stream Mach number

γ = ratio of specific heats of air = 1.41

The results of our calculations from Equation 6.3 are also shown in Fig. 6.1.1. A comparison of the boundary layer thickness estimations from Fig. 6.1.1 shows that the 3-dimensional compressible boundary layer (Equation 6.3) is thinner for $x/L < 0.565$, because the flow area normal to the surface of the body of revolution increases as the square of the distance, whereas, the flow area increases directly with the distance above a flat plate. The rapid growth of the compressible boundary layer for $x/L > 0.565$ is due to the adverse pressure gradient and the onset of

boundary layer separation which, according to the compressible theory, occurs at some position beyond $x/L \geq .75$.

Velocity distribution within the boundary layer is shown in Fig. 6.1.3. This distribution was calculated from Prandtl's empirical equation:

$$\frac{u}{u_s} = \left(\frac{y}{\delta}\right)^{1/7} \tag{6.5}$$

In the following section, this velocity distribution is compared with that existing in the wind tunnel.

6.2 Boundary Layer in Wind Tunnel

Boundary thickness predictions based on Equations 6.1 and 6.3 were also made for the high-velocity wind tunnel used in our deagglomeration studies. Agreement with measurement for this case should be good, due to the negligible compressibility effects associated with parallel flow along the tunnel walls. Results of the calculations are shown in Fig. 6.2.1 for the various tunnel Mach numbers used in our studies. Location of the agent ejector is shown on the abcissia; notice that ejection occurs well within the turbulent flow regime. The transition to turbulent flow occurs approximately at the location shown for each of the three Mach numbers. These transition locations were obtained by assuming a transition Reynolds' number of 5×10^5. Transition to turbulent flow may occur earlier, but not later than the locations shown, because of the moderately large free-stream turbulence in our tunnel.

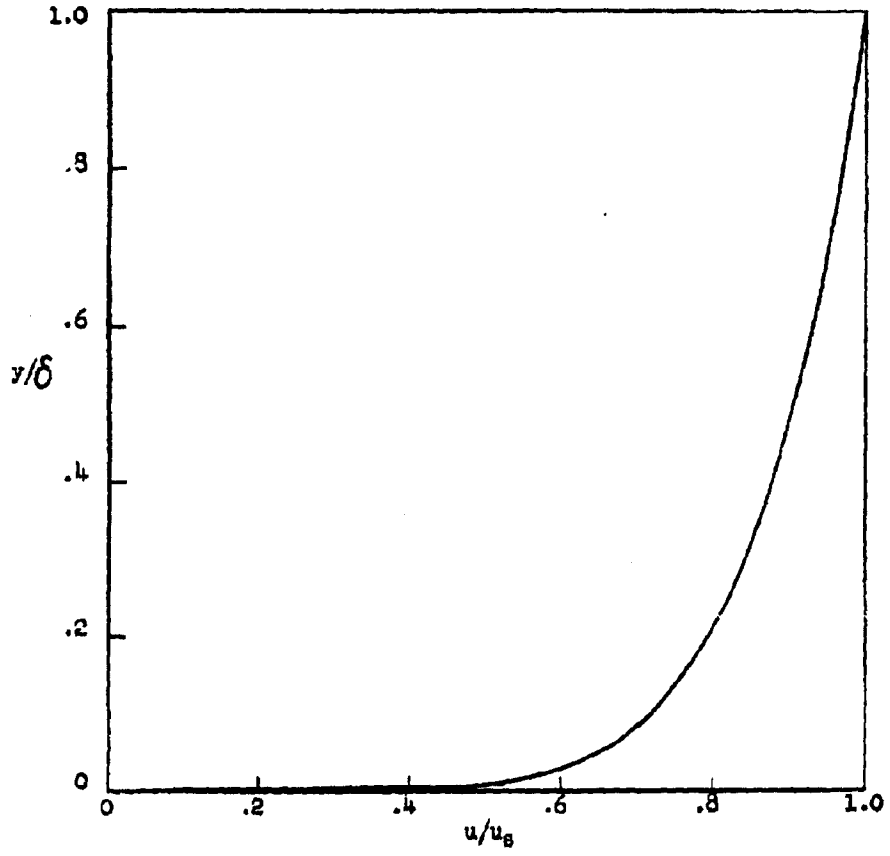

FIG. 6.1.3 VELOCITY PROFILE IN TURBULENT BOUNDARY LAYER

FIG. 6.2.1 BOUNDARY LAYER DEVELOPMENT IN HIGH VELOCITY WIND TUNNEL

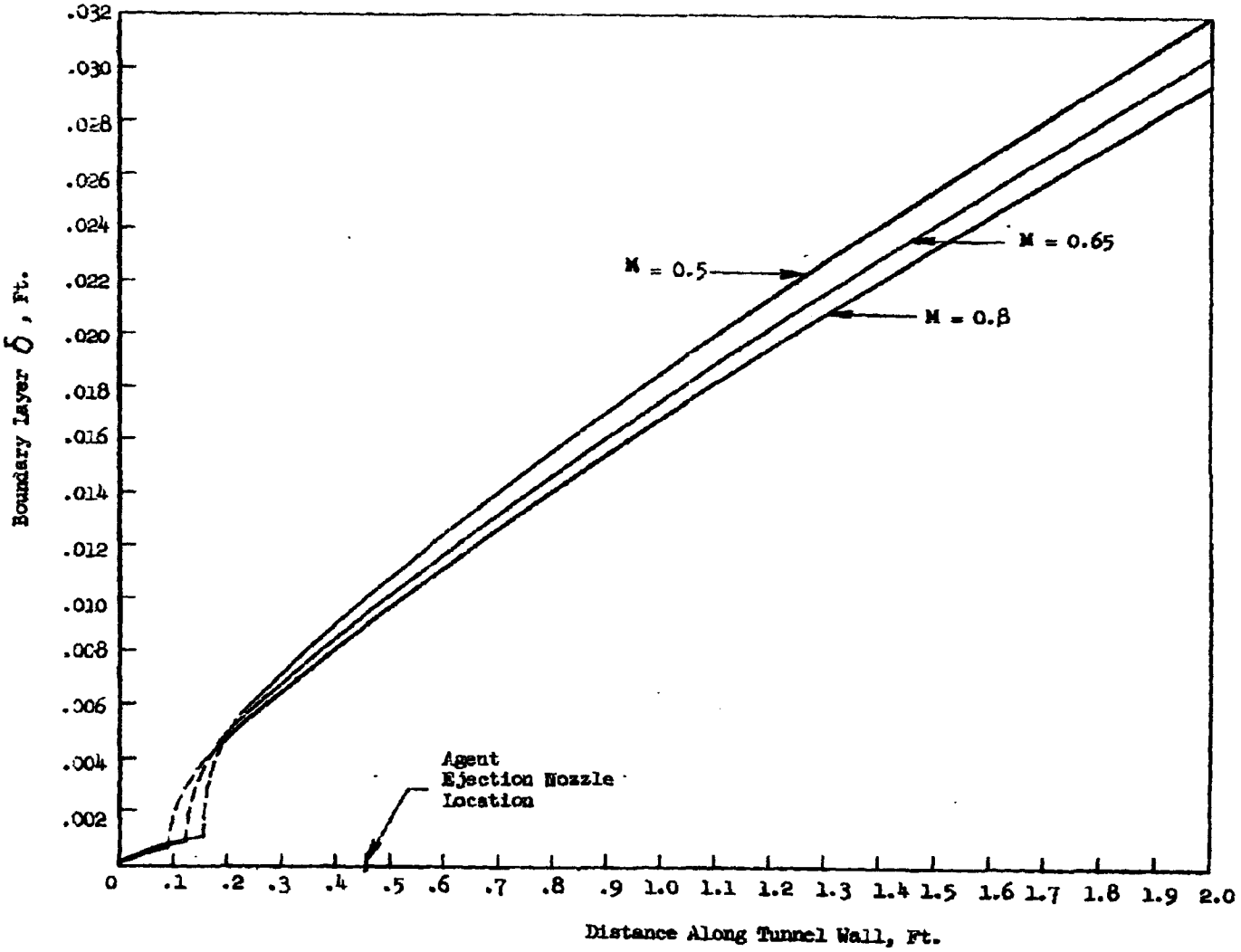

A comparison between the boundary layer velocities occuring in the tunnel and on the agent store for a tunnel Mach number of 0.8 at the point of ejection is shown in Fig. 6.2.2. Agent ejection is assumed to occur from the surface at one half the axial chord (x = 8.5 ft.) in this example. Both boundary layers are turbulent, but the store boundary layer is approximately 10 times thicker, due to the greater distance that the air has traveled at the ejection point. The effect of the different Mach numbers (0.8 in tunnel, 0.9 for store) is small.

Fig. 6.2.2 indicates that the velocities are quite similar in the two cases at distances of 0.02 to 0.04 ft. from the surface. This region is of considerable interest, since it has been found that the finely-divided material can be injected approximately this distance. It is believed that the results shown on Fig. 6.2.2 indicate that the deagglomeration effects measured in the wind tunnel will be slightly conservative since the velocity gradient in the region is essentially zero, while there is a modest velocity gradient indicated for the actual flight case.

FIG. 6.2.2 VELOCITY IN BOUNDARY LAYER FOR AGENT STORE AND HIGH VELOCITY WIND TUNNEL

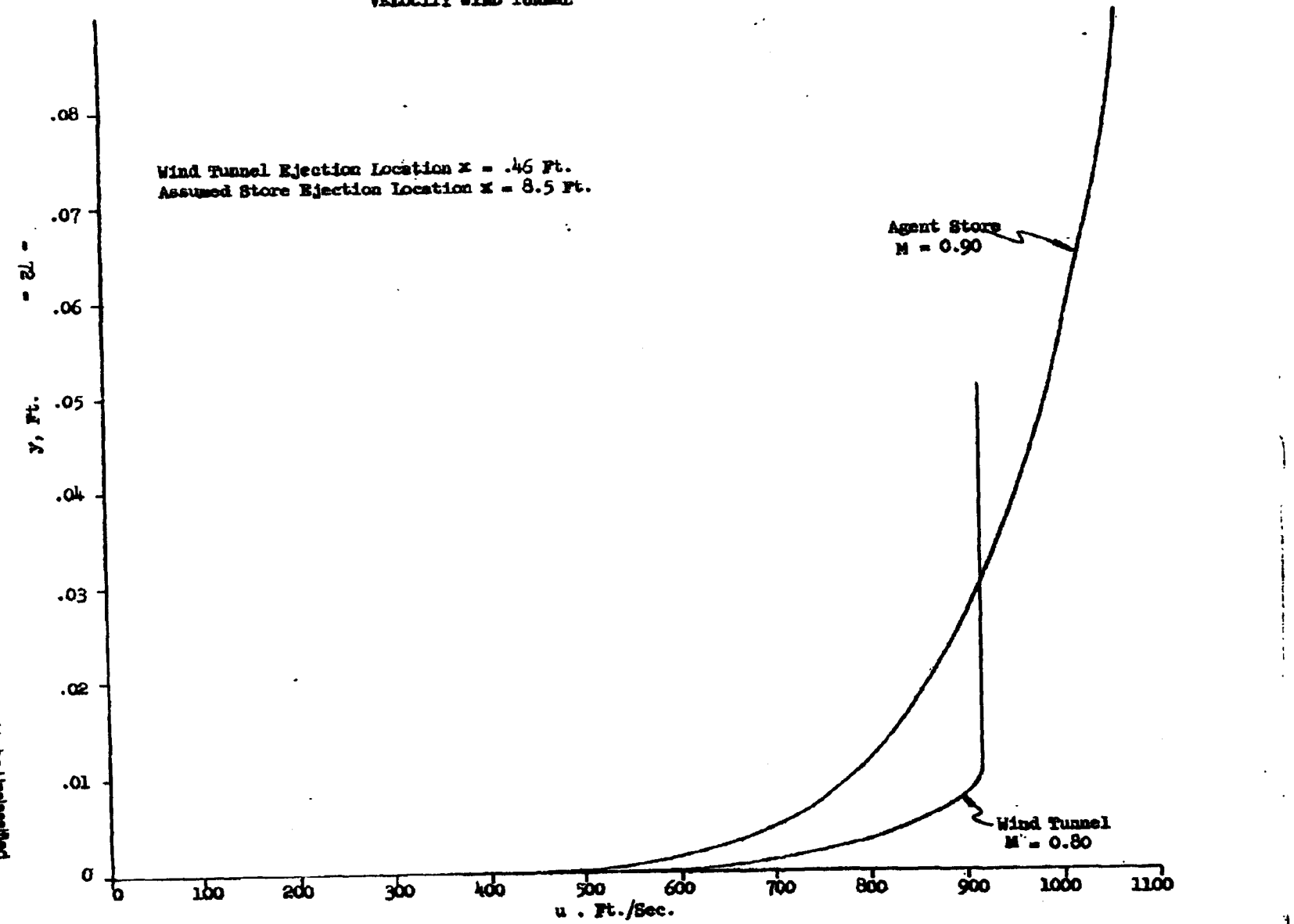

7. DISSEMINATION AND DEAGGLOMERATION STUDIES

Studies on the dissemination of Sm simulant in the high-subsonic velocity wind tunnel were initiated during this reporting period. A series of high speed motion pictures were taken of the aerosolization process within the tunnel and samples of Sm were obtained with the high velocity sampling system.

7.1 Motion Picture Study of Sm Dissemination

Visual observations of the aerodynamic break-up process during the dissemination of Sm have been accomplished by photographing the area of injection inside the wind tunnel at 3000 frames per second. The photographic equipment employed in this work consisted of an Eastman High Speed Camera (No. 3) and an Edgerton, Germeshausen, and Grier Inc. lighting system. The latter has a speed of 1.5 μ sec., which was fast enough to stop agglomerates larger than 0.1 mm in these pictures. Three factors were investigated in this study: (1) bulk density, (2) tunnel Mach number, and (3) moisture content.

Samples from two separate batches of Sm, "A"* and "B"**, were used in this work. The material was injected into the wind tunnel with a piston-type device [7.1.1] at an average velocity of 4 meters/sec. The samples were prepared in three different bulk densities: 0.33, 0.43, and 0.49 gm/cc. At the low density, the material was in its loose form while at the higher

---

* Shipment GBL A-3416691
** Run S1-Sm-342

7.1.1 General Mills Report No. 2161, Second Quarterly Progress Report on "Dissemination of Solid and Liquid BW Agents" (Unclassified Title) Feb. 13, 1961, p. 36 (Confidential).

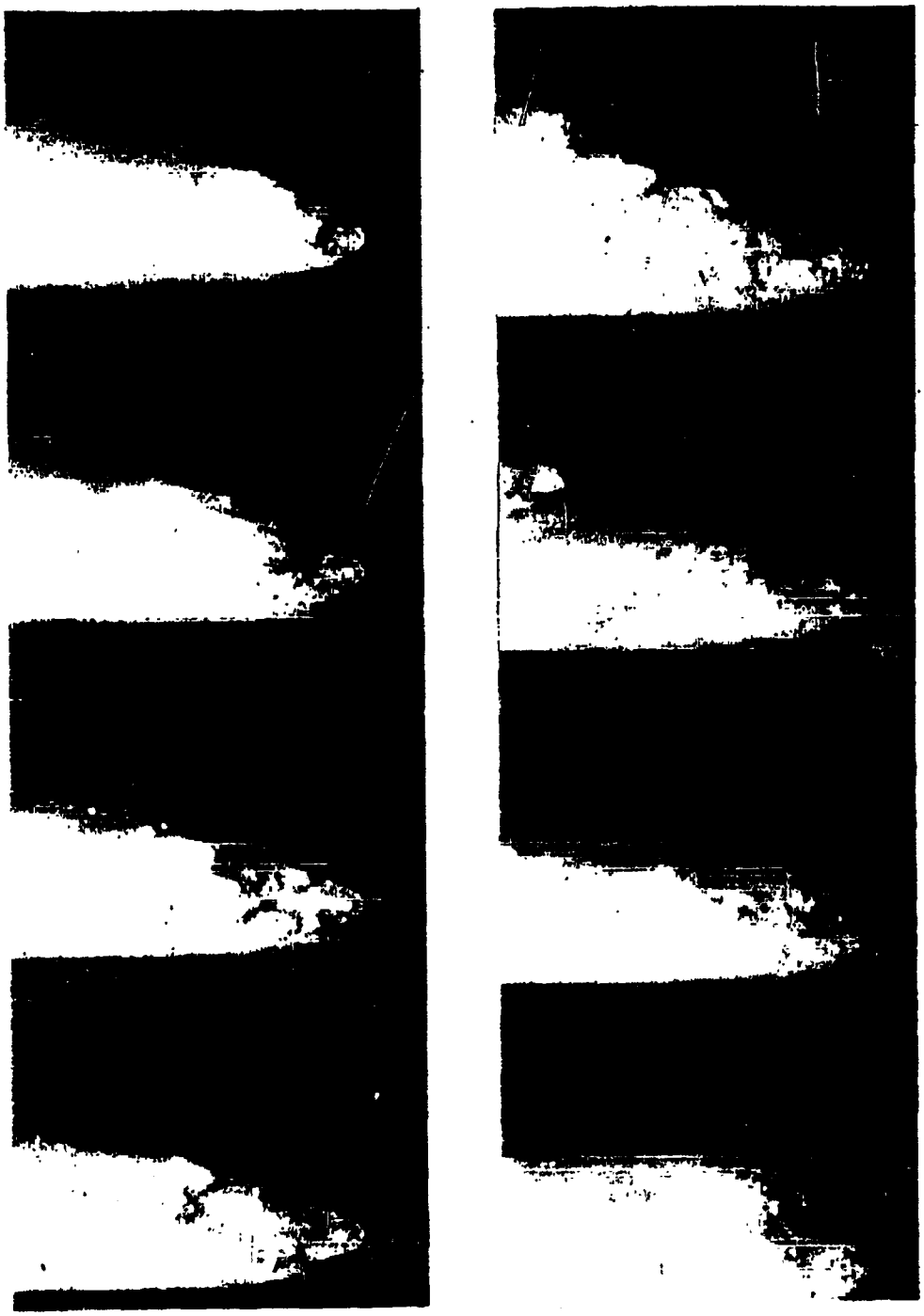

FIGURE 7.1.1 DISSEMINATION OF Sm "A" WITH BULK DENSITY 0.33 gm/cc IN MACH 0.50 AIR STREAM

FIGURE 7.1.1 CONTINUED

densities it was compacted into cylindrical slugs, 0.63 cm dia., by using a low friction piston device. Since compaction studies show that it is necessary to form compressed slugs in stepwise manner to assure a uniform density throughout, (see Section 3), seven steps were used and each segment was compressed to a length-to-diameter ratio of 0.3. Each of the density groups was photographed at tunnel Mach numbers 0.50, 0.65, and 0.80.

The Sm moisture contents were determined by the Flosdorf-Webster vacuum oven method. Approximately 2 gm of Sm was filled in a bottle which had a known tare weight. The sample was placed in an oven maintained at 50°C, at an absolute pressure of about 100 microns of mercury. After 22 hours it was weighed again. The reduction in weight of Sm divided by its original weight gave the moisture content which for Sm "A" was 4.0 percent and Sm "B" 1.0 percent.

From the standpoint of dissemination, an Sm moisture content of 4 percent is considered to be high. This motion picture study shows that such material can form strong agglomerates which are difficult to break up completely in a high velocity air stream. Thus, the importance of controlling moisture content is demonstrated in this work.

Figures 7.1.1, 7.1.2 and 7.1.3 show injections of loose Sm "A". Much of the material appears to be aerosolized within a short time, 3 frames or 0.001 sec. However, there are some relatively large agglomerates, approximately 0.50 mm in size, which seem to be unaffected by the air stream. These are shown in Figure 7.1.1, in the upper part of Frame 10.

In comparison, Figures 7.1.4 and 7.1.5 show that Sm "B" has few of these hard agglomerates and the material seems to break up faster. This

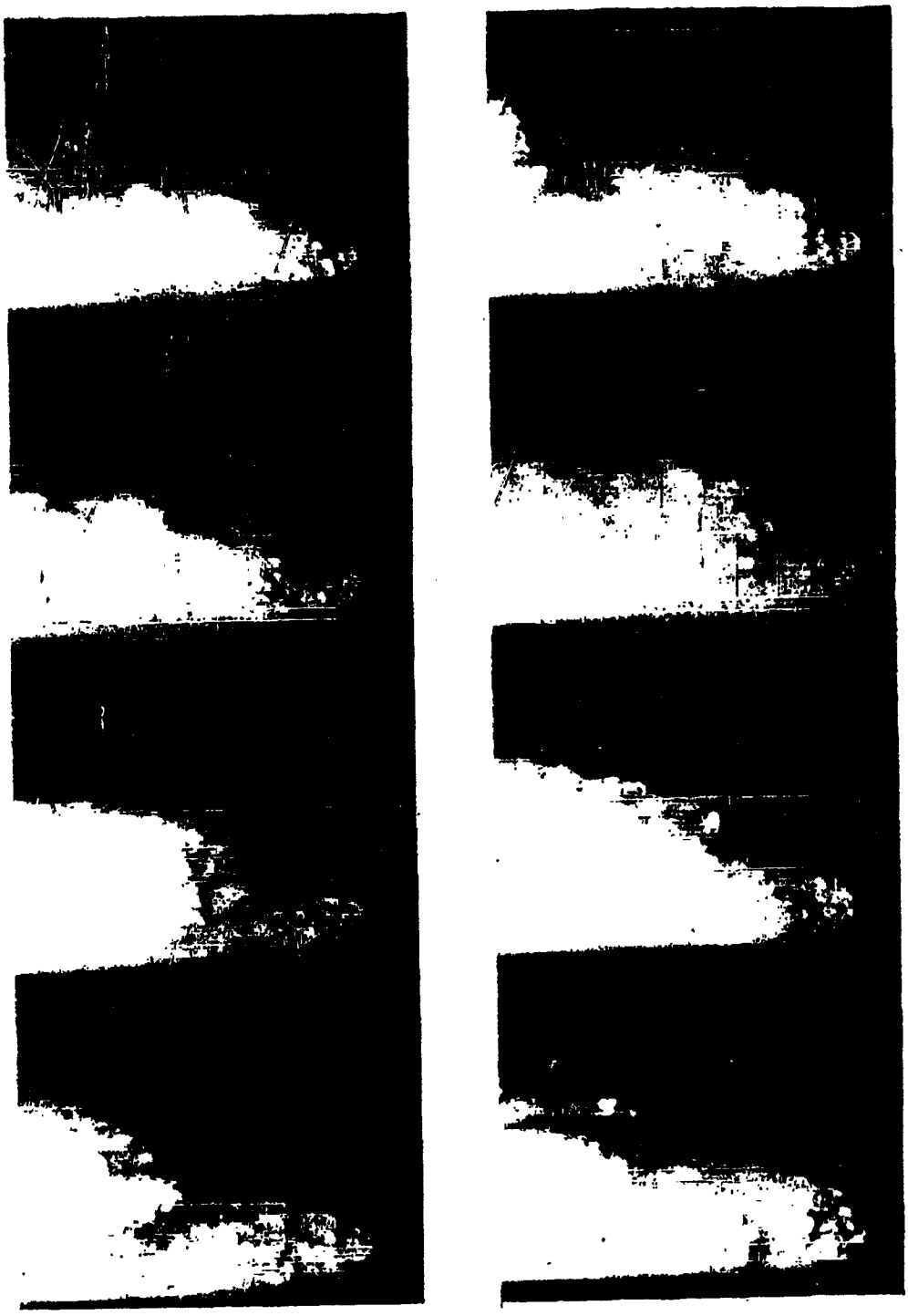

FIGURE 7.1.2 DISSEMINATION OF Sm "A" WITH BULK DENSITY 0.33 gm/cc IN MACH 0.65 AIR STREAM

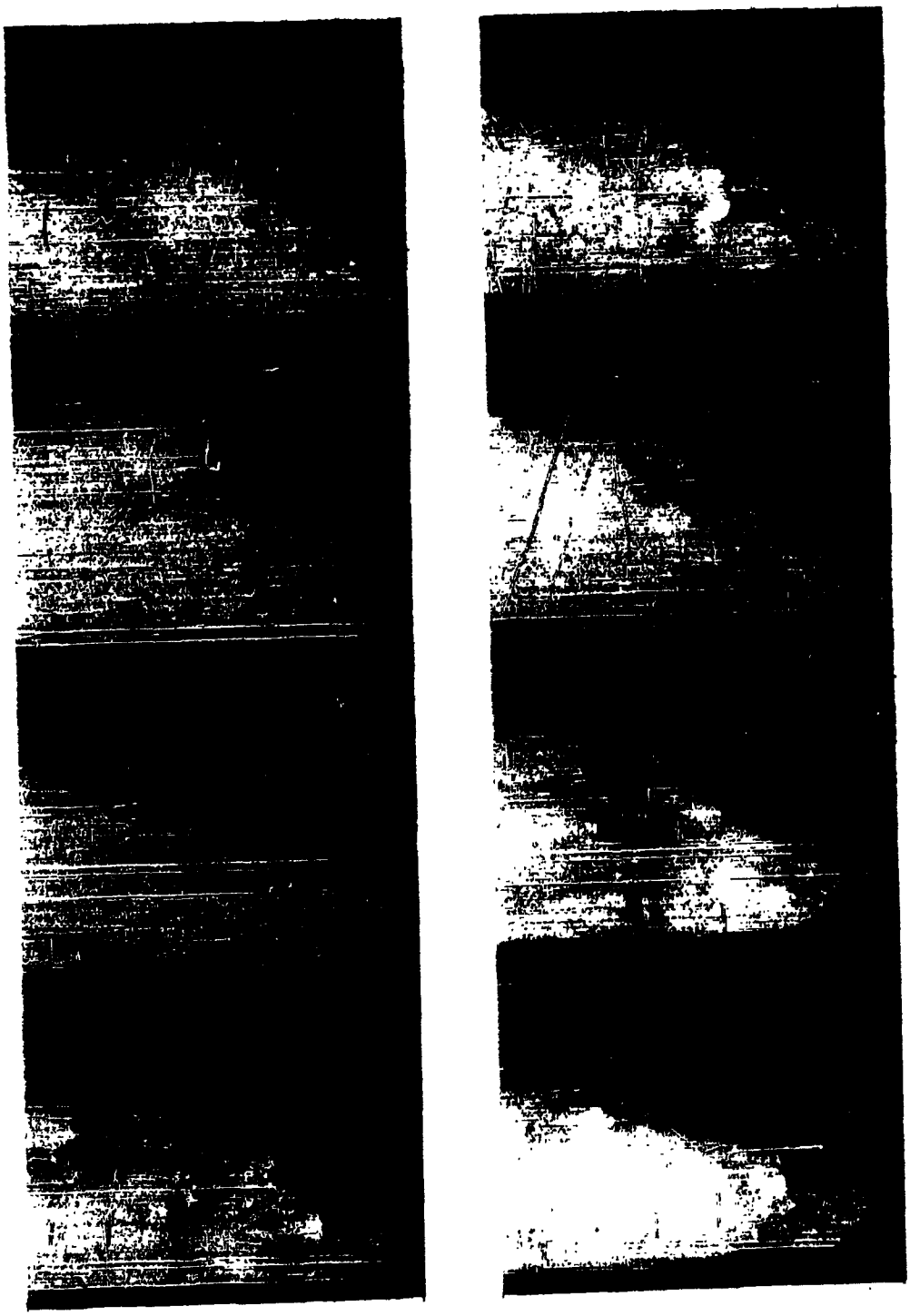

FIGURE 7.1.2 CONTINUED

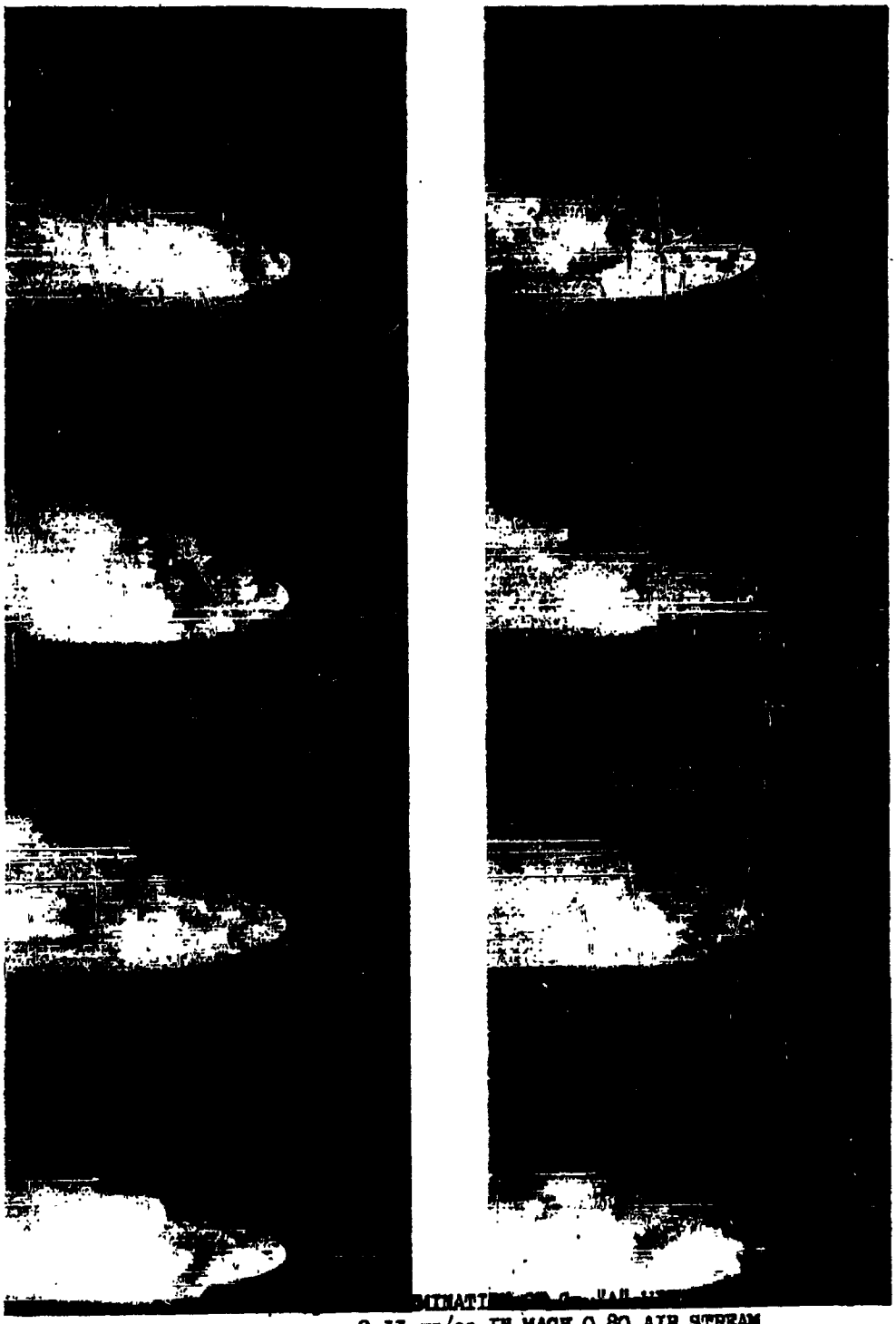

0.33 gm/cc IN MACH 0.80 AIR STREAM

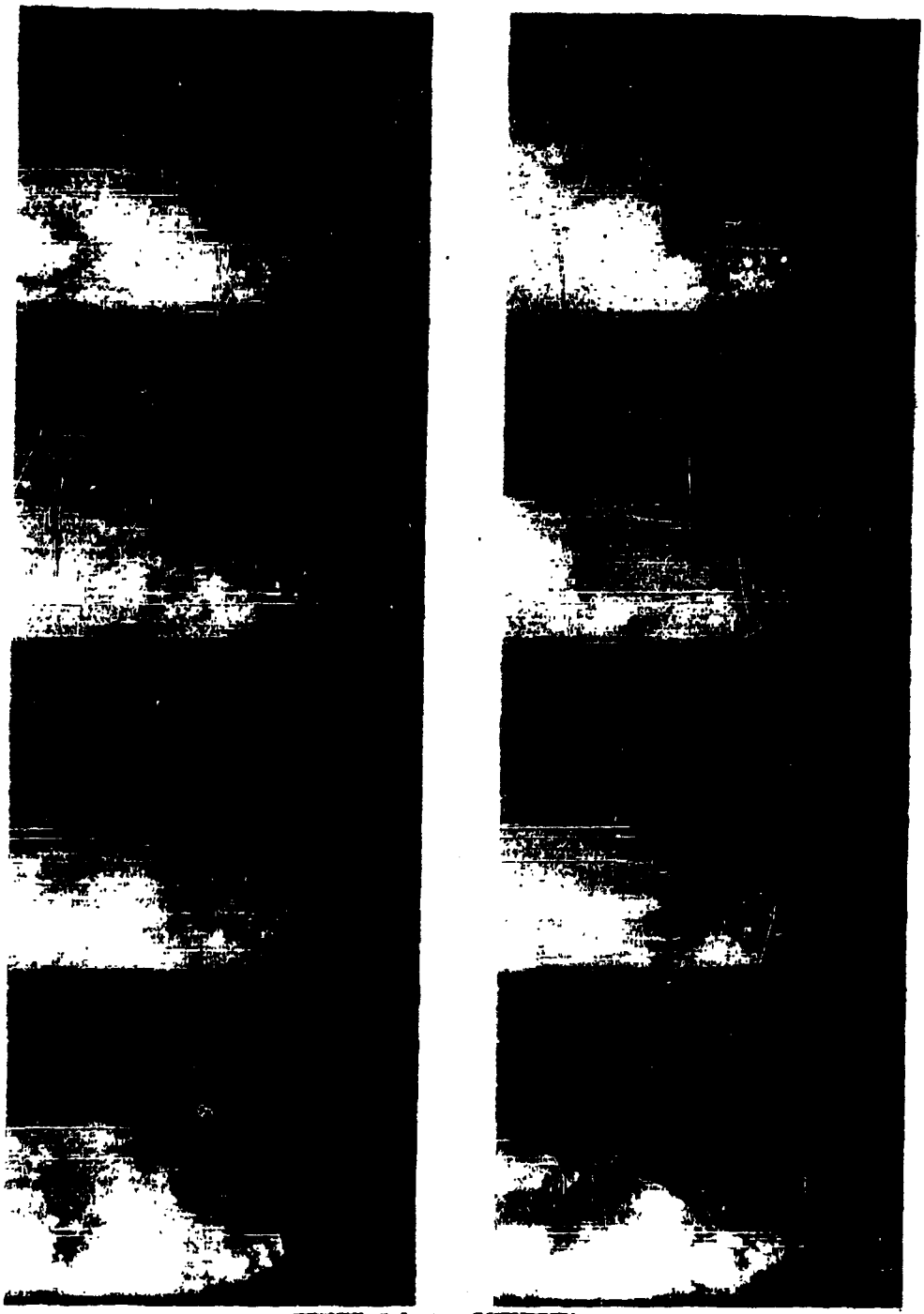

FIGURE 7.1.3 CONTINUED

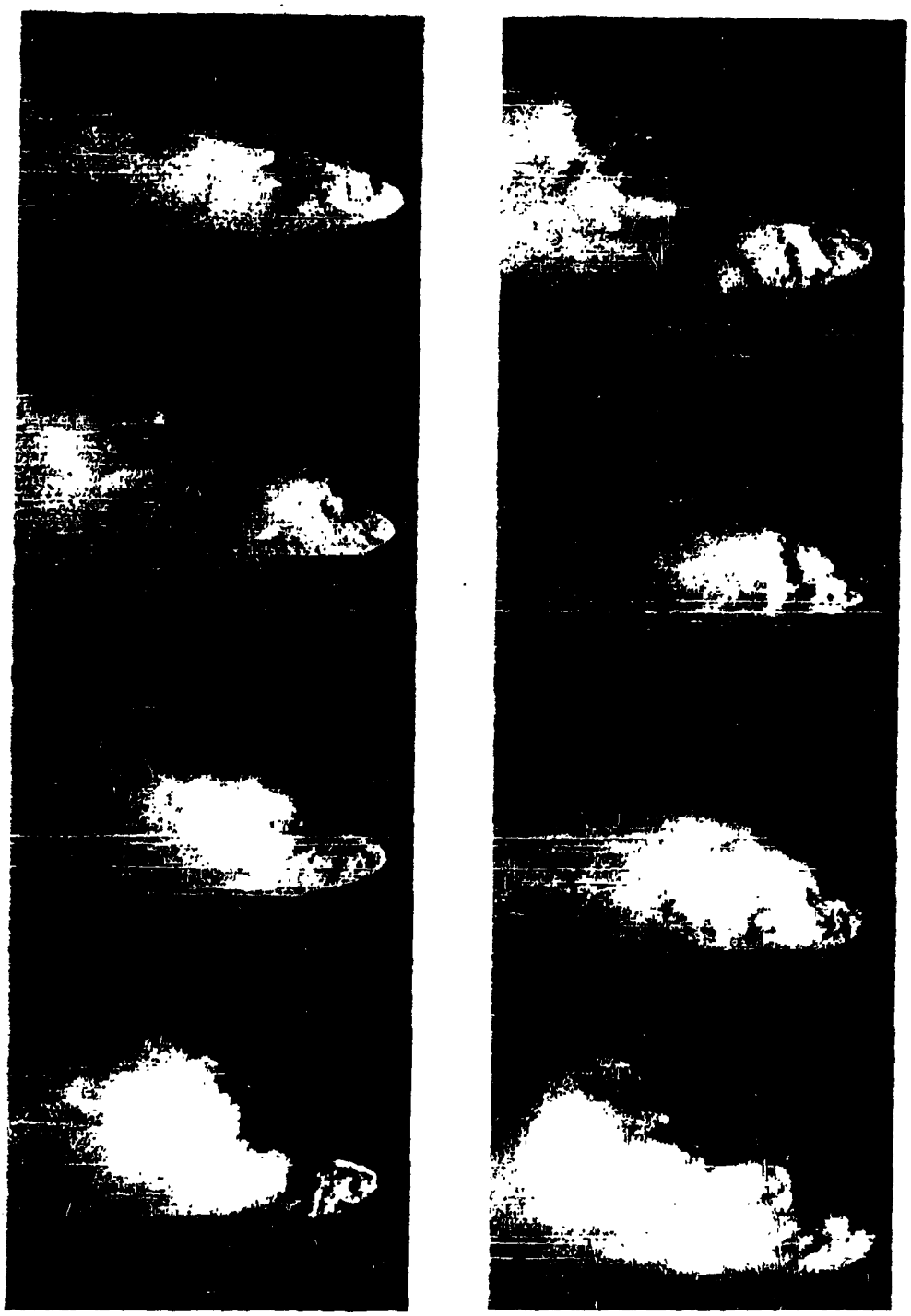

FIGURE 7.1.4 DISSEMINATION OF Sm "B" WITH BULK DENSITY 0.33 gm/cc IN MACH 0.5 AIR STREAM

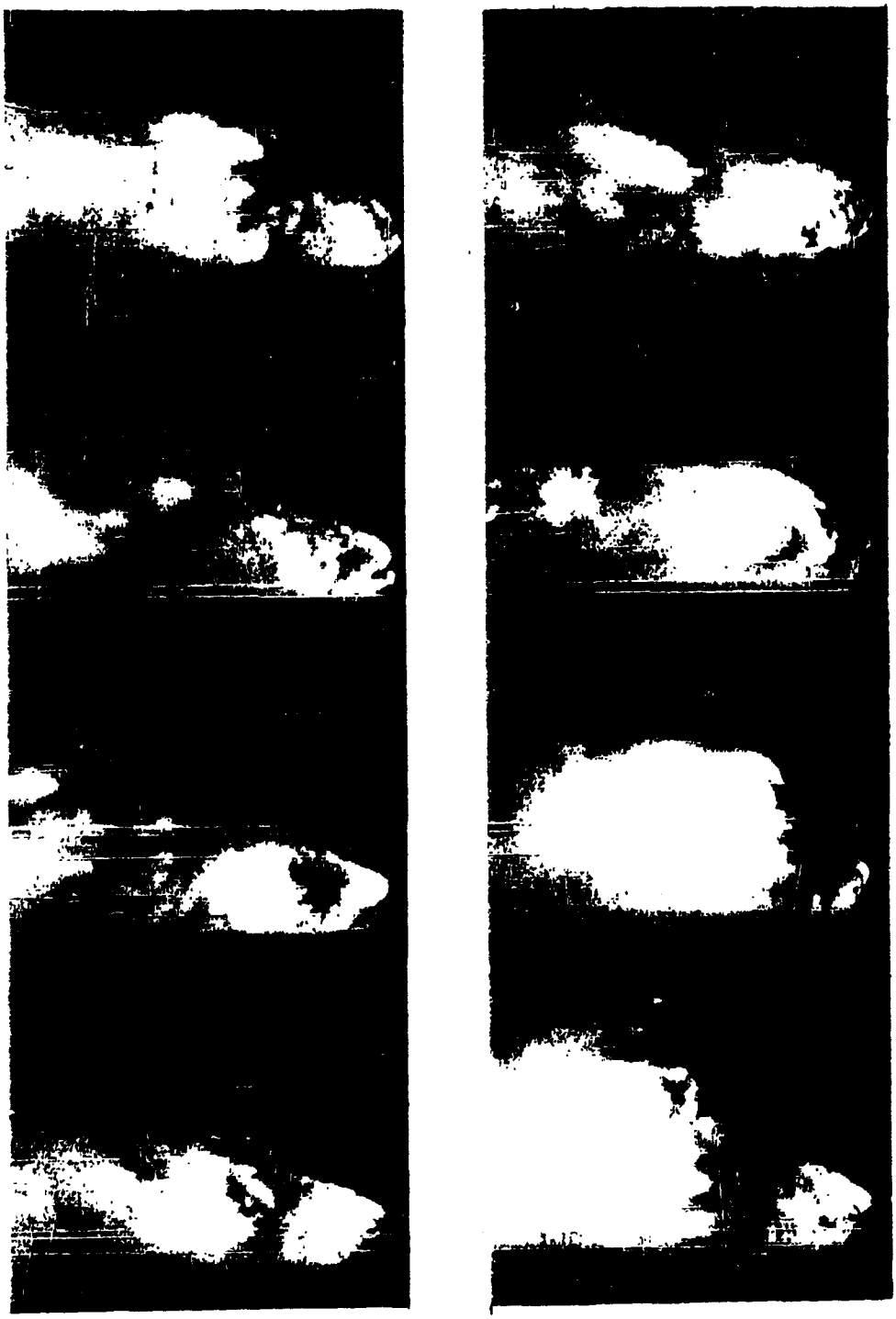

FIGURE 7.1.4 CONTINUED

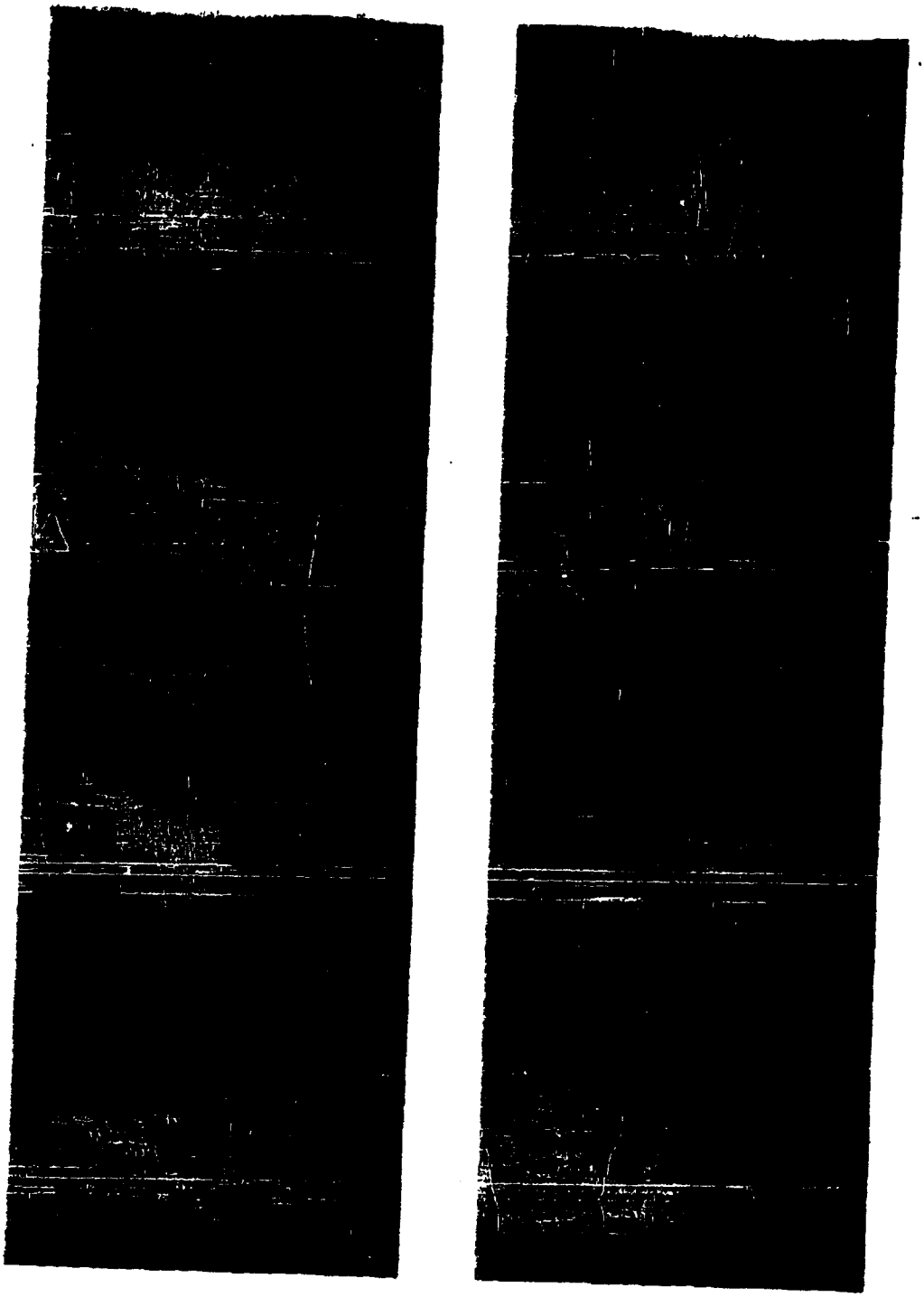

FIGURE 7.1.5 DISSEMINATION OF Sm "B" WITH BULK DENSITY 0.33 gm/cc IN MACH 0.80 AIR STREAM

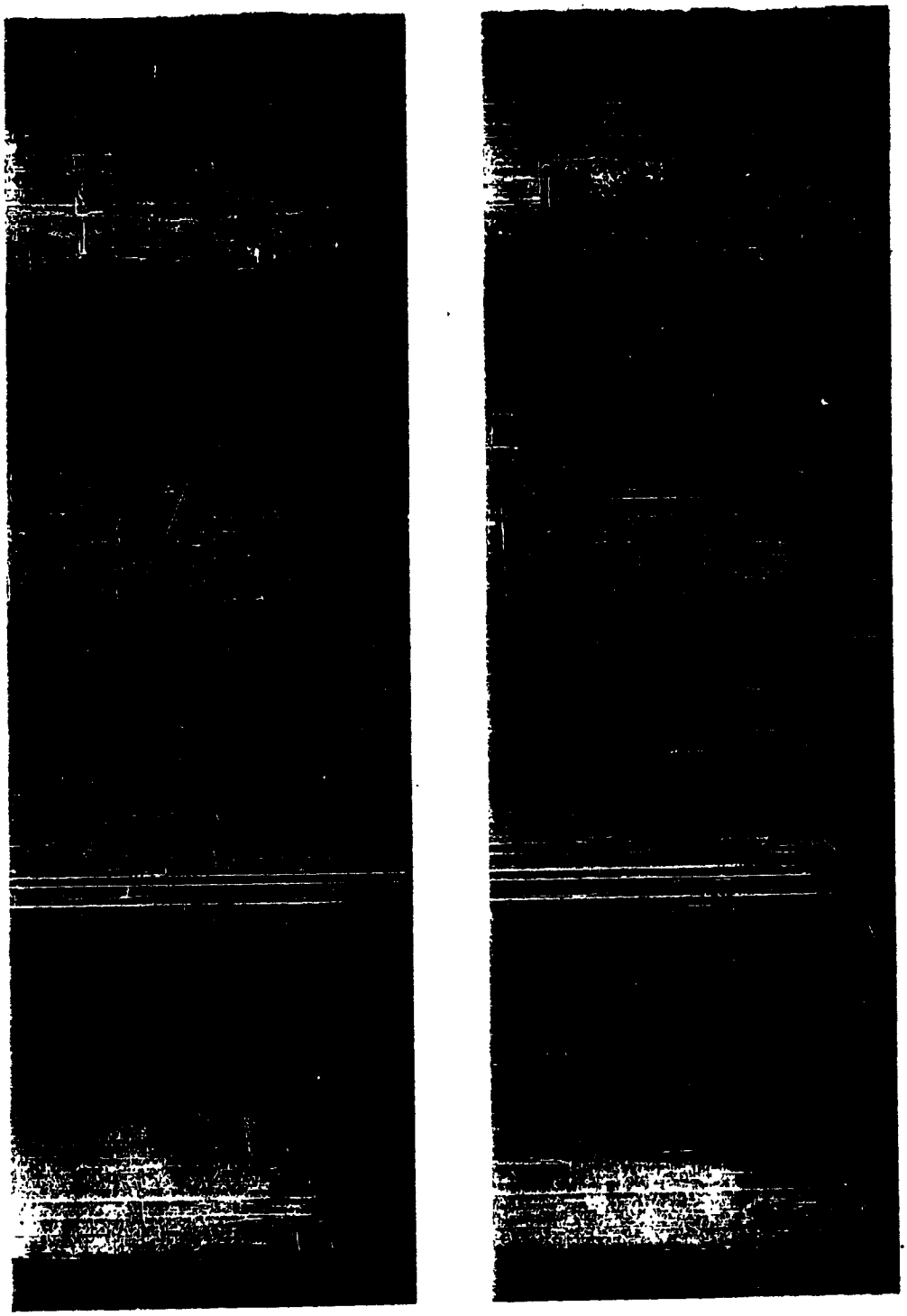

FIGURE 7.1.5 CONTINUED

difference is attributed to their moisture contents given above.

Figures 7.1.6, 7.1.7 and 7.1.8 show the dissemination of Sm "A", compacted to a density 0.43 gm/cc. Note that the end of the slug is sheared or eroded very rapidly as it enters the air stream. Aerodynamic break-up appears to be as satisfactory as that of the lower density.

The results at density 0.49 gm/cc, Figures 7.1.9, 7.1.10 and 7.1.11, can be compared with the previous group to show the significant effect of compaction of relatively moist Sm beyond the density 0.43 gm/cc. At Mach number 0.50, the Sm slug protrudes into the stream an estimated 0.5 cm before being broken by aerodynamic drag forces. This is beyond the boundary layer which was calculated to be 0.33 cm thick at the point of injection. As the compacted pieces flow farther into the stream they break up rapidly. For example, note the change between Frames 4 and 6 in Figure 7.1.9. With increasing Mach number the slugs are broken up closer to the tunnel wall. In this group of pictures there appears to be a significant number of particles formed in the 0.1 to 0.5 mm size range which do not show signs of completely deagglomerating. Thus, it seems likely that this combination of compaction density and moisture content may be beyond the limits for satisfactory dissemination with a simple injection-type apparatus such as was employed in this study.

Generally, the maximum particle injection distance from the wall into the tunnel decreases with increasing Mach number. For example, in Figure 7.1.1 (M = 0.5), the material flows out as far as 2.0 cm before passing out of view, while in Figure 7.1.3 (M = 0.8), it flows to 1.2 cm. It

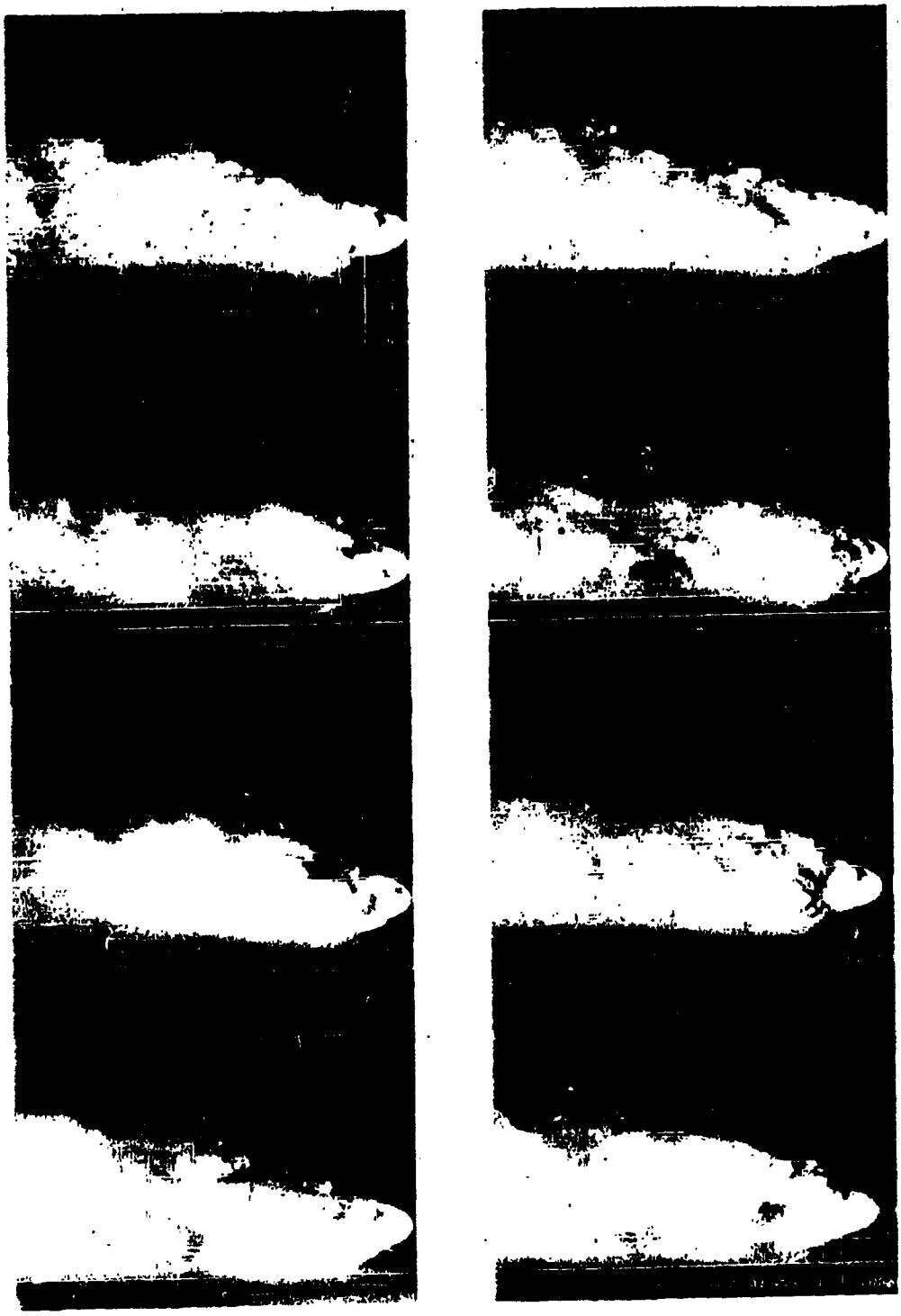

FIGURE 7.1.6 DISSEMINATION OF Sm "A" WITH BULK DENSITY 0.43 gm/cc IN MACH 0.50 AIR STREAM

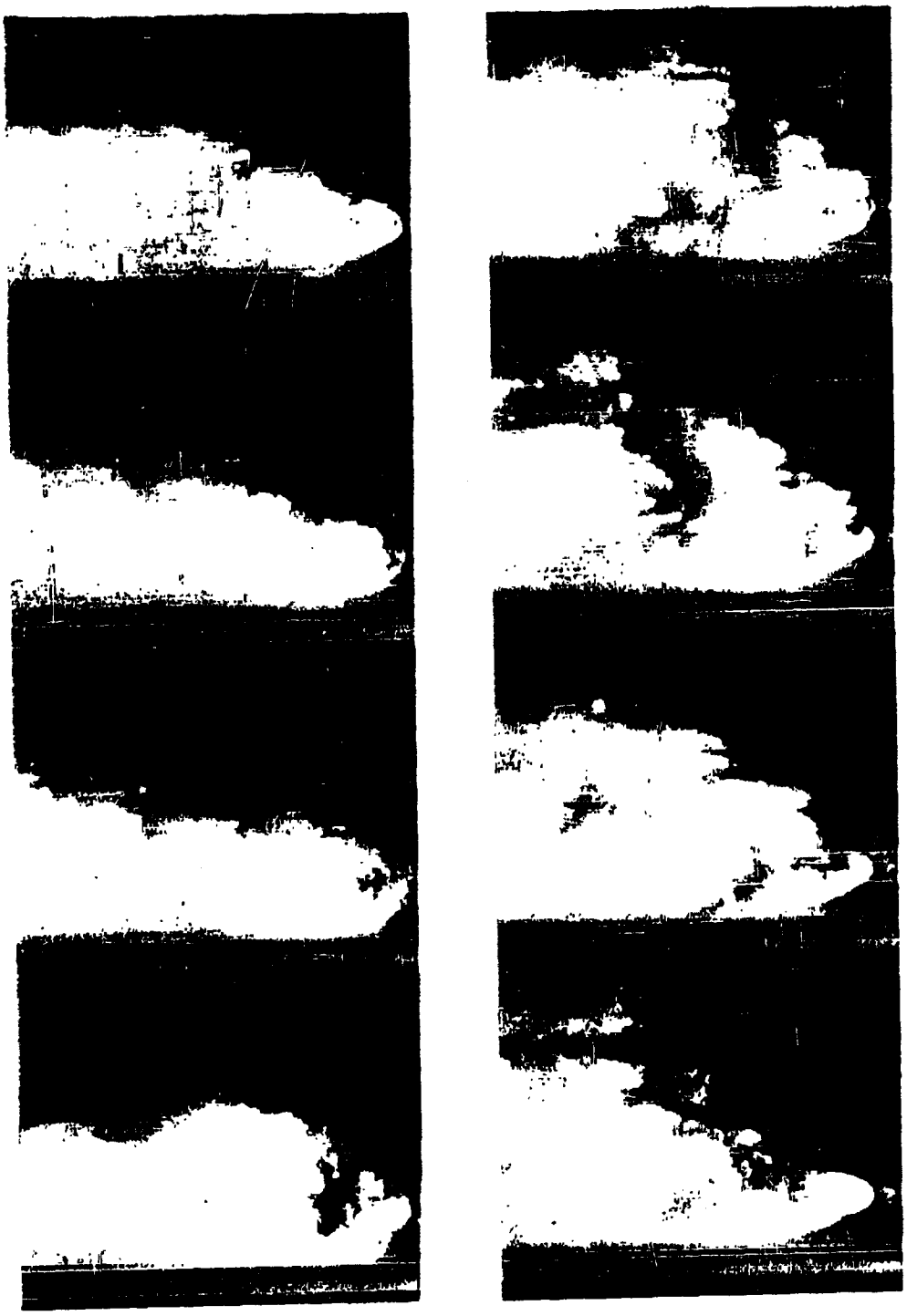

FIGURE 7.1.6 CONTINUED

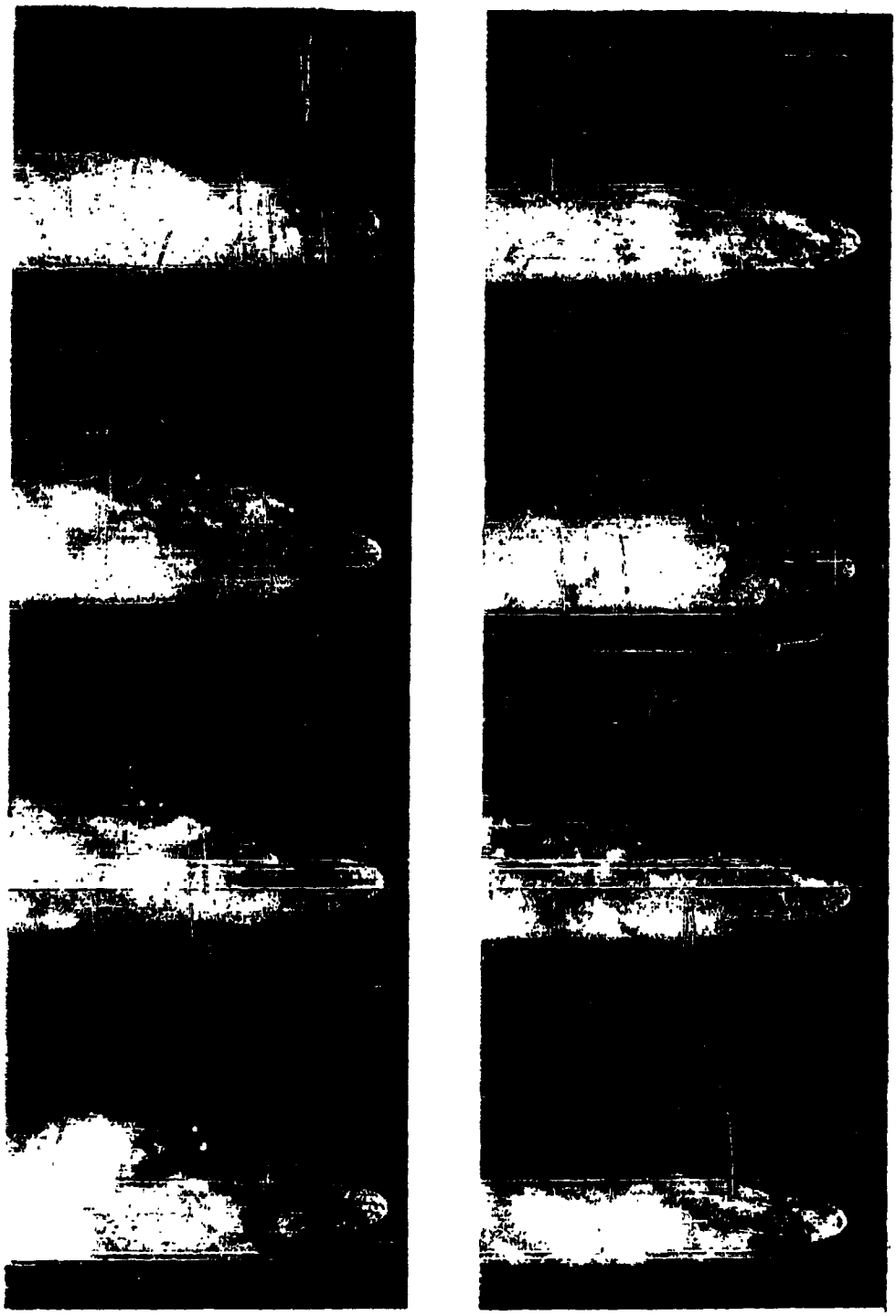

FIGURE 7.1.7 DISSEMINATION OF Sm "A" WITH BULK DENSITY 0.43 gm/cc IN MACH 0.65 AIR STREAM

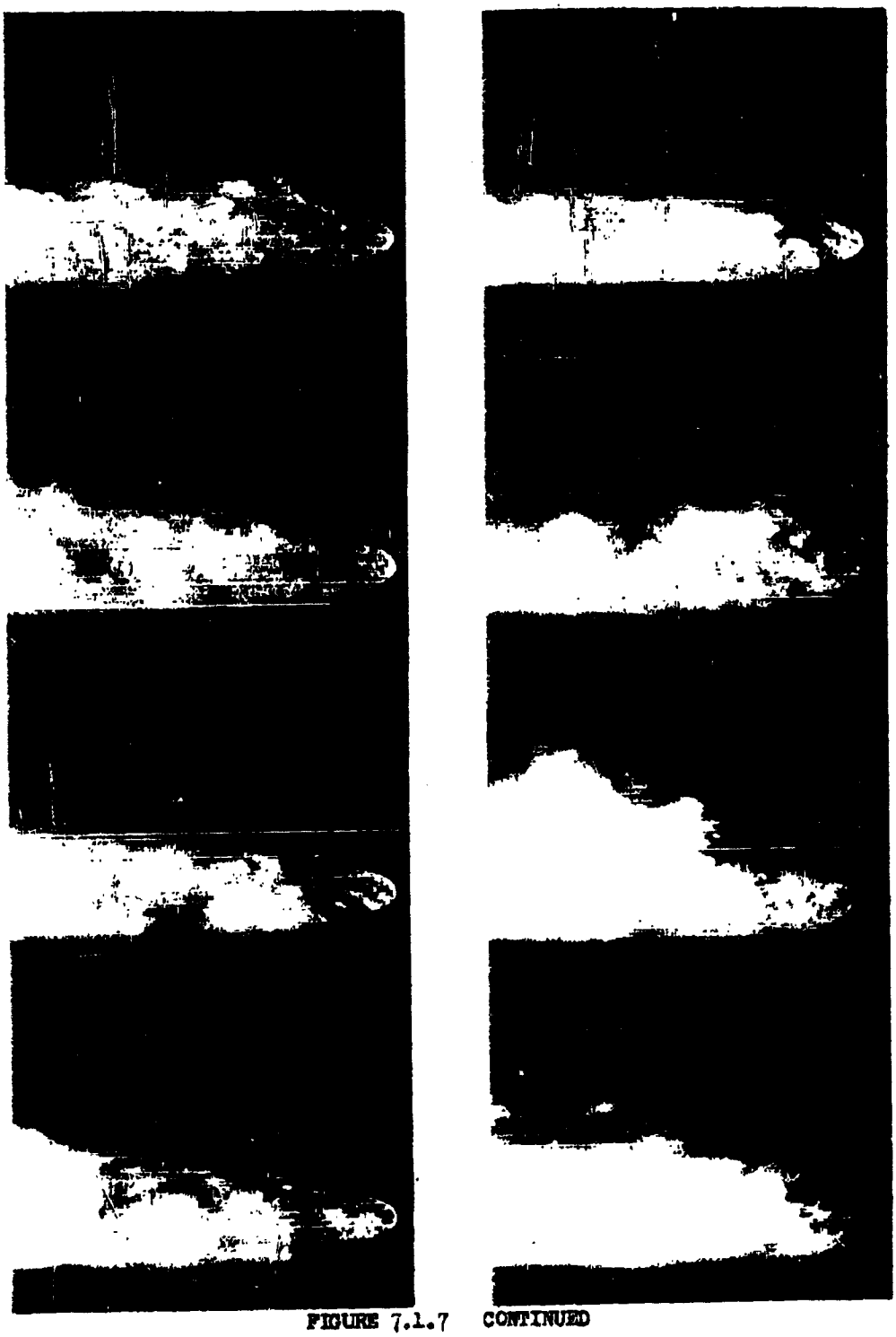

FIGURE 7.1.7 CONTINUED

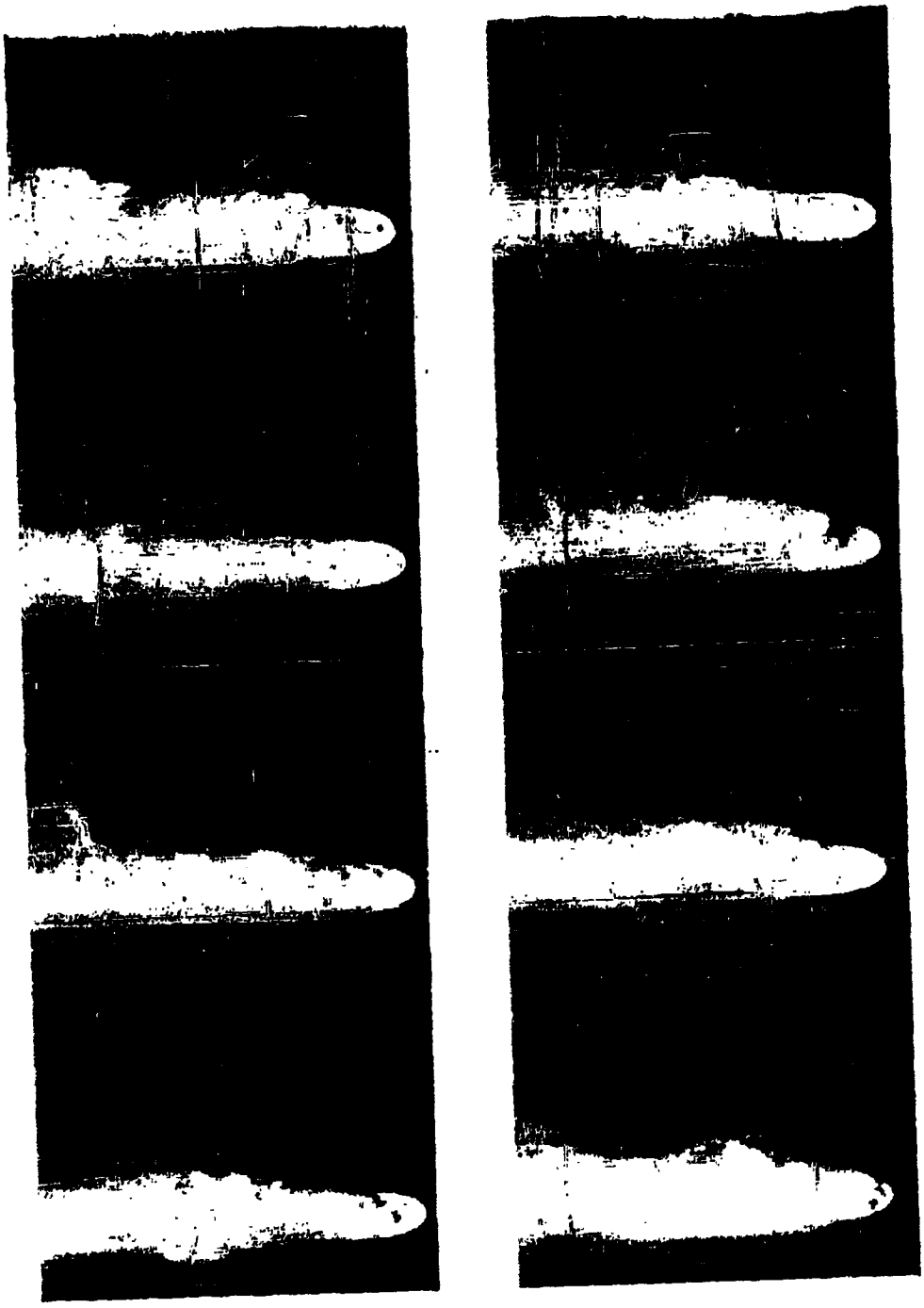

FIGURE 7.1.8 DISSEMINATION OF Sm "A" WITH BULK DENSITY 0.43 gm/cc IN MACH 0.80 AIR STREAM

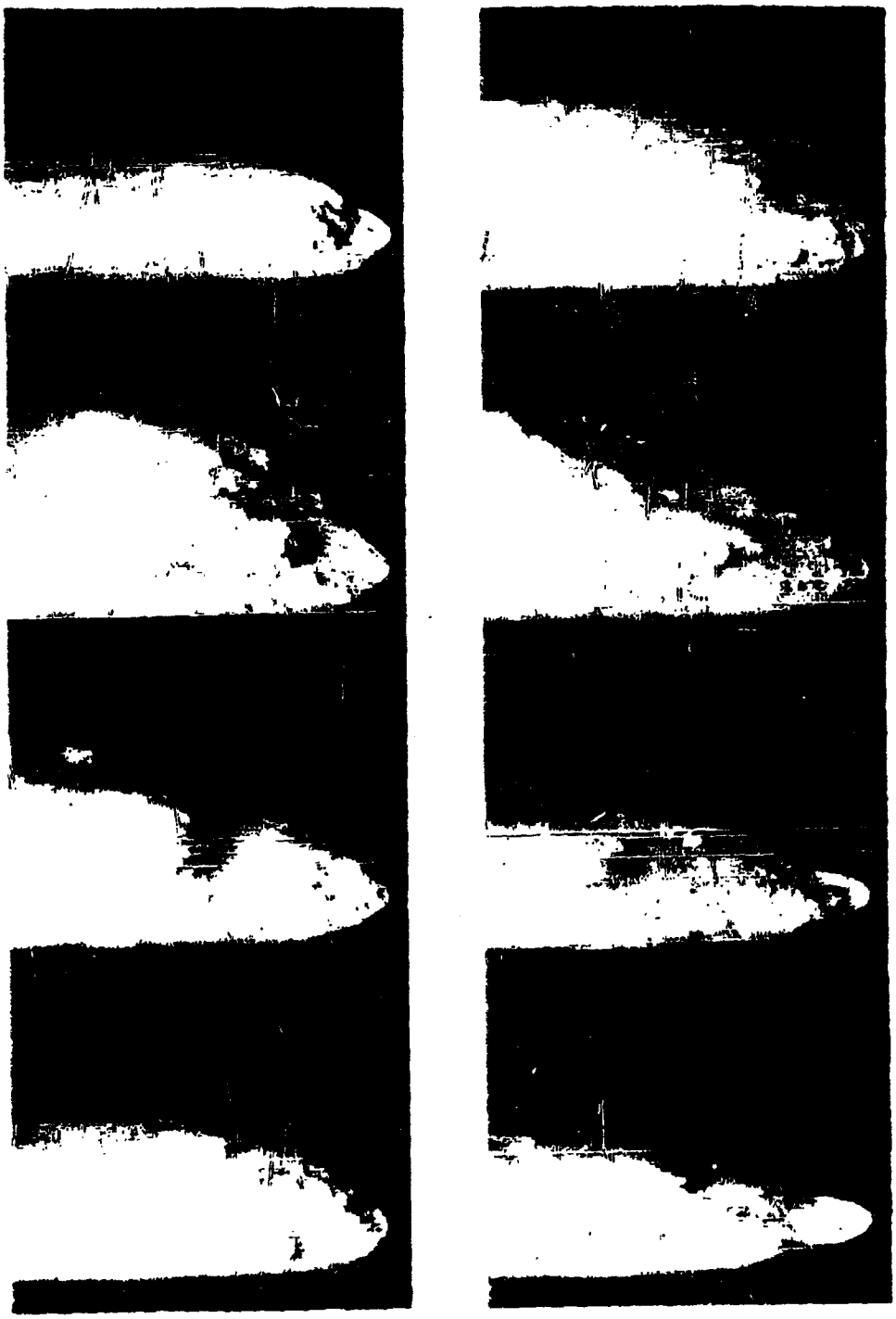

FIGURE 7.1.8 CONTINUED

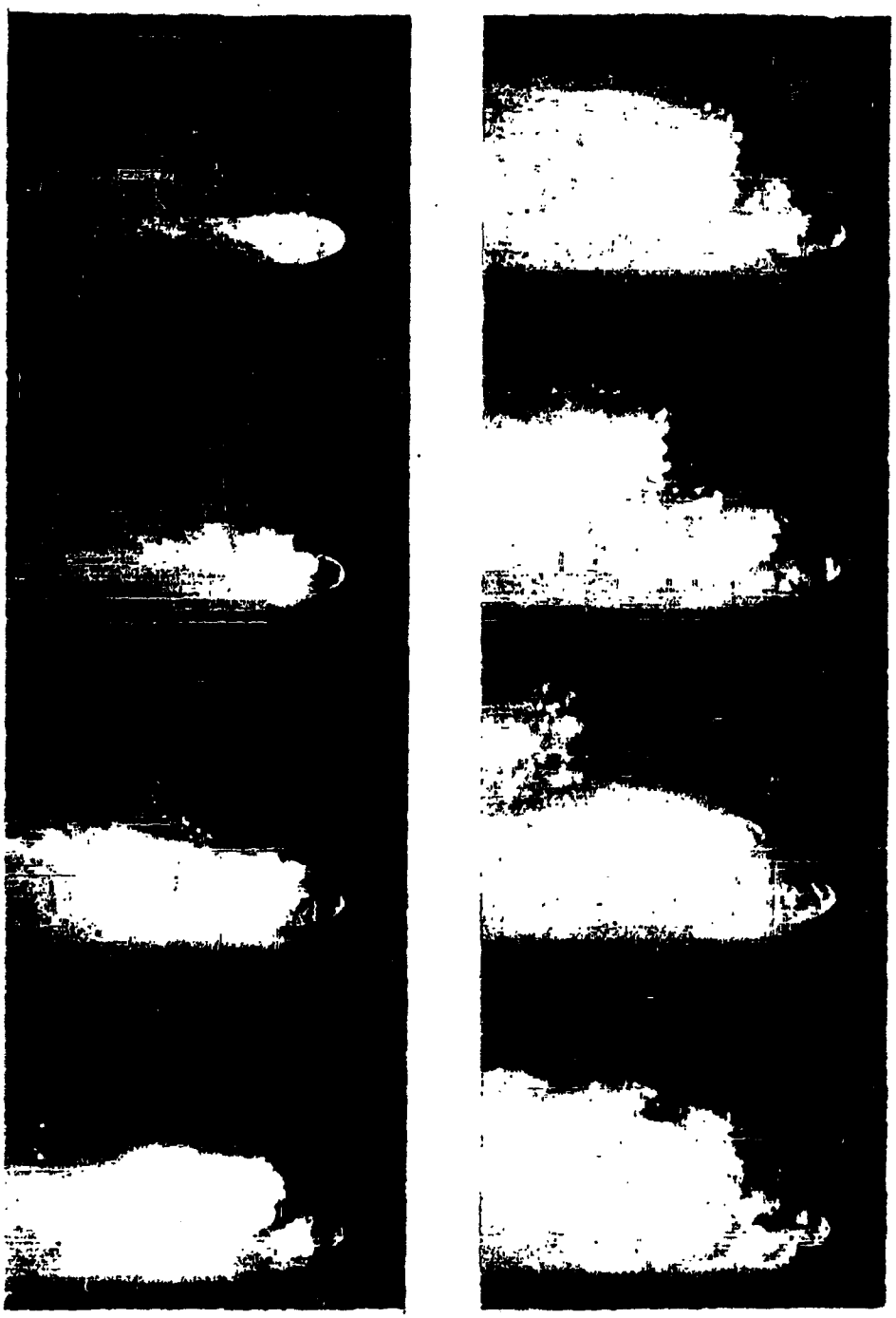

FIGURE 7.1.9 DISINTEGRATION OF Sn "A" WITH BULK DENSITY 0.49 gm/cc IN MACH 0.50 AIR STREAM

FIGURE 7.1.9 CONTINUED

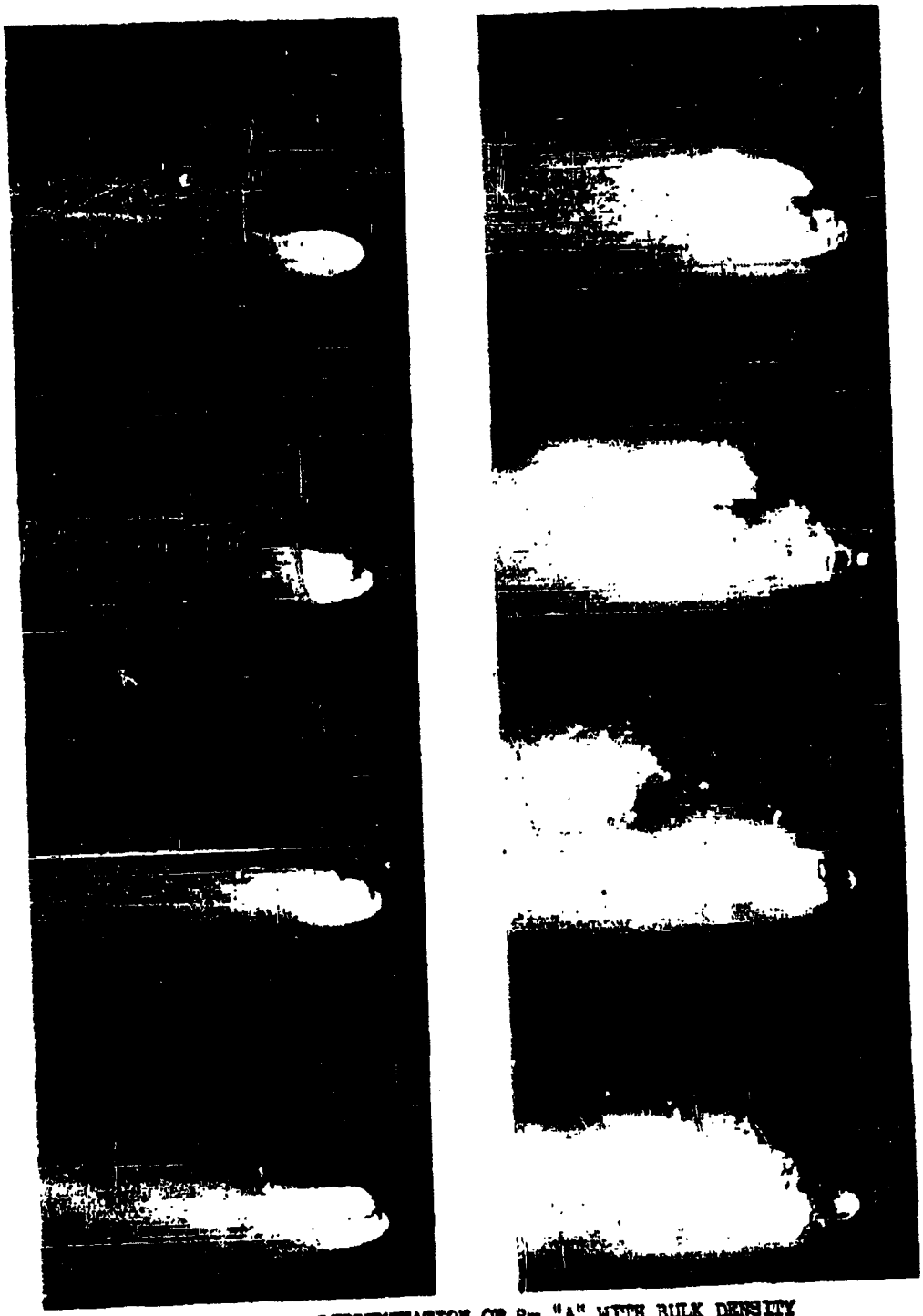

FIGURE 7.1.10 DISSEMINATION OF Sm "A" WITH BULK DENSITY 0.49 gm/cc IN MACH 0.65 AIR STREAM

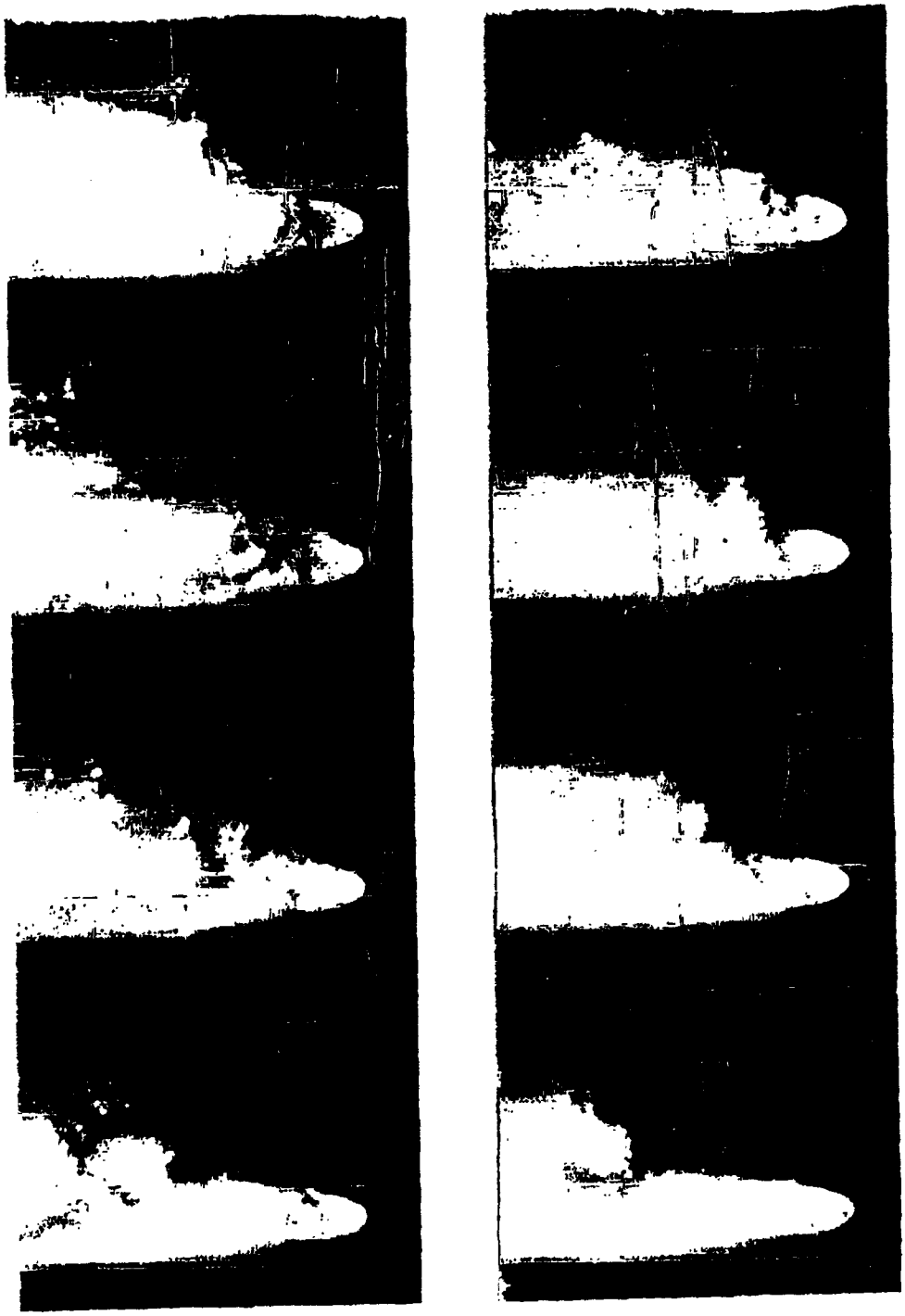

FIGURE 7.1.10 CONTINUED

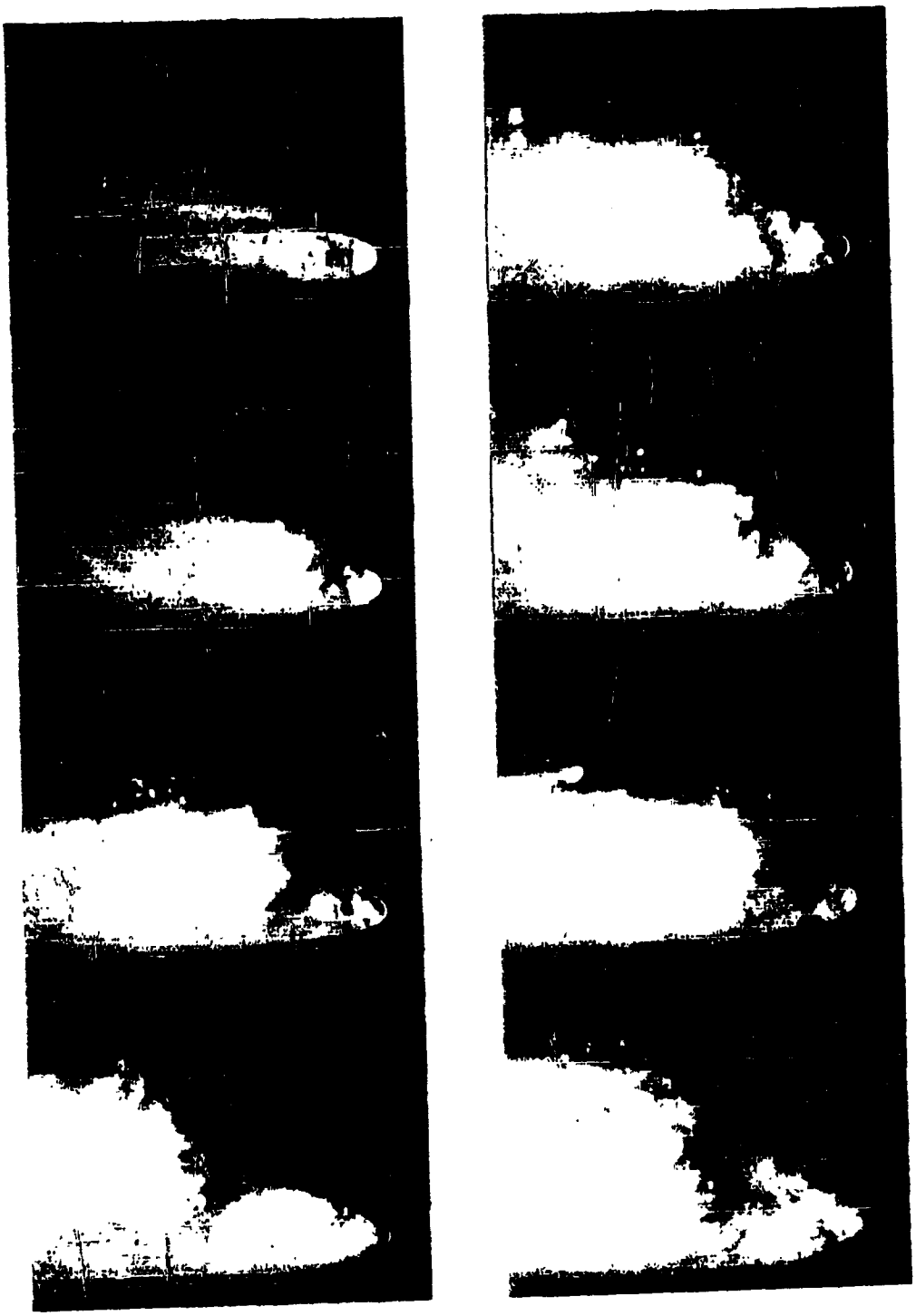

FIGURE 7.1.11 DISSEMINATION OF Sm "A" WITH BULK DENSITY 0.49 gm/cc IN MACH 0.80 AIR STREAM

FIGURE 7.1.11 CONTINUED

should be noted here that Sm does collect on the wall as a result of its close proximity.

In careful study of these pictures, possibly two of the chief mechanisms by which deagglomeration occurs in the wind tunnel may be observed. First, it appears that unequal pressure distributions around large slugs during acceleration cause them to break up suddenly into a large number of finer particles. Figure 7.1.9, Frames 4 and 5, shows this phenomenon, where a piece of slug was shattered in the period of 0.0003 sec. It should be noted that this mechanism does not appear to fully deagglomerate the material in this case. Numerous particles, on the order of 0.2 mm, were produced in the process.

Secondly, the mechanism of fluid shear, in connection with fluid boundary layers around agglomerates and clusters, is considered to be very important in dissemination. It causes erosion of small particles from the material during the acceleration process. For example, Figure 7.1.1, Frame 16, shows clearly the formation of clouds of fine particles around clusters of Sm. A large percentage of the break up of Sm into its basic particle size appears to occur in this manner. Due to the high acceleration of these fine particles, the cloud is oriented in the downstream direction.

The motion of 0.5 mm agglomerates has been traced in these motion pictures to determine their acceleration in the air stream. For the flow condition Mach number 0.5, calculations show that they undergo accelerations greater than 3000 times gravity. Evaluations of their pressure and friction drag coefficients indicate that the former is approximately 50 times greater

than the latter. Thus, acceleration is primarily caused by non-uniform pressure distributions around the agglomerates.

It has not been determined whether fluid shear in turbulent or laminar boundary layers is most effective in deagglomeration; however, it is a well known fact that the shear stress at a boundary is higher in the former case.

7.2 Sm Dissemination - Particle Size Distribution

Experiments have been conducted to determine the degree of deagglomeration of Sm simulant in the wind tunnel. In these studies Sm "S" was injected at an approximate velocity of 4 m/sec into an air stream maintained at Mach number 0.50. The resulting aerosol was then sampled at a distance of 67 cm downstream of the injector with the high velocity sampling probe and 76 mm Millipore filters.

The degree of deagglomeration was determined by studying the material under a microscope. Segments of the samples were prepared for the observations by inverting them on slides and dissolving the filter material with one drop of acetone. By sealing a cover slip over the sample, good particle contrast could be maintained for long periods of time. The analysis was made by first scanning the prepared slides to determine the type of particles that were present. Agglomerates could be distinguished from basic particles so that a qualitative understanding could be obtained of the degree of deagglomeration. The second step was to determine the particle size distribution (by number) of the sample.

These tests indicate that dry (one percent moisture) Sm with a density of about 0.33 gm/cc can be disseminated to produce an aerosol in the wind tunnel which is fully deagglomerated. The samples were found to consist of basic Sm particles. On a number basis, where the statistical Martin's diameter* was measured with a Filar micrometer eyepiece, approximately 90 percent of the particles were smaller than 5μ.

This work will be continued with both loose and compacted Sm at air stream velocities, Mach 0.50 and 0.80. The results should provide a good understanding of the degree of deagglomeration of dry Sm in a high velocity airstream.

---

* Length of a line intercepted by the particle profile boundary which approximately bisects the area of the profile. The measurement is taken in the same direction for all particles.

8. A STUDY OF THE EFFECT OF COMPACTION ON THE VIABILITY OF A DRY SIMULANT MATERIAL

Our Third Quarterly Progress Report included a study of the influence of effective filling density on aerodynamic drag of solid agent external stores. The filling density is a product of the mean bulk density of a finely-divided solid agent and the fraction of the total volume enclosed by the skin of the store which is occupied by the agent. This study pointed out that drag is minimized if the external store has a large filling density. From a structural point of view, it is desirable to have the store as small as possible. It can be concluded from this that it is desirable to use the most dense agent that can be produced.

Our work on the physical characteristics of powders shows that the higher powder densities require increasing higher compaction forces. Preliminary work by Fort Detrick suggests that these high compaction forces may greatly reduce the visibility of agent. To explore the effects produced on a simulant, a series of compaction-viability tests using Sm have been initiated.

Figure 8.1 shows the compaction device which was fabricated for the compaction-viability tests. It is composed of five separate parts: the base, cylinder, closure plug, piston, and funnel. This particular design was chosen to allow for accurate density measurement, ease of applying a load, ease of handling, and provisions for keeping the agent under test sufficiently cool. Cooling was considered since viability may be greatly affected by the heat generated during compression.

FIGURE 8.1 COMPACTION DETAIL, DISASSEMBLED CHAMBER, SOLAR REFLECTOR

In all tests made to date the compaction device and Sm was brought to approximately 4°C prior to conducting the tests at room temperature. This has appeared to be adequate cooling for the low loading rate used in these tests. The procedure is to insert the closure plug into the cylinder and in turn insert these into the base. The Sm is poured into the cylinder in small lots. Tests in this type apparatus have shown that density decreases with distance from the piston. To keep the density variation acceptably small the pellet was formed in layers, each about 1/3 the 250 mg total. The piston was then inserted and slowly loaded with the mass capable of producing the desired density. The piston was removed and the procedure repeated until the full 250 mg pellet was formed.

The length of the pellet was measured with an optical height gage so that the volume and subsequently the density of the test pellet could be determined. The resulting pellet was next weighed and placed into a dispersing solution from which viability assessments were conducted.

Compaction tests, using loading rates as low as 16 grams per second and piston loads up to approximately 16 atmospheres, gave Sm densities up to 0.65 grams per cubic centimeter. Preliminary results suggest that the effect of compaction on viability is not excessive. Based on the procedure described above and a content sample, it appears that the viability recovery of Sm may be as high as 80 percent. Further tests are currently being made to firmly establish this compaction-viability relationship.

9. SYSTEMS STUDY

To obtain a numerical evaluation of target area coverage as a function of the various parameters (flow rate, aerosol diffusion, height of release, etc.), the appropriate equations were programmed on a Bendix G-15 digital computer. The model used was similar to the one used by North American Aviation, Inc.,[1] but with a different expression for the lethal dosage as a function of down wind distance. The model used in this report is the one due to K. Calder with the additional modification of a variable decay rate. The symbols used are defined in Table I below.

We assume that the plane is flying crosswind and disseminates a line source. The line source strength is given by:

$$q = \frac{f.C.H}{v} \tag{9.1}$$

Assuming that this line source is effectively infinite in length, we obtain the ground level lethal dosage via the equation:

$$D_L = (2/\pi)^{1/2} \left[q/\sigma u(x/x_1)^{\beta} \right] \exp\left[-h^2/2\sigma^2 (x/x_1)^{2\beta} \right] \cdot \exp\left[- \text{decay factor.} \right] \tag{9.2}$$

We have a variable decay rate and the "decay factor" is assumed to be:

$$\frac{.05x}{u} \text{ for } 0 < x/u \leq 0.5,$$

$$.01\left(\frac{x}{u} - 0.5\right) + .025 \text{ for } 0.5 < x/u \leq 6.0,$$

and

$$.001\left(\frac{x}{u} - 6.0\right) + .025 + .055 \text{ for } 6.0 < x/u. \tag{9.3}$$

---

1. North American Aviation, Inc., Report No. NA-59-632, "Airborne Biological Warfare at Low Altitudes", Vol. II, 16 June 1959, pp. 183 and following.

TABLE 9.1

Symbol	Definition	Units	Numerical Value Used for this Report
P	Probability of infection	Unitless	
ID_{50}	No. of organisms required to infect 50% of the people	Organisms	
q	Source strength	Org/ft.	Variable
k	Agent decay rate	%/hr.	5 for $0 \leq t \leq .5$ hr. 1 for $0.5 < t \leq 6$ hrs. 0.1 for 6 hrs. $< t$
x	Down wind cloud travel	Miles	Variable
u	Wind speed	Miles/hr.	Variable
h	Height of release	Feet	100
σ	Weather parameter	Feet	.66
β	Weather parameter	Unitless	3.8
x_1	Height for which σ and β are determined	Miles	.0622
b	Breathing rate of man	$Ft.^3/hr.$	25.43
f	Dissemination flow rate	$Ft.^3/min.$	Variable
C	Agent concentration	$Org/ft.^3$	
E	Dissemination efficiency	Unitless	0.20
v	Delivery speed	Ft./min.	48,000 (=545 mph = Mach .76)
D_L	Ground level dosage of lethal agent	$Org\text{-}hr./ft.^3$	

That is, the decay rate is five percent per hour during the first half hour, one percent per hour for the next five and one half hours, and one tenth of one percent thereafter.

It should be noted that time has been integrated out of the expression for D_L and hence D_L is in terms of viable organisms present per cubic foot for one hour. If we multiply D_L by the total intake of air of one person for one hour we obtain the dosage, d, for that person. Knowing d, we obtain the probability of infection, P, from the equation

$$P = 1 - 2^{-d/ID_{50}}. \qquad (9.4)$$

In the exponent d/ID_{50} the quantity C/ID_{50} occurs and this will be treated as a variable.

Curves of P versus down wind distance, x, are plotted and shown in Fig. 9.1. The parameters are C/ID_{50}, wind speed u, and flow rate f. These curves can be related to a specific agent through the parameter C/ID_{50}, assuming we have used the proper decay rate. Since these curves are not restricted to a particular agent they can be thought of as universal curves.

It is of considerable interest to compare these curves with the experimental results contained in the North American Report, pp. 103-117, especially Figure O-6, p. 115. We observe that all data has a characteristic shape which rises sharply in the beginning, starts to drop, rises again and then falls into an exponential decay. This structure is precisely that exhibited in our computed curves. This agreement with experimental data gives considerable credence to the theory of a variable decay rate.

FIGURE 9.1 PROBABILITY OF INFECTION FOR INFINITE LINE SOURCE
(h=100 ft., Open Terrain, Favorable Weather Conditions)

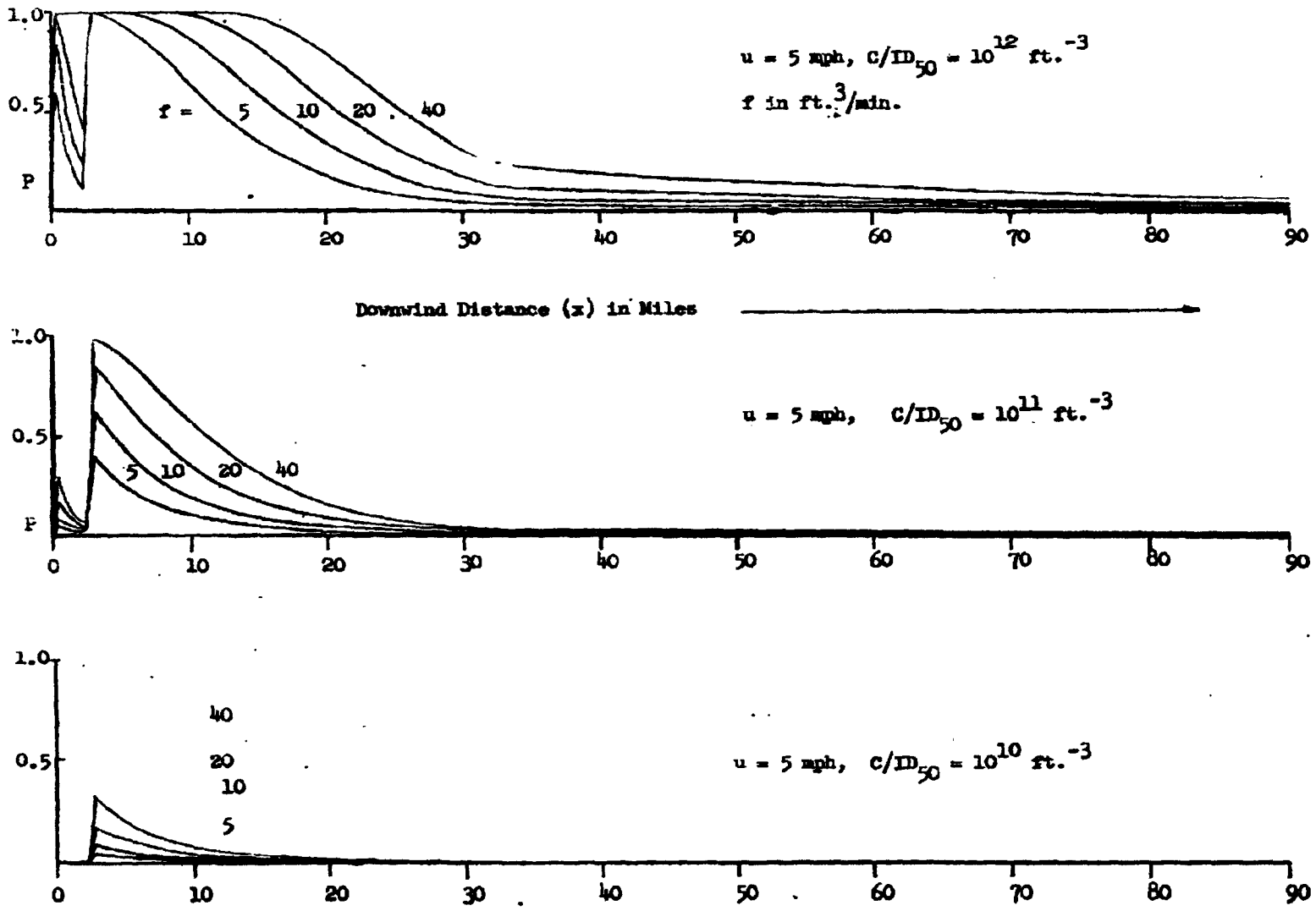

FIGURE 9.1 - CONTINUED

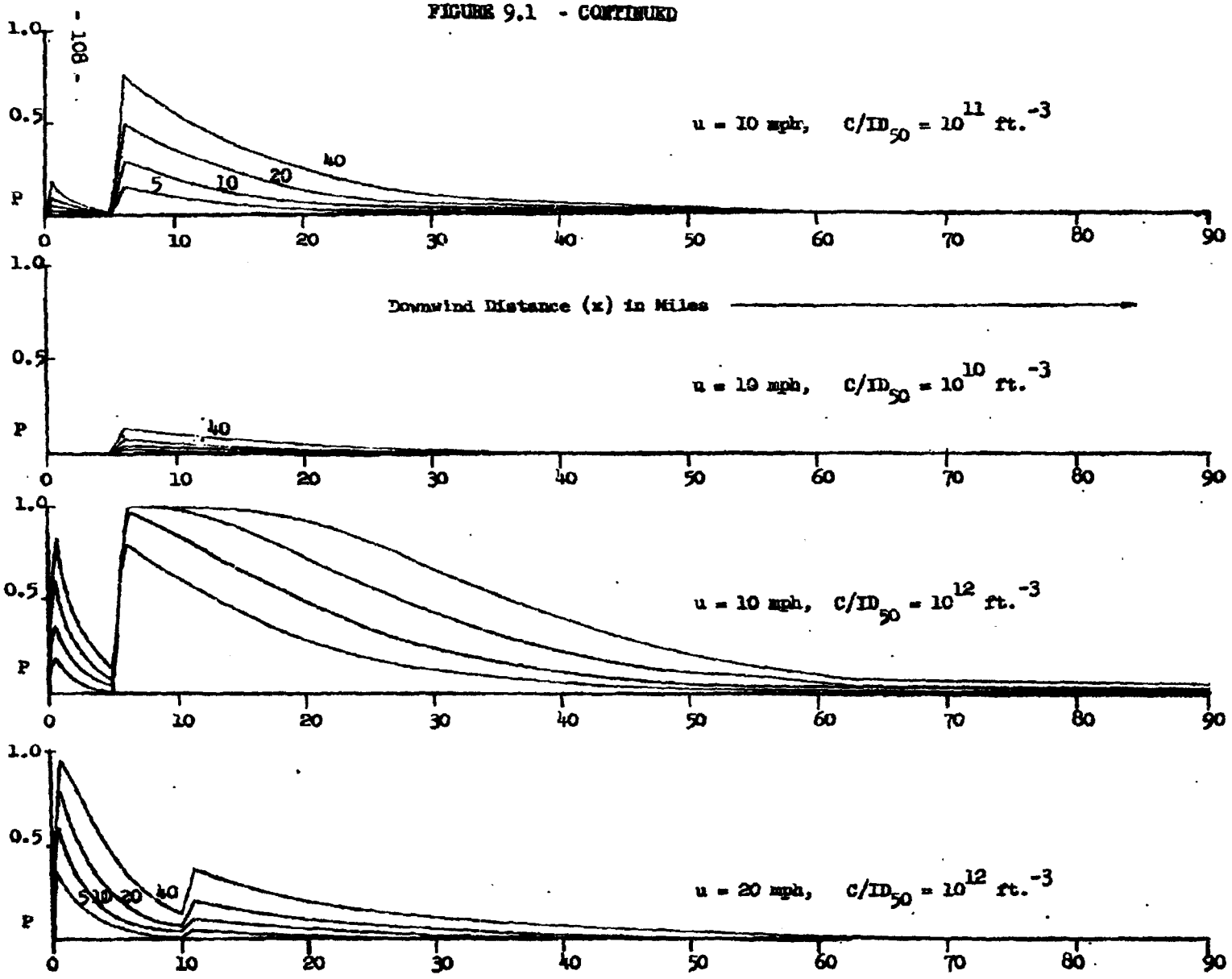

Since the theory of a variable decay rate seems even more plausable now, a mathematical model is being developed which will account for this. This model entails particle size as one of its parameters.

10. WORK ON LIQUID AGENT DISSEMINATING STORE

As reported in our Third Quarterly Progress Report, General Mills, Inc. was asked to consider the potential store-carrying capabilities of the AN/USD-5 Drone, before selecting the final configuration of the research prototype liquid agent disseminating store. In order to thoroughly investigate this potential application, General Mills, Inc. issued subcontracts to Fairchild Aircraft and Missiles Division and North American Aviation, Inc. for studies on this subject. The work statements for each of these studies were included in our Third Quarterly Progress Report.

Both of these studies have been completed. The final report prepared by Fairchild is included as Appendix A. The final report prepared by North American Aviation is included as Appendix B. The reader is referred to these appendices for the detailed findings of these studies. Conclusions are summarized in Section 11.

11. SUMMARY AND CONCLUSIONS

During this reporting period, the Phase II studies were continued. This phase includes research related to solid agent dissemination and the design and fabrication of a research model of a liquid agent store, intended for future field experiments.

Experimental studies of the effect of exposure to heated air streams on the viability of Sm aerosols have been made. Results for an exposure time of 1.7 seconds show a very substantial loss of viability at elevated temperatures. For example, exposure at 125°C causes 99 percent loss of viability. This work indicates that mixing of the aerosol with the jet plume of a carrier aircraft should be avoided. (Section 2)

The study of frictional forces between various powders and various surfaces has been continued. With the use of a piston-cylinder apparatus, measurements were made of the product $C_1\mu$, where C_1 is the constant of proportionality between forces acting perpendicular to and parallel to the direction of the applied force, and μ is the coefficient of friction. Measurements were also made of μ directly, using a tilting-table method. It was possible to calculate C_1 from these measurements. The average value for C_1 was found to be 0.484 for talc and 0.414 for Sm.

A study was made of average bulk density of a column of compressed powder, as a function of column length, for various compressive stresses. Measurements were made on both talc and Sm. An empirical formula was found to fit the experimental data quite well. (Section 3)

A theoretical analysis of the force required to lift an imbedded disk from a bed of dilatant material was carried out, under the assumption that attractive forces between particles are negligible. The removal force was found to depend on the density γ and the shear angle ϕ of the particulate material, the force being proportional to the factor:

$$\frac{\gamma \sin \phi}{1-\sin \phi}.$$

The agreement between theory and experiment was found to be good for glass beads of 100 and 200 micron diameter. (Section 4)

The viscosity of egg slurries W.E.S. #1, #2, #3 and #4 was redetermined, using a new shipment of frozen samples. The thermal conductivity of these slurries also was determined at intervals of 1.5°C in the temperature range from 0 to 32°C. The thermal conductivity values varied from 78 to 97 percent of the value for water.

The rheological properties of Sm slurries without a surface active agent were investigated at 20°C. The slurries exhibited initial thixotropy (apparent viscosity decreases with shear) followed by rheopectic behavior (increase in apparent viscosity with shear). A slurry containing 28.6 percent by weight Sm was too thick to handle in the coaxial cylinder viscometer. A capillary viscometer is being constructed to extend the rheological investigation to greater solids concentration and higher shear rates. (Section 5)

Boundary layer studies showed that the boundary layer of an aircraft external store is approximately 10 times thicker than the boundary layer in our wind tunnel. However, with a reduced wind tunnel

Mach number, the deagglomeration measured in the wind tunnel is conservative, since the velocity gradient at the apparent injection distance (0.02 to 0.04 ft.) is greater for the agent store than for the wind tunnel, while the velocity at this distance is almost identical. (Section 6)

Studies on the dissemination of Sm simulant in the high-velocity wind tunnel were conducted during this reporting period. A series of high-speed motion pictures, taken of the aerosolization process within the tunnel, showed the aerodynamic breakup characteristics of Sm at various bulk densities, moisture contents, and tunnel Mach numbers. The degree of deagglomeration is strongly dependent on the moisture content of Sm; values in the range of 1-2 percent by weight appear to be most satisfactory for dissemination. The two mechanisms which seem to be primarily responsible for deagglomeration are non-uniform pressure distributions around agglomerates and fluid shear stresses at their boundaries.

Samples were taken of Sm aerosols produced in the tunnel at an air stream velocity, Mach number 0.5. For the case of dry Sm with density 0.33 gm/cc, it was found that the sample consisted of basic Sm particles; i.e., full deagglomeration was obtained. (Section 7)

Experiments were conducted to determine the effect of compaction on the viability of dry Sm. Early results indicate that the viability recovery for samples subjected to approximately 16 atmospheres pressure was in the order of 80 percent. (Section 8)

A numerical evaluation of the target area coverage was conducted as a function of the various parameters, including the factor of a variable decay rate. The result of this study is a family of infection probability curves, with a characteristic shape which has been demonstrated in actual field experiments. This agreement with experimental results adds considerable strength to the variable decay rate theory. (Section 9)

The USD-5 is capable of carrying external stores at three locations with very small penalties in structure weight. It was determined that the near optimum store for universal use on manned aircraft is substantially larger than the near optimum store for the USD-5. In addition, the manned aircraft store can reasonably include an independent power source. On this basis, it was decided that the most useful unit for this program is one designed for a manned aircraft. (Section 10)

[redacted]

APPENDIX A

STUDY OF COMPATIBILITY OF EXTERNAL WING-MOUNTED EW STORES WITH THE AN/USD-5 (XE-1) DRONE

Conducted Under General Mills, Inc.
Purchase Order No. MD-82550

By

Fairchild Stratos Corporation
Hagerstown, Maryland

[redacted]

Book No. 4

~~CONFIDENTIAL~~

AIRCRAFT & MISSILES DIVISION • HAGERSTOWN MARYLAND
FAIRCHILD STRATOS CORPORATION

SUBJECT STUDY OF COMPATIBILITY OF EXTERNAL WING-MOUNTED BW STORES WITH THE AN/USD-5 (XE-1) DRONE

PREPARED BY R. H. ROTHENBERGER
CHECKED BY R. H. PUTNAM
APPROVED BY G. SEYTON
APPROVED BY G. F. NORTON
APPROVED BY

REPORT NO. R 361-000
MODEL M-361
COPY NO.
NO. OF PAGES
DATE May 26, 1961

REVISIONS

REVISION DATE	PAGES AFFECTED	APPROVED

NS-800-698

~~CONFIDENTIAL~~

~~CONFIDENTIAL~~

REPORT NO. R 361-000 FAIRCHILD Aircraft and Missiles Div. OF FAIRCHILD ENGINE & AIRPLANE CORPORATION			PAGES | PAGE
MODEL M-361	PREPARED BY R. N. Rothenberger	CHECKED BY R. H. Putnam	APPROVED BY E. E. Morton
SUBJECT:- Study of Compatibility of External Wing-Mounted BW Stores with the AN/USD-5 (XE-1) Drone			DATE May 26, 1961 REVISED

TABLE OF CONTENTS

~~CONFIDENTIAL~~

~~CONFIDENTIAL~~

REPORT NO. R 361-000 FAIRCHILD Aircraft and Missiles Div. OF FAIRCHILD ENGINE & AIRPLANE CORPORATION			PAGES PAGE 1-1
DEPT. M-361	PREPARED BY R.N. Rothenberger	CHECKED BY R. H. Putnam	APPROVED BY E. E. Morton
SUBJECT:- Study of Compatibility of External Wing-Mounted BW Stores with the AN/USD-5 (XE-1) Drone			DATE May 28, 1961 REVISED

SECTION 1. SUMMARY.

To assess the compatibility of external wing-mounted BW stores with the AN/USD-5 (XE-1) drone, the initial investigation considered the installation of tanks 18, 20 and 22 inches in diameter located at wing butt lines 37, 74 and 85. Parametric analysis of these tank sizes and locations at 0.7 Mach number indicated the most desirable configuration to be a 22-inch diameter tank located at wing butt line 85. Further investigation based on the selected configuration indicated a sea level radius of action capability of 111 nautical miles with a BW agent capacity of 1240 pounds.

~~CONFIDENTIAL~~

DEPT. M-361	PREPARED BY R. N. Rothenberger	CHECKED BY R. H. Putnam	APPROVED BY E. E. Morton

SUBJECT:- Study of Compatibility of External Wing-Mounted BW Stores with the AN/USD-5 (XE-1) Drone

DATE May 20, 1961

REVISED

SECTION 2. INTRODUCTION.

This report presents the results of a study to investigate the compatibility of external wing-mounted BW stores with the AN/USD-5 (XE-1) Drone.

Under a contract with the United States Army Chemical Corps, General Mills undertook the development of external stores for line-source dissemination of solid and liquid BW agents from low flying manned and unmanned aircraft. In order that the resulting stores be adaptable to a large number of delivery vehicles, investigation of the potential capabilities of the AN/USD-5 (XE-1) drone for carrying external stores was requested.

The primary mission is line-source dissemination of BW agents from a low altitude drone. Basic assumptions are:

a. Modification of drone components other than the wing structure will be minimized.
b. Weight allowance will be made for installation of functional BW control package.
c. Normal surveillance equipment will be installed.
d. Installation of a wind determination system will be considered.
e. Drone will be returned and recovered.
f. Launch will be made at the highest practical gross weight consistent with the operating limitations of the AN/USD-5 (XE-1) drone.
g. Agent dissemination will be made at minimum feasible altitude and 0.7 Mach number.
h. External BW tanks will be ejected after dissemination run.
i. Minimum radius of operation will be 300 nautical miles.
j. A.C.E.P. of three nautical miles for a 60-minute flight duration will be acceptable.

Basic design data of the BW external tanks as compiled by North American Aviation Company is contained in Appendix I of this report. The following additional data was furnished by General Mills - - - :

a. Density of payload: 8.33 pounds per gallon.
b. Rate of payload dissemination: 9 gal/min/tank.
c. Tank drag (isolated store drag coefficient); 0.08
d. Electrical power requirements of tanks and control: 28 volts dc, 2 amps.

SECTION 2. (Continued)

e. Tank size and weight:

Tank Size (diameter)	Tank Wt. (lb)	Agent Wt. (lb)	Tank Cap (gal)	Total Wt. (2 tanks) (lb)
18 in.	440	233	28	1346
20 in.	520	491	59	2022
22 in.	600	783	94	2766
* 22 in.	460	1241	149	3401

* Alternate tank weight and capacity supplied after completion of preliminary investigation.

The study was conducted in two phases. The objective of Phase I was the determination of the best tank configuration considering tank size and location on the wing. Tanks of 18, 20 and 22-inch diameter located at wing butt lines 37, 74 and 85 were investigated. The effect of each configuration on drone structure, stability and control, and performance was analyzed to establish the most desirable tank configuration.

The objective of Phase II was a study of the selected configuration considering the design, flutter stability, lateral stability, load analysis and stress checks, weight, center of gravity and moment of inertia. A sea-level dissemination mission was calculated utilizing the selected BW tank configuration as well as a summary of design load factors for the tanks.

SECTION 3. SYMBOLS.

B. L. . . . . butt line

C_D . . . . drag coefficient = $\frac{D}{q S}$

C. E. P. . . . . circular error probability

C_L . . . . lift coefficient = $\frac{L}{q S}$

$\mathcal{L}$ . . . . center line

C_m . . . . pitching moment = $\frac{M}{q S l}$

C_n . . . . yawing moment = $\frac{N}{q S l}$

C_{n_β} . . . . static directional stability parameter = $\frac{d C_n}{d \beta}$

C_y . . . . side force coefficient = $\frac{Y}{q S}$

C_x . . . . axial force coefficient

D . . . . drag

F. S. . . . . fuselage station

G. W. . . . . gross weight

I . . . . moment of inertia

I_x . . . . roll moment of inertia

I_y . . . . pitching moment of inertia

I_z . . . . yawing moment of inertia

I_{x_o} . . . . mass moment of inertia of the drone about a centroidal axis parallel to the x datum axis

L. E. . . . . leading edge

M . . . . Mach number 0.7

MAC . . . . mean aerodynamic chord

Mi/lb . . . . nautical mile per pound of fuel

MRP . . . . military rated power

REPORT NO. R 361-000 FAIRCHILD Aircraft and Missiles Div. OF FAIRCHILD ENGINE & AIRPLANE CORPORATION			PAGES PAGE 3-2
MODEL M-361	PREPARED BY R. N. Rothenberger	CHECKED BY R. H. Putnam	APPROVED BY E. E. Merton

SUBJECT:- Study of Compatibility of External Wing-Mounted BW Stores with the AN/USD-5 (XE-1) Drone

DATE May 26, 1961

REVISED

SECTION 3. (Continued)

M_y	. . . . fuselage moment about horizontal axis
M_z	. . . . wing moment about vertical axis
N. Mi	. . . . nautical mile
NRP	. . . . normal rated power
$P_{x_o z_o}$	. . . . product of inertia in the xz plane with respect to centroidal x and z axes
R/A	. . . . radius of action
R/C	. . . . rate of climb
S	. . . . area in square feet
T. E.	. . . . trailing edge
$T._{T.E.}$	. . . . wing torque about trailing edge
V	. . . . airspeed
V_z	. . . . vertical shear
Wt.	. . . . weight
Δ	. . . . incremental change
α	. . . . angle of attack in degrees
α_a	. . . . airplane angle of attack
β	. . . . angle of sideship - degrees
δ	. . . . control surface deflection angle
π	. . . . indicates a coefficient based on maximum cross-sectional area.
ϕ	. . . . roll angle - degrees
$\dot{\phi} = p$	. . . . rolling velocity of drone about longitudinal axis - rad/sec
ψ	. . . . angle of roll
$\dot{\psi}$	. . . . rolling velocity
$\ddot{\psi}$	. . . . rolling acceleration
$\dot{\psi} = r$	. . . . yawing velocity of drone about vertical axis - rad/sec

8-800-23A

SECTION 3. (Continued)

a . . . . aileron

c.g. . . . . center of gravity

l . . . . length

n_x . . . . longitudinal load factor; positive - forward

n_y . . . . lateral load factor; positive - right

n_z . . . . normal load factor; positive - up

q . . . . dynamic pressure = $1/2\ \rho V^2$

r . . . . rudder

w . . . . wing

x . . . . longitudinal center of gravity

y . . . . lateral center of gravity

z . . . . vertical center of gravity

REPORT NO. R 361-000 FAIRCHILD Aircraft and Missiles Div. OF FAIRCHILD ENGINE & AIRPLANE CORPORATION			PAGES PAGE 4-1
DEPT. M-361	PREPARED BY R. N. Rothenberger	CHECKED BY R. H. Putnam	APPROVED BY E. E. Morton
SUBJECT:- Study of Compatibility of External Wing-Mounted BW Stores with the AN/USD-5 (XE-1) Drone			DATE May 28, 1961 REVISED

SECTION 4. FACTUAL DATA

4.1 PARAMETRIC ANALYSIS OF TANK SIZE AND LOCATION - PHASE I

4.1.1 PERFORMANCE ANALYSIS

The performance analysis consisted of a study of the effects of tank size, tank location and cruise altitude on radius of action (Phase I) and the calculation of the mission performance for one selected tank size, weight and wing location (Phase II).

4.1.1.1 Basic Performance Data

The thrust required for the drone without tanks installed is based on the lift and drag coefficients obtained from wind tunnel tests of a AN/USD-5 (XE-1) model. The thrust requirements with tanks installed are based on the addition of an incremental drag coefficient due to the tank installation to the basic AN/USD-5 (XE-1) data. The drag breakdown is given in Table I and a plot of incremental drag coefficient versus tank capacity is presented in Figure 4-1. The tank capacities used in this figure and later figures are the agent capacities specified by General Mills for the Phase I parametric study. The drag coefficients are based primarily on data supplied by North American Aviation and General Mills. The drag coefficients are applicable up to $M = 0.7$.

The thrust available is the same as that used for the AN/USD-5 (XE-1). When calculating cruise performance, the present normal rated power (NRP) of the engine was exceeded when necessary to meet the $M = 0.7$ speed requirement; however, military rated power (MRP) was not exceeded.

Specific range data are presented in Figures 4-2 thru 4-5.

REPORT NO. R 361-000 FAIRCHILD Aircraft and Missiles Div. of FAIRCHILD ENGINE & AIRPLANE CORPORATION

MODEL M-361 | PREPARED BY R. N. Rothenberger | CHECKED BY R. H. Putnam | APPROVED BY E. R. Morton | PAGES | PAGE 4-2

SUBJECT: Study of Compatibility of External Wing-Mounted BW Stores with the AN/USD-5 (XE-1) Drone

DATE May 26, 1961 REVISED

S-800-23A

TABLE I. INCREMENTAL TANK INSTALLATION DRAG COEFFICIENTS

ITEM	TANK DIAMETER 18 Inch	TANK DIAMETER 20 Inch	TANK DIAMETER 22 Inch	COMMENTS
Usable tank capacity per tank	28 gal	59 gal	94 gal	Specified by General Mills for Phase I Study
Tank frontal area	1.762 sq ft	2.182 sq ft	2.640 sq ft	
C_{D_w} for isolated tank	0.05	0.05	0.05	NAA data per TWX dated March 31, 1961
C_{D_w} for fins	0.01	0.01	0.01	NAA data supplied by General Mills
C_{D_w} for pylons	0.0103	0.0103	0.0103	General Mills allowed 0.08 per TWX dated March 31, 1961
	0.0703	0.0703	0.0703	
C_{D_w} for ram air turbine drag	0.1587	0.1281	0.1039	C_D = 0.013 based on area of 21.5 sq ft
Total ΔC_{D_w} per tank	0.2290	0.1984	0.1762	
Total ΔC_D for cruise out (Based on wing area)	0.00402	0.00432	0.00463	Two tanks
ΔC_D for dissemination nozzles	0.00070	0.00070	0.00070	Based on drag of two faired cylinders per tank, 42 in. long, 1 in. diam. and inclined 60° to vertical
Total ΔC_D for dissemination (Based on wing area)	0.00472	0.00502	0.00533	
Usable tank capacity, two tanks	56 gal	118 gal	188 gal	

SECTION 4. FACTUAL DATA (Continued)

4.1.1.2 Missions

The missions investigated were all radius-of-action missions and consisted, basically, of a boosted launch, cruise out to dissemination point, disseminate liquid agent, drop tanks and pylons 25 nautical miles after dissemination, and return to base for recovery. The rules for the missions are given below:

4.1.1.2.1 Sea Level Cruise Mission

a. Fuel allowance (67 lbs) is provided for two minutes operation at NRP for pre-launch check out.

b. Launch and cruise out at Mach number = 0.7 at sea level.

c. Disseminate agent at Mach number = 0.7 at sea level. Agent is disseminated from both tanks simultaneously at rate of 9 gal/min/tank.

d. Range does not include dissemination distance.

e. Drop tanks and pylons after 25 nautical miles of cruise back.

f. Cruise back at Mach number = 0.7.

g. Recover.

h. No reserve fuel.

4.1.1.2.2 Altitude Cruise Mission

a. Fuel allowance (67 lb) is provided for two minutes operation at NRP for pre-launch check out.

b. Launch and climb to 30,000 ft with MRP at best rate of climb.

c. Cruise at 30,000 ft and Mach number = 0.7 until weight decreases to point where service ceiling (R/C = 100 ft/min at NRP) is 35,000 ft.

d. Climb to 35,000 ft with MRP.

e. Cruise to dissemination point at Mach number = 0.7.

f. Descend to dissemination area. No credit is taken for range in descent.

SECTION 4. FACTUAL DATA (Continued)

g. Disseminate agent at Mach number = 0.7 at sea level. Agent is disseminated from both tanks simultaneously at rate of 9 gal/min/tank.

h. Range does not include dissemination distance.

i. Climb to 35,000 ft with MRP. Drop tanks and pylons after 25 nautical miles range in climb.

j. Cruise back at 35,000 ft and Mach number = 0.7 to recovery area.

k. No credit is taken for range during descent to recovery area.

l. No reserve fuel.

Typical mission profiles and the results of the radius-of-action calculations are given in Figures 4-6 thru 4-9. Weight and fuel data are given in the Gross Weight Summary.

NOTE: Gross Weight Summary has been submitted by Weights Section.

It should be noted that none of the tank installations considered were able to meet the minimum desired radius of action of 300 nautical miles at sea level.

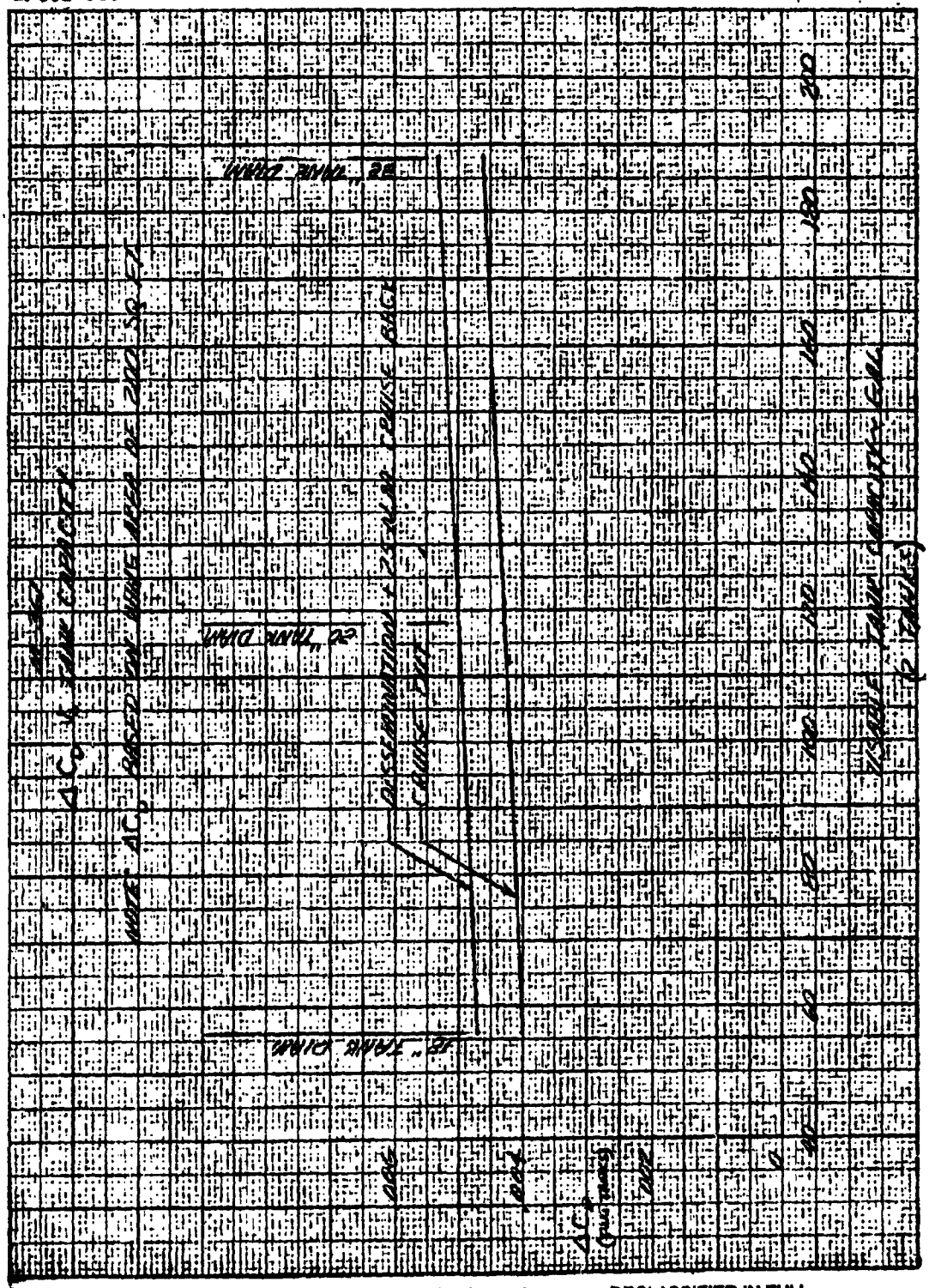

4-1. ΔC_D vs Tank Capacity

~~CONFIDENTIAL~~

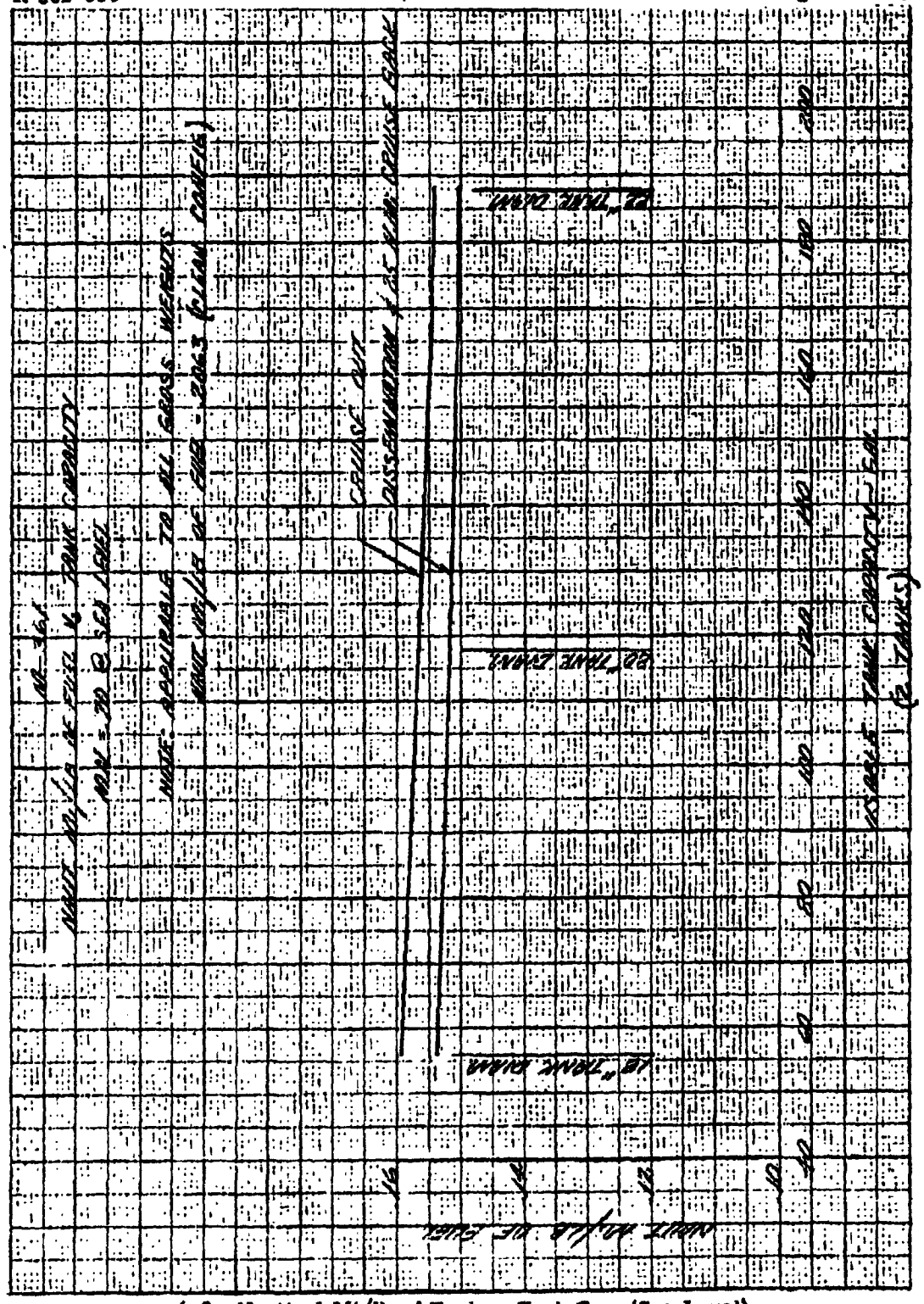

4-2. Nautical Mi/lb of Fuel vs Tank Cap. (Sea Level)

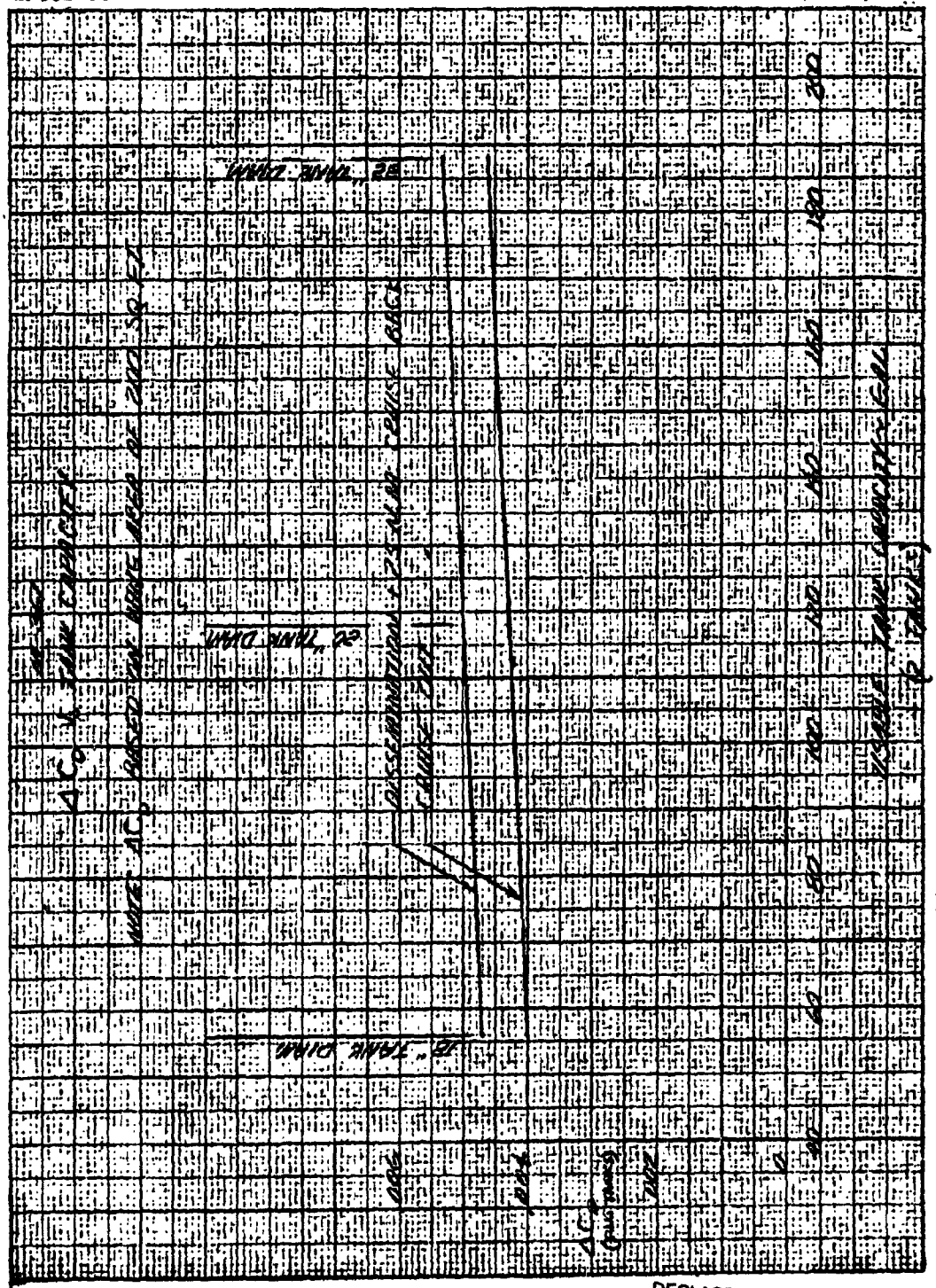

4-1. ΔC_D vs Tank Capacity

~~CONFIDENTIAL~~

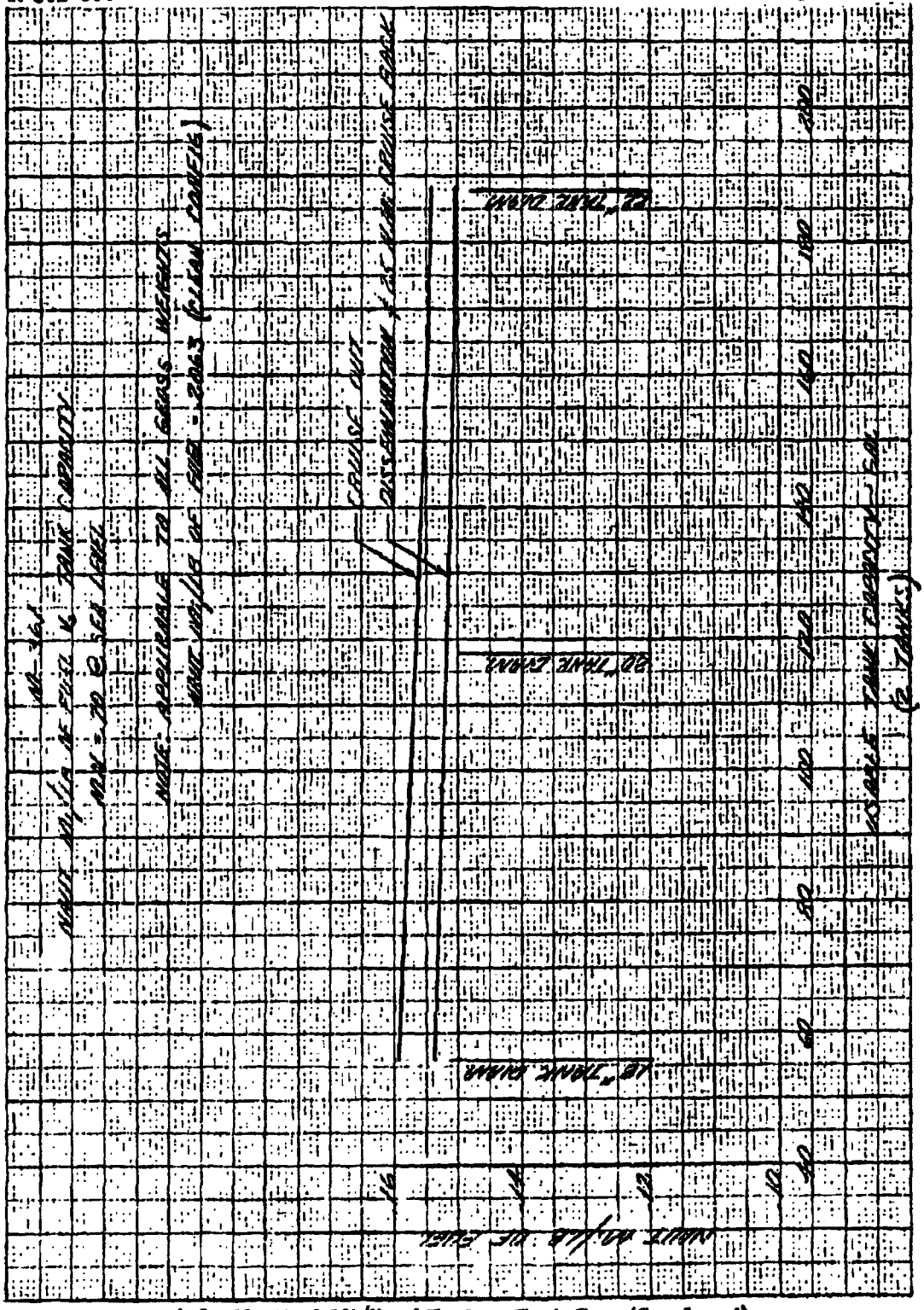

4-2. Nautical Mi/lb of Fuel vs Tank Cap. (Sea Level)

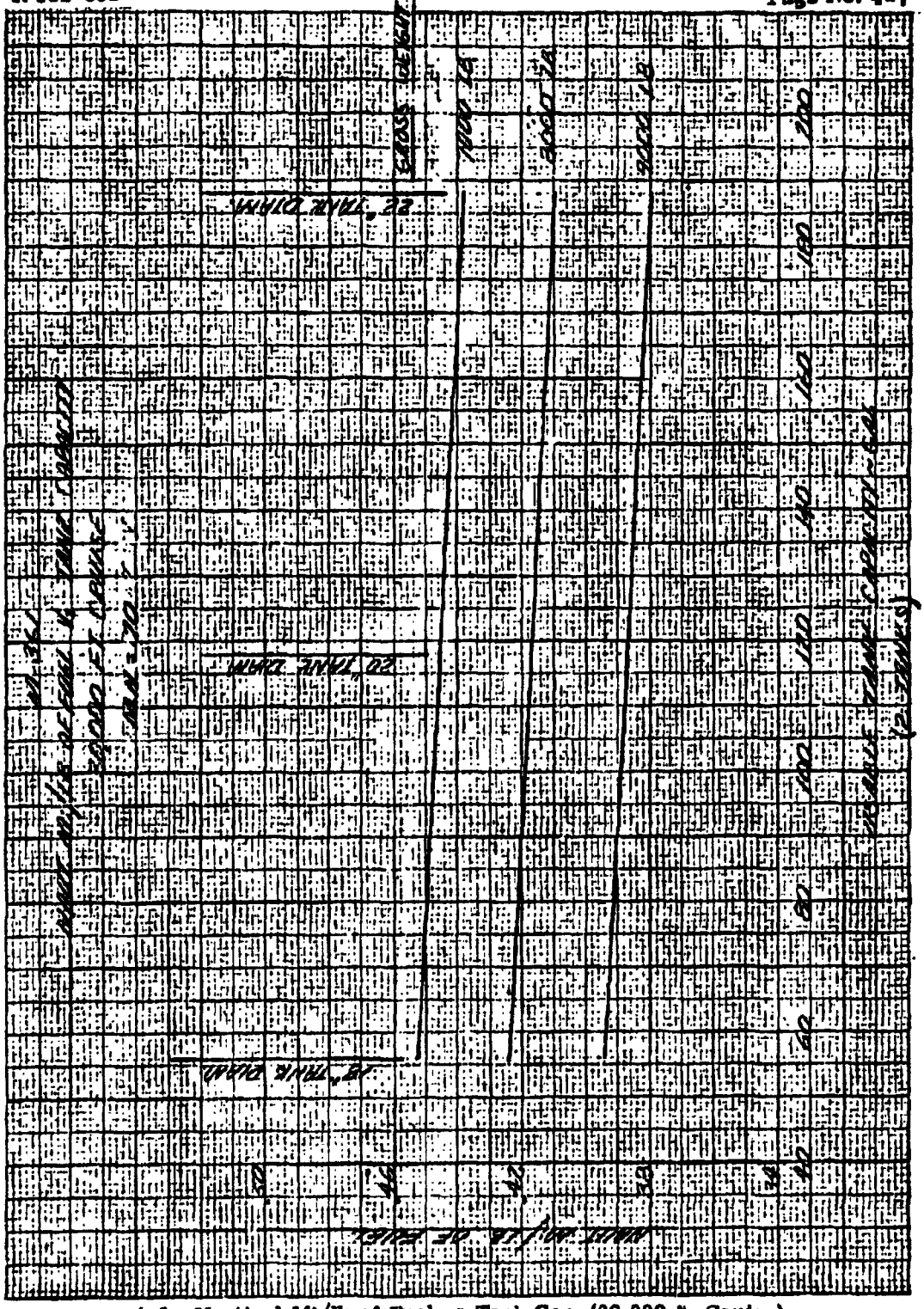

4-3. Nautical Mi/lb of Fuel vs Tank Cap. (30,000 ft. Cruise)

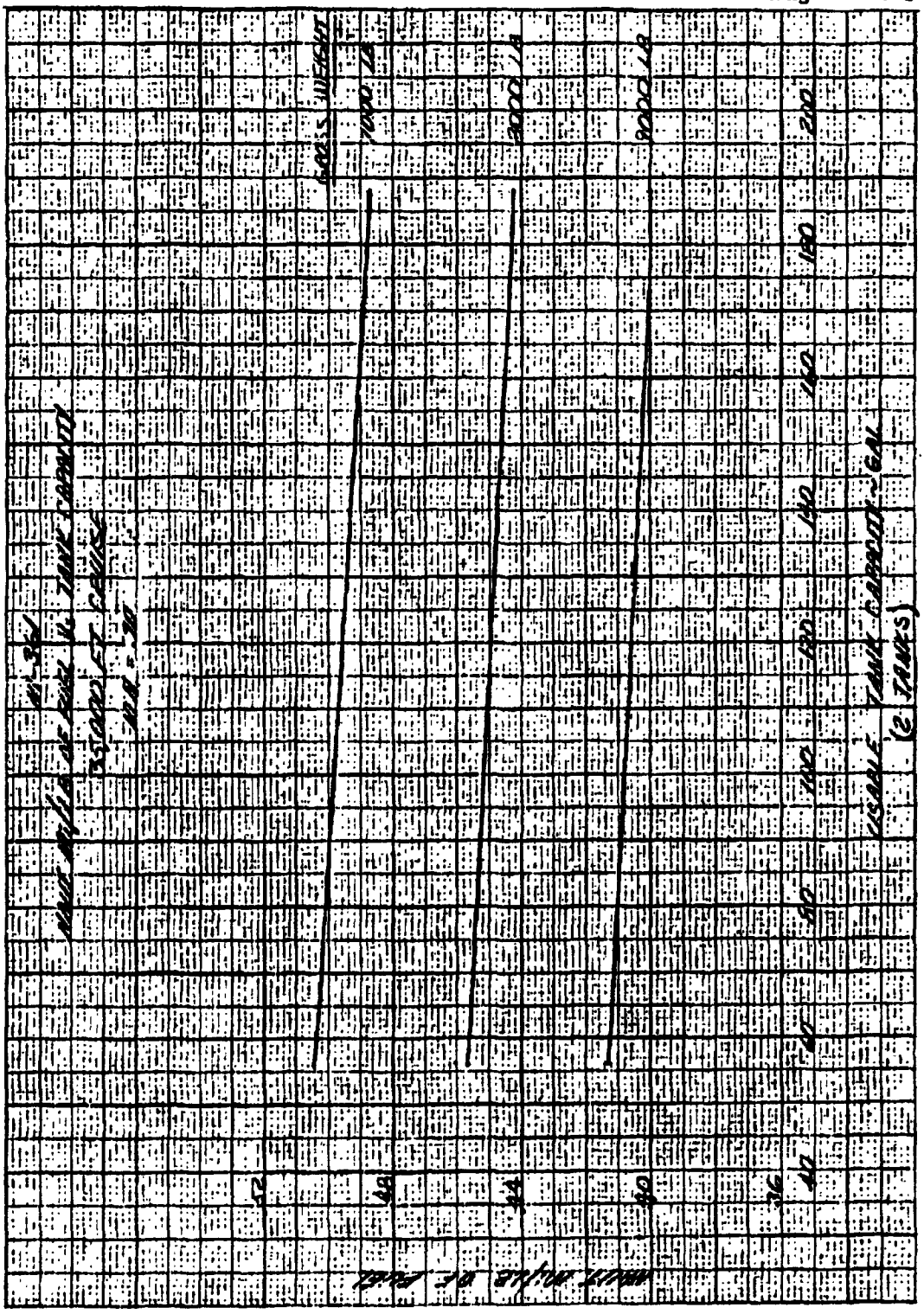

4-4. Nautical Mi/lb of Fuel vs Tank Cap. (35,000 ft. Cruise)

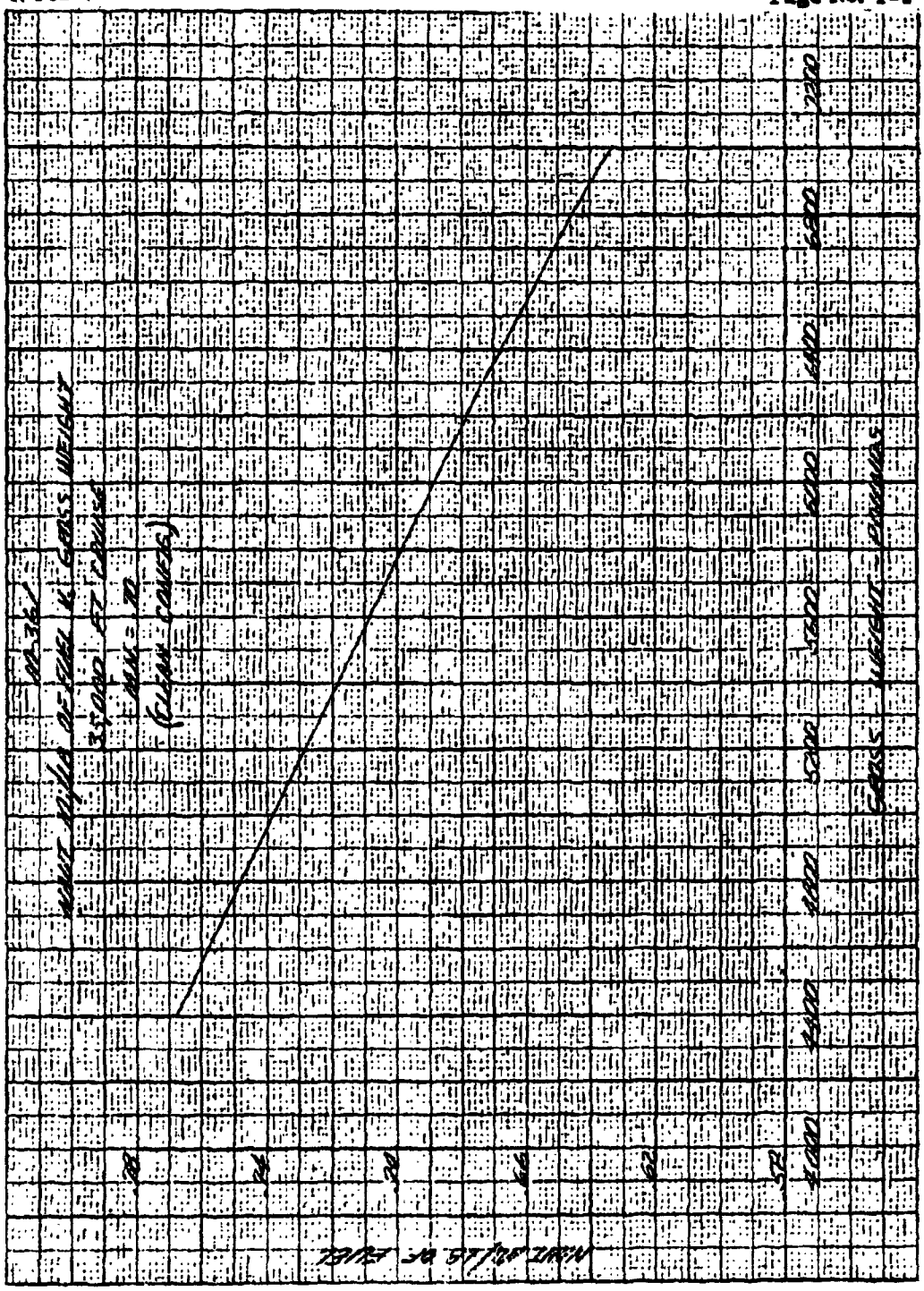

4-5. Nautical Mi/lb of Fuel vs Gross Weight (35,000 ft. Cruise)

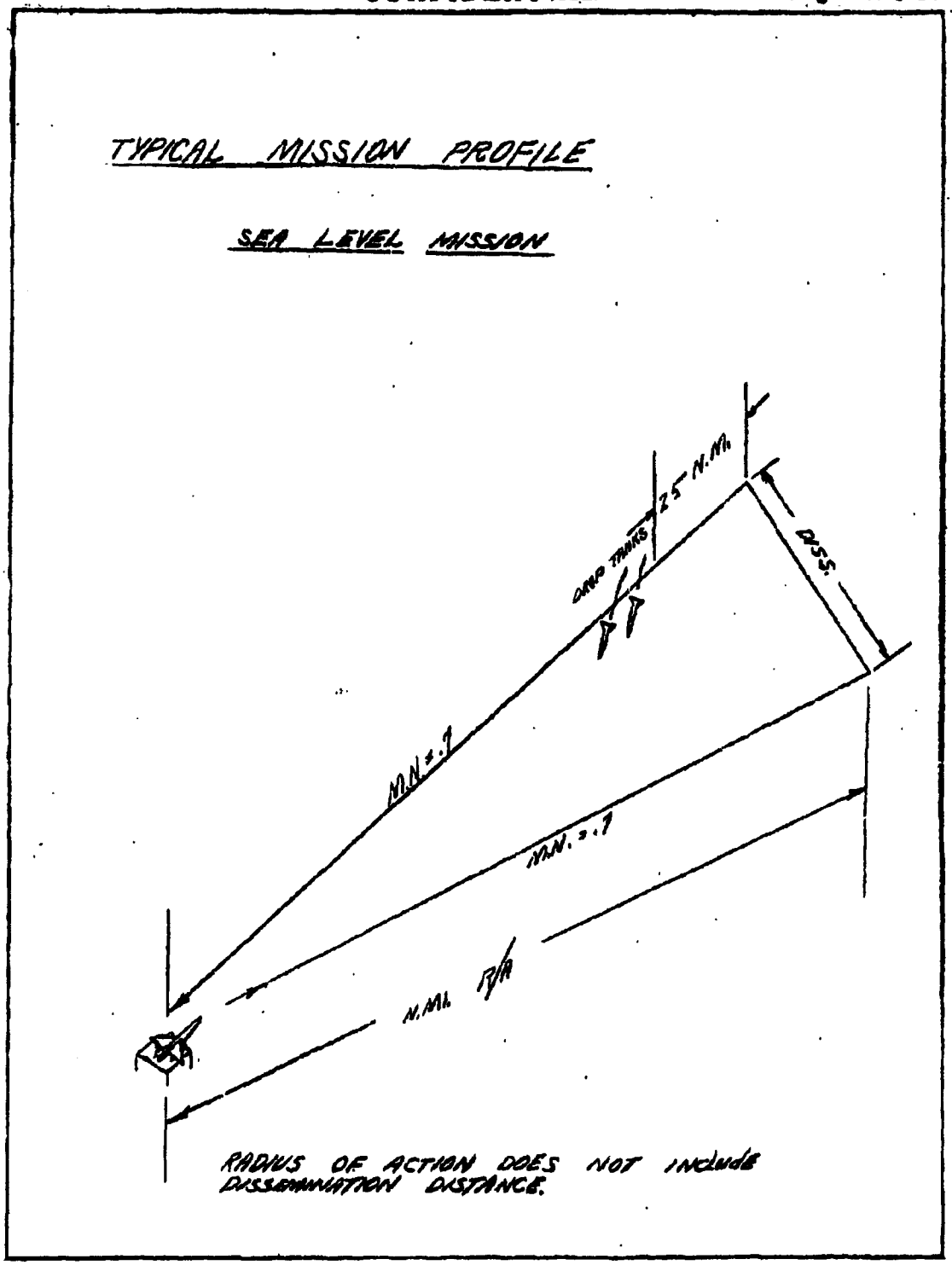

4-6. Typical Mission Profile (Sea Level)

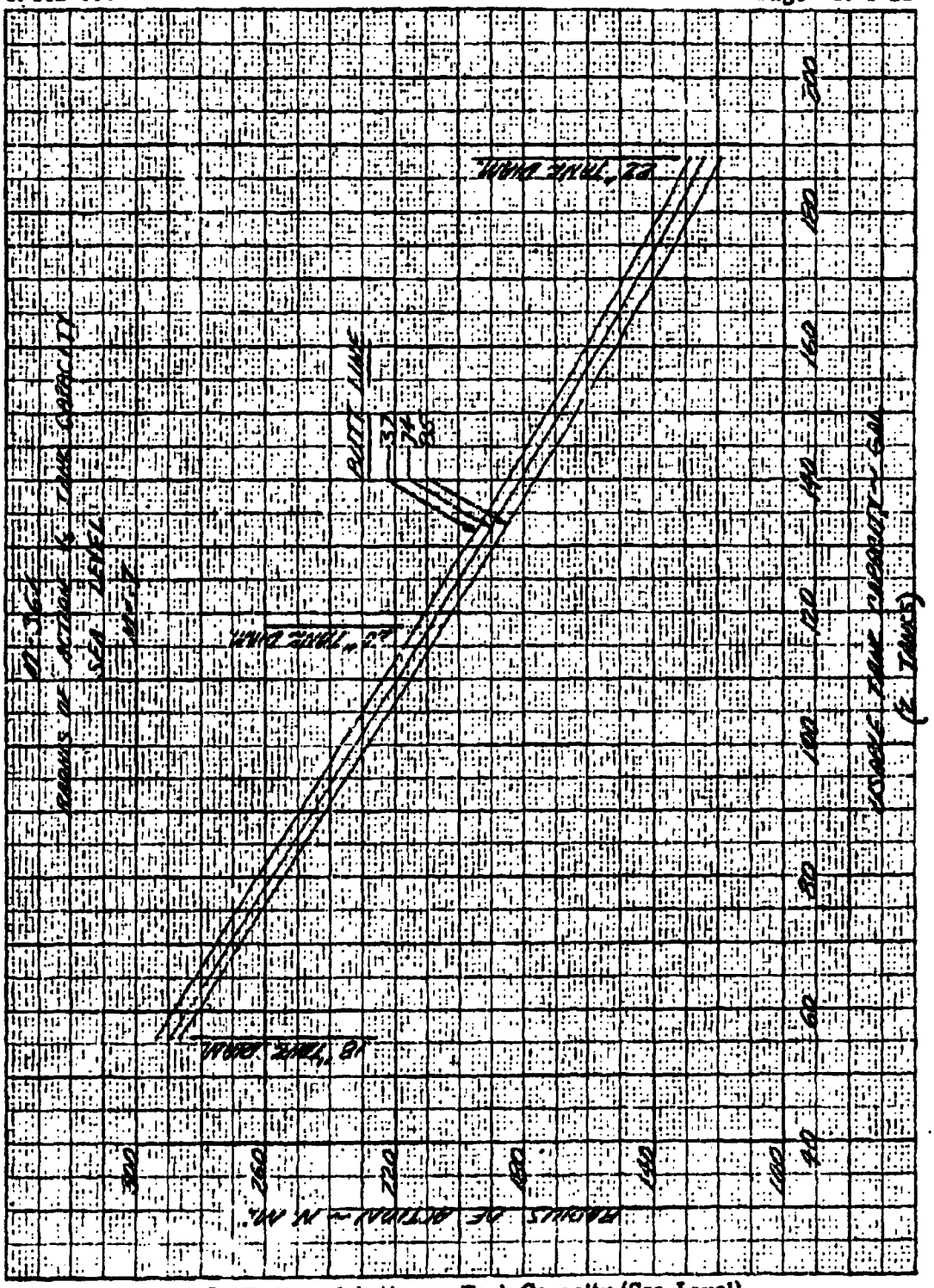

4-7. Radius of Action vs Tank Capacity (Sea Level)

~~CONFIDENTIAL~~

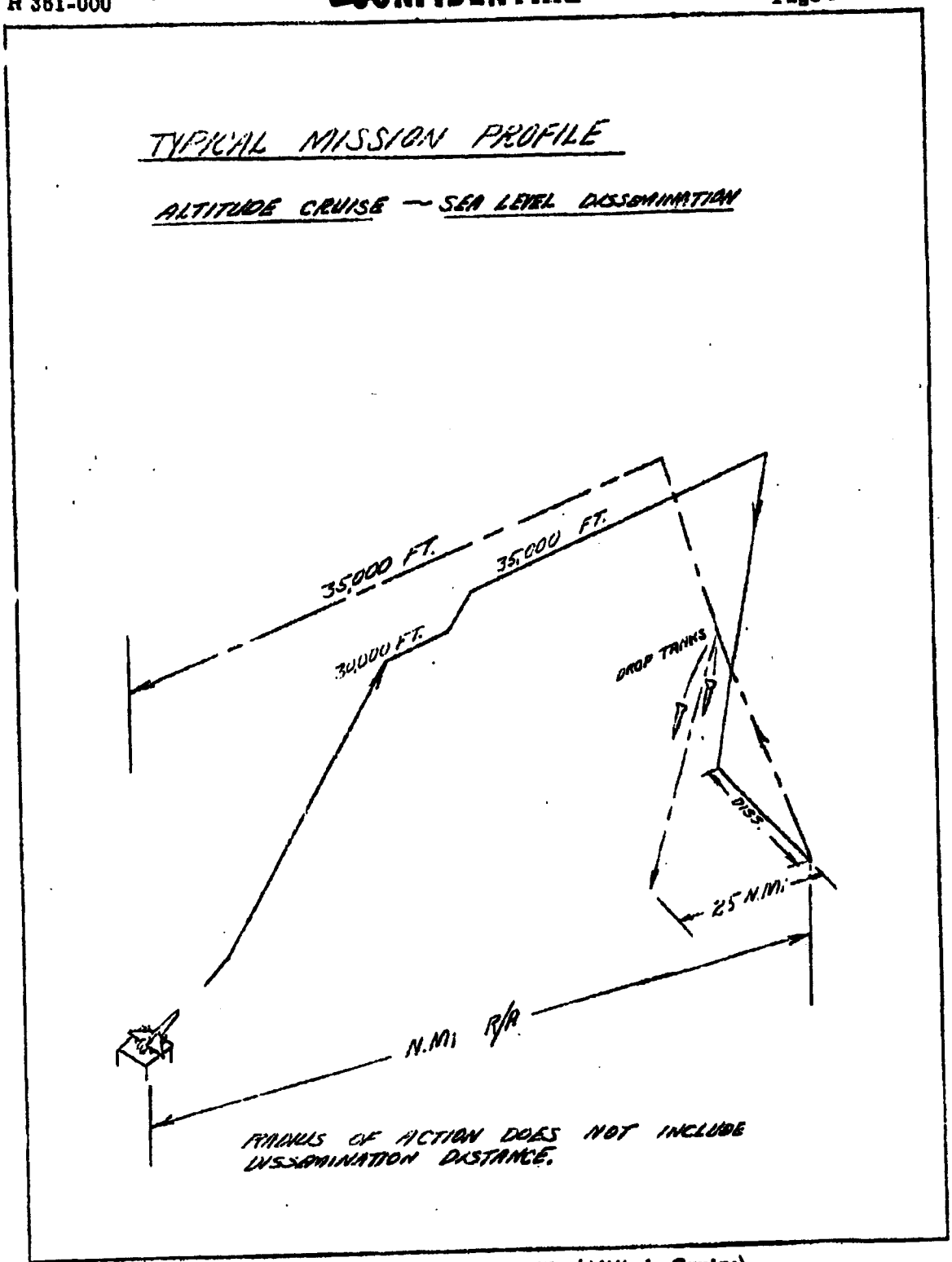

4-8. Typical Mission Profile (Altitude Cruise)

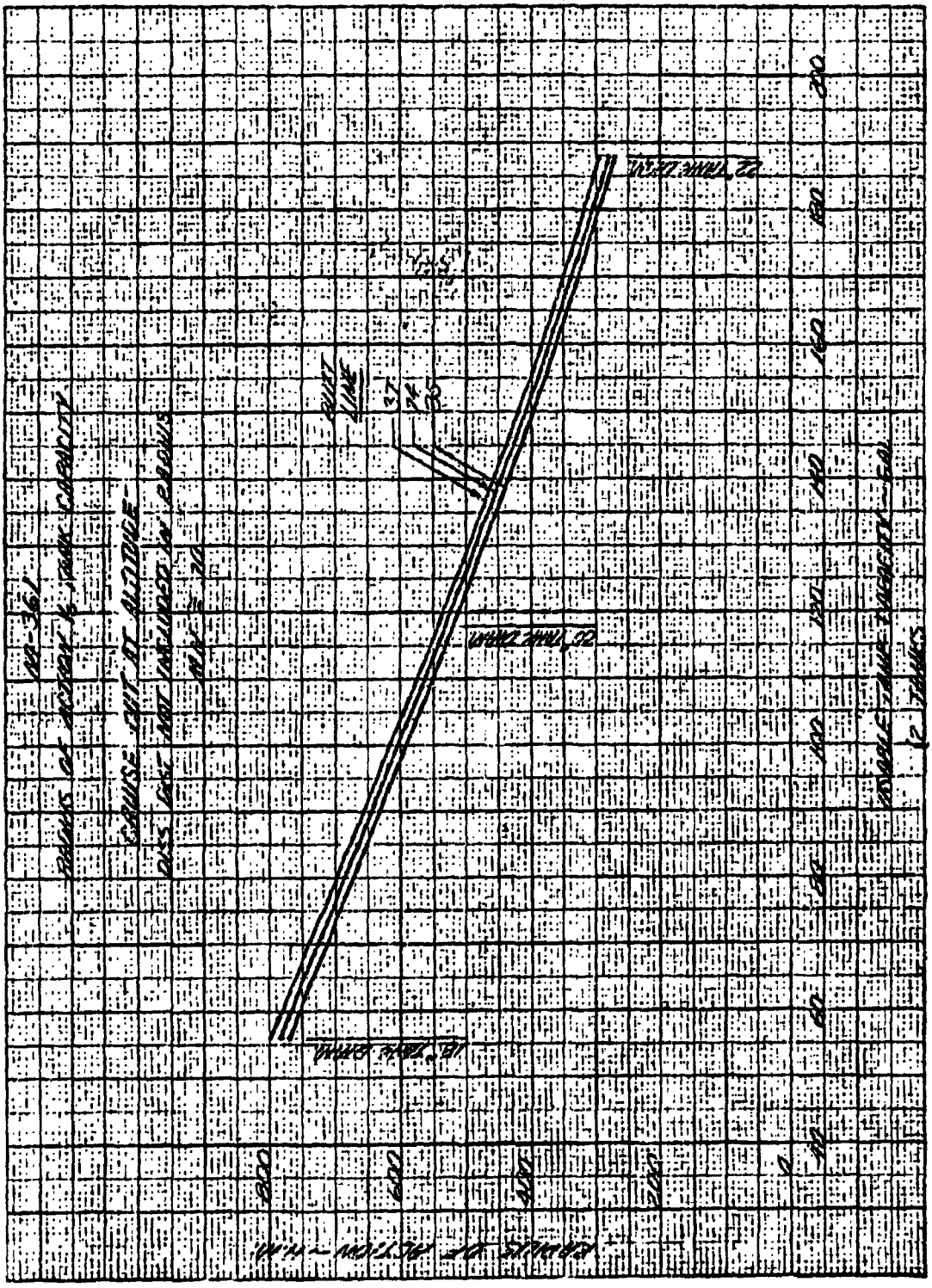

4-9. Radius of Action vs Tank Capacity (Cruise Out at Altitude)

SECTION 4. FACTUAL DATA (Continued)

4.1.2 STATIC STABILITY AND CONTROL CHARACTERISTICS

A brief static stability and control analysis was made of the various tank configurations in order to determine their feasibility. The study was made without consideration of aeroelastic effects. The results are given below.

4.1.2.1 Longitudinal

The addition of tanks with horizontal fins is estimated to produce a forward shift of the neutral point as much as 3.5% MAC (see Figure 4-10). The greatest effect is obtained with the large tanks in the outboard location. The shift in neutral point will be handled by restricting the aft c.g. limit. This solution is expected to introduce problems in c.g. control. It is recommended that horizontal fins be used to minimize the adverse effect of tanks on longitudinal stability.

No control problems are indicated based on static considerations.

4.1.2.2 Lateral-Directional.

The static directional stability parameter, C_{n_β} is reduced significantly when tanks without vertical fins are added to the basic AN/USD-5 (XE-1) configuration. See Figure 4-10. Further study may indicate the desirability of adding vertical fins to the tanks.

Lateral control is sufficient to handle unsymmetrical dissemination of agent.

4.1.2.3 General.

The changes to the AN/USD-5 (XE-1) stability and control characteristics become greater as the tanks are moved outboard on the wing; however, the results of this static analysis has not indicated any insurmountable difficulties.

The results of a brief lateral dynamic-stability study indicate a potential problem at V = 200 kts. The lateral oscillation is damped, but large rudder to sideslip angle ratios are required to control the motion.

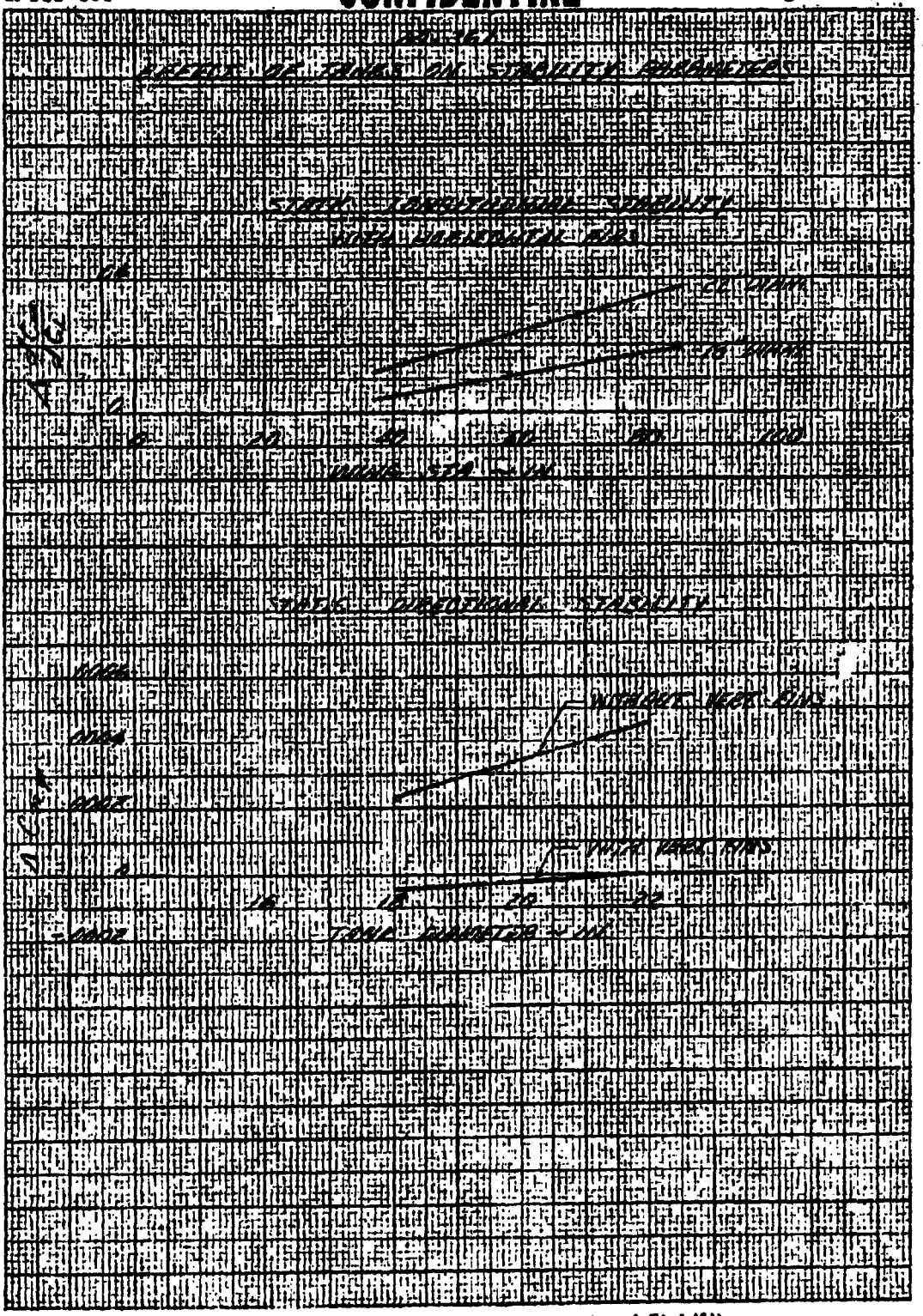

4-10. Static Longitudinal and Directional Stability

REPORT NO. R 361-000 FAIRCHILD Aircraft and Missiles Div. OF FAIRCHILD ENGINE & AIRPLANE CORPORATION			PAGES PAGE 4-18
MODEL M-361	DEPARTMENT R. N. Rothenberger	CHECKED BY R. H. Putnam	APPROVED BY E. E. Morton
SUBJECT:- Study of Compatibility of External Wing-Mounted BW Stores with the AN/USD-5 (XE-1) Drone			DATE May 26, 1961 REVISED

SECTION 4. FACTUAL DATA (Continued)

4.1.3 STRESS

4.1.3.1 Structural Modifications Required to Fuselage

For all stores at all locations on the wing the fuselage bending moments and shears are higher than the design values for the AN/USD-5 (XE-1). The area affected is between Station 207.5 and 259.5. Therefore, there will be some changes in the longerons and shear panels in this area.

For the 1383 lb store at either B.L. 85 or B.L. 74, the tie bar in the fuselage frame at the front spar (Station 207.5) must be increased in size.

For all stores there may be a slight change in the fasteners where the rear spar fitting attaches to the fuselage lower longeron.

4.1.3.2 Structural Modifications Required to Wing

For all stores at all locations on the wing it is necessary to increase the strength of the root rib at the joint where the leading edge portion attaches to the main portion of the rib.

For all stores at B. L. 37 the existing fuel bulkhead must be converted into a structural rib.

For all stores at B. L. 74 or B. L. 85 a structural rib must be added.

For the 1011 lb store at B. L. 74 an 0.02 inch doubler must be added to the wing skin for 10 inches inboard of the rib.

For the 1383 lb store at B. L. 74 an 0.03 inch doubler must be added to wing skin for 10 inches inboard of the rib.

For the 1011 lb store at B. L. 85 an 0.02 inch doubler must be added to the wing skin for 10 inches inboard of the rib.

For the 1383 lb store at B. L. 85 the wing skin gage must be increased from the existing 0.06 inch thickness to 0.07 (an 0.01 inch increase) from B. L. 85 to the root rib, and an 0.03 inch doubler must be added for 10 inches inboard of B. L. 85.

For all stores at B. L. 85 and B. L. 74 the front spar fitting would have to be changed slightly to add more material.

SECTION 4. FACTUAL DATA (Continued)

4.1.3.2 Structural Modifications Required to Wing (Continued)

For all stores at B. L. 74 or B. L. 85, a swept pylon is required because the store c.g. is so far forward in relation to the wing section. A swept pylon is far more complex than a straight pylon from both a design and a manufacturing standpoint and, due to the fact that the c.g. is so far forward in relation to the wing section, the greatly increased moments and torques require much heavier structure in the pylon.

SECTION 4. FACTUAL DATA (Continued)

4.1.4 THERMODYNAMICS.

4.1.4.1 J-60 Turbojet Engine Estimated Jet Wake Diagram

An estimated jet wake diagram on the J-60 turbojet engine, based on sea-level condition and M = 0.7, was obtained by cross-plotting Pratt and Whitney data for other conditions and is, in the opinion of Thermodynamics, conservative for the purpose since it does not account for the effects of the secondary air-flow in the cooling ejector. See Figure 4-11. The cooling ejector is part of the basic design of the AN/USD-5 (XE-1) in all its versions.

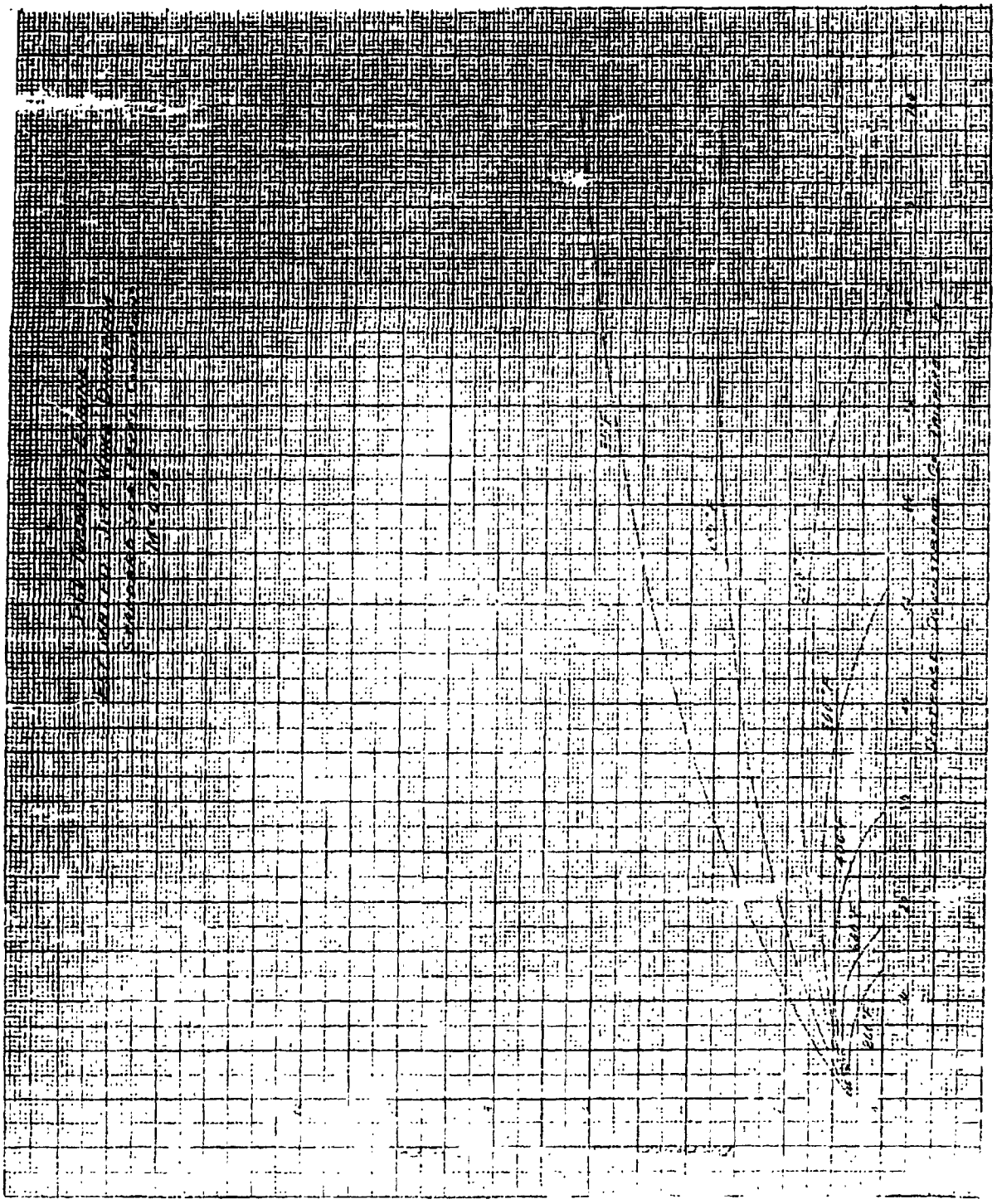

4-11. J-58 Turbojet Engine Estimated Jet Wake Diagram

SECTION 4. FACTUAL DATA (Continued)

4.1.5 WEIGHTS.

4.1.5.1 Basis for Analysis.

a. Maximum launch gross weight shall be 10,800 lb.

b. Basic drone shall be the operational AN/USD-5 (XE-1).

c. Agent tanks shall be full (96%) for launch.

d. Fuel tanks shall be partially full for launch.

e. C. G. of all external stores shall be at F. S. 228.0 (20.9 % MAC). Refer to Figure 4-14.

f. Maximum diameter of tank at B. L. 37.0 shall be 22 inches.

g. Pylon constant for all tank diameters at a given butt line location.

4.1.5.2 Applied Changes to Operational AN/USD-5 (XE-1) Drone. Refer to Figure 4-13.

a. Add circuitry in guidance and electrical systems for stores functions.

b. Revise wing fuel plumbing to provide for partially filled wing fuel tanks at launch.

c. Add beef-up in skin panels and longerons (F. S. 187-270) of fuselage to sustain increase in bending loads.

d. Wing structural beef-up is required and varies with agent tank size and location as follows:

(1) All conditions require changes to root rib joints and the rear spar fitting.

(2) For all stores at B. L. 37 the existing fuel bulkhead must be converter into a structural rib.

(3) For all stores at B. L. 74 a structural rib and local skin doublers must be added.

(4) For the 18 and 20-inch diameter tanks at B. L. 85 a structural rib and local skin doublers must be added.

SECTION 4. FACTUAL DATA (Continued)

4.1.5.2 Applied Changes to Operational AN/USD-5 (XE-1) Drone. (Refer to Figure 4-13) (Continued)

(5) For the 20-inch diameter tank at B. L. 85 a structural rib will be added and the wing skin increased by 0.01 inches from the root rib to B. L. 85 rib.

(6) Design of the structural ribs at B. L. 37, 74 and 85 is based on the 22-inch diameter tank.

e. A straight pylon can be used from B. L. 37 thru B. L. 60.5 and the weight is estimated as a constant. For all stores outboard of B. L. 60.5 a canted pylon is required because the tank center of gravity is projected forward of the wing by the sweep back of the wing leading edge and the pylon becomes far more complex and heavier. Figure 4-12 shows the influence of the pylon weight on the expendable stores configuration and Figure 4-13 reflects the penality to the empty drone weight.

4.1.5.3 Summary Build Up of Drone Gross Weight.

Refer to Table II for the summary build up of drone gross weight from the AN/USD-5 (XE-1) weight empty to the M-361 launch gross weight.

4.1.5.4 Longitudinal Balance.

Longitudinal balance of the nine recovery gross weight conditions falls between 22 and 23% MAC and appears to be satisfactory. Until such time that c.g. envelopes can be established, it is assumed that the longitudinal centers of gravity for flight can be satisfied by selective placement and programming of the drone fuel.

4.1.5.5 Alignment Angle.

The effect of agent tank size, agent tank location and placement of drone fuel on the booster alignment angle has not been included in this phase of study. Once a configuration has been selected, booster alignment will be resolved.

~~CONFIDENTIAL~~

REPORT NO. R361-000 | FAIRCHILD Aircraft and Missiles Div. OF FAIRCHILD ENGINE & AIRPLANE CORPORATION | PAGES | PAGE 4-22

MODEL M-361 | PREPARED BY R. N. Rothenberger | CHECKED BY R. H. Putnam | APPROVED BY E. E. Morton

SUBJECT:- Study of Compatibility of External Wing-Mounted BW Stores with the AN/USD-5 (XE-1) Drone

DATE: May 26, 1961

REVISED

TABLE II. GROSS WEIGHT SUMMARY

	B.L. 37.0			B.L. 74.0			B.L. 85.0		
Basic AN/USD-5 (XE-1) (Calc.) Per/Nov/11/60	4495	4495	4495	4495	4495	4495	4495	4495	4495
M-361 Modifications (Est)	65	65	65	93	93	93	101	101	123
Electrical System	4	4	4	4	4	4	4	4	4
Guidance System	1	1	1	1	1	1	1	1	1
Fuel System	10	10	10	10	10	10	10	10	10
Fuselage Structure	10	10	10	10	10	10	10	10	10
Wing Structure	40	40	40	68	68	68	76	76	98
Total Empty Weight	4560	4560	4560	4588	4588	4588	4596	4596	4618
Fuel - Unusable	50	50	50	50	50	50	50	50	50
Total Recovery G.W.	4610	4610	4610	4638	4638	4638	4646	4646	4668
Fuel - Usable	3531	2855	2111	3481	2805	2061	3445	2769	2003
Stores - Expendable	1426	2102	2846	1448	2124	2868	1476	2152	2896
Pylon (2)	80	80	80	102	102	102	130	130	130
Tank (2)	880	1040	1200	880	1040	1200	880	1040	1200
Agent 8.33 lb/Gal	466	982	1566	466	982	1566	466	982	1566
Total Drone G.W. (less booster)	9567	9567	9567	9567	9567	9567	9567	9567	9567
Booster	1300	1300	1300	1300	1300	1300	1300	1300	1300
Total Drone G.W. (plus booster)	10867	10867	10867	10867	10867	10867	10867	10867	10867
Booster Drop Off G.W. (level attitude)									
- Wt. - lb									9500
- I_{xo} (roll) - slug-ft^2									7513
- I_{zo} (yaw) - slug-ft^2									16646
- P_{xozo} - slug-ft^2									- 160
Agent Tanks Empty G.W. (level attitude)									
- Wt. - lb									6487
- I_{xo} (roll) - slug-ft^2									3464
- I_{zo} (yaw) - slug-ft^2									11063
- P_{xozo} - slug-ft^2									- 79
Tank Dia. - inches	18	20	22	18	20	22	18	20	22
Length - inches	153	170	187	153	170	187	153	170	187
Volume - gal (to outside skin contour)	105	145	190	105	145	190	105	145	190
Volume - gal (usable)	28	59	94	28	59	94	28	59	94

~~CONFIDENTIAL~~

S-800-23A

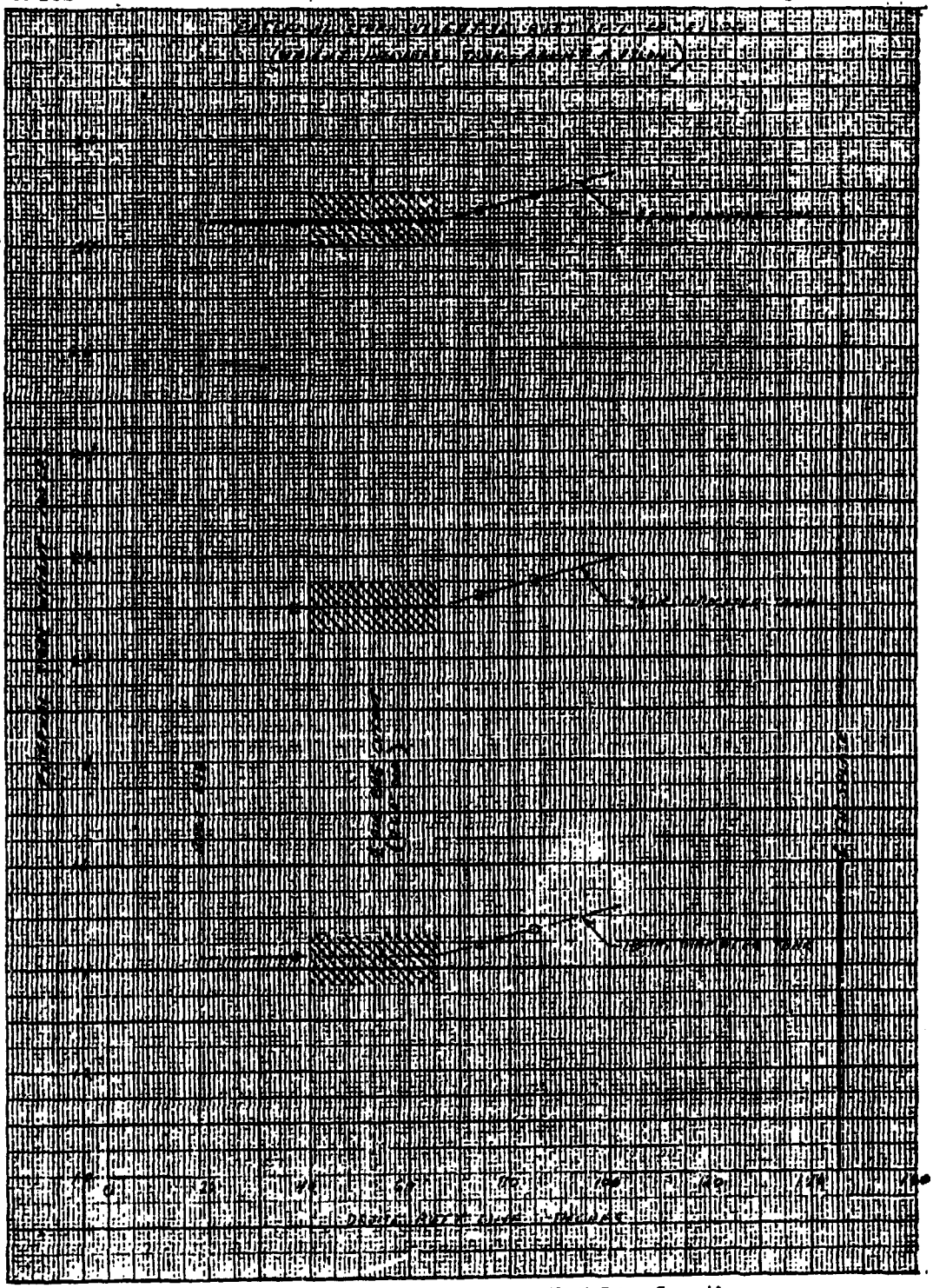

4-12. External Store Weight vs Butt Line Location

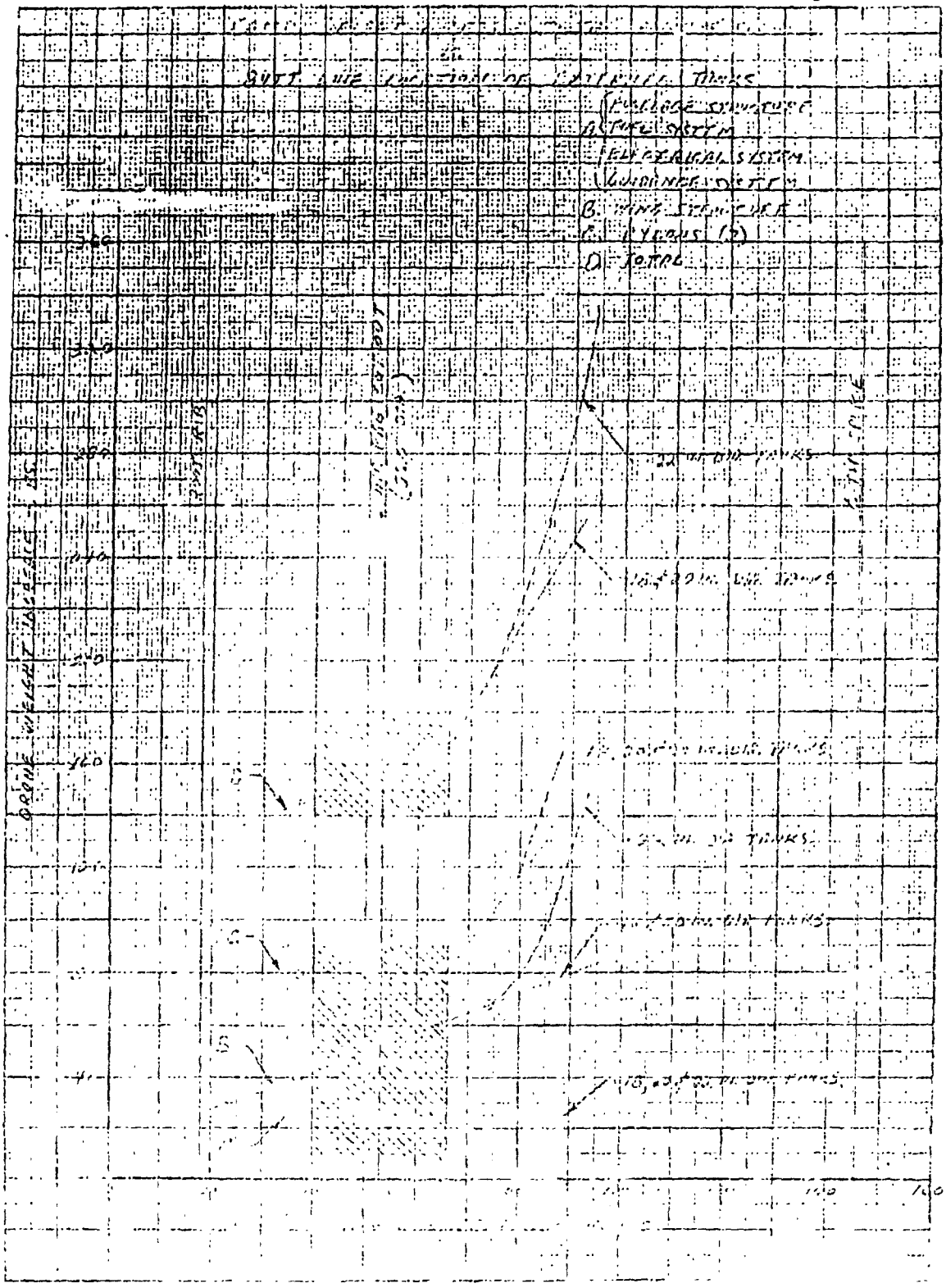

Figure 4-5 Drone vs Putt Line Location of Personnel Parks

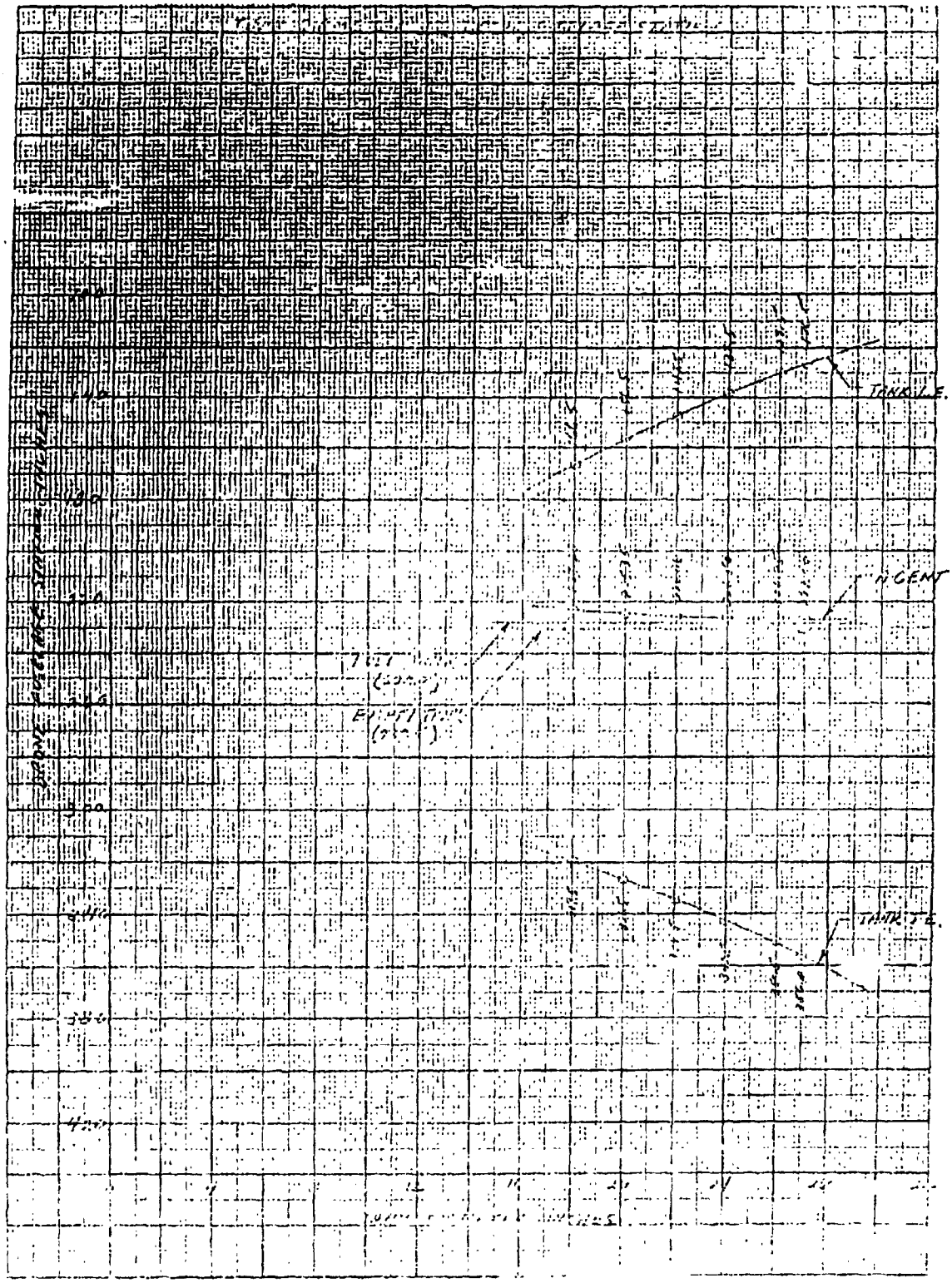

4-1. Tank Diameter vs Drone Fuselage Station

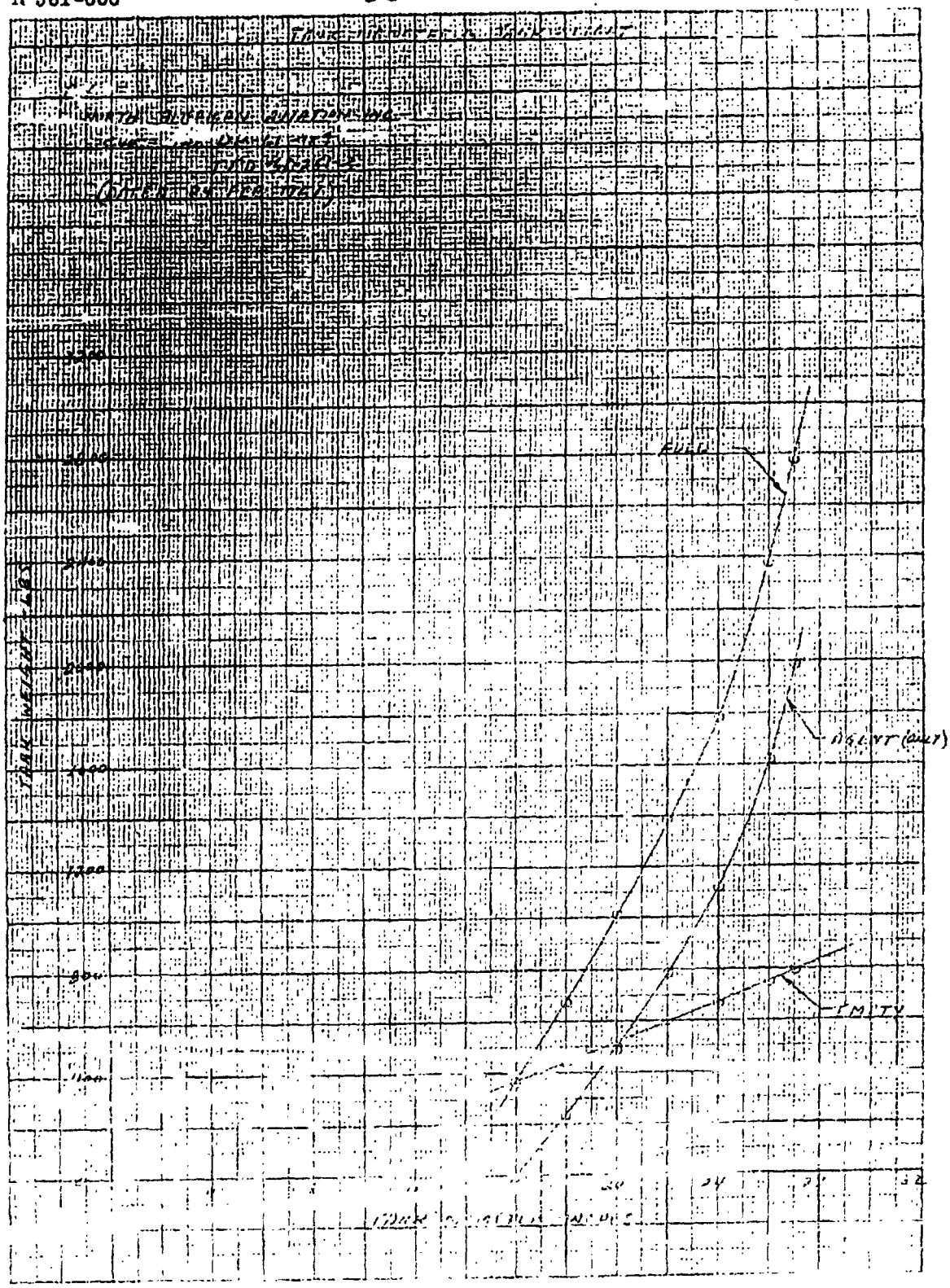

4-15. Tank Diameter vs Tank Weight

REPORT NO. R 361-000 FAIRCHILD Aircraft and Missiles Div. OF FAIRCHILD ENGINE & AIRPLANE CORPORATION			PAGES PAGE 4-27
MODEL M-361	PREPARED BY R. N. Rothenberger	CHECKED BY R. H. Putnam	APPROVED BY E. E. Morton
SUBJECT:- Study of Compatibility of External Wing-Mounted BW Stores with the AN/USD-5 (XE-1) Drone			DATE May 26, 1961 REVISED

SECTION 4. FACTUAL DATA (Continued)

4.2 STUDY OF SELECTED CONFIGURATION - PHASE II

4.2.1 DESIGN

4.2.1.1 General Arrangement.

The general arrangement and overall dimensions of the M-361 modified drone are shown on Figure 4-16.

4.2.1.2 Mobile Launcher Clearances.

The launcher clearances are given in Figure 4-17. The M-361 modified drone is shown in the launch and also the transport positions.

[redacted]

1

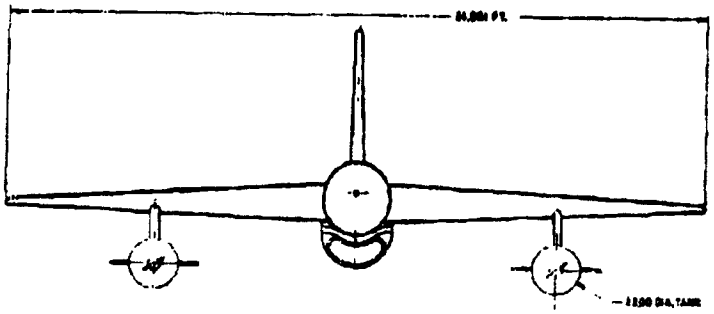

[redacted]

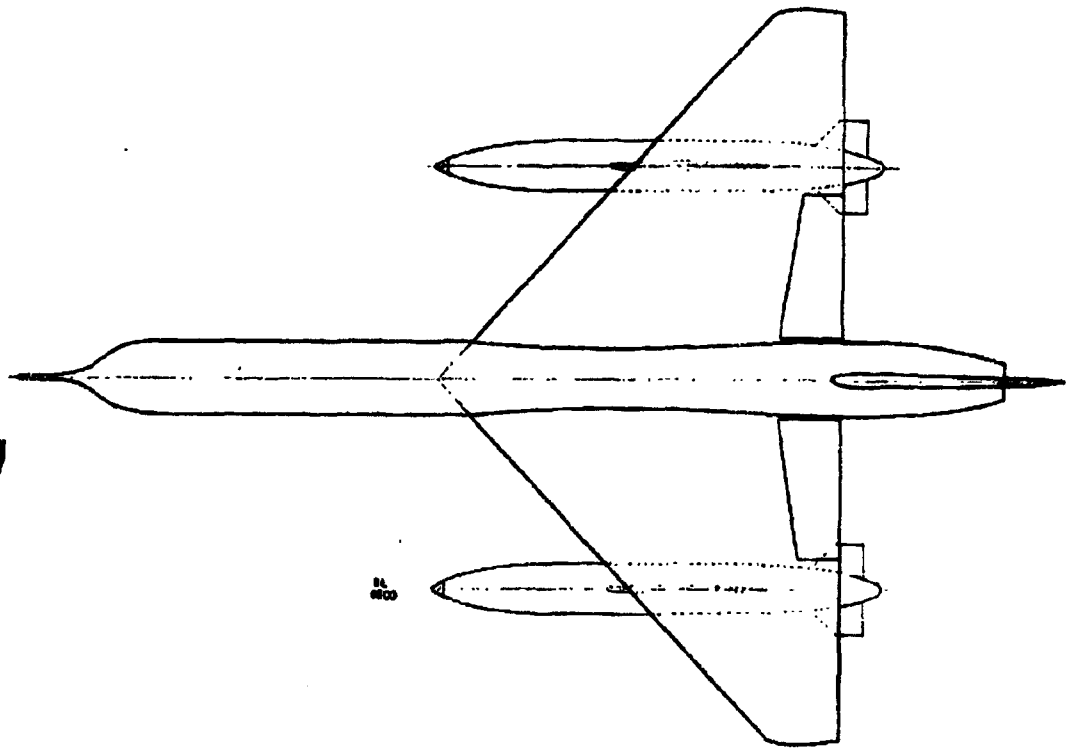

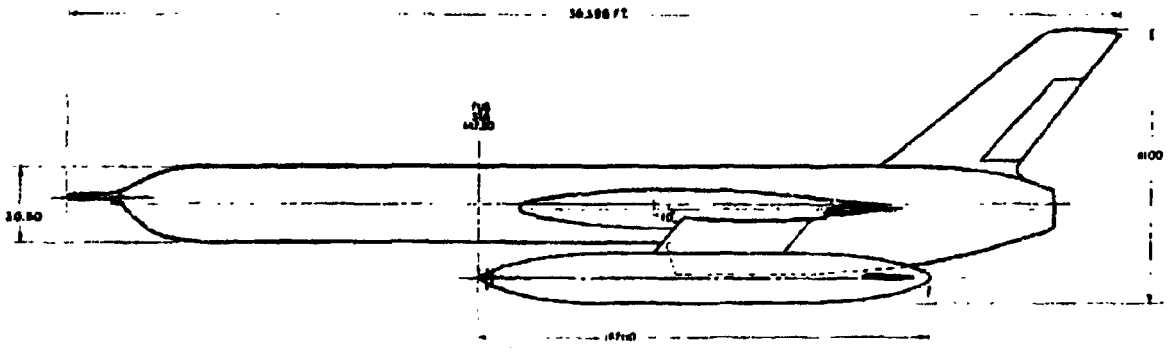

CONFI

Figu

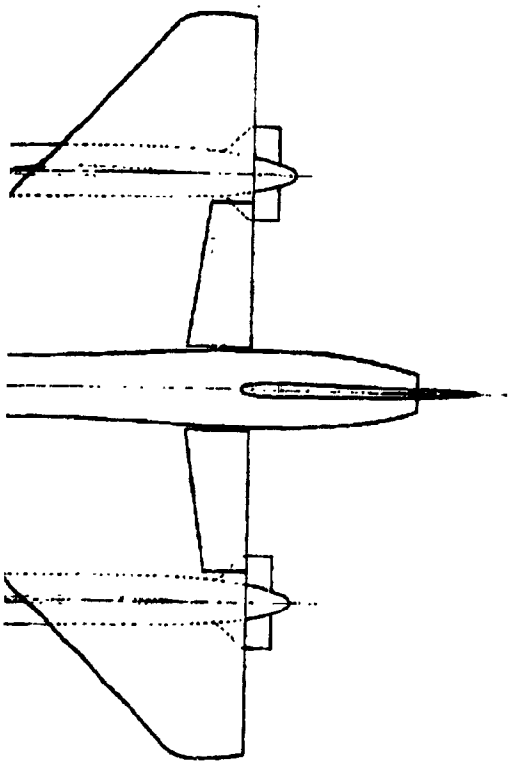

3

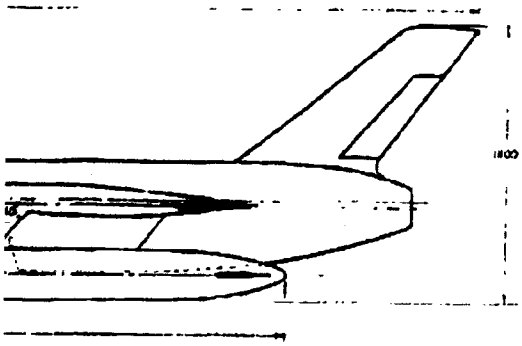

M361 USQ6 MOD
MISSILE
GENERAL
ARRANGEMENT
P361001

Figure 4-16. General Arrangement

Page No.
301-000

CONFIDENTIAL

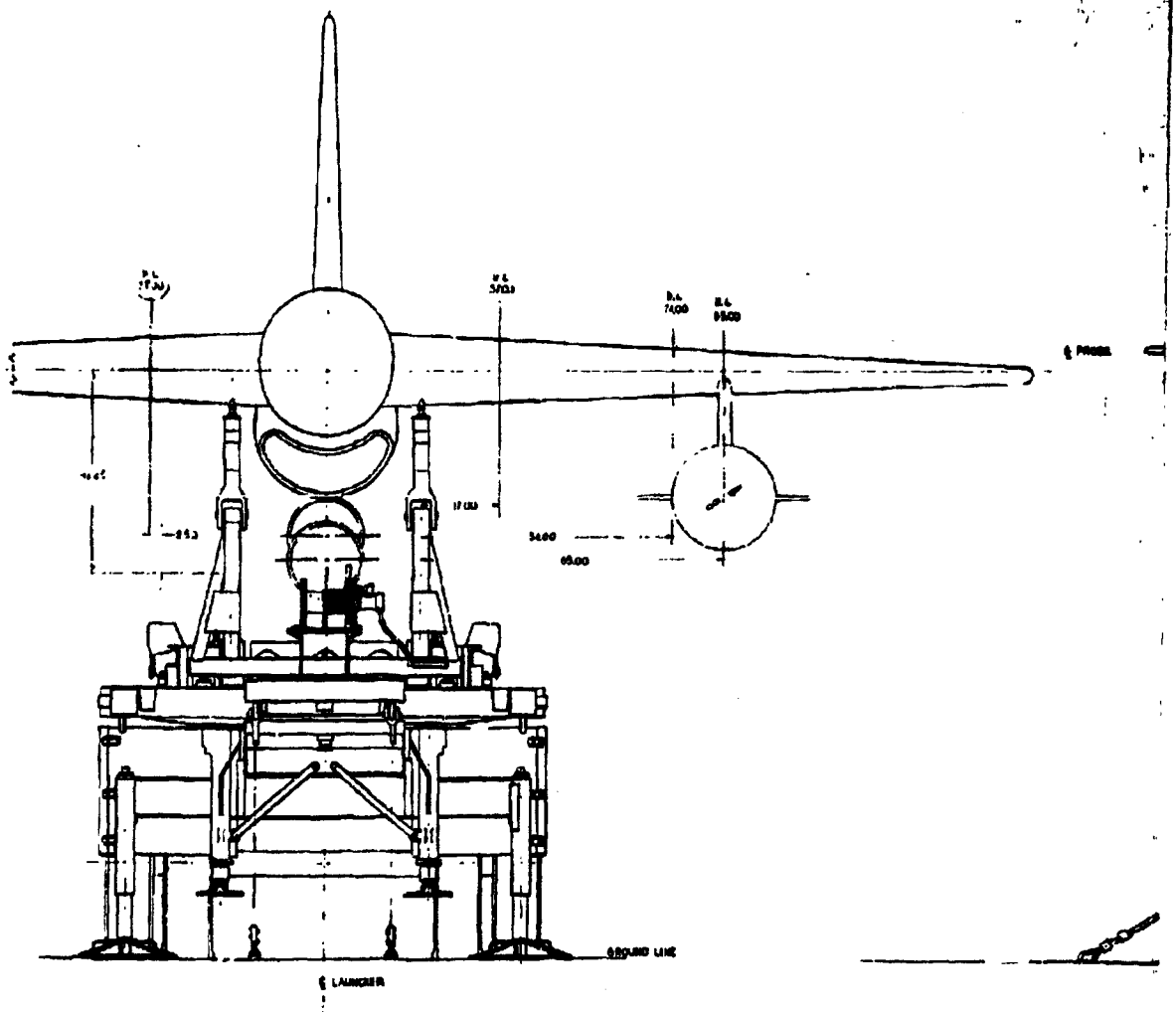

1

CONFIDENTIAL

2

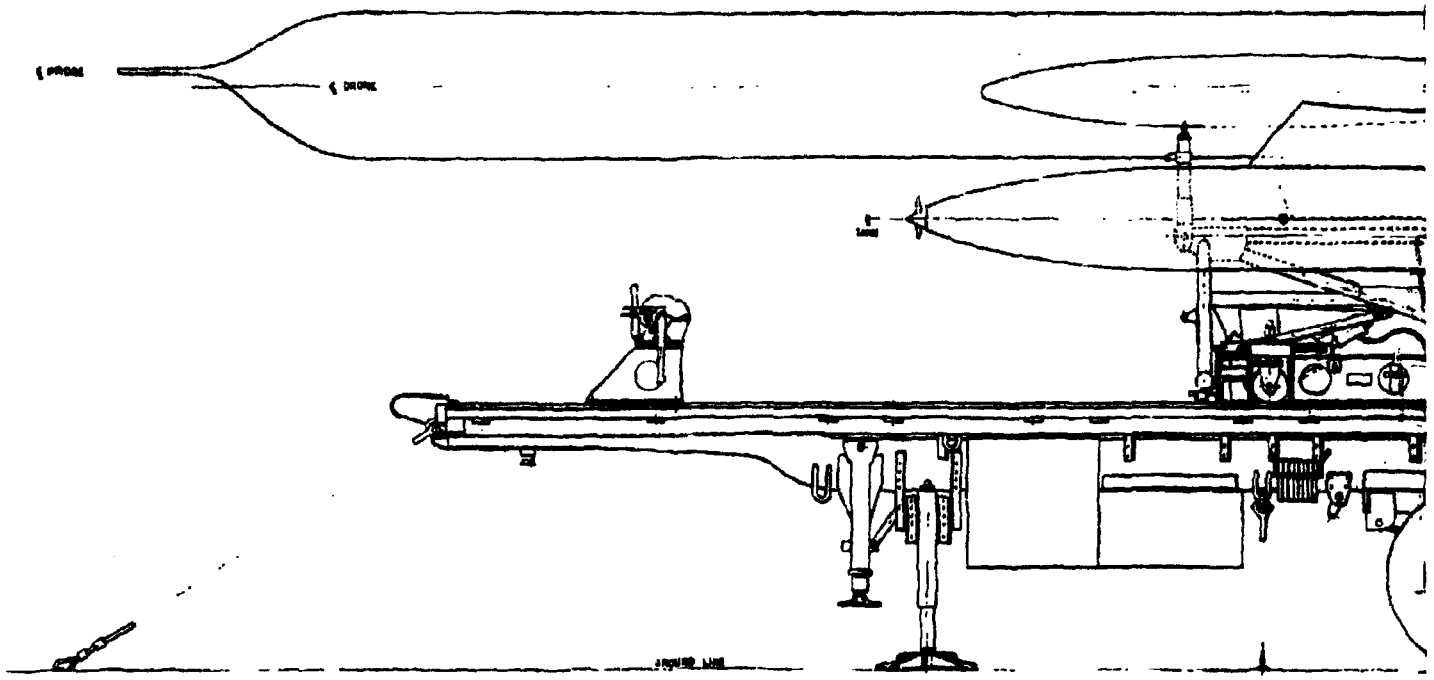

MISSILE IN TRANSPORT POSITION

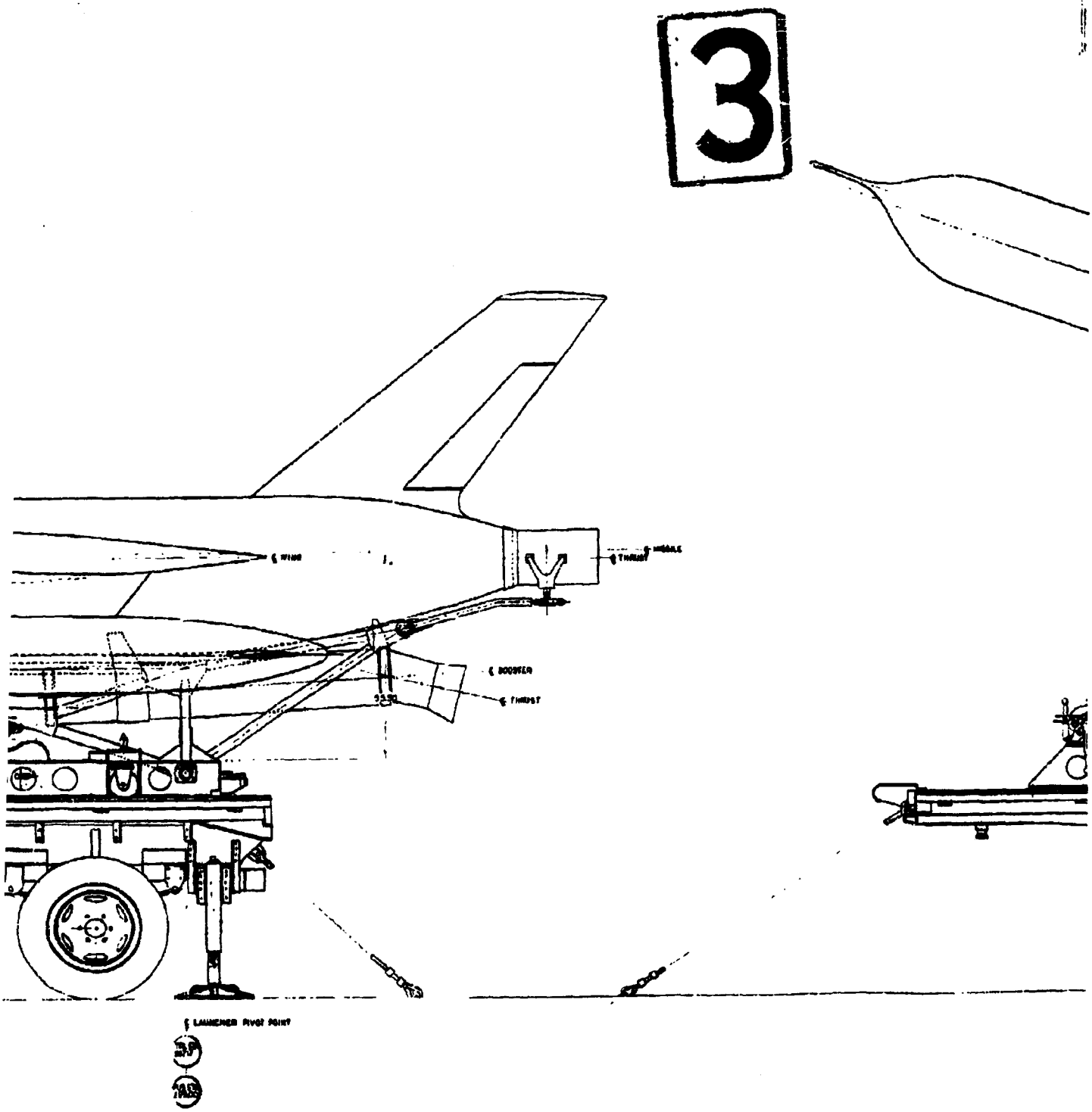

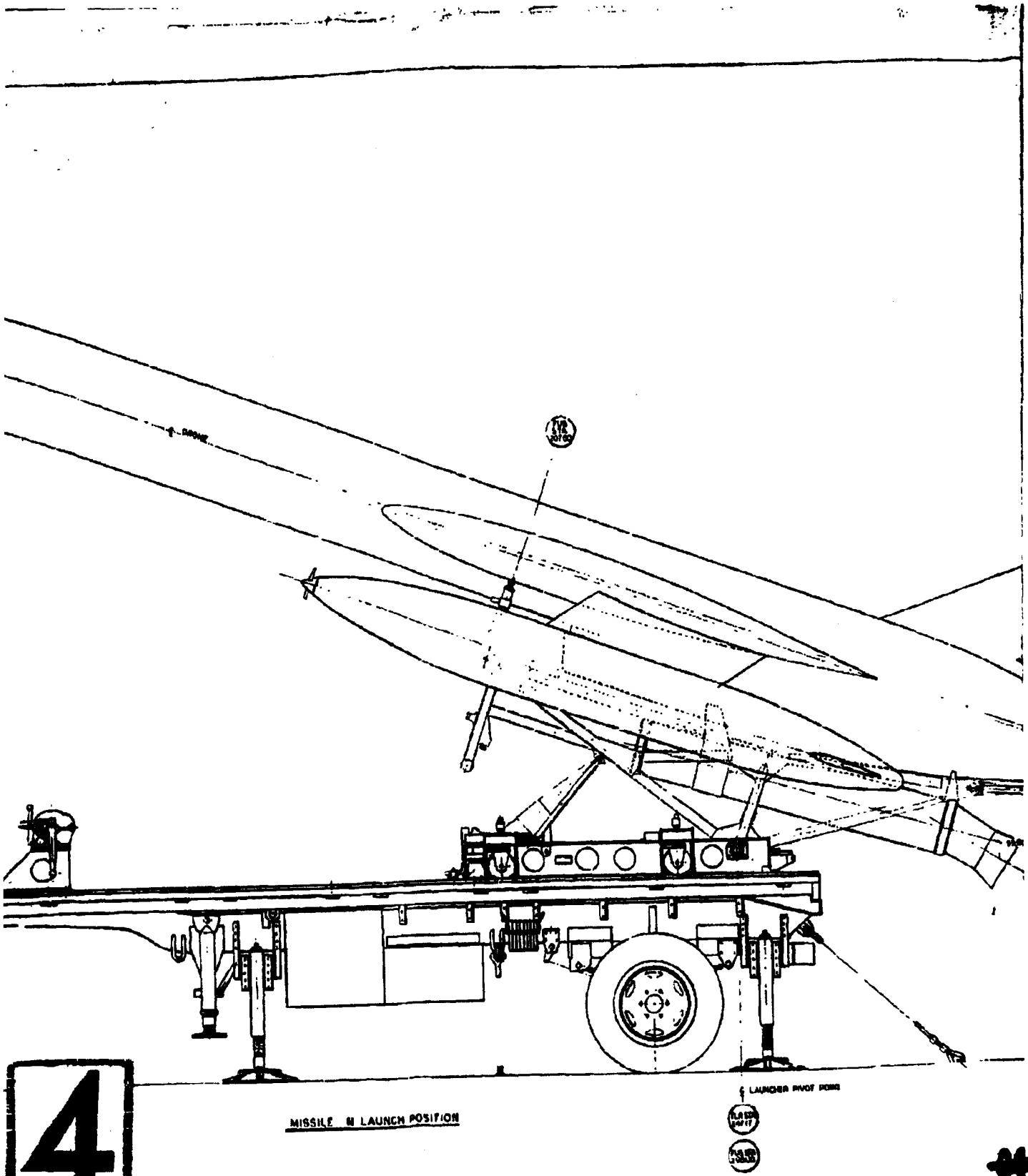

4

MISSILE IN LAUNCH POSITION

CONFIDENTIAL

5

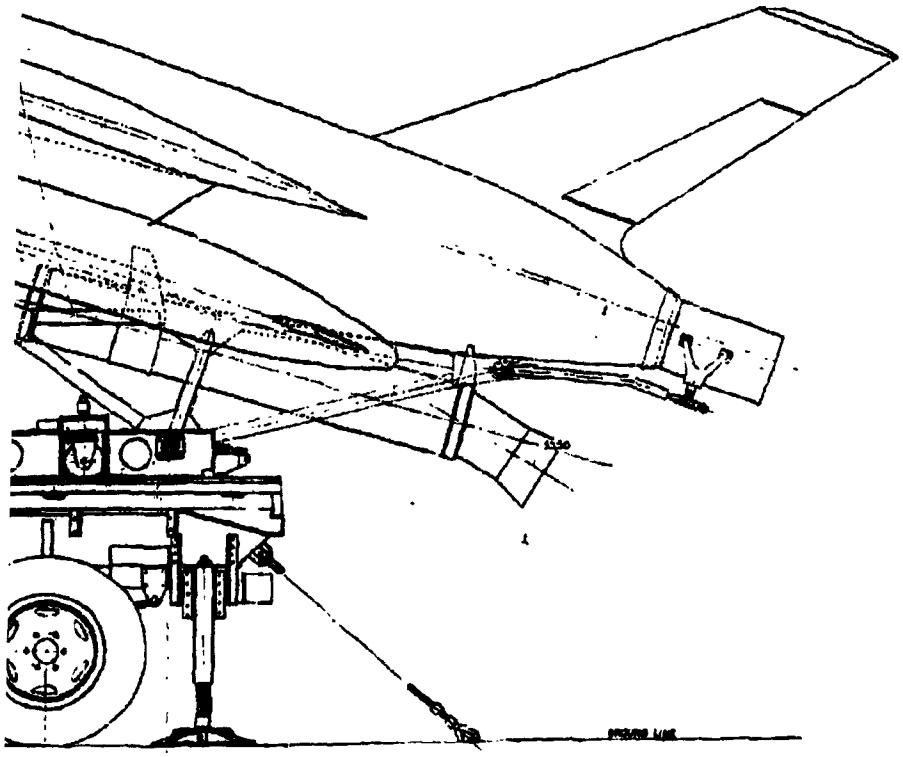

CONFIDENTIAL

Figure 4-17. Launcher Clearances

SECTION 4. FACTUAL DATA (Continued)

4.2.2 FLUTTER STABILITY

The addition of concentrated masses to a wing will generally affect the flutter stability of the wing. The effect can be beneficial in some cases, but often it will adversely affect the flutter speed. No flutter analysis of concentrated masses on the AN/USD-5 (XE-1) wing has been accomplished. Because no simplified method exists for estimating the effects of concentrated masses on a delta wing, a formal flutter investigation must be made before the final design is frozen in regard to spanwise and chordwise location of the external stores center of gravity and flexibility of the pylon mounting structure. Since the AN/USD-5 (XE-1) wing is free from flutter without external stores, it is reasonable to assume that a flutter-free design can be achieved with external stores. A parameter study will be required to obtain the correct pylon flexibility consistent with the requirements for location of the external stores center of gravity.

The only general rule of thumb available in regard to external stores is that the center of gravity should always be forward of the "effective" torsional axis of the wing. The present design does not violate this rule.

SECTION 4. FACTUAL DATA (Continued)

4.2.3 LATERAL STABILITY

4.2.3.1 Lateral Stability Study

The following presents the results of a PACE analog computer study of the lateral stability of the selected configuration, allowing three degrees of freedom. The basic equations of airframe motion are listed below:

In the classical dynamic equations for airframe motion all aerodynamic coefficients are assumed constant for any particular condition of Mach number and gross weight and small angle approximations (i.e., $\cos \alpha = 1$, $\sin \alpha = \tan \alpha = \alpha$ (radians) are employed. The two orientation angle computations are:

$$\dot{\phi} = p$$

$$\dot{\psi} = r$$

Transfer functions of the lateral autopilot used in the simulation are derived from Reference 5.3

$$\phi_r = 1.0 \left[\frac{1}{.05\,S+1}\right] r$$

$$\phi_a = (1.017 + .61\,S) \left[\frac{1}{.05\,S+1}\right] \phi$$

The steering loop has been omitted from the analysis. It is also noted that no coupling between the lateral and longitudinal modes has been considered.

The aerodynamic coefficients are taken from References 5.1 and 5.2.

The configuration investigated was the 22 inch wing tank located at B. L. 86. Gross weights of 6500 lb and 9500 lb at speeds of 0.3 MN and 0.7 MN were chosen as the conditions to be investigated. Weight and Moment of Inertia data are supplied by Reference 5.4.

SECTION 4. FACTUAL DATA (Continued)

4.2.3.1 Lateral Stability Study (Continued)

Step inputs were applied to ϕ, β, p and r individually while the resulting responses were monitored by observing the traces on a brush recorder. The step inputs were as follows:

step input to	magnitude of step
ϕ	+ 10°
β	+ 4°
p	+ .4 rad/sec
r	+.2 rad/sec

The resulting traces, Figures 4-18 thru 4-33, show that the system investigated is stable in the lateral modes for the conditions considered.

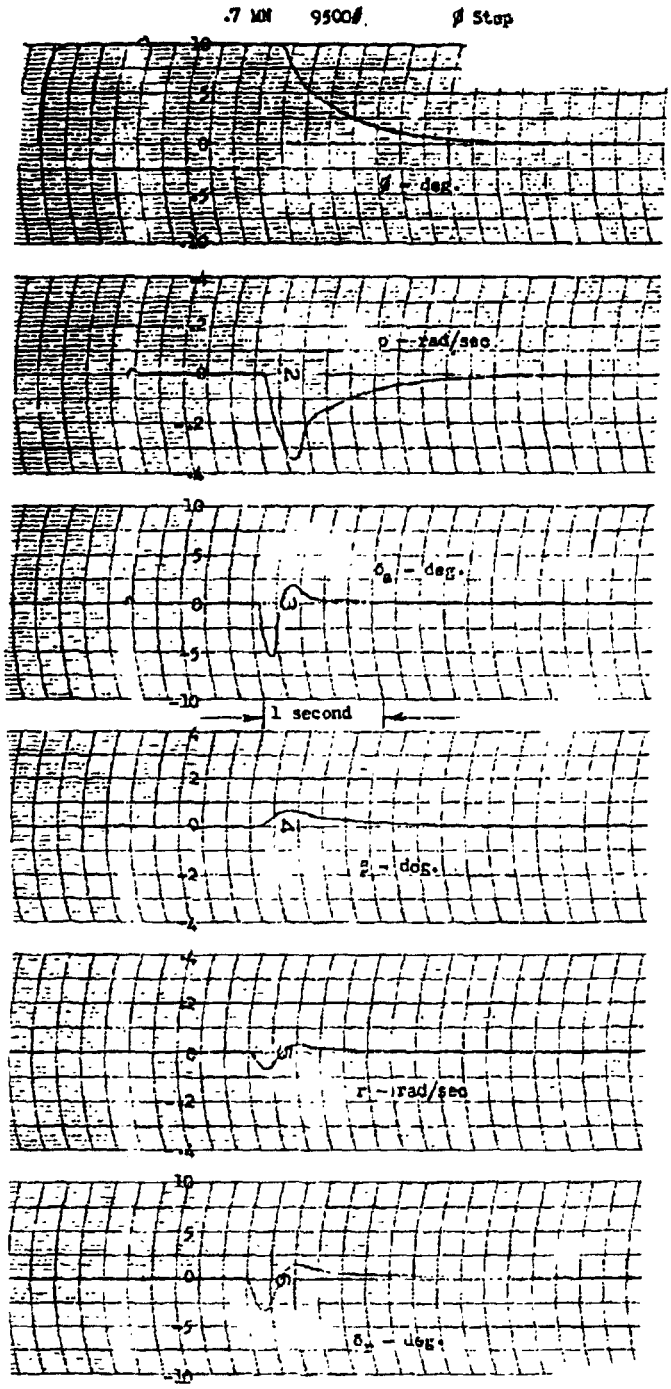

4-18. Lateral Stability Study Result Tracing

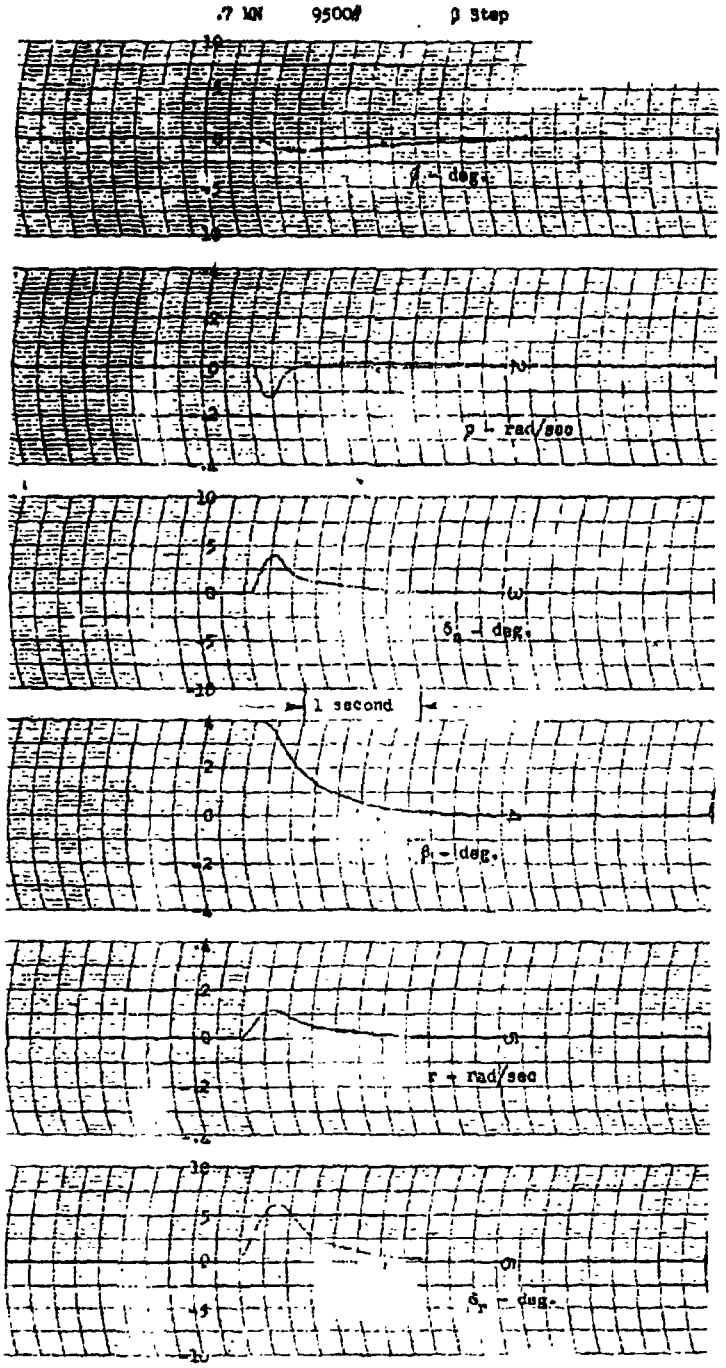

4-19. Lateral Stability Study Result Tracing

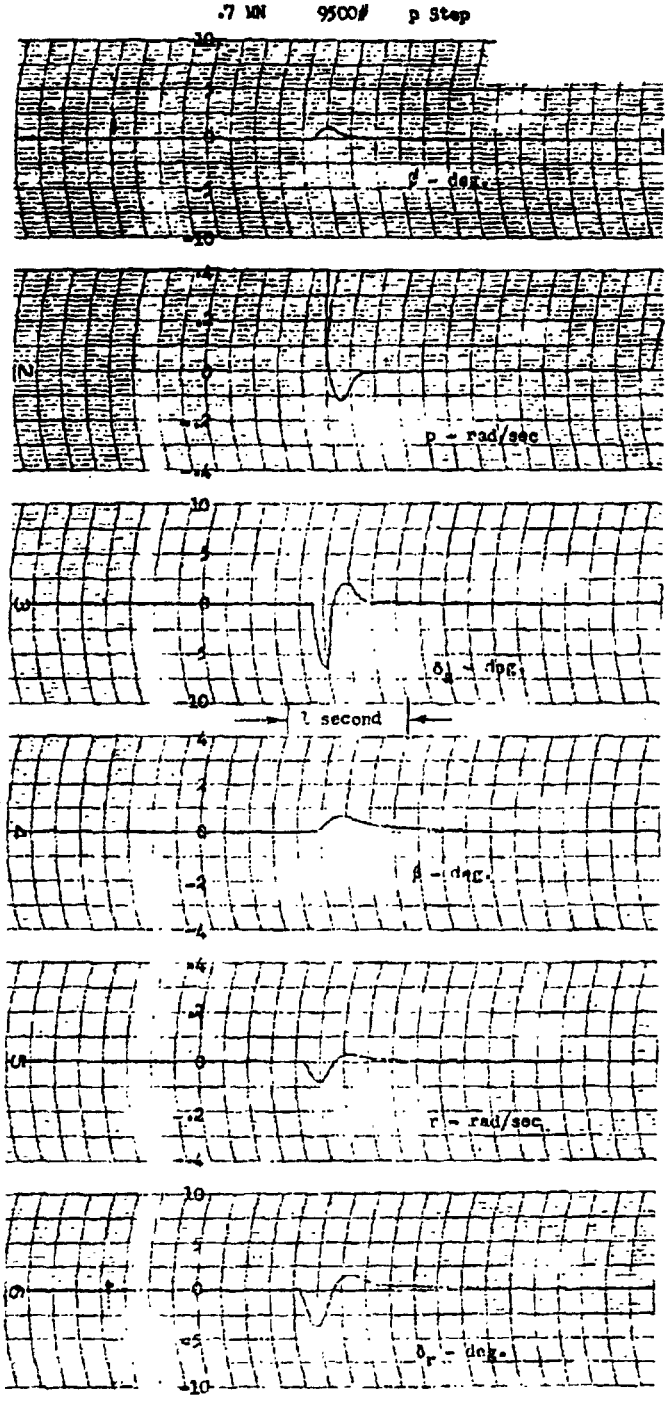

4-20. Lateral Stability Study Result Tracing

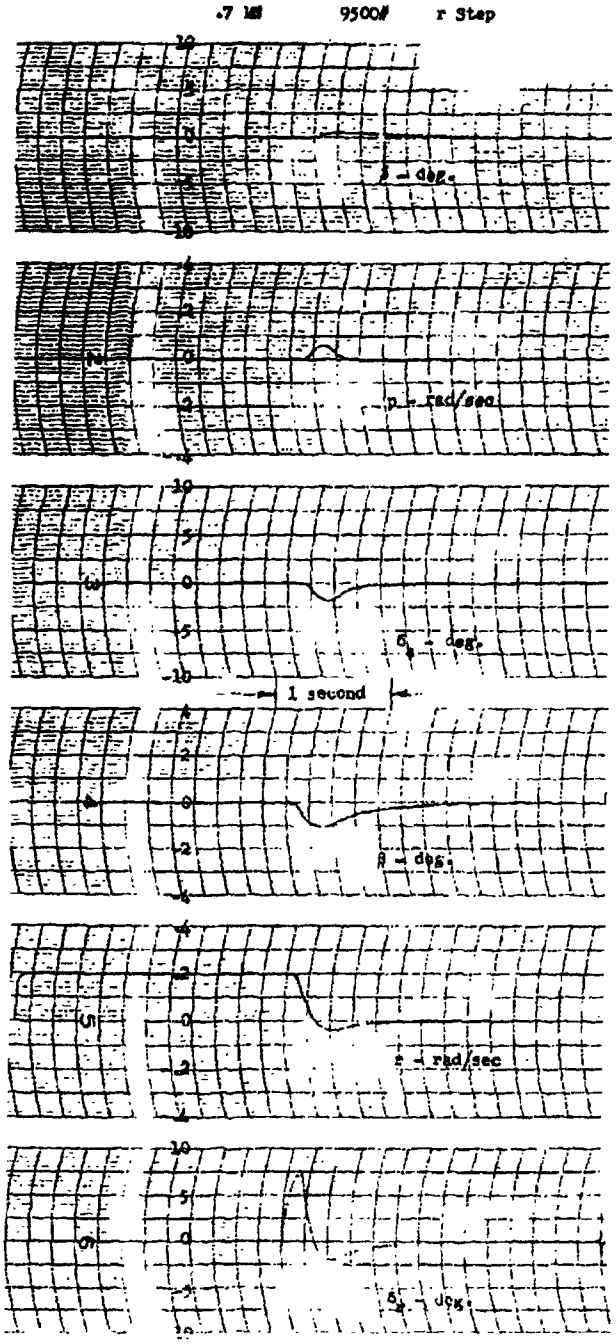

4-21. Lateral Stability Study Result Tracing

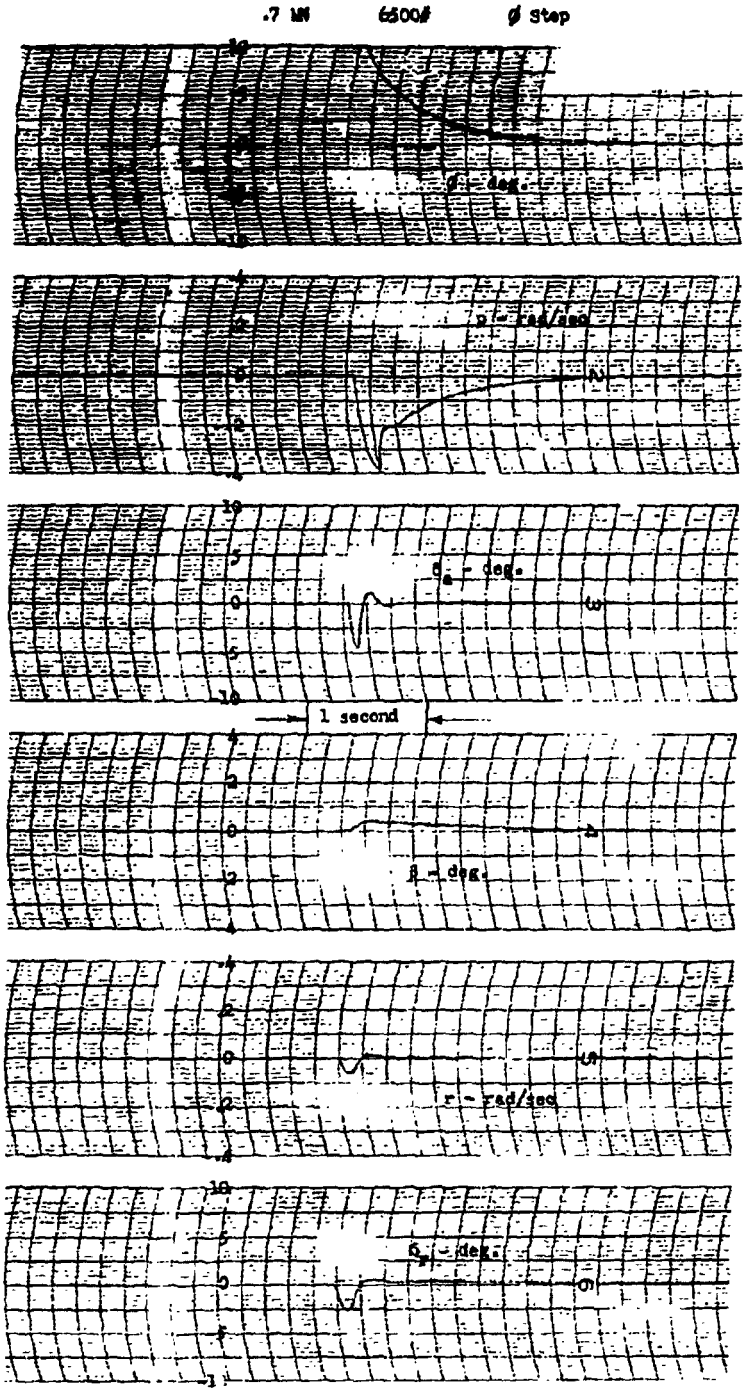

4-22. Lateral Stability Study Result Tracing

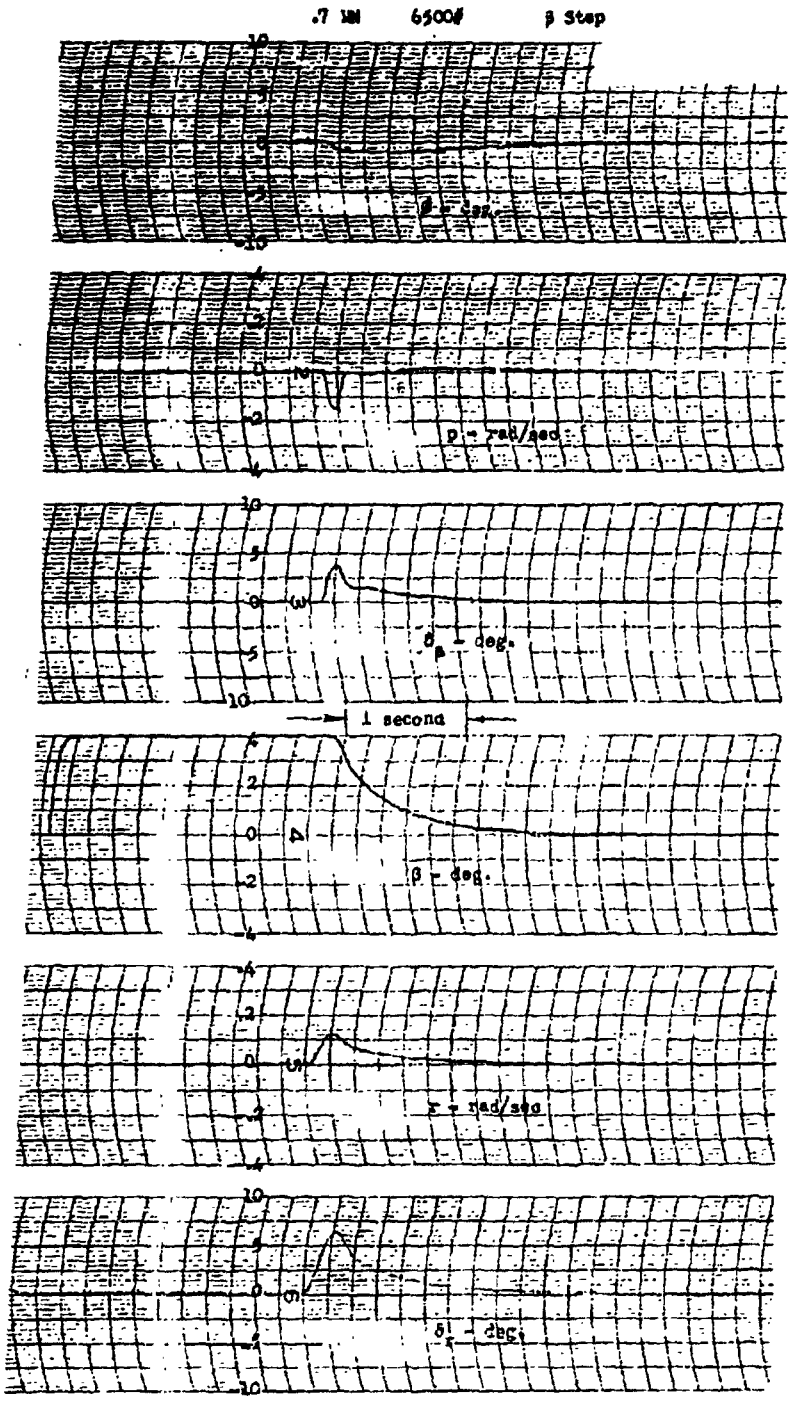

4-23. Lateral Stability Study Result Tracing

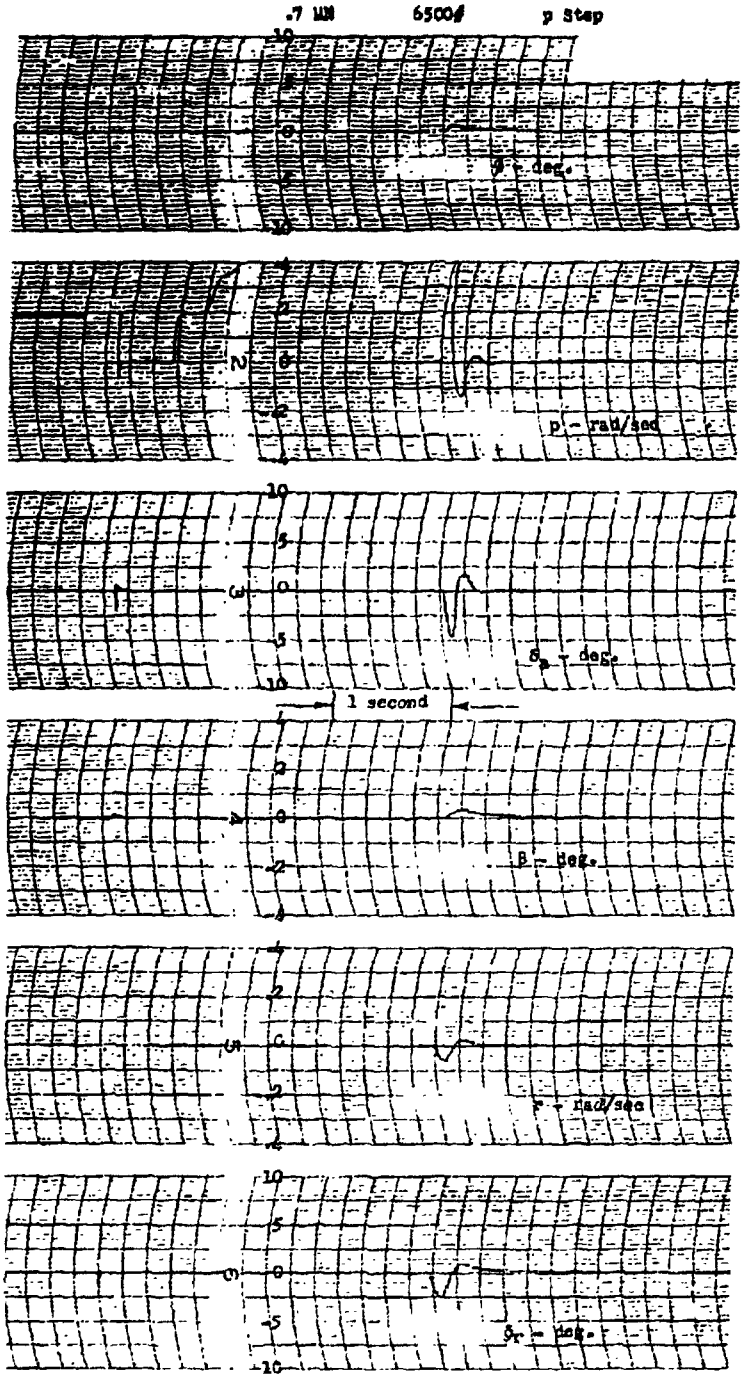

4-24. Lateral Stability Study Result Tracing

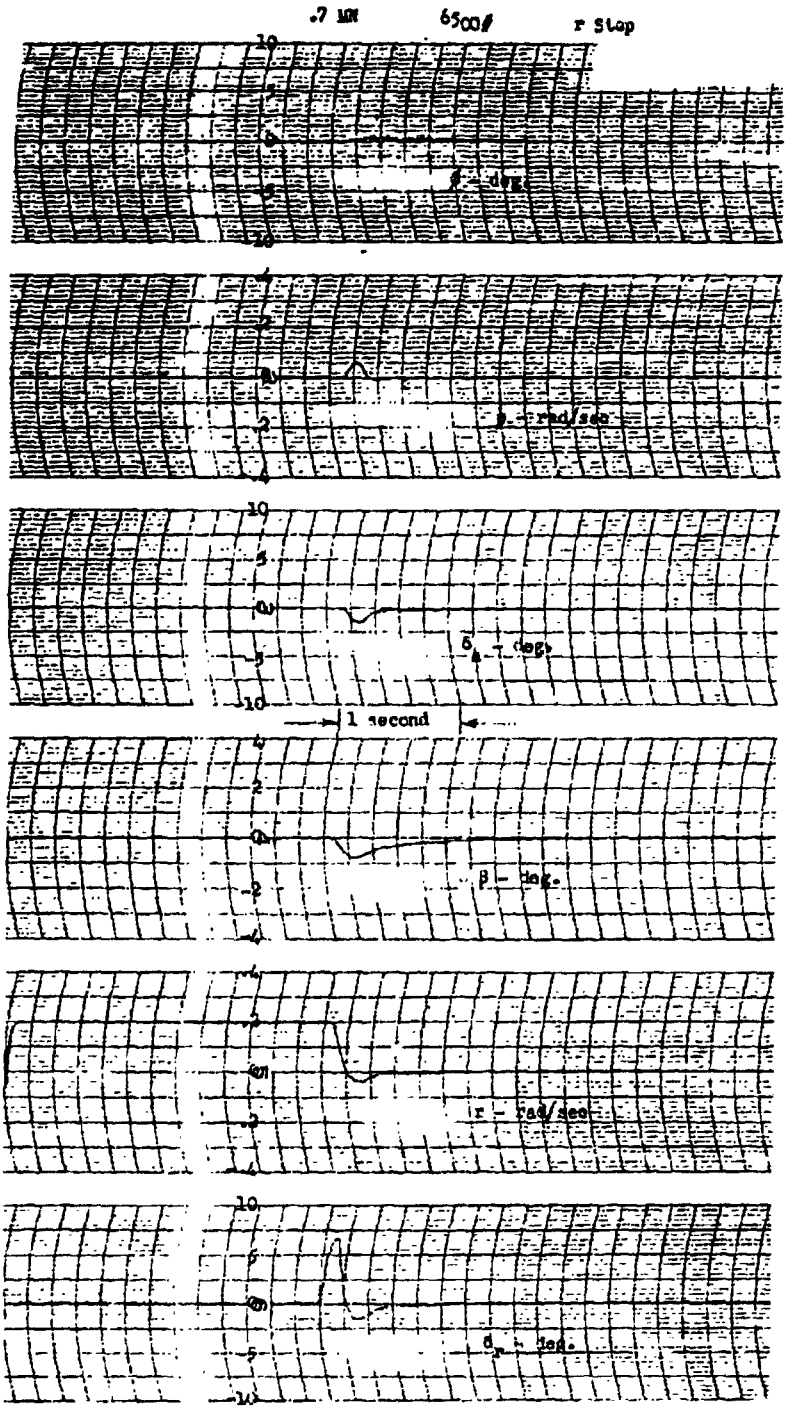

4-25. Lateral Stability Study Result Tracing

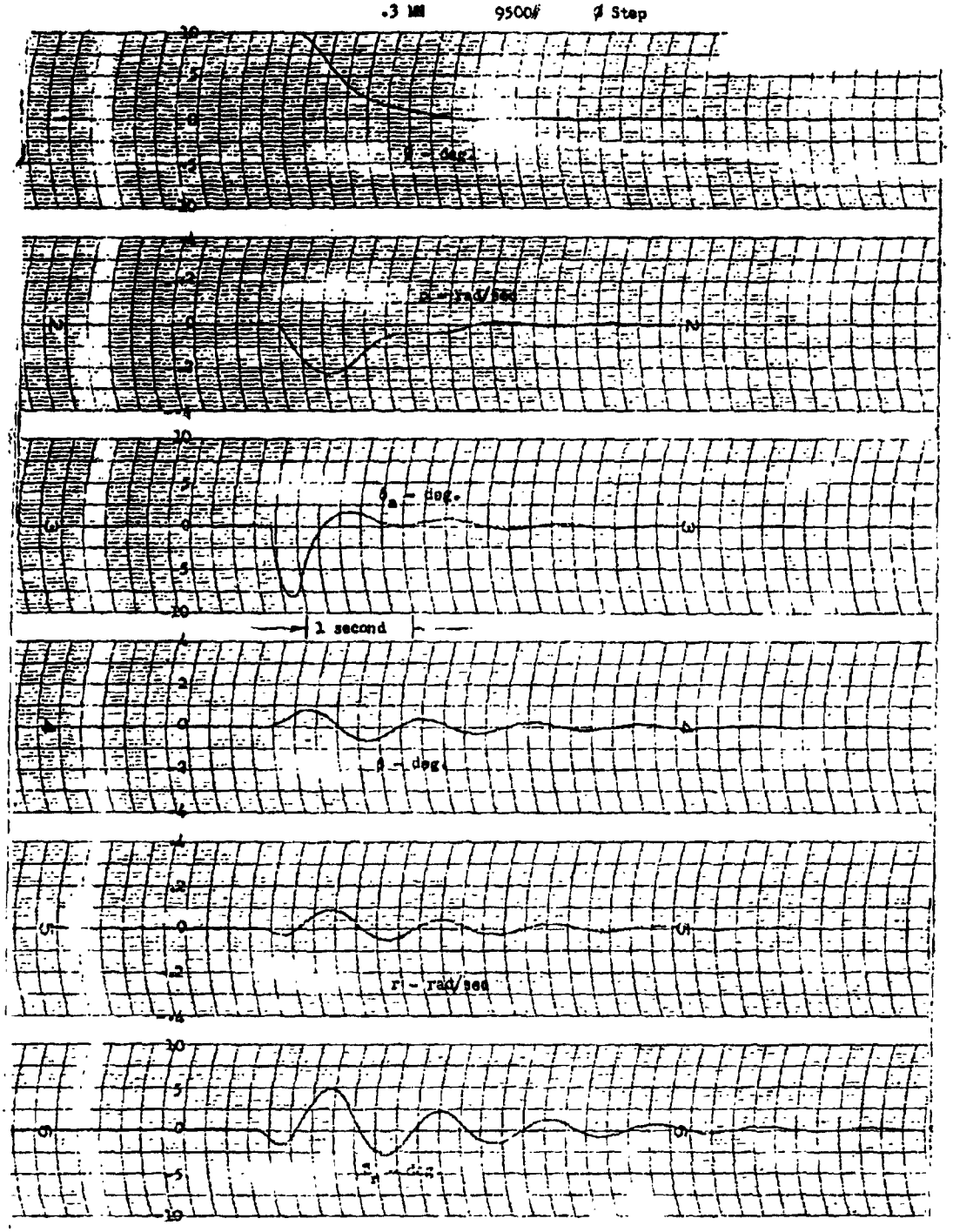

4-26. Lateral Stability Study Result Tracing

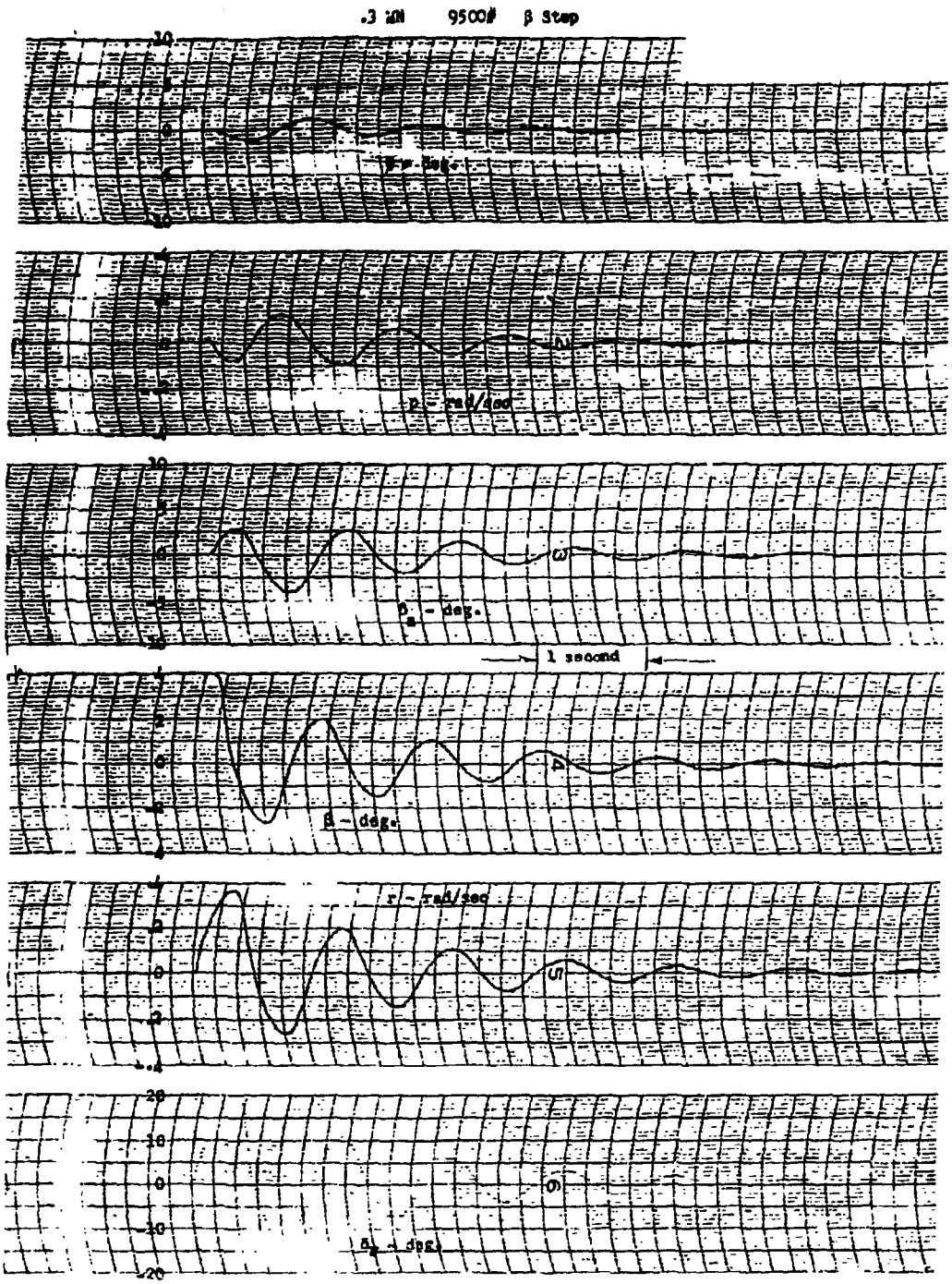

4-27. Lateral Stability Study Result Tracing

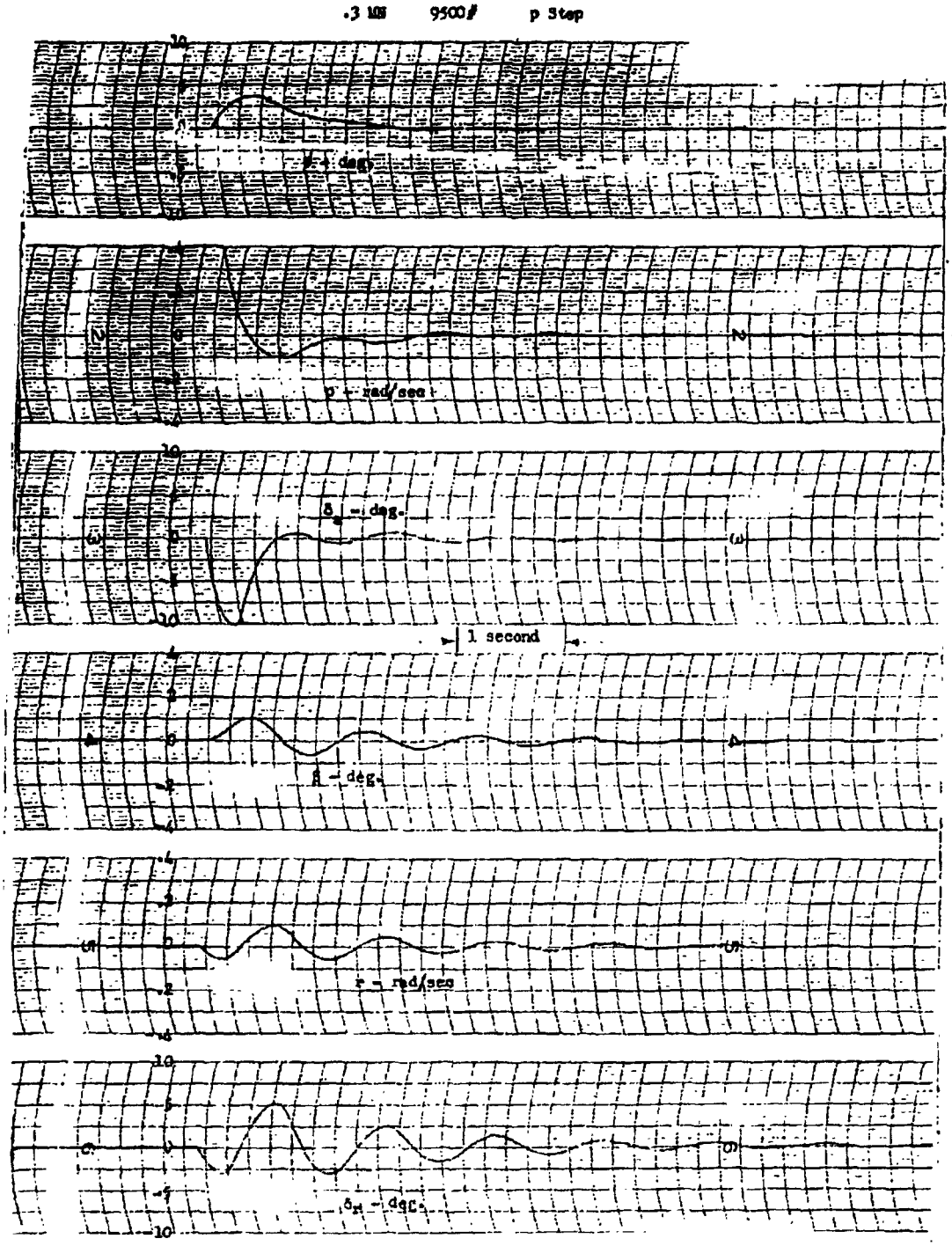

4-28. Lateral Stability Study Result Tracing

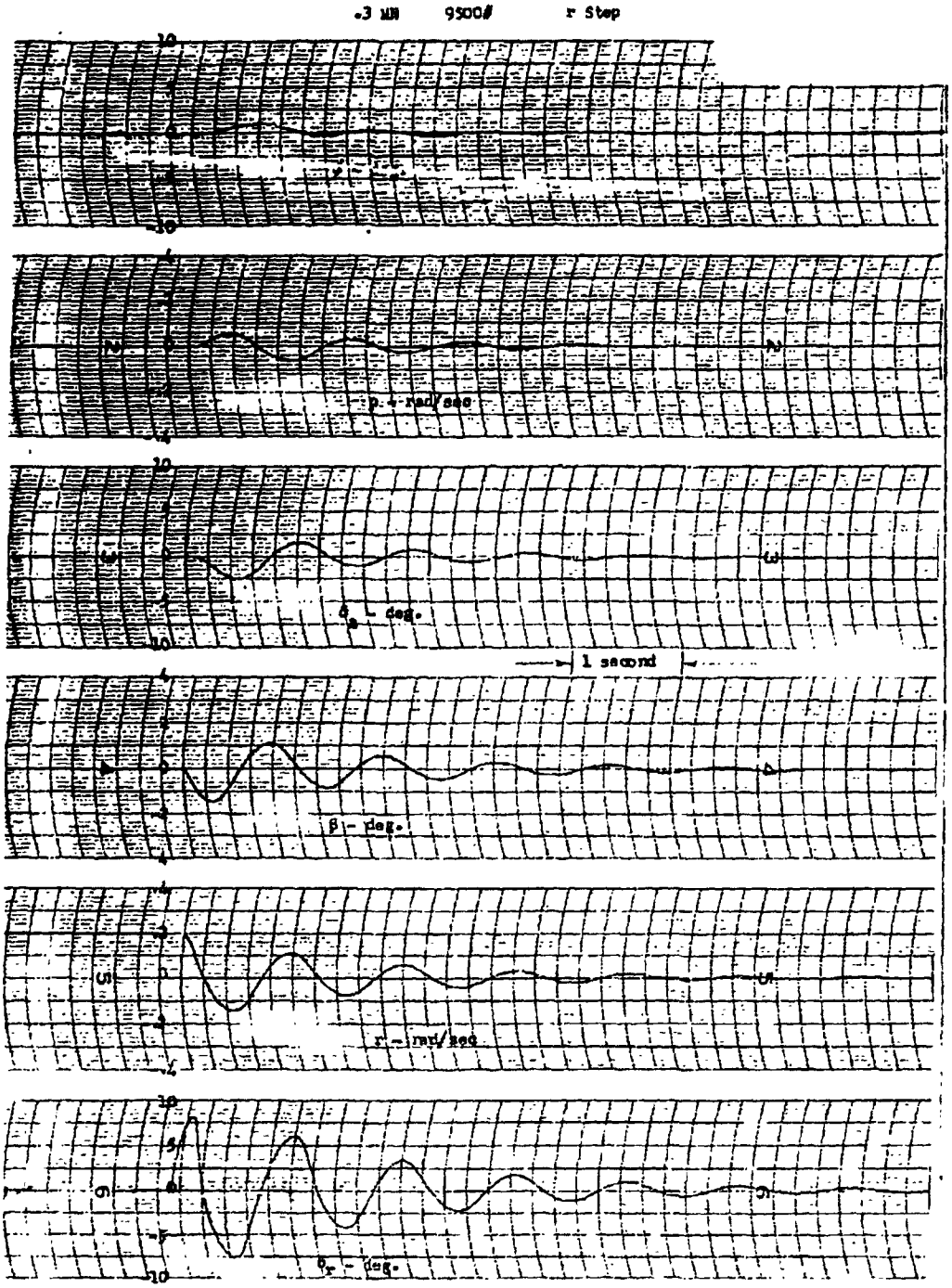

4-29. Lateral Stability Study Result Tracing

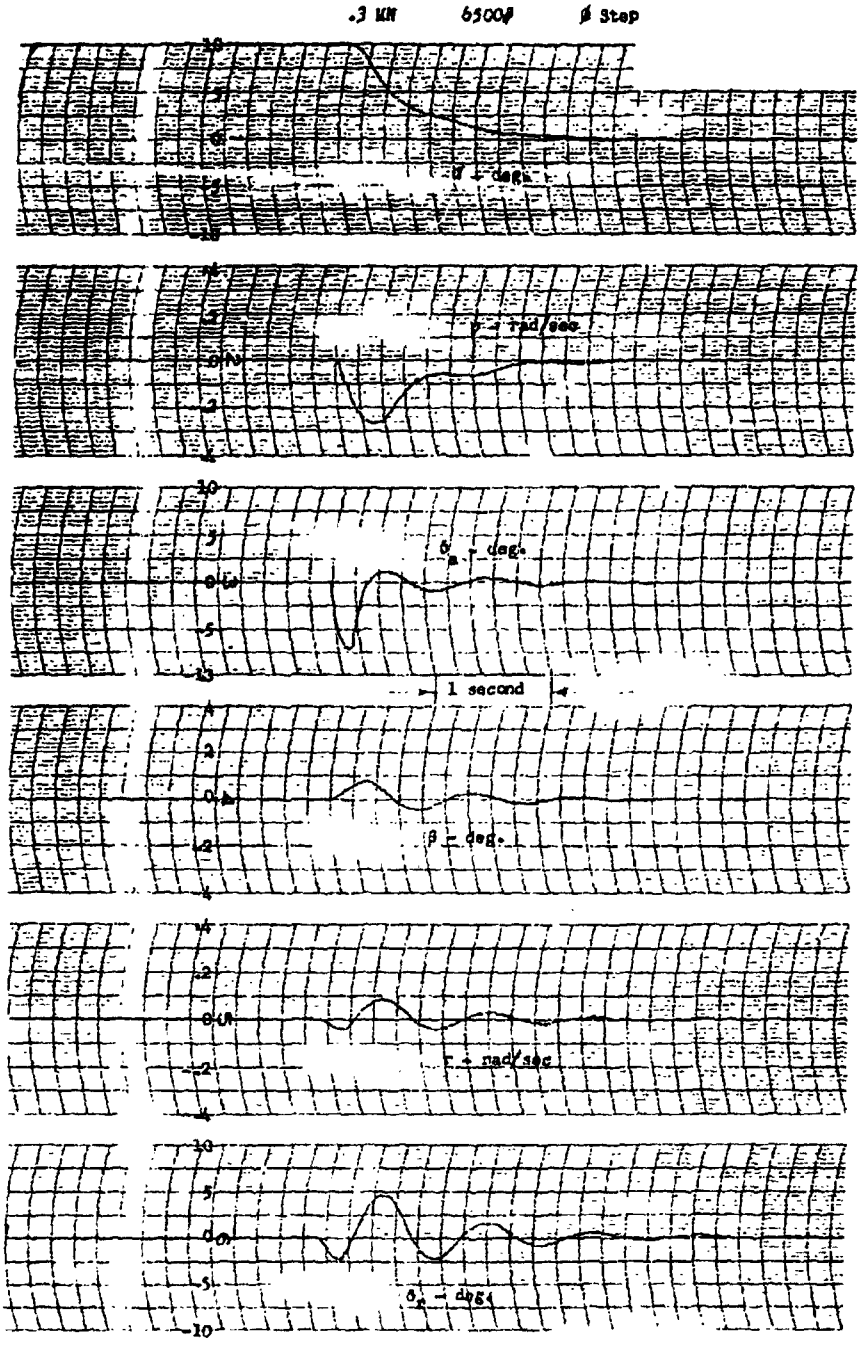

4-30. Lateral Stability Study Result Tracing

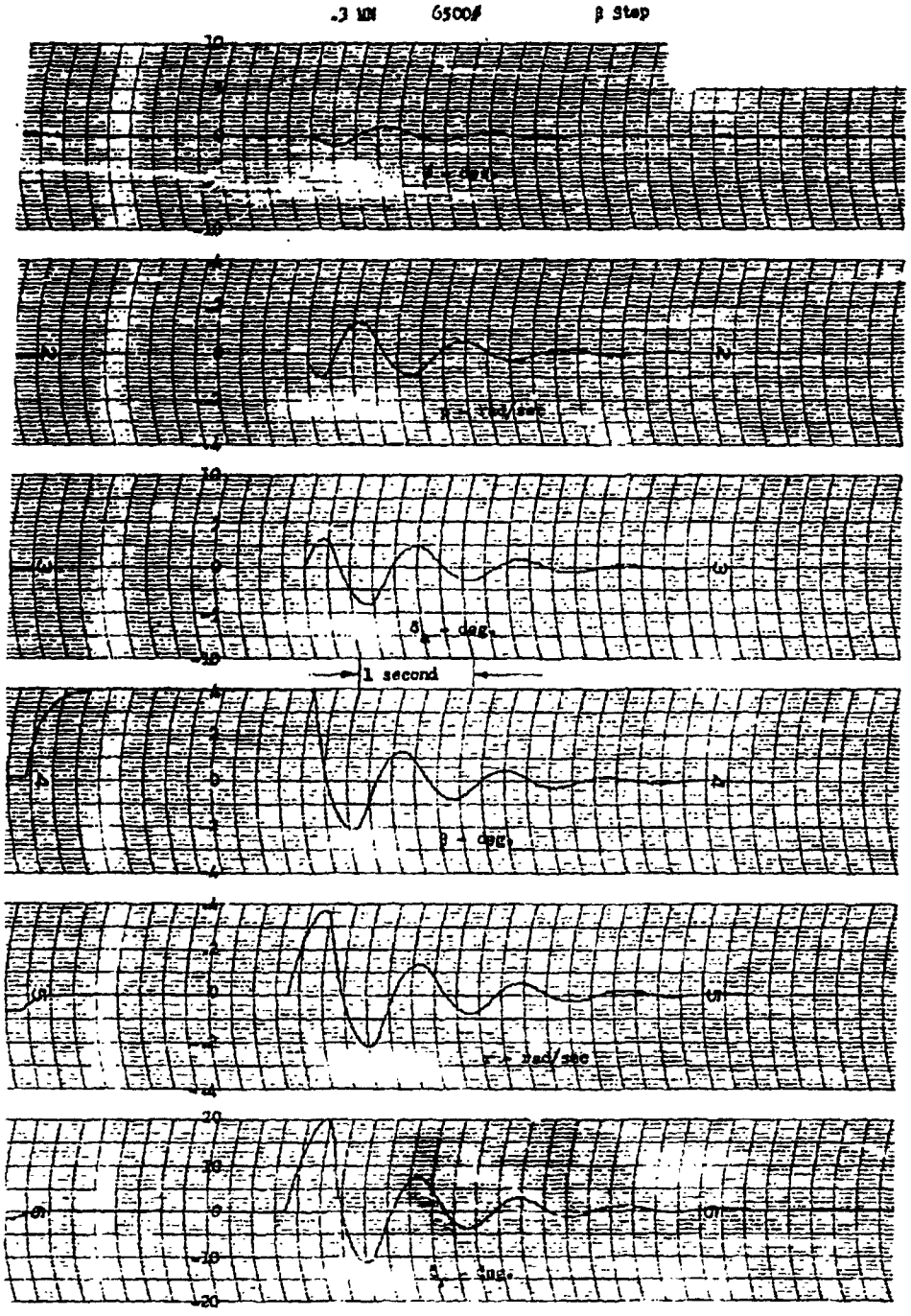

4-31. Lateral Stability Study Result Tracing

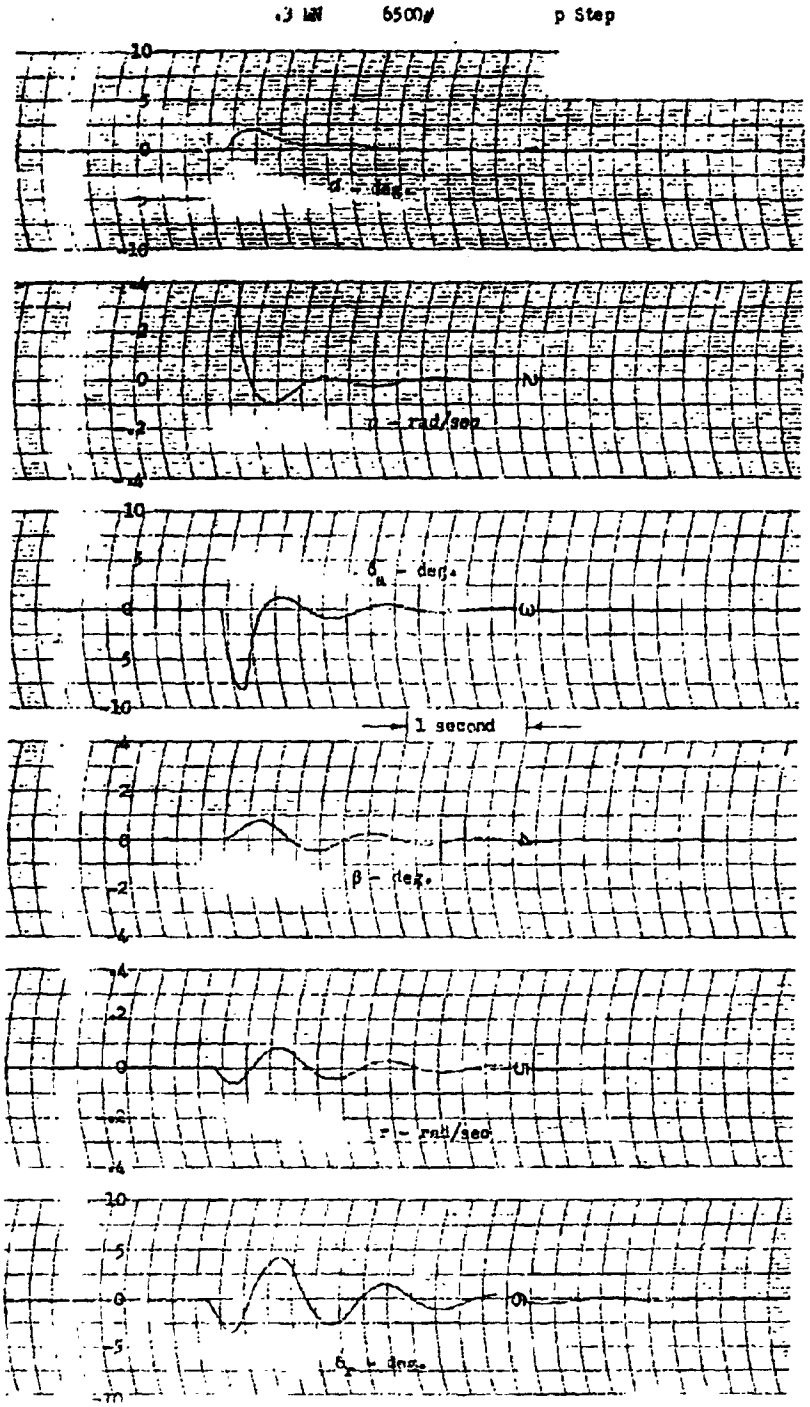

4-32. Lateral Stability Study Result Tracing

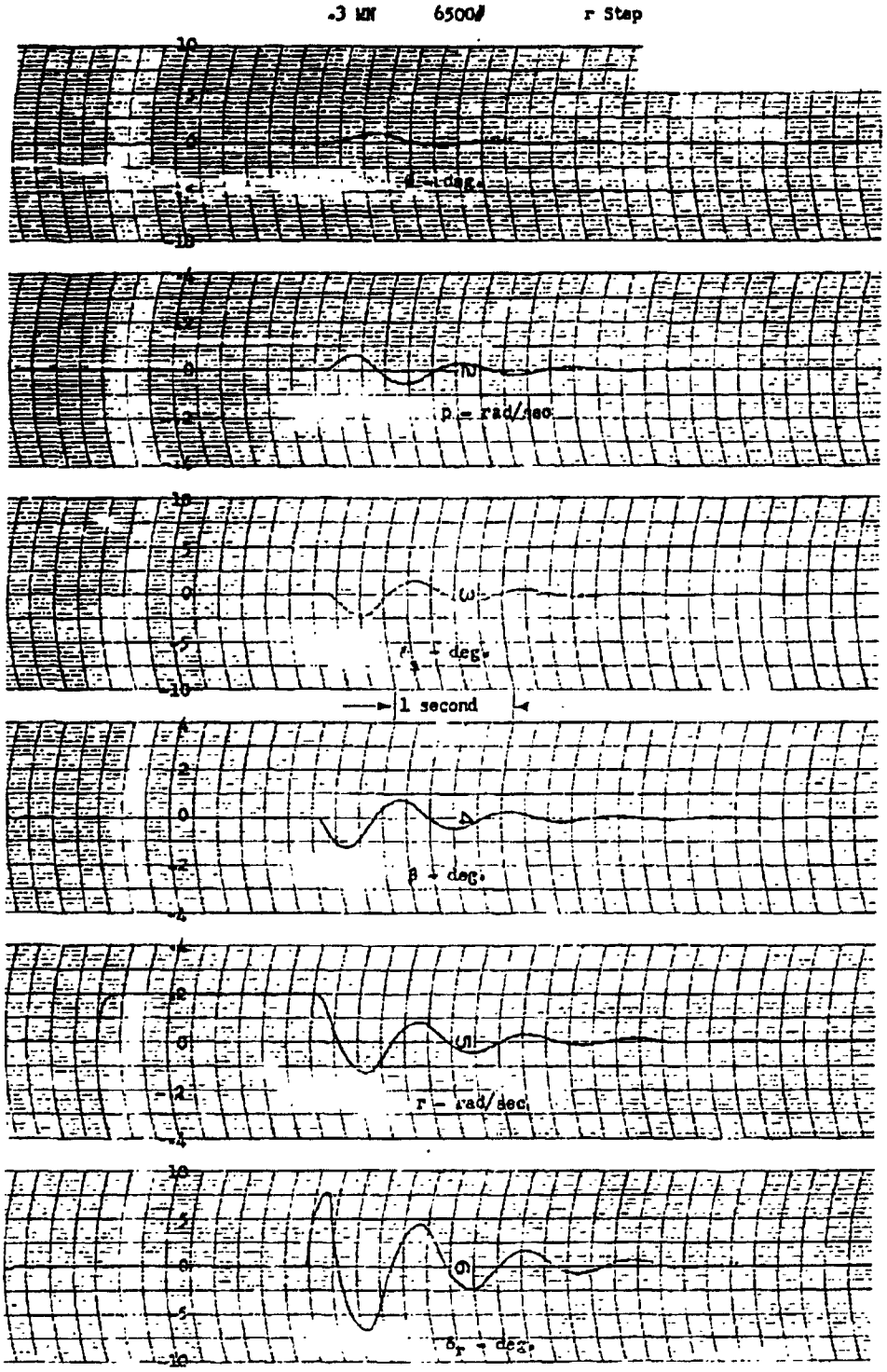

4-33. Lateral Stability Study Result Tracing

SECTION 4. FACTUAL DATA (Continued)

4.2.4 STRESS

4.2.4.1 Load Analysis

A loads analysis was made of the AN/USD-5 (XE-1) drone with three different stores (673 lb, 1011 lb and 1383 lb) at three different locations (B.L. 37, B.L. 74, and B.L. 85). In each case it was assumed that the top of the store was at W.L. - 19.75. This analysis was done for several loading conditions which appeared to be the most critical for the drone with external stores.

Following the loads analysis, stress checks were made on items in the most critically loaded areas to determine what modifications would be required to insure positive margins of safety in all of the structure.

4.2.4.2 Loads

The curves on Figures 4-34 thru 4-39 show the increases in loads on the wing and fuselage due to the various stores at the various butt lines.

The wing moment about the fore and aft axis is not increased as a result of mounting these stores on the wing at any butt line.

The wing fore and aft shear is greater than that for which the AN/USD-5 (XE-1) wing was designed, especially when the stores are mounted at one of the outboard locations. However, due to the long chord of the delta wing, this is not an important design consideration.

In no case is the wing vertical shear greater than that for which the wing was designed.

Wing moments about the vertical axis and wing torque about the trailing edge for stores at B.L. 37 are not greater than those for which the wing was designed.

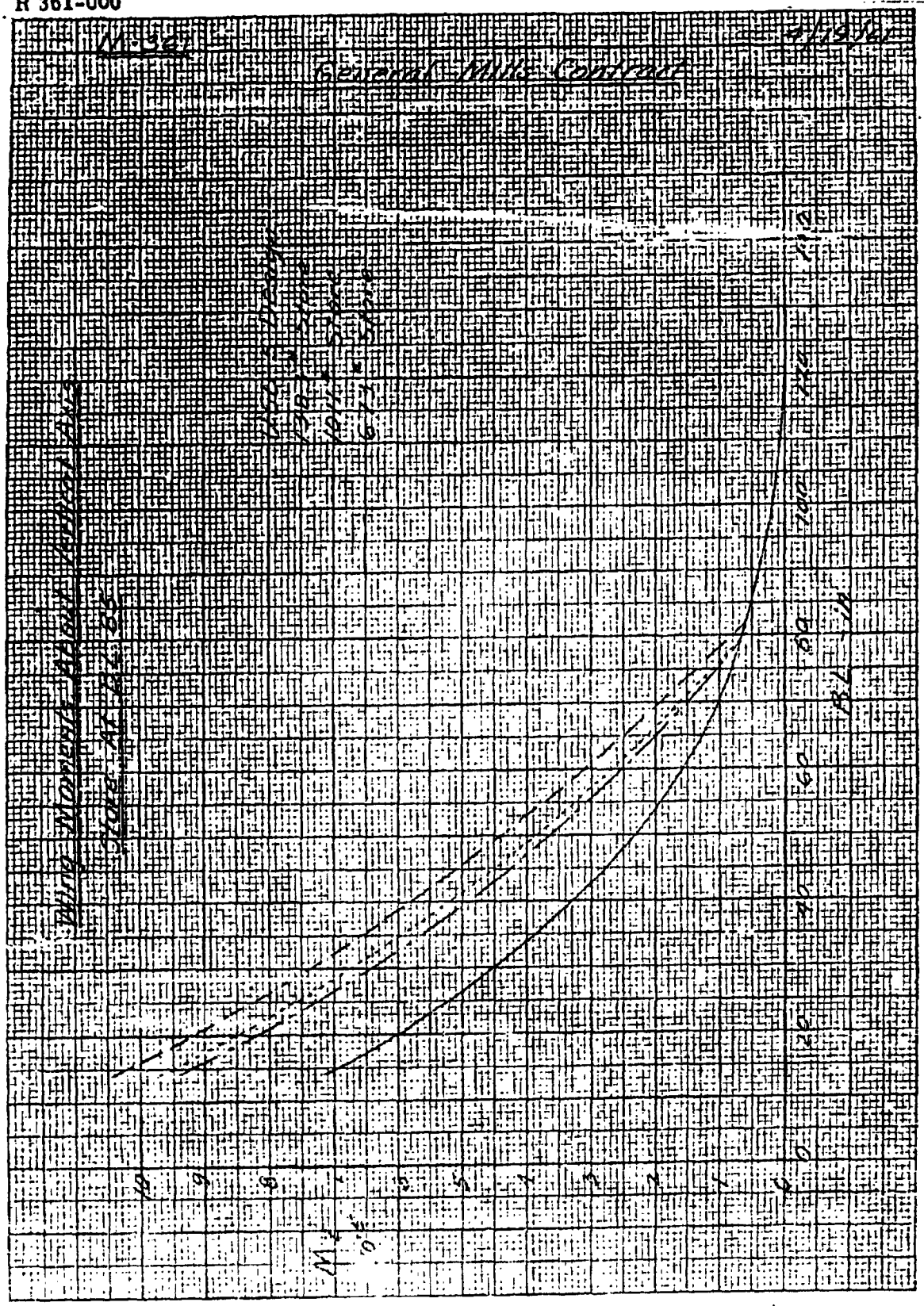

4-34. Wing Moments about Vertical Axis (Store at B.L. 85)

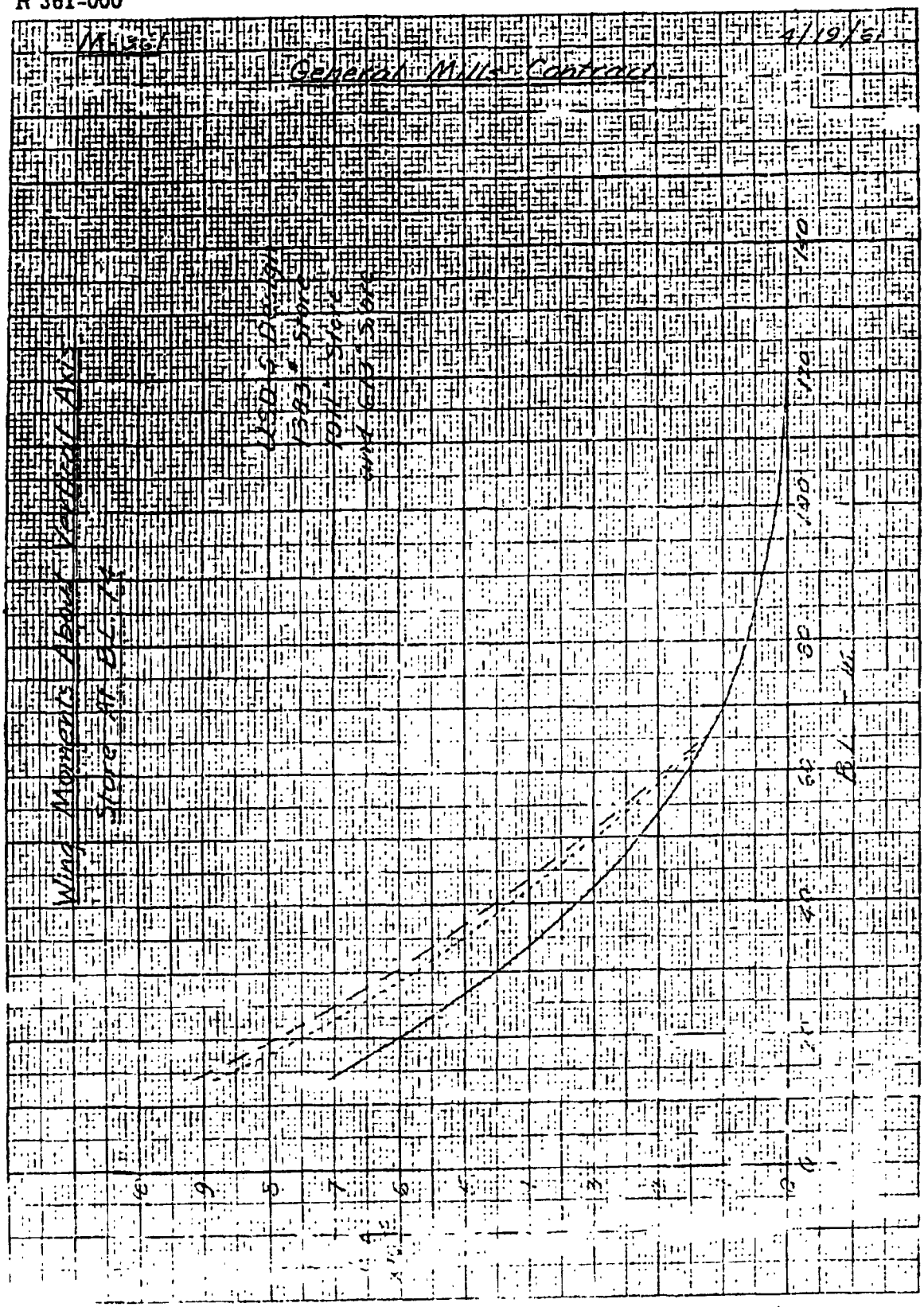

4-35. Wing Moments about Vertical Axis (Store at B.L. 74)

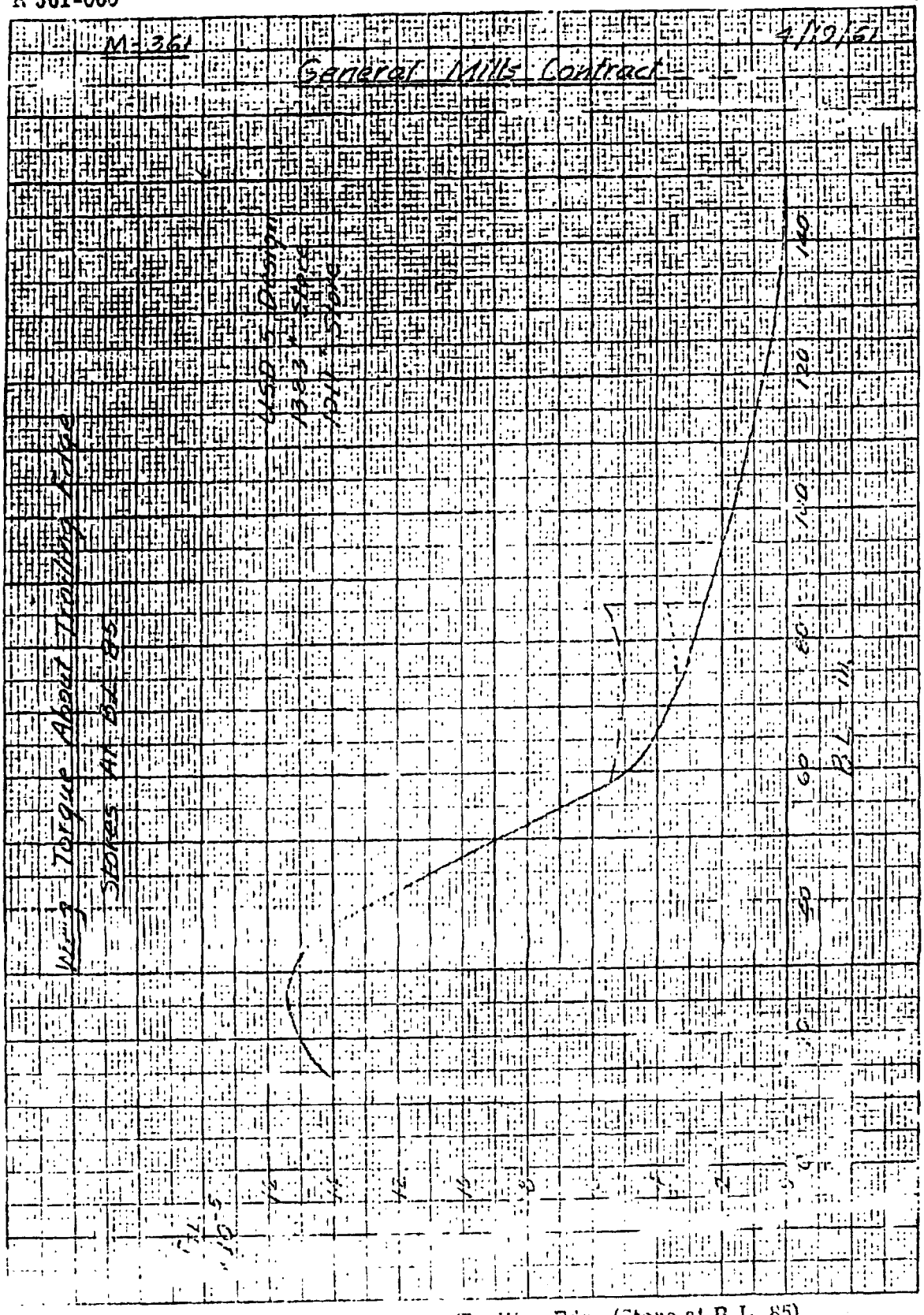

4-36. Wing Torque about Trailing Edge (Store at B.L. 85)

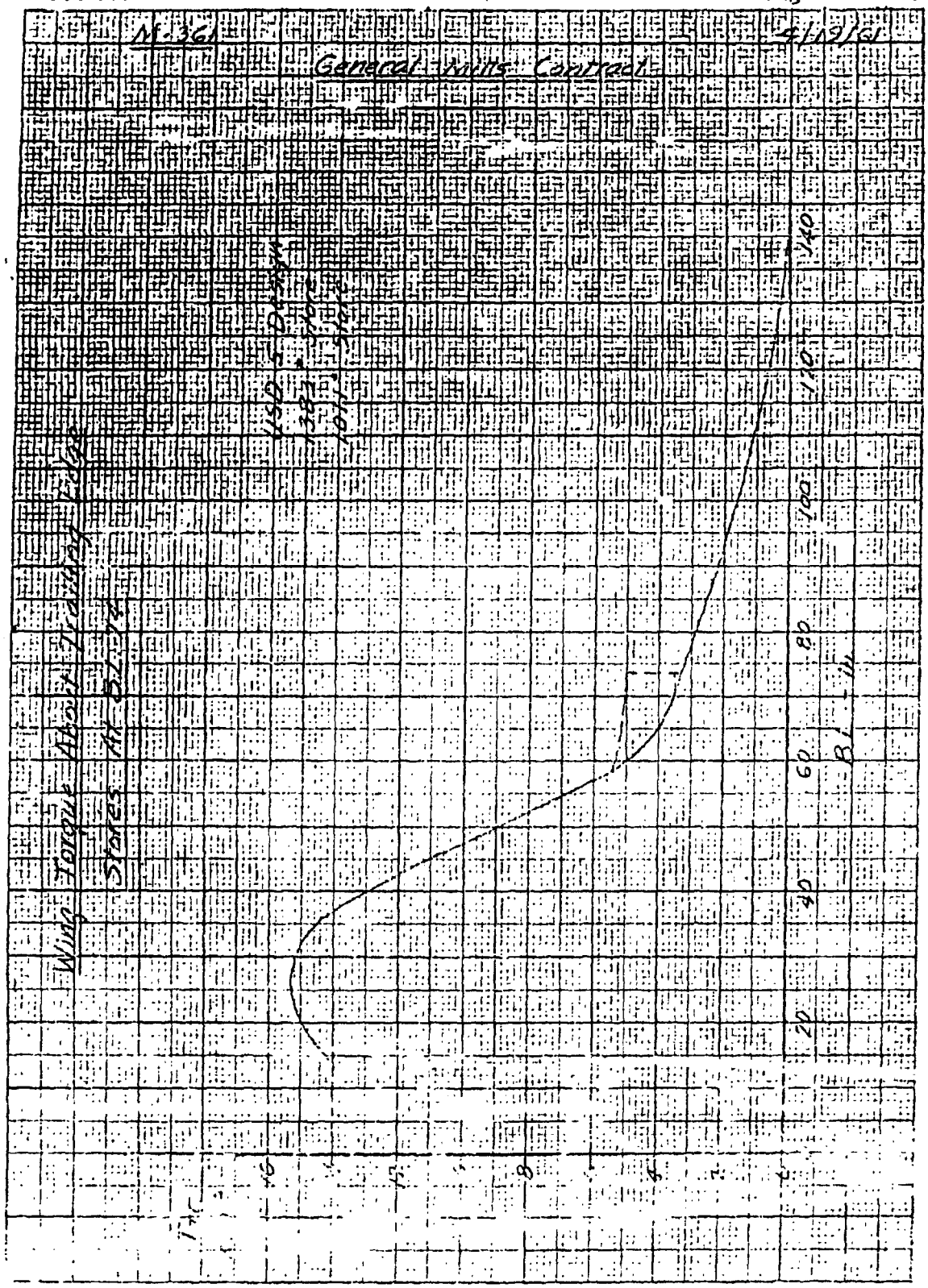

4-37. Wing Torque about Trailing Edge (Store at B.L. 74)

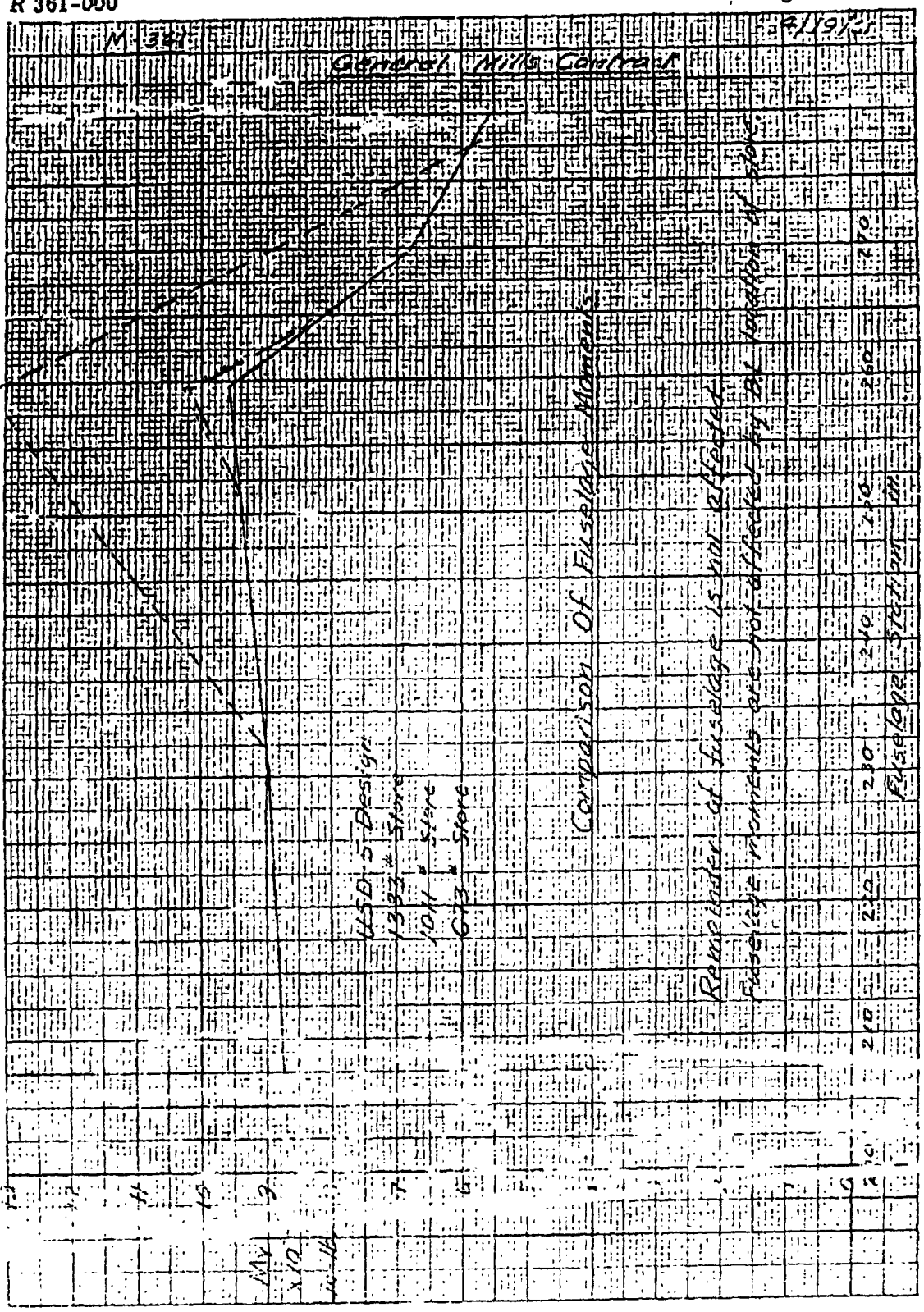

4-38. Comparison of Fuselage Moments

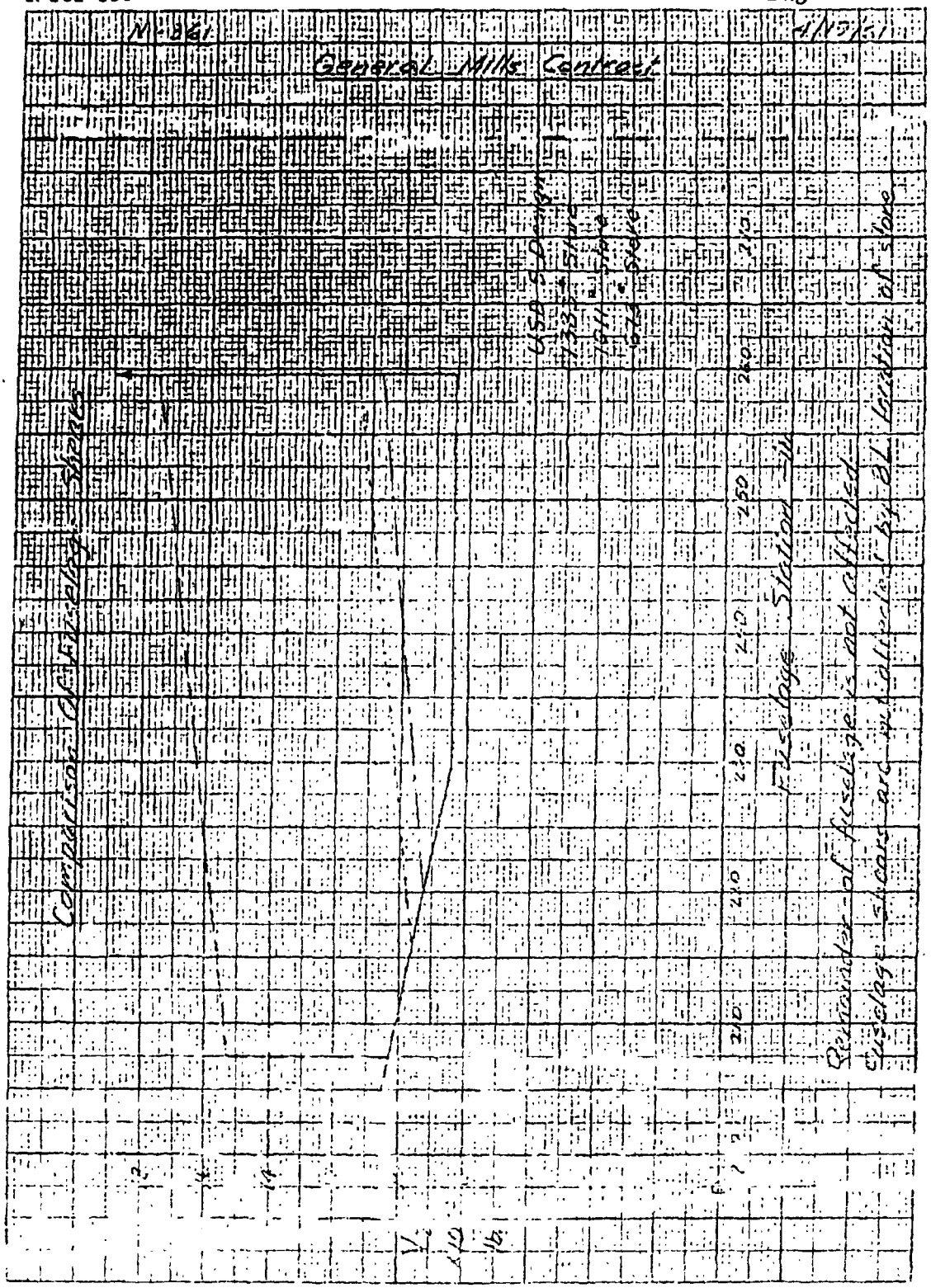

4-39. Comparison of Fuselage Shears

SECTION 4. FACTUAL DATA (Continued)

4.2.5 WEIGHTS

4.2.5.1 Drone Configuration

The weight, center of gravity and moment of inertia were compiled on the basis of a drone configuration as defined by Reference 5.5. The conditions set forth in the drone configuration are as follows:

a. A 22-inch diameter tank located at drone B. L. 85.

b. A redesign of the agent tank, empty weight 460 pounds was 600 pounds, and usable volume 149 gallons was 94 gallons in lieu of the tank shown in Phase I study. Refer to Table II, Section 4.1.5.

c. Partial filling of the redesigned agent tanks in preference to reducing the drone fuel load to maintain the fixed launch gross weight of 10,800 pounds.

Item			Weight
Total Recovery Gross Weight			4668
Fuel - Usable @ 6.5 lb/gal	(308.2 gal)		(2003)
Wing Inboard	179.7 gal		1168
Wing Outboard	62.0 gal		403
Fwd. Fuselage	54.0 gal		351
Sump	12.5 gal		81
Stores - Expendable			(2896)
Pylon		(2)	130
Tank (149 gal usable volume)		(2)	920
Agent @ 8.33 lb/gal	(110.8 gal)	(2)	1846
Total Drone Gross Weight (less booster)			9567
Booster			1300
Total Drone Gross Weight (plus booster)			10867
Fuel - Prelaunch checkout			67
Total Launch Gross Weight			10800

SECTION 4. FACTUAL DATA (Continued)

4.2.5.1 Drone Configuration (Continued)

Booster Drop Off GW (level attitude) - Weight : 9,500 lb

I_{x_c} (Roll) : 7,513 slug-ft^2

I_{z_o} (Yaw) : 16,646 slug-ft^2

$P_{x_o z_o}$: -160 slug-ft^2

Agent Tanks Empty GW (level attitude) - Weight : 6,457 lb

I_{x_o} : 3,464 slug-ft^2

I_{z_o} : 11,063 slug-ft^2

$P_{x_o z_o}$: - 79 slug-ft^2

Agent Tank	Diameter	: 22 inches
	Length	: 187 inches
	Volume (outside skin contours)	: 190 gal
	Volume (usable)	: 149 gal

NOTE: The drone center of gravity and moment of inertia as influenced by partially filled agent tanks has not been investigated.

SECTION 4. FACTUAL DATA (Continued)

4.2.6 SEA-LEVEL MISSION.

One sea-level mission was calculated for the 22-inch diameter tank located at butt line 85. The agent weight and tank weights are different from those used in the Phase I study; however, the sum of the agent and tank weights are the same. The calculation of this mission is shown in Table I and the mission profile is given in Figure 4-40.

~~CONFIDENTIAL~~

REPORT NO. R 361-000 FAIRCHILD Aircraft and Missiles Div. OF FAIRCHILD ENGINE & AIRPLANE CORPORATION			PAGES PAGE 4-59
MODEL M-361	PREPARED BY R. N. Rothenberger	CHECKED BY R. H. Putnam	APPROVED BY E. E. Morton

SUBJECT:- Study of Compatibility of External Wing-Mounted BW Stores with the AN/USD-5 (XE-1) Drone

DATE May 26, 1961

REVISED

SECTION 4. FACTUAL DATA (Continued)

TABLE I

SEA-LEVEL MISSION CALCULATION

Butt Line 85		Tank Diameter 22 Inches
Take-Off Gross Weight	lb	10,867
Total Fuel	lb	2,003
Fuel for Reserve	lb	0
Fuel Used For Check Out	lb	67
Climb Gross Weight	lb	10,800
Drop Booster	lb	1,300
Gross Wt. @ Start of Cruise Out	lb	9,500
Fuel Assumed For Cruise Out	lb	720
Avg. G. W. For Cruise Out	lb	9,140
Naut. Mi/Lb of Fuel		0.1543
Range in Cruise Out	n.. mi.	111.1
Average Speed	kn	463.2
Time to Cruise Out	hr	0.2398
End of Cruise G.W.	lb	8,780
Arrival Gross Weight	lb	8,780
Dispense Agent (Cargo)	lb	1,846
Dissemination Speed	kn	463.2
Dissemination Rate	gal/min/drone	18
Usable Agent	gal/tank	110.8
Dissemination Time	hr	0.2057
Dissemination Range	n. mi.	95.3
Avg. Wt. During Dissemination	lb	7,541
Naut. Mi/Lb of Fuel		0.1507
Fuel Used During Diss.	lb	632.3
G.W. @ End of Dissemination	lb	6,302
Wt. @ Start of Cruise Back	lb	6,302
Naut. Mi/Lb of Fuel		0.1507
Range in Cruise Back	n. mi.	25
Average Speed	kn	463.2
Time to Cruise 25 n. mi.	hr	0.0539
Fuel Used to Cruise 25 n. mi.	lb	165.9
Wt. @ End of 25 n. mi. Cruise	lb	6,136
Drop Tanks	lb	1,050
End Weight	lb	5,086

~~CONFIDENTIAL~~

3-800-23A

REPORT NO. R 361-000 FAIRCHILD Aircraft and Missiles Div. OF FAIRCHILD ENGINE & AIRPLANE CORPORATION			PAGES PAGE 4-60
MODEL M-361	PREPARED BY R. N. Rothenberger	CHECKED BY R. H. Putnam	APPROVED BY E. E. Morton

SUBJECT:- Study of Compatibility of External Wing-Mounted BW Stores with the AN/USD-5 (XE-1) Drone

DATE May 28, 1961

REVISED

SECTION 4. FACTUAL DATA (Continued)

TABLE I (Continued)

SEA-LEVEL MISSION CALCULATION

Butt Line 85 Tank Diameter 22 Inches

G. W. for Return	lb	5,086
Fuel for Return	lb	418
Avg. Gross Weight	lb	4,877
Naut. mi/lb of Fuel		0.2063
Range in Cruise Back	n. mi.	86.2
Avg. Speed	kn	463.2
Time to Cruise Back	hr	0.1861
Radius of Action	n. mi.	111.2
Total Mission Time	hr	0.6855
Recovery Weight	lb	4,668

8-800-23A

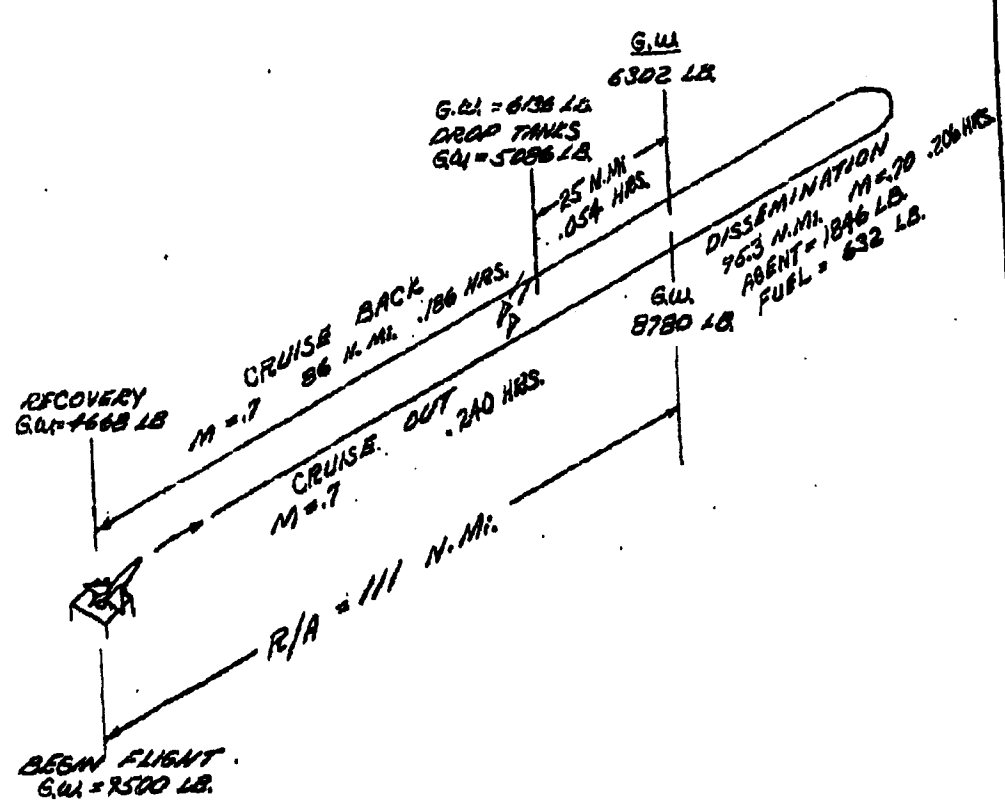

9-800-23A

4-40. Sea-Level Mission with Final Tank Configuration

~~CONFIDENTIAL~~

SECTION 4. FACTUAL DATA (Continued)

4.2.6.1 Tank Loads.

A summary of the design load factors for the tanks is presented in Table II. These load factors are based on the design conditions for the basic drone. Inertia loads and airloads on the tanks are presented in Table III.

CONFIDENTIAL

TABLE II. DESIGN LOAD FACTORS FOR FINAL TANKS

Design Loading Condition	Drone Gross Wt., lb	Altitude	Mach Number	Limit Load Factor	Ultimate Factor of Safety
Launch Phase	10,800 (with max. agent)	S.L.	200 knots	$n_x = 5.0$ $n_z = 2.33$	1.5
Flight Phase					
Symmetrical Flight	8,500 (with max. agent)	S.L.	maximum	$n_z = 4.72, -2.72$	1.5
Sideslipping Flight	8,500 (with max. agent)	S.L.	maximum	$n_y = \pm 1.0$ $n_z = 1.0$	1.5
Rolling Flight	8,500 (with max. agent)	S.L.	maximum	$n_z = 3.0$	1.5
Accelerated				$\ddot{\psi} = \pm 6.8$ rad/sec^2	
Steady				$n_z = 2.33$ $\dot{\phi} = \pm 3.05$ rad/sec	

n_x - longitudinal load factor; positive-forward

n_y - lateral load factor; positive - right

n_z - normal load factor; positive - up

$\ddot{\psi}$ - rolling acceleration; positive - right wing down

CONFIDENTIAL

MODEL M-361 | PREPARED BY R. N. Rothenberger | CHECKED BY R. H. Putnam | APPROVED BY E. E. Morton

SUBJECT:- Study of Compatibility of External Wing-Mounted BW Stores with the AN/USD-5 (XE-1) Drone

DATE May 26, 1961

REVISED

TABLE III. TANK LOADS FOR FLIGHT PHASE

DROKE FLIGHT CONDITIONS		SYMMETRICAL FLIGHT		SIDESLIPPING FLIGHT		ROLLING FLIGHT ACCELERATED		ROLLING FLIGHT STEADY		POS. DIRECTION
						RT. ROLL	LT. ROLL	RT. ROLL	LT. ROLL	
n_z		-2.72	4.72	1	-1	3	3	2.33	2.33	
n_y		0	0	1	-1	0	0	0	0	
$\dot{\phi}$	rad/sec^2	0	0	0	0	5.5	-5.5	0	0	
$\ddot{\phi}$	rad/sec^2	0	0	0	0	0	0	3.05	-3.05	
$\ddot{\psi}$	rad/sec^2			-3	3	0	0	0	0	
α	deg.	-2.2	3.8	.7	.7	2.5	2.5	2.0	2.0	
β	deg.	0	0	-5.5	5.5	0	0	0	0	
Tank Inertia Loads										
Normal load factor		2.72	-4.72	-1	-1	-3.33	1.57	-3.0	-3.0	lb inboard
Side load factor		0	0	-1	1	.59	-.98	-2.0	-2.0	
Tank Airloads										lb Nose up / Rearward / inboard / Nose right (view from top)
Normal force	lb	640	550	600	600	570	570	338	580	
Pitching moment	ft-lb	-4000	-3500	-4400	-4400	-4100	-4100	-4000	-4000	
Chord force	lb	187	336	275	275	363	363	336	220	
Side force (With vert. fins)	lb	1300	220	2800	-800	998	998	550	550	
Yawing moment (With vert. fins)	ft-lb	-3000	-800	-6000	2140	-1250	-1250	-1470	-1470	
Side force (Without vert. fins)		1000	250	1450	-190	400	400	575	575	
Yawing moment (Without vert. fins)		-480	-1000	120	-2800	-925	-925	-870	-870	

NOTES:
1. All loads and load factors are limit values
2. Values are for left tank
3. Horizontal fins are on tanks in all cases
4. Aerodynamic moments are referred to 90% tank length

S-800-23A

REPORT NO. R361-000 FAIRCHILD Aircraft and Missiles Div. OF FAIRCHILD ENGINE & AIRPLANE CORPORATION			PAGES PAGE 5-1
MODEL M-361	PREPARED BY R. N. Rothenberger	CHECKED BY R. H. Putnam	APPROVED BY E. E. Morton
SUBJECT:- Study of Compatibility of External Wing-Mounted BW Stores with the AN/USD-5 (XE-1) Drone			DATE May 26, 1961 REVISED

SECTION 5. REFERENCES

5.1 FAMD Report R252-019, "Summary of Aerodynamics Coefficients Advanced Surveillance System M-252" November 1958 (Confidential).

5.2 FAMD Report R252-076, "Analysis of Phase II Wind Tunnel Data High Speed Model AN/USD-5," November 1959 (Confidential).

5.3 FAD Report No. 74R-133, "Guidance and Flight Control, Final System AN/USD-5 ( ) Drone," September 9, 1960 (Confidential).

5.4 FAMD EW-132, "Model M-361 General Mills BW Drone Study," April 19, 1961 (Confidential).

5.5 Interoffice Memorandum, "General Mills Contract - M-361," EPD-3464, May 4, 1961.

REPORT NO. R361-000	FAIRCHILD Aircraft and Missiles Div. OF FAIRCHILD ENGINE & AIRPLANE CORPORATION	PAGES	PAGE 6-1
MODEL M-361	PREPARED BY R. N. Rothenberger	CHECKED BY R. H. Putnam	APPROVED BY E. E. Morton
SUBJECT:- Study of Compatibility of External Wing-Mounted BW Stores with the AN/USD-5 (XE-1) Drone			DATE May 26, 1961 REVISED

SECTION 6. APPENDIX

9-800-23A

DP-61-179 1

PREPARED BY: R. S. N. — NORTH AMERICAN AVIATION, INC.	TFD-61-251-1
CHECKED BY:	REPORT NO. 1
DATE: FEB. 23, 61	MODEL NO. 60 2593

GENERALIZED LIQUID AGENT STORE
AERODYNAMIC DIMENSIONAL DATA

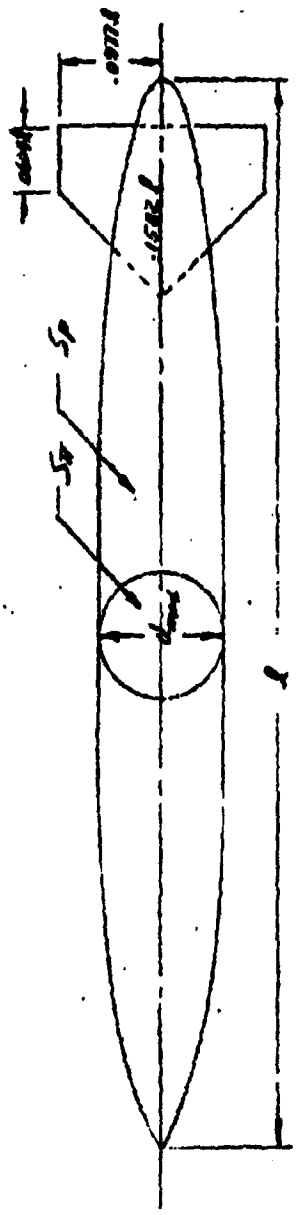

PLAN VIEW

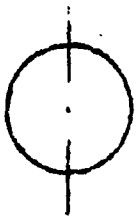

REAR VIEW

$\frac{S_p}{S_w} = 0.83$

$\frac{l}{d_{max}} = 8.5$

DP-61-190

NORTH AMERICAN AVIATION, INC.

CONFIDENTIAL

PREPARED BY

CHECKED BY

DATE 24 FEB. 61

TLD 61-251-2

PAGE NO

REPORT NO

MODEL NO G.O. 2533

DIMENSIONAL CHARACTERISTICS OF A GENERALIZED LIQUID AGENT DISSEMINATING STORE

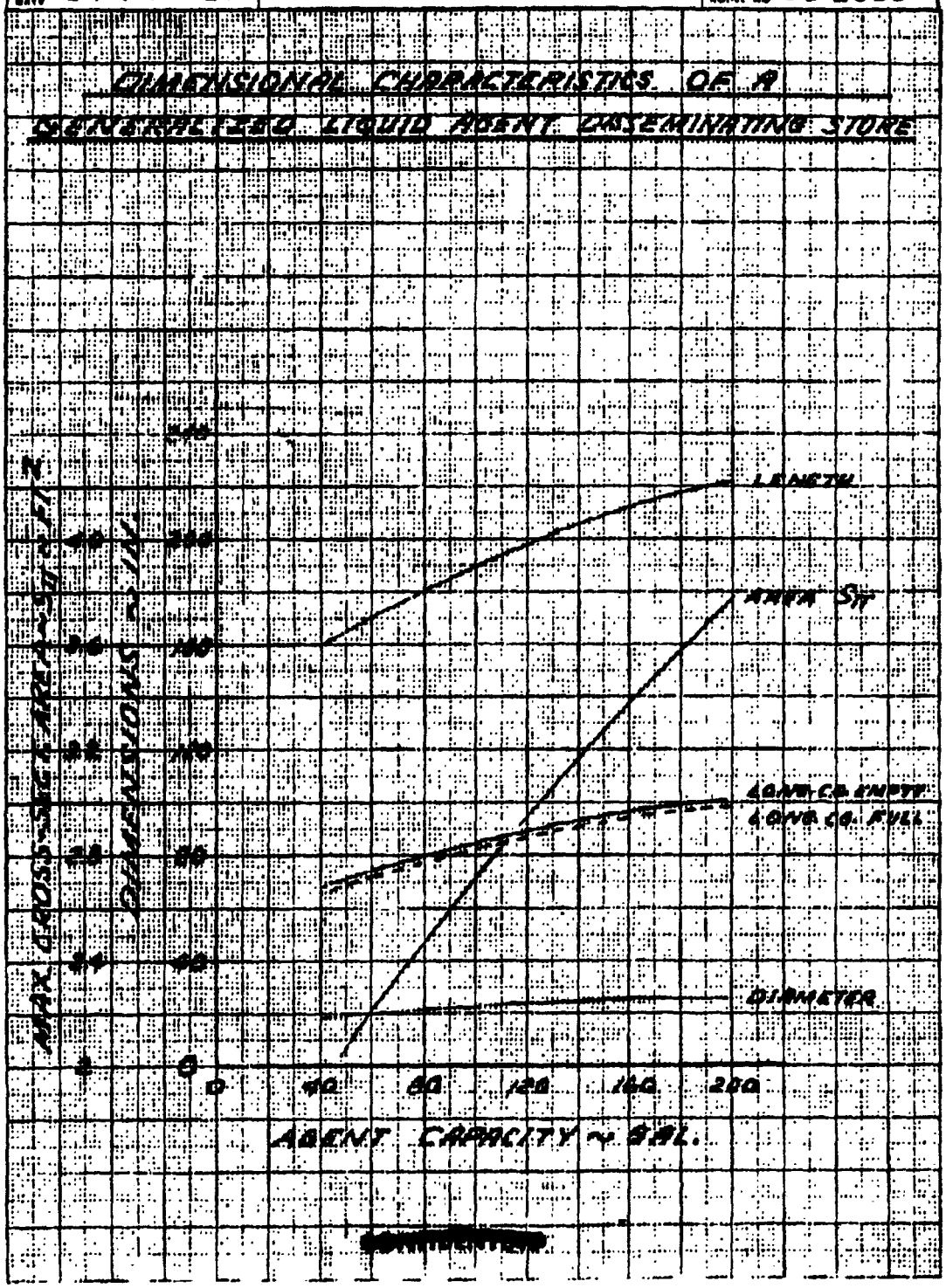

CONFIDENTIAL

SP-61-189

NORTH AMERICAN AVIATION, INC.

CONFIDENTIAL

4

DATE 24 FEB. 61

G.O. 2533

WEIGHT & INERTIA CHARACTERISTICS OF A GENERALIZED LIQUID AGENT DISSEMINATING STORE

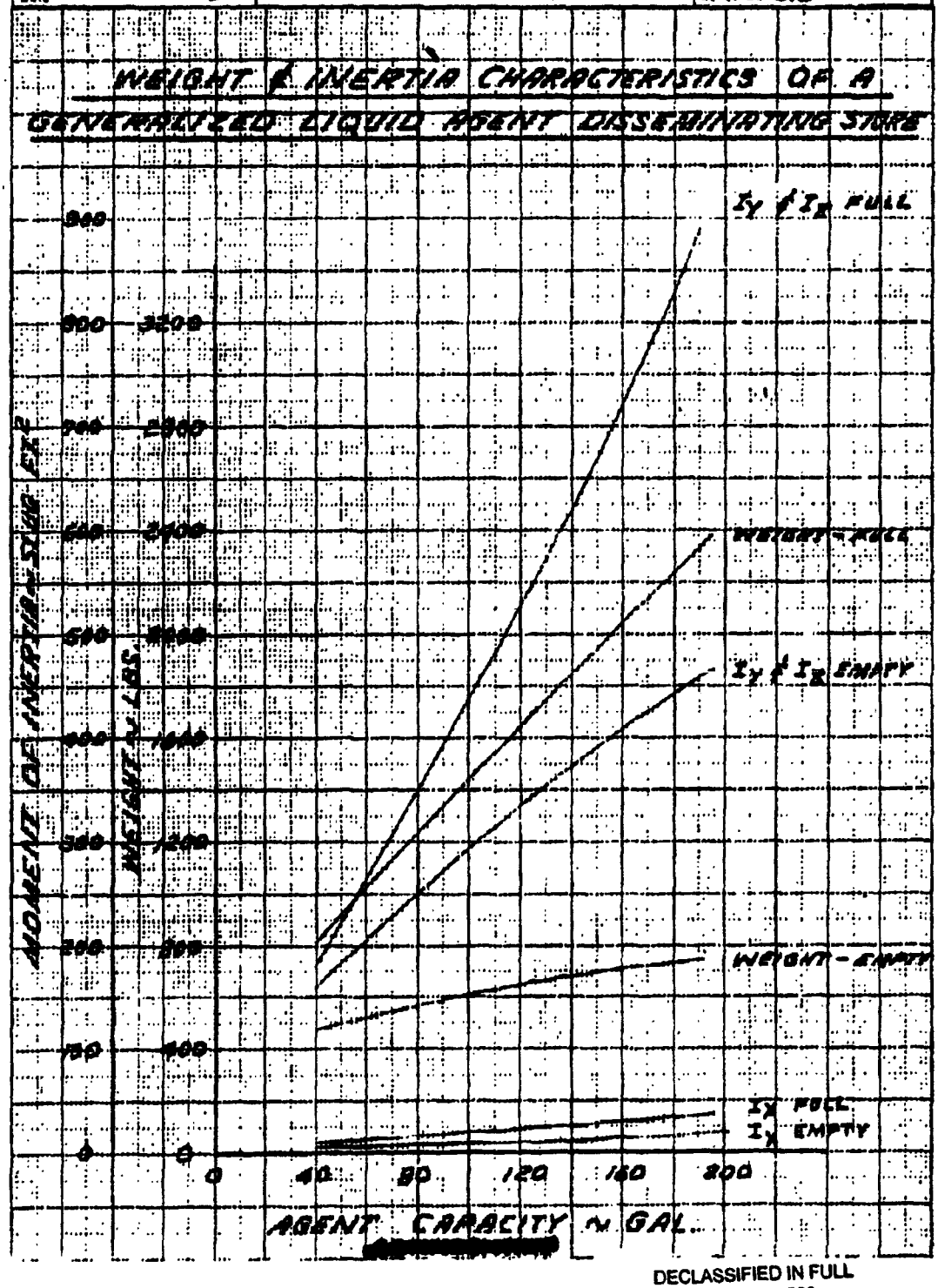

PREPARED BY RSN	NORTH AMERICAN AVIATION, INC.	TFD-61-251-4
CHECKED BY		REPORT NO
DATE FEB. 17, 61		MODEL NO GQ 2533

GQ 2533

ISOLATED STORE ESTIMATED AERODYNAMIC CHARACTERISTICS

LIFT, DRAG AND PITCHING MOMENT

FINLESS CONFIGURATION

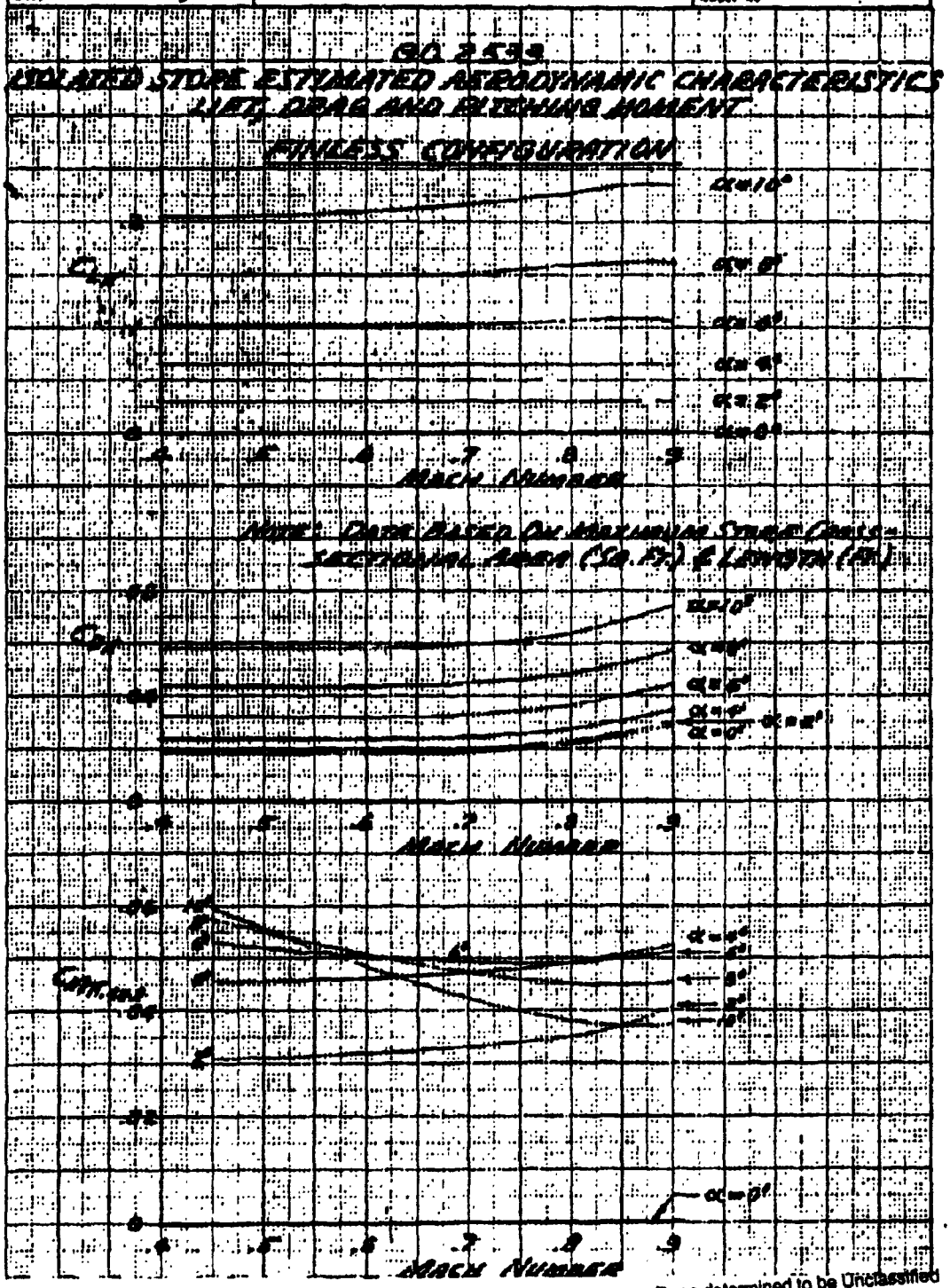

NOTE: DATA BASED ON MAXIMUM STORE CROSS-SECTIONAL AREA (Sq. Ft.) & LENGTH (Ft.)

DP-61-181

NORTH AMERICAN AVIATION, INC.

TFD-61-251-5

REPORT NO

ORIG. NO G.O. 2533

DATE 23 FEB. 61

G.O. 2533 ISOLATED STORE

ESTIMATED AERODYNAMIC CHARACTERISTICS

ZERO COEFFICIENT

FINNED CONFIGURATION

NOTE: DATA BASED ON MAX. STORE CROSS-SECTIONAL AREA (3 sq. ft.)

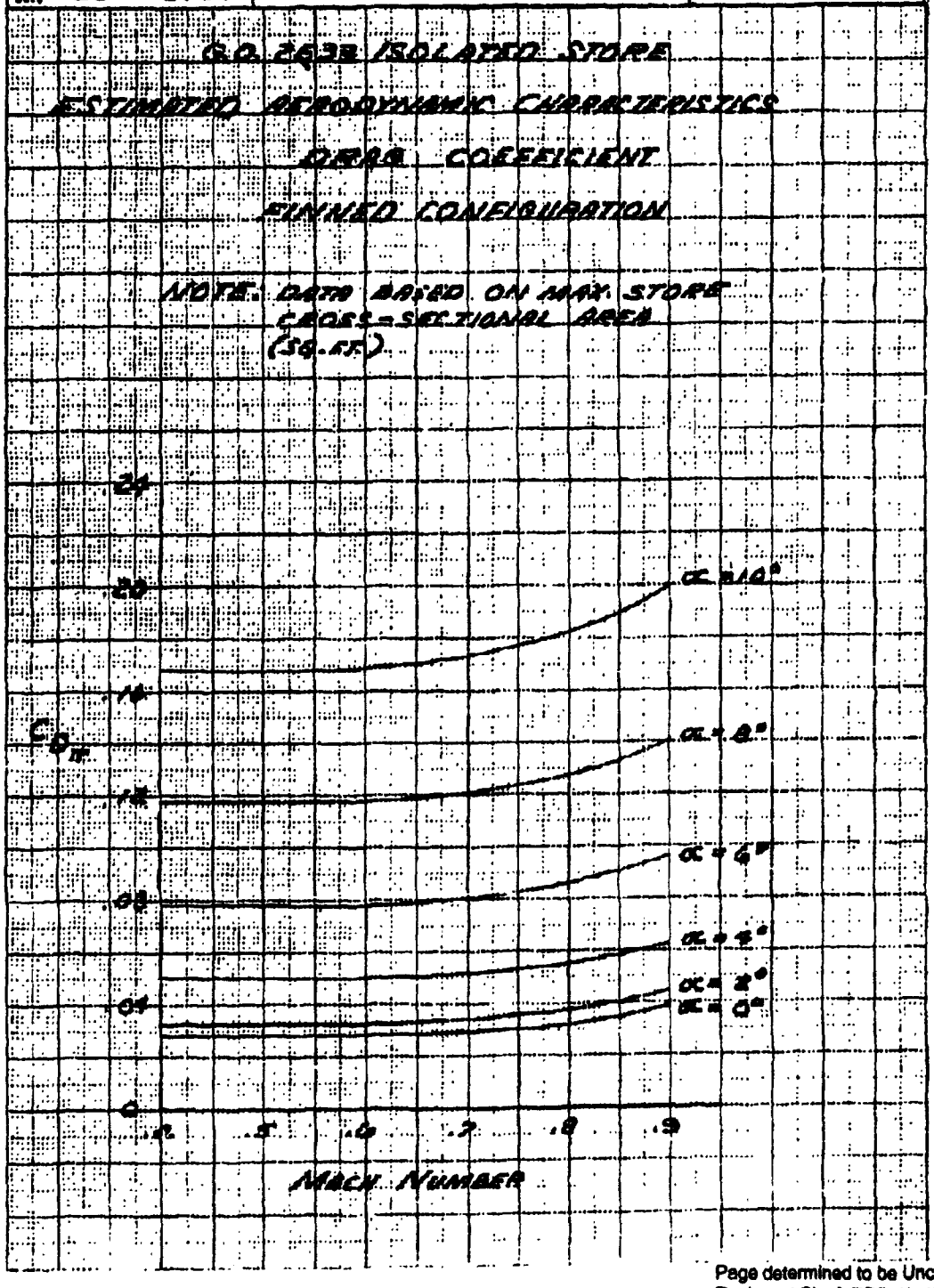

DP-61-182

NORTH AMERICAN AVIATION, INC.

TFD-61-251 6

DATE 17 FEB. 61

G.O. 2533

G.O. 2533 ISOLATED STORE

ESTIMATED AERODYNAMIC CHARACTERISTICS

LIFT COEFFICIENT

FINNED CONFIGURATION

NOTE. DATA BASED ON MAX. STORE CROSS-SECTIONAL AREA (5.0 SQ. FT.)

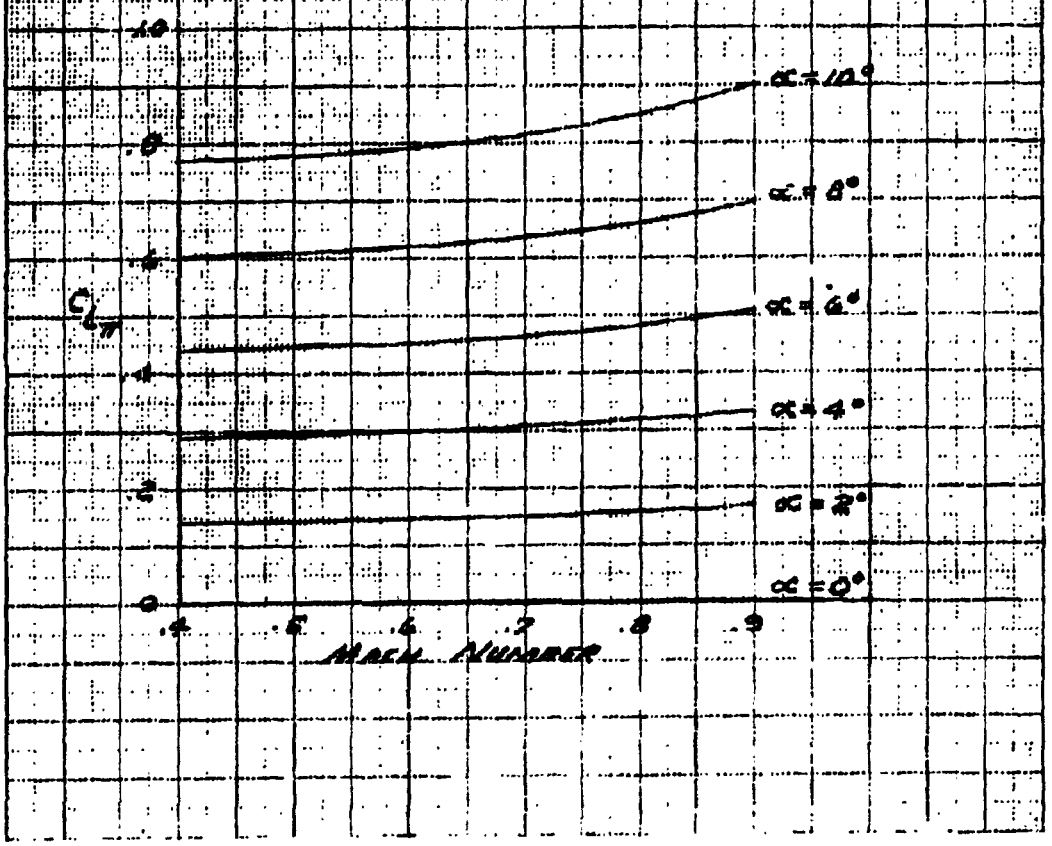

DP-61-183

NORTH AMERICAN AVIATION, INC.

DATE 17 FEB. 61

G.O. 2533

G.O. 2533 ISOLATED STORE

ESTIMATED AERODYNAMIC CHARACTERISTICS

PITCHING MOMENT COEFFICIENT

FINNED CONFIGURATION

NOTE: DATA BASED ON MAX. STORE CROSS-SECTIONAL AREA (SQ. FT.) & LENGTH (FT.)

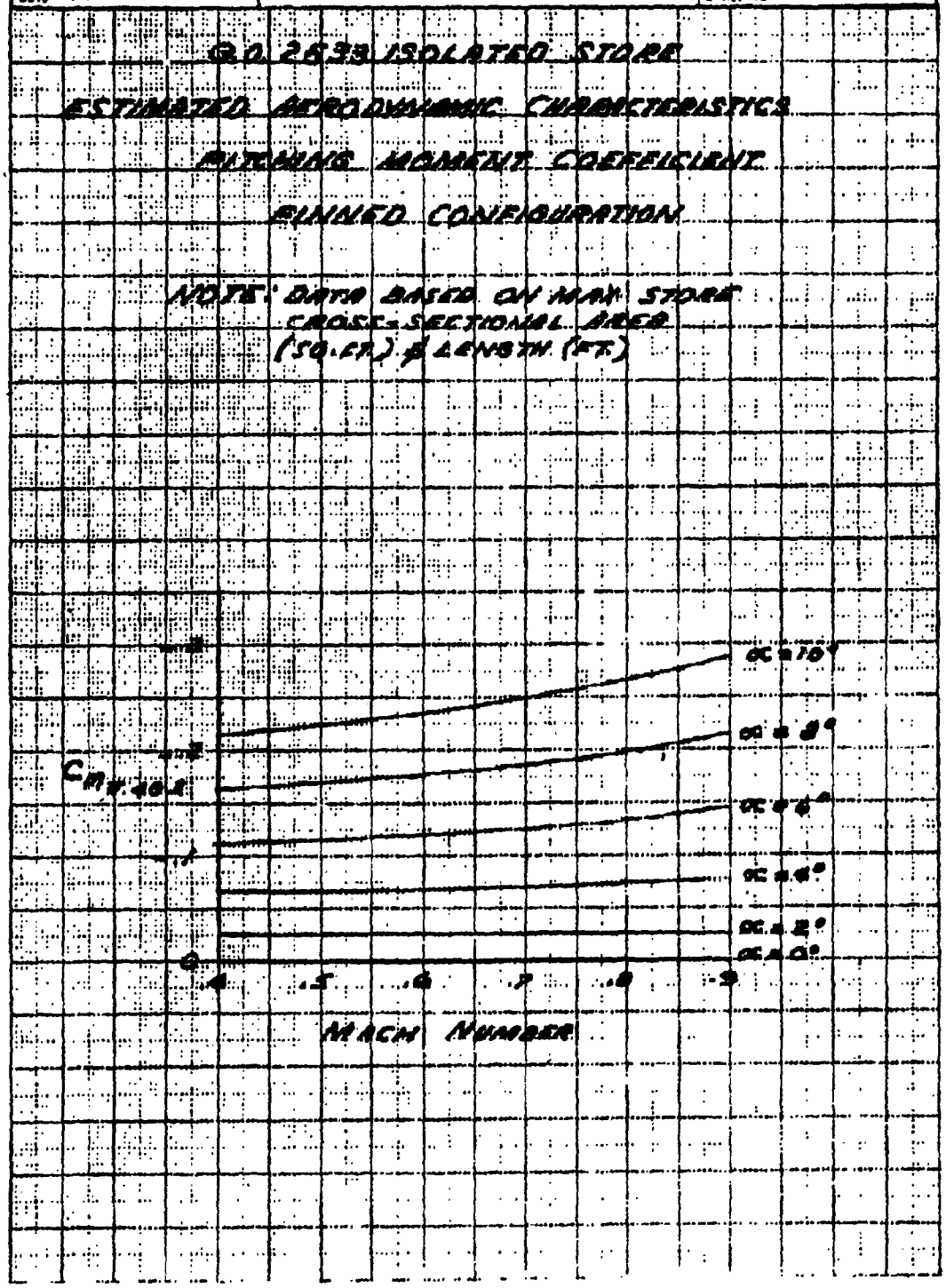

DP-61-184

DESIGNED BY H.J.	NORTH AMERICAN AVIATION, INC.	TEL 6-25-8
CHECKED BY		
DATE 23 FEB. 61		G.O. 2533

G.O. 2533

ESTIMATED STORE NORMAL FORCE AND PITCHING MOMENT COEFFICIENTS AS MOUNTED AT INBD WING STA. OF F-100 AIRPLANE

NOTE: 1) DATA BASED ON STORE PLANVIEW AREA (SQ. FT) & LENGTH (FT) $\frac{S_p}{S_w} = 0.22$

2) DATA FOR LEFT WING STORE

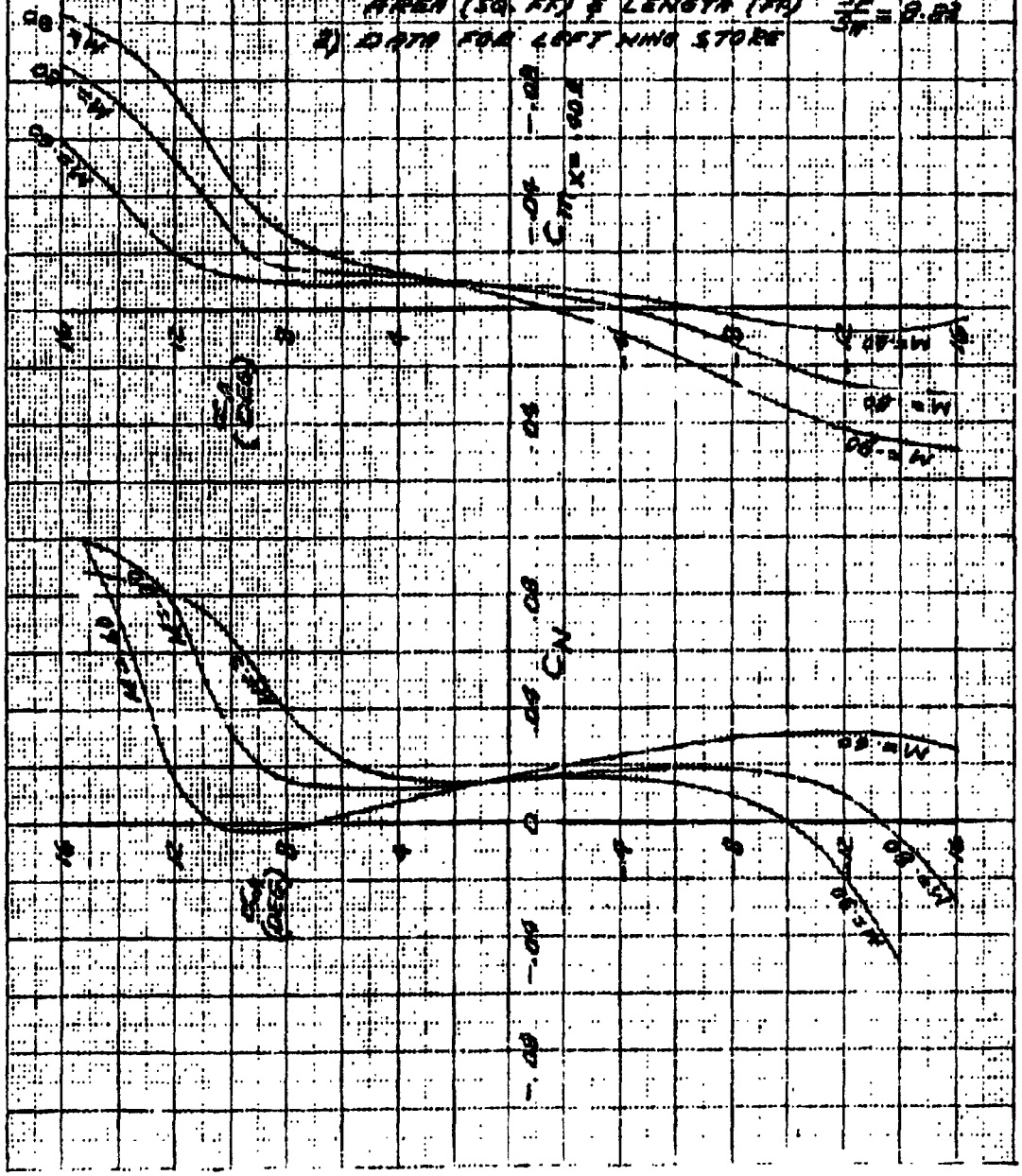

DP-61-185

PREPARED BY RSN

NORTH AMERICAN AVIATION, INC.

DATE FEB. 23, 61

MODEL NO G.O. 2533

G.O. 2533

ESTIMATED STORE AXIAL FORCE COEFFICIENTS AS MOUNTED AT INBOARD WING SECTION OF THE F-100 AIRPLANE

FAIRED CONFIGURATION

NOTES: DATA BASED ON STORE PLANFORM AREA (SQ. FT.) & LENGTH (FT.)

$\frac{S_A}{S_m} = 0.03$

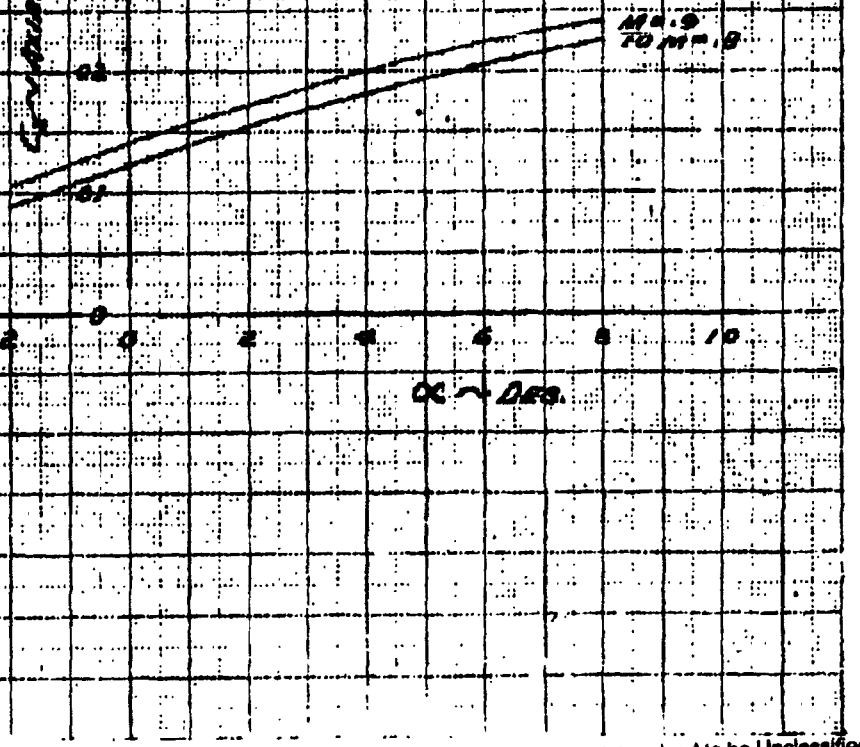

DP-61-186

NORTH AMERICAN AVIATION, INC.

PREPARED BY H.J. | TFD-61-231-10

CHECKED BY | MODEL NO.

DATE 23 FEB. 61 | MODEL NO. G.O. 2533

G.O. 2533

ESTIMATED STORE YAWING MOMENT AND SIDE FORCE COEFFICIENTS AS MOUNTED AT INBD WING STA. OF F-100 AIRPLANE

NOTE: 1) DATA BASED ON STORE PLANFORM AREA (SQ. FT.) & LENGTH (FT.)

$\frac{S_p}{L_p} = 8.88$

2) DATA FOR LEFT WING STORE

3) DATA INCLUDES EFFECTS OF VERTICAL FINS

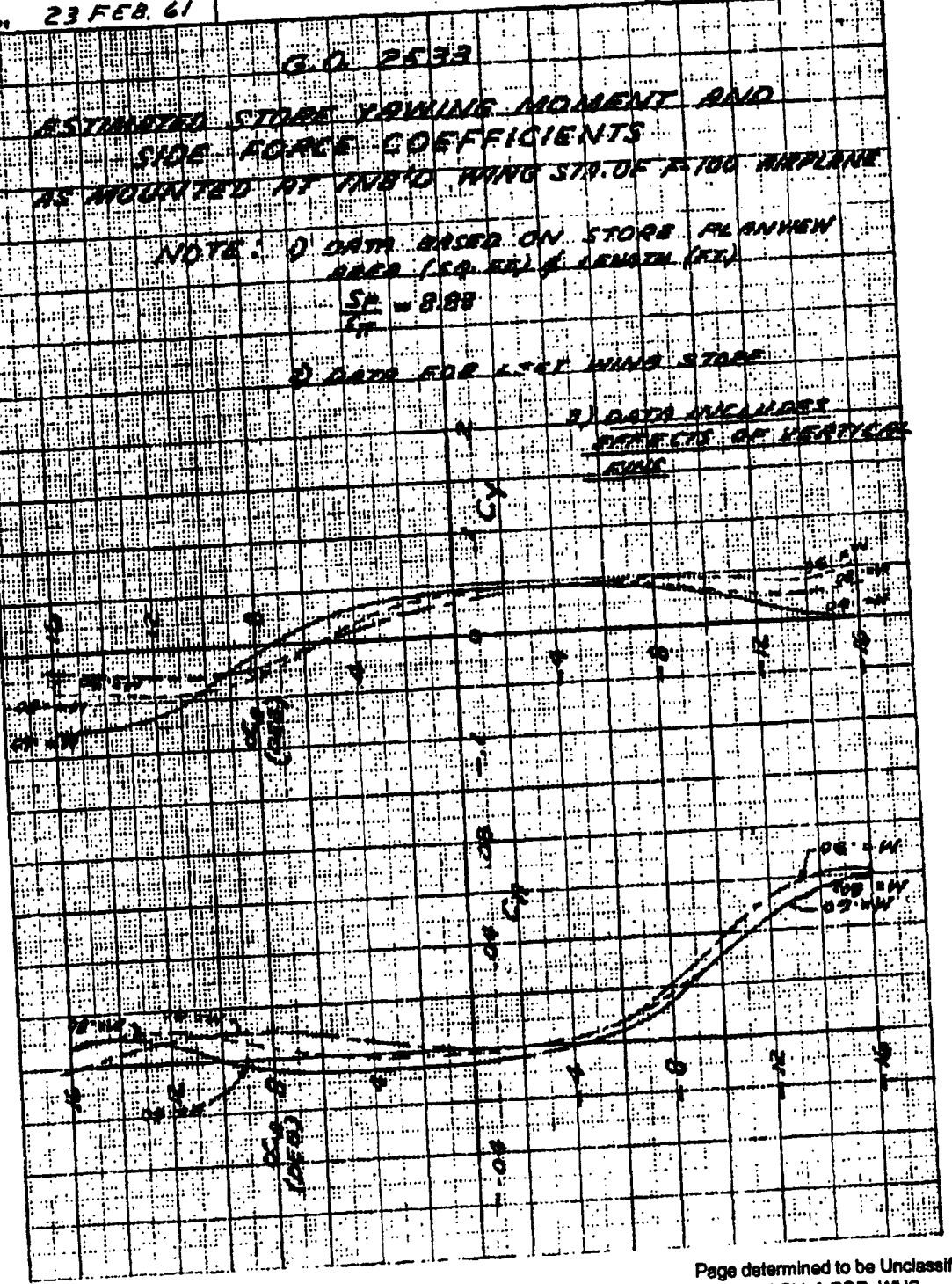

DP-61-187

PREPARED BY H.J.	NORTH AMERICAN AVIATION, INC.	TFD-61-251-11
CHECKED BY		REPORT NO
DATE 23 FEB. 61		MODEL NO G.O. 2533

G.O. 2533

INCREMENTAL NORMAL FORCE AND PITCHING MOMENT COEFFICIENTS DUE TO YAW ON THE STORE MOUNTED AT INBD WING STA. OF THE F-100 AIRPLANE FINNED CONFIGURATION

$D \& M \leq .90$

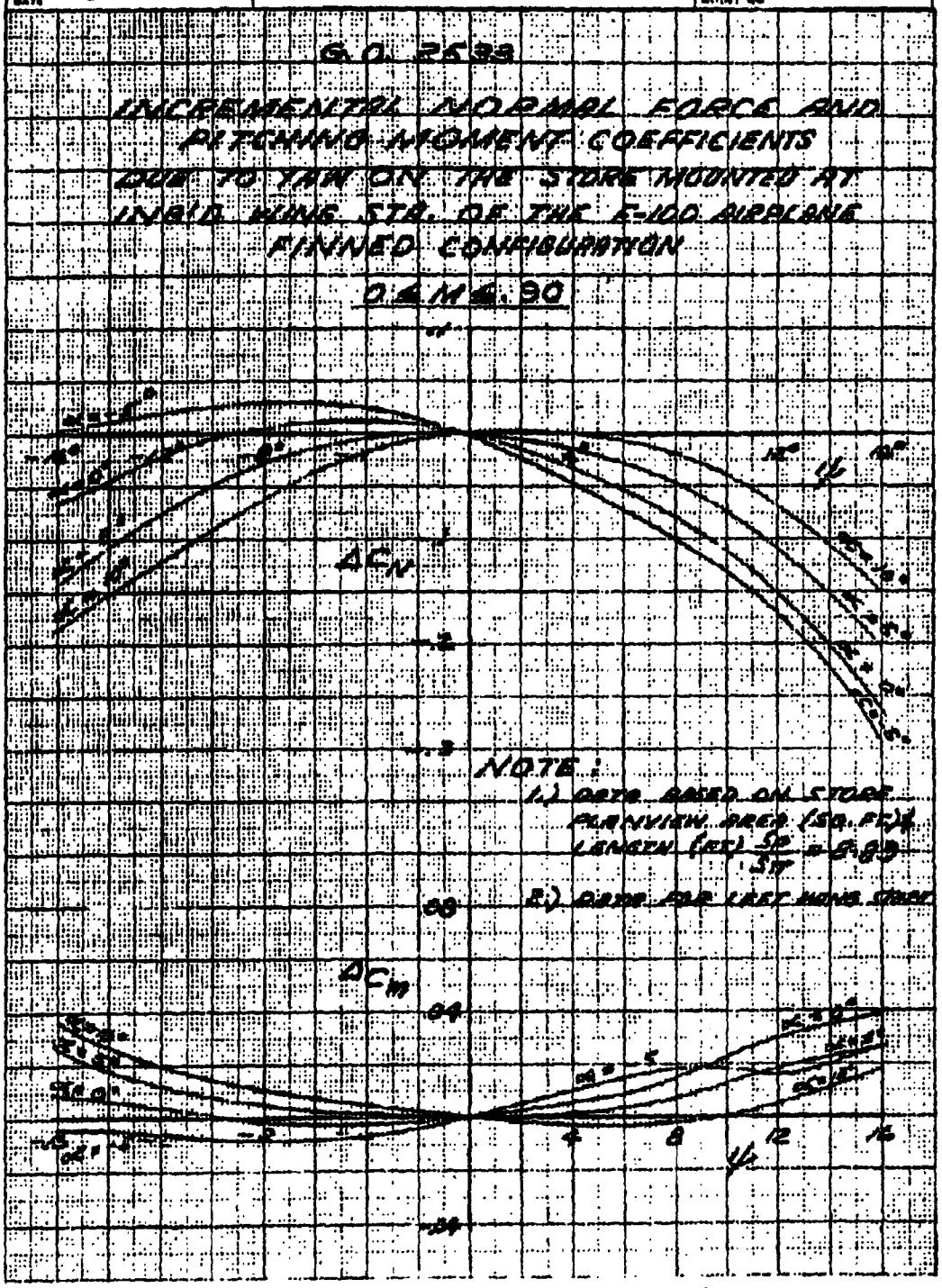

DP-61-188

PREPARED BY RSN	NORTH AMERICAN AVIATION, INC.	71-61 25-12
CHK'D BY		REPORT NO
DATE FEB. 23, 61		MODEL NO 90.2533

90.2533

INCREMENTAL SIDE FORCE AND YAWING MOMENT COEFFICIENTS DUE TO YAW ON THE STORE MOUNTED AT INB'D WING STA. OF THE F-100 AIRPLANE

FINNED CONFIGURATION

TO M=.80

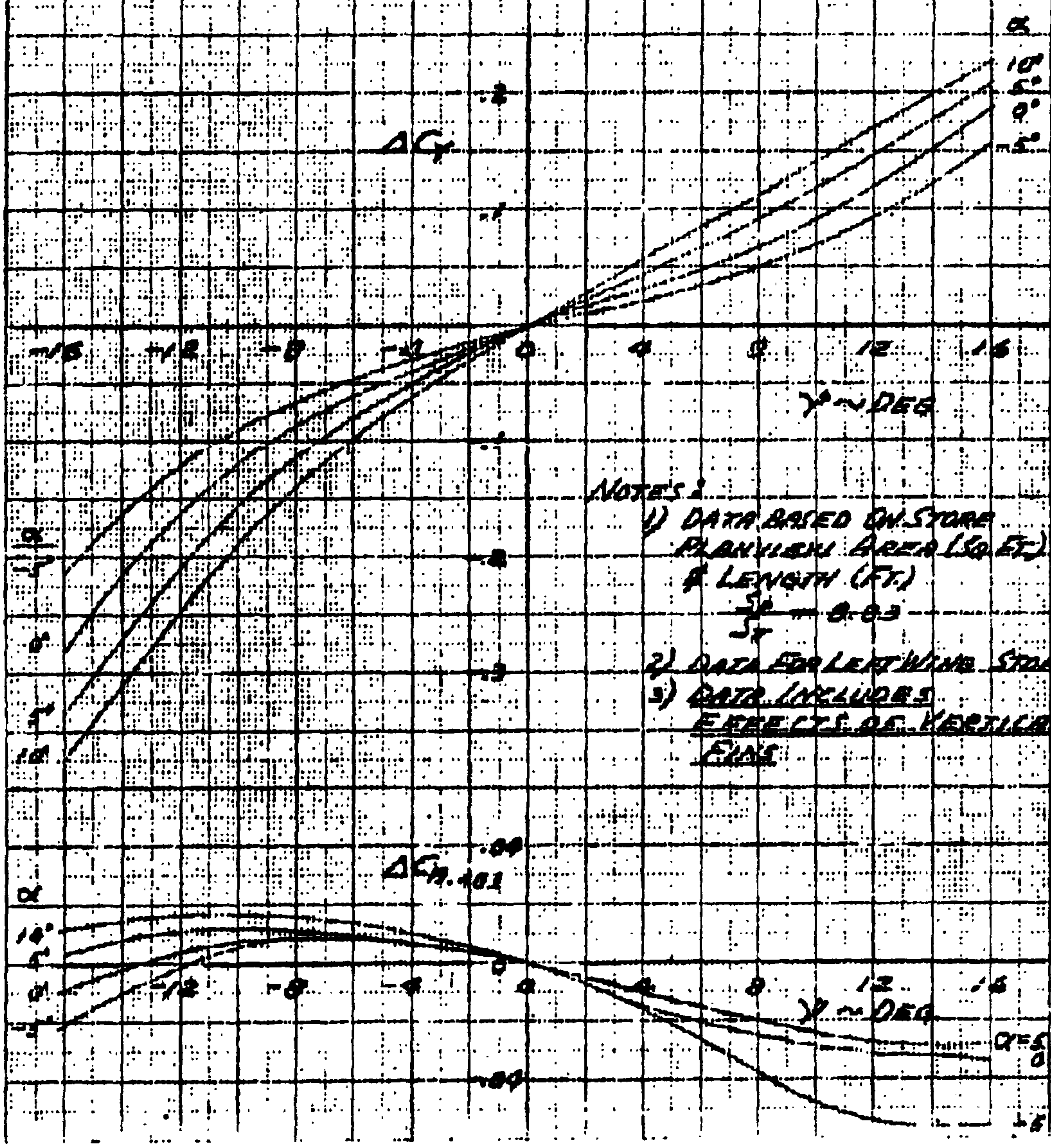

CONFIDENTIAL

APPENDIX B

PRELIMINARY DESIGN OF AN AIRBORNE UNIVERSAL EXTERNAL STORE FOR LINE SOURCE DISSEMINATION OF LIQUID BW AGENTS

Conducted Under General Mills, Inc.
Purchase Order No. MD-78766

By

North American Aviation, Inc.
Los Angeles, California

[redacted]

Serial No. .....

File No. ....

Report No. NA-61-758

NORTH AMERICAN AVIATION, INC.

INTERNATIONAL AIRPORT
LOS ANGELES 45, CALIFORNIA

ENGINEERING DEPARTMENT

THE PRELIMINARY DESIGN OF AN AIRBORNE UNIVERSAL EXTERNAL STORE FOR LINE SOURCE DISSEMINATION OF LIQUID BW AGENTS

[redacted]

PREPARED BY

Aero-Thermo Special Projects

APPROVED BY

L. P. Greene, Manager
Research and Development

No. of Pages 32

Date 3 July 1961

REVISIONS

DATE	REV BY	PAGES AFFECTED	REMARKS

[redacted]

FD-699 APV 1-60

[redacted]

ABSTRACT

TITLE: The Preliminary Design of an Airborne Universal External Store for Line Source Dissemination of Liquid BW Agents.

AUTHOR: Marshall H. Roe, Aero-Thermo Special Projects

This report presents generalized aerodynamic, weight, and inertia characteristics of a universal external aircraft store for dissemination of liquid biological agents. These data were prepared to examine compatibility of the store with an Army surveillance drone. Also included are the results of a configuration study preliminary to detailed engineering design of the store.

DESCRIPTIVE TERMS

Biological warfare
External stores for aircraft
Line-source dissemination
General Mills, Inc.
Liquid BW agents
BW/CW

FOREWORD

The studies described in this report were conducted in accordance with Amendment 2 of the General Mills, Inc., Contract MD-78766, subcontract to Army Chemical Corps Contract No. DA-18-064-CML-2745. The study period was from 13 February 1961 through 26 May 1961

[redacted]

TABLE OF CONTENTS

[redacted]

LIST OF ILLUSTRATIONS

LIST OF TABLES

[redacted]

INTRODUCTION

North American Aviation, Inc., is participating as a subcontractor to General Mills, Inc., in an Army Chemical Corps program to develop external stores for the line source dissemination of liquid and dry BW agents. NAA has completed the phase of this development program of design studies of a universal liquid agent dissemination store for use with operational manned aircraft. The present work is concerned with examining the compatibility of the Army SD-5 surveillance drone with a liquid agent store, and proceeding with the preliminary design of a prototype store. It is planned that the detailed design and fabrication of the prototype store will follow review and approval by GMI and the Biological Laboratories of the preliminary design resulting from this phase of the program.

[redacted]

[redacted]

DISCUSSION

The scope of the work covered by this report is defined by the work statement of Amendment 2 of GMI Contract MD 78766, which is quoted below:

"1. Complete the design requirements for a prototype external store liquid agent dissemination system. The results already obtained under this contract with General Mills, Inc. shall be used. The design requirements to be established shall apply insofar as possible to a universal store; however, detailed design shall consider installation of the store on the AN/USD-5 drone and also the F-100D airplane, which is anticipated as a test vehicle.

a. As part of this work, data shall be submitted to General Mills, Inc. for purposes of evaluating compatability with the drone. These data shall consist of preliminary aerodynamic, weight and inertia characteristics.

b. Coordinate with General Mills, Inc., the Army Chemical Corps, and the drone manufacturer in establishing a mutally acceptable store configuration at General Mills, Inc. direction.

c. Preparation of Layout Drawings - Layout drawings of the external store shall be prepared, which shall include external geometry, definition of components (such as turbine, generator, valves, pumps, nozzle assembly and actuators), controls and control sequencing, jettison provisions, agent capacity, insulation, agitation and heating and maintenance provisions.

2. Prepare a reproducible technical report covering the work under Item 1 above."

Upon completion of items 1a and 1b, NAA was redirected by GMI to eliminate any further consideration of store compatibility with the USD-5 drone as required by item 1.

[redacted]

GENERALIZED STORE DATA FOR DRONE COMPATIBILITY STUDY

For purposes of a comparative evaluation of store characteristics versus drone capabilities, aerodynamic, weight, and inertia characteristics as a function of store size were prepared. These data are based on the store configuration as shown in an earlier proposal report, reference 8, and reflect a somewhat heavier empty weight than the store that has evolved from the present work.

Geometrical data defining the generalized store are shown in figures 1 and 2. A fineness ratio of 8.5:1 was chosen since it has an adequately high drag - divergence Mach number as well as adequate capacity. The stabilizing fins shown are optional, depending on the need for reduction or the destabilizing effects of the stores and for free drop jettisoning of the stores.

Aerodynamic Characteristics

Aerodynamic characteristics consisting of lift, drag, and pitching moment coefficients for the isolated store are shown as a function of Mach number and angle of attack in figures 3 through 6.

The isolated store aerodynamic characteristics consisting of lift, drag and pitching moment coefficients of the finless configuration were initially estimated on the basis of data contained in reference (1) which dealt with the high subsonic Mach number wind tunnel testing of a similar external store model. The fins-on data were also derived from the above referenced report with necessary corrections made for the fin effects. A North American report, NA-55-1108, was also referenced in the comparison of the body alone (finless) data. (These initial data were forwarded to GMI by cover letter and later revised by wire.)

Subsequent analysis of the drag data in the referenced Douglas report and a comparison of those data with data in references (3), (4) and (5) indicated that the drag data of reference (1) are optimistic, probably because of improper corrections for the base drag. All of references (3), (4) and (5) show the low speed zero-lift drag level of 0.05 of a fins-off low-drag body similar to the store shapes concerned now; particularly, the configuration #7 in reference (3) is almost the exact shape. Therefore, the initial drag estimate was revised to that shown in figure 3, which gives a drag coefficient of 0.05 at low speed, zero lift. Effects of angle of attack and fins on the store drag remain the same as estimated from reference (1).

Weight and Inertia Characteristics

Weight and inertia data are shown as a function of agent capacity in figure 7.

These data were estimated from an arrangement as depicted in NAA drawing No. 2521-900001, as shown in reference 8. Using this configuration as a reference model, variations in tank capacity and geometry were established and are identified in the following manner.

Tank No. 1	50 Gals Agent Capacity
Tank No. 2	125 Gals Agent Capacity
Tank No. 3	190 Gals Agent Capacity

Since the preliminary design phase did not include detailed design information, the structural weights were estimated from previous North American Aviation tank configurations. Weights for the secondary power supply and pumping equipment were obtained from equivalent off-the-shelf units and hardware items.

A summary of weight, C.G., and inertia data is shown in Table I below. Weight build-ups for the three stores are shown in Tables II through IV.

CONFIDENTIAL

TABLE I

WEIGHT, INERTIA AND BALANCE SUMMARY

CONDITION	WEIGHT LBS	$\bar{X}$ TANK STA INCHES	$\bar{Z}$ WL INCHES	I_X RCLL SLUG FT^2	I_Y PITCH SLUG FT^2	I_Z YAW SLUG FT^2	I_{XZ} SLUG FT^2
TANK #1 (50 GALS) - 19.3 INCHES MAX DIA, 165 INCHES LENGTH							
Empty-Rooms Retr.	499	70.5	- .2	5.3	182.8	182.8	+ 1.4
" " Ext.	499	70.2	- .9	7.6	180.0	177.7	- 6.4
Full " Retr.	916	68.9	- .1	8.0	225.8	225.9	+ 1.4
" " Ext.	916	68.7	- .5	10.4	222.9	220.6	- 6.5
TANK #2 (125 GALS) - 23.5 INCHES MAX DIA, 200 INCHES LENGTH (125 GALS)							
Empty Rooms Retr.	649	90.0	- .1	10.4	345.1	345.1	- 2.5
" " Ext.	649	89.7	- .7	12.9	341.2	338.8	- 8.5
Full " Retr.	1691	88.2	0	21.3	550.7	550.8	- 2.5
" " Ext.	1691	88.1	- .3	23.8	546.8	544.3	- 8.6
TANK #3 (190 GALS) - 26 INCHES MAX DIA, 220 INCHES LENGTH							
Empty-Rooms Retr.	736	99.3	- .1	14.8	457.8	457.9	- 2.4
" " Ext.	736	99.0	- .6	17.3	453.8	451.4	- 8.6
Full " Retr.	2319	97.7	0	34.3	893.2	893.3	- 2.4
" " Ext.	2319	97.6	- .2	36.8	889.2	886.7	- 8.7

INERTIAS ARE ABOUT AXES PASSING THRU CG AND PARALLEL TO REFERENCE AXES

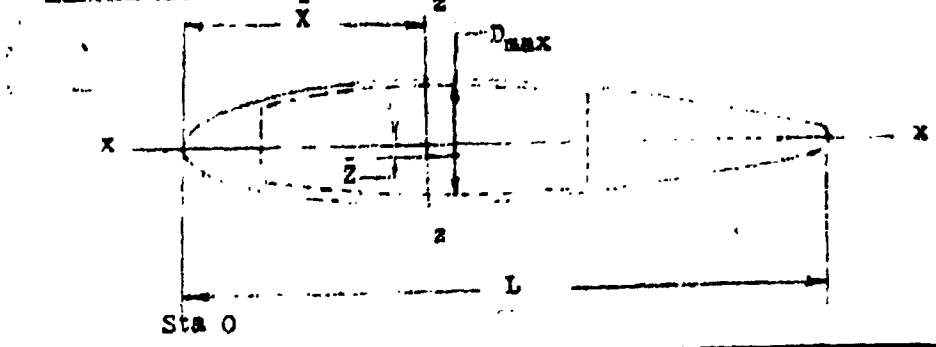

CONFIDENTIAL

CONFIDENTIAL

TABLE II

WEIGHT SUMMARY FOR

TANK #1 (50 GAL)

ITEM	WT-LBS
Body Group (Outer Shell Struct)	166
Fins	10
Insulation	11
Tank Assembly	155
Power Supply	
Turbine Assembly	29
Generator Assem (Incl Supts)	40
Electronic Prov.	14
Spray Provisions	
Pumps & Piping	12
Boom Assem.	30
Actuators & Controls	13
Indicators & Controls	5
MISC.	18
TOTAL TANK ASSEMBLY (EMPTY)	499
AGENT 50 GAL	417
TOTAL TANK ASSEMBLY (INCL. AGENT)	916

CONFIDENTIAL

CONFIDENTIAL

TABLE III

WEIGHT SUMMARY FOR

TANK #2 (125 GAL)

ITEM	WT-LBS
Body Group (Outer Shell Struct)	210
Fins	14
Insulation	18
Tank Assembly	245
Power Supply	
Turbine Assem	25
Generator Assem (Incl Supts)	40
Electrical Prov	15
Spray Provisions	
Pumps & Piping	14
Boom Assem	30
Actuators & Controls	13
Indicators & Controls	6
MISC.	19
TOTAL TANK ASSEMBLY (EMPTY)	649
AGENT 125 GAL	1042
TOTAL TANK ASSEMBLY (INCL. AGENT)	1691

CONFIDENTIAL

CONFIDENTIAL

TABLE IV

WEIGHT SUMMARY FOR

TANK #3 (190 GAL)

ITEM	WT-LBS
Body Group (Outer Shell Struct)	850
Fins	16
Insulation	21
Tank Assembly	284
Power Supply	
Turbine Assem	25
Generator Assem (Incl Supts)	40
Electrical Prov	15
Spray Provisions	
Pumps & Piping, etc.	16
Boom Assem.	30
Actuators & Controls	13
Indicators & Controls	6
MISC.	20
TOTAL TANK ASSEMBLY (EMPTY)	736
AGENT 190 GAL	1583
TOTAL TANK ASSEMBLY (INCL AGENT)	2319

CONFIDENTIAL

DESIGN PARAMETERS FOR MANNED AIRCRAFT STORE

Following the decision by the Biological Laboratories to delete the requirement for store compatibility with the SD-5 drone, design requirements for the prototype store for manned aircraft were determined and applied in the design layout shown in figure 8. A discussion of these requirements follows.

Geometrical Parameters

In establishing the overall store dimensions the following criteria were considered:

1. The store should be capable of operational demonstration on the first-line tactical aircraft (fighter-bombers, ground support types) of the Air Force, Navy, and Marine Corps.

2. Since area coverage requirements have not been established by the using commands, the amount of agent to be carried was assumed to be the maximum possible, consistent with the requirement of item (1) above.

The aircraft considered in item (1) were: F-100C, D and F, F-105B and D, B-66B, A3J-1, FJ-4B, and the A4D. Reference 6 shows the following capabilities of these particular aircraft.

Airplane	Store Station	Fuel Tank Capability	Store Weight Capability	Lug Spacing
F-100C,D & F	106 in.	450 Gal.	3170 lb.	14,20,30 in.
F-105 B & D	0	450	3170	30
	138	450	3170	30
B-66B	254	450	3200	30
A3J-1	110	400	4000	30
FJ-4B	122	344	2450	14,30
A4D	0	300	3575	14,30

From consideration of these capabilities evolved the store geometry of 226 in. length, 26 in. diameter, 190 gallon volume of agent tank, and 30 inch lug spacing.

Preliminary Structural Design

The structure of the BW Store, as shown on NAA drawing 2533-900001 figure 8, was based on the following preliminary loads analysis. Air loads used in this study were based on a 275 gal fuel tank which is similar to the proposed BW store. The amount of inertia for the 275 gal fuel tank was also used as a basis for the external shell of the BW store. The inner tank values were computed and incorporated into the overall results which were the basis for the design consideration made.

Following is a discussion of the loads used and the method of analysis.

Symbols

W	=	weight of store including all disposable loads, lbs.
N_x	=	load factor in fore-and-aft direction
N_y	=	load factor in lateral direction
N_z	=	load factor in vertical direction
$\ddot{\theta}$	=	pitching acceleration, rad/sec^2
$\ddot{\psi}$	=	yawing acceleration, rad/sec^2
α_s	=	angle of attack of store, degrees
β_s	=	angle of sideslip of store, degrees
q	=	$1/2\rho V^2$, dynamic press lb/ft^2
ρ	=	air density, slugs/ft^3
V	=	air velocity, ft/sec

[redacted]

BW Tank
30" Lug Suspension

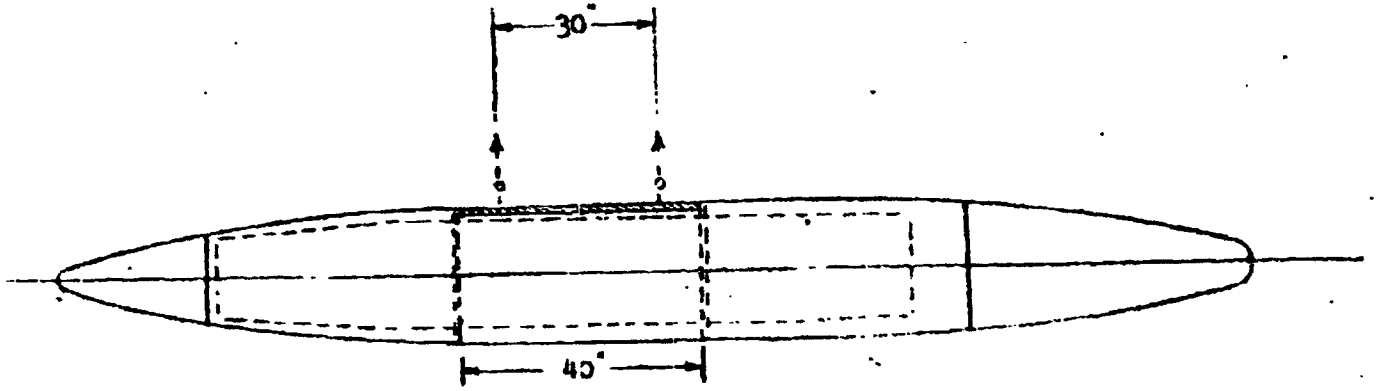

Outer tank
Assume tank Wt = 300# } Estimate based on data
$I_y = I_z = 475{,}000$ lb-in^2 } for 275 gal fuel tank
Inner Tank:
Wt of Tank = 100# } $I_y = I_x = 2{,}470{,}000$ lb-in^2
Wt of Liquid = 1630# }
Total Wt = 2030 lbs
Total I = 3,445,000#-in^2

Inner Tank: 190 Gallon Capacity

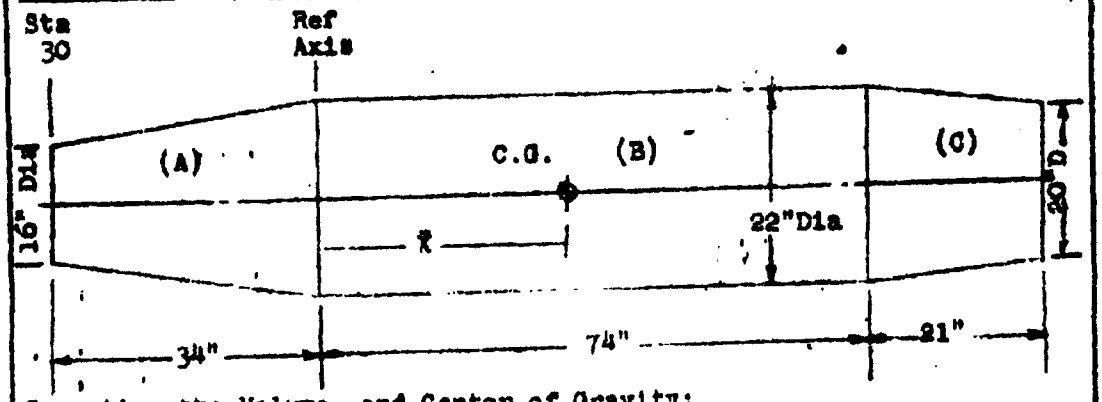

Computing the Volume and Center of Gravity:

Portion	Volume (in^3)	x	(Vol.)x
(A)	9720	-16.1	-15.7×10^4
(B)	28,100	37	104.0×10^4
(C)	7280	84.3	61.4×10^4
	45,100		149.7×10^4

$$\bar{x} = \frac{149.7}{45,100} \times 10^4 = 33.2"$$

Agent Wt = 8.3 lb/Gal
1 Gal = 231 in^3

Capacity of Tank = 196 gal
Wt of Agent = 1630 lb.

Assume Inner Tank 1/8" Thick
Fiberglass Wt = .070lb/in^3
Portion (A)
Volume = 270 in^3

Portion (B)
Volume = 600 in^3

Portion (C)
Volume = 180
= 1050^3 in^3

Wt = 1050x.07 = 73.5 lb.
use a weight of 100 lb.

Inner Tank
Estimate I_y and I_z

Assume Cylinder 22" dia x 129" long
Wt = 1730 lb.

$$M = \frac{1730}{386} = 4.5 \ \frac{\text{lb. sec}^2}{\text{in.}}$$

$$I_y = I_z = M\left\{\frac{r^2}{4} + \frac{l^2}{12}\right\} = 4.5\left\{\frac{11^2}{4} + \frac{129^2}{12}\right\} = \underline{6300 \text{ lb. sec}^2 \text{ in.}}$$

$I_y = I_z = 6300 \times 386 = 2{,}470{,}000$ lb. -in.^{2}

Locate Composite C.G. of Inner Tank, Outer Tank and Liquid.

Outer Tank:
Assume C.G. at Sta. 110 Wt. = 300 lb.

Inner Tank C.G. at Sta 30+34_33.2 = Sta. 97.2 Wt - 1730 lb.

$$X' = \frac{300 \times 100 + 1730 \times 97.2}{1730 + 300} = 99" \text{ (Sta. 99)}$$

Use tank sta 100 as C.G.
Air load reference point is at .4 x 220 = Sta 88
For symmetrical lugs about tank C.G. lugs should be at Sta 85 and 115

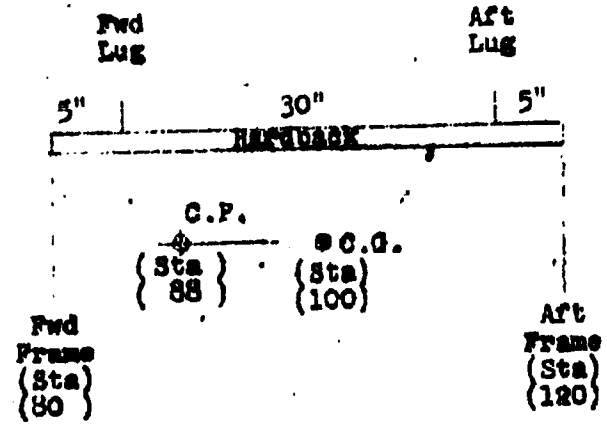

use sway brace angle of 20° per spec. MIL-A-8591B(ASD) Reference 8
inertia moments at C.G. for external tank only

$$M_y = \frac{I_y \ddot{\theta}}{g} = \frac{935000}{386} \ddot{\theta} = 25200 \ddot{\theta} \quad M_z = 2520 \ddot{\psi}$$

for inner tank

$$M_y = \frac{2{,}470{,}000}{386} \ddot{\theta} = 6300 \ddot{\theta} \quad M_z = 6300 \ddot{\psi}$$

Limit Load Factors (Reference MIL-A-8591B)

Wt = 2030 lbs (estimated)

Inertial	1*	2*	3*	ARR Ldg*	Catapult*
N_z	8.67	4.0	6.0	+3 or -1	+3 or -1
N_y	±1.5	±1.5	±5.0	±1.5	±1.5
N_x	±2.0	±2.0	±2.0	9.0	-9.0
$\ddot{\theta}$	±6.0	±6.0	±6.0	±12.0	±12.0
$\ddot{\psi}$	0	0	0	±6.0	±4.0

Signs

$+N_z$ Down $+\ddot{\theta}$ Nose Up

$+N_y$ Left $+\ddot{\psi}$ Nose Left

$+N_x$ Fwd

*Max Design Limit Load Factors from Page 11 of MIL-A-9591B (ASG)

Air Loads For a 275 Gallon Tank from NA 52-186 (Reference 9)

Condition 380R (M .90 at 3000 ft., q = 980 lb/ft^2)
P_z = 653 lb. P_y = 1490 lb.
M_y = 9611 in. lb. M_z = 66282 in. lb.
P_x = 1293 lb.

Condition 329R (M .96 at 3000 ft., q = 1220 lb/ft^2)
P_z = 764 lb. P_y = 1472 lb.
M_y = 9545 in. lb. M_z = 52716 in. lb.
P_y = 1881 lb.

Condition 300S (M 1.10 at 10000 ft., q = 1220 lb/ft^2)
P_z = 982 lb. P_y = 781 lb.
M_y = 59079 in. lb. M_z = 98161 in. lb.
P_x = 2821 lb.

For Negative condition, use condition 420 multiplied by 1.44 (for 1220q)
P_z = 99 x 1.44 = -143 lb.
M_y = 85389 x 1.44 = -123,000 in. lb.
P_y = 608 x 1.44 = -875 lb.
M_z = 35420 x 1.44 = -51,000 in. lb.
P_x = 750 x 1.44 = 1080 lb.

F100A Airloads for q = 1220 lb/ft^2 For 275 Gal Tank

Condition *	P_z	M_y	P_y	M_z	P_x	
1042	560	-83619	640	147242	2271)	
3008	-982	59079	781	98161	2821)	Pos. N_z
324N	-764	4545	1472	52716	1881)	
420	143	-123000	-875	-51000	1080	-Neg N_z

Combine Airload Condition 1042 With Inertia Condition 1
" " " 420 " " " 2
" " " 1042 " " " 3

	For Condition 1 and 3	Condition 2
Max Vertical Loads on Fwd. Frame for	$-N_x$, $-\ddot{\theta}$	$+N_x$, $+\ddot{\theta}$
Max Horizontal " " " " "	$+N_y$ + $\ddot{\psi}$	$-N_{y1}$ - $\ddot{\psi}$
Max Vertical " " Aft " "	$+N_x$ $+\ddot{\theta}$	$-N_x$ $-\ddot{\theta}$
Max Horizontal " " " " "	$-N_y$ - $\ddot{\psi}$	$-N_y$ - $\ddot{\psi}$

Condition	Dash No	N_x	N_y	$\ddot{\theta}$	$\ddot{\psi}$
1	-1	-	+	-	+
	-2	+	-	+	-
2	-1	+	-	+	-
	-2	-	+	-	+
3	-1	-	+	-	+
	-2	+	-	+	-

* Condition

1042 is a symmetrical flight maneuver without pitching acceleration

3008 is an unsymmetrical flight maneuver, steady roll

3242 is an unsymmetrical flight maneuver, steady roll

420 is an unsymmetrical flight maneuver, abrupt roll

Agent Tank Design

The selection of a filament wound fiber glass agent tank was based on considerations of strength (safety), corrosion, weight, sealing, decontamination, heat transfer, and producibility. The Lamtex Corporation of Farmingdale, N.Y., was consulted on design, fabrication, and structural testing of this unit.

Other materials considered, but rejected in favor of the filament wound fiber-glass were: aluminum alloys, stainless steel, self sealing cells, bladder cells, and honeycomb fiberglass.

HEATING AND INSULATION

To fulfill the requirement of maintaining the temperature of the liquid agent within 35°F to 70°F, the agent tank is insulated and the nozzle and plumbing components are heated.

The heat transfer characteristics of the BW store are a function of the outside film coefficient, the amount of insulation, the heat capacity, and film coefficient of the agent. The effect of the insulation is to negate the effect of the outside film coefficient.

Figure 9 shows the effect of various thicknesses of fiberglass batting insulation on agent temperature after a three hour exposure at 43,000 ft cruise altitude with a ram temperature of -7°F. As can be noted, the change in agent temperature is insignificant for insulation thicknesses in excess of 1/2 inch. However, when the store is partially full as shown on figure 9, the agent reaches its limit sooner, as the heat capacity is not available in the agent.

A time - temperature history for agent temperature with a 1/2 inch thick insulation and only 25 gal. of agent in the store is shown on figure 10. This curve assumes that the starting agent temperature was 40°F and the airplane was cruising above 35,000 ft with a ram temperature of -7°F.

As can be noted, the agent will reach 35°F after 105 minutes. With the full tank of course, the agent temperature did not approach 35°F in three hours.

The amount of heat required to maintain the temperature level of the disseminating booms above freezing is a function of the ambient temperature, airplane speed and the film coefficient of the booms. Figure 11 graphically illustrates the heating requirements for the most critical condition of maintaining the extended disseminating booms at 35°F for a

sea level run. The ordinate of figure 11 is the 85% ram recovery temperature, which is a function of both ambient temperature and airplane speed. The heating required will vary then in relation to the ram temperature and the airplane speed. These values are also related to the ambient temperature which is cross plotted on the curve.

A review of the minimum temperature for likely target areas indicates that -40°F is the lowest temperature that need be considered. Reference to figure 11 indicates that a heating density of 8 watts per square inch will be adequate for all airspeeds of approximately 0.7 Mach number and higher. It can be seen that 8 watts per square inch will provide satisfactory heating at any speed for ambient temperatures of -28°F or higher.

Pump and Nozzle Assembly

The design flow rate of the dissemination system has been taken as 18 gallons per minute in accordance with the findings of reference 6. The pump selected is nominally rated at 20 gallons per minute at 50 psi. An adjustment of plus-or-minus two gallons per minute is provided so that the desired rate can be set during bench tests.

The nozzle design is based on earlier test results as reported in reference 7. On the basis of that information the nozzle assembly incorporates 50 individual slit-type orifices, 0.360 inches in length and 0.005 inches in width. This will result in a flow rate of 18 gallons per minute at approximately 35 psi at the nozzle.

Turbine-Generator

Analysis of the electrical load imposed on the generating system indicates that a 4 KVA output is adequate. Estimated requirements for the various electrical components are listed below.

Pump	2.16 KVA
Actuator	1.15 KVA
Boom heaters	1.32 KVA max (boom extended)
Flex line heaters	0.34 KVA max
Valve and plumbing heaters	0.60 KVA max
Solenoid valves(per valve)	1.00 KVA starting, 0.06 KVA holding

The functioning of the controls, as described in a later portion of this report, is sequenced so that the electrical load does not exceed the 4 KVA output of the generator.

The Allison Division of the General Motors Corporation and the AiResearch Division of the Garrett Corporation were contacted relative to supplying the turbine-generator system, and both companies have submitted cost and schedule estimates.

Controls

The control panel to be located in the pilots cockpit is shown schematically in figure 8. In addition to the two switches shown on the panel, the pilots trigger switch will be incorporated as the prime disseminating control. The control switches will utilize the airplane's d.c. power to activate control relays. A schematic of the circuitry is shown in figure 12.

Functions of the controls and indicator lights are described below.

Master control switch (3 position switch)

Position 1: generator off (no power to store components)

Position 2: generator on (power available to store components, assuming air speed is 250 knots IAS or greater)

Position 3: generator on, pump on, recirculation valve open

Boom control switch (2 position switch)

Position 1: nozzle boom extends (assuming generator on)

Position 2: nozzle boom retracts (assuming generator on)

Trigger switch (on-off switch)

Switch depressed: heaters off, pump on, discharge valve opened

Switch released: pump off, discharge valve closed, heaters on

Indicating lights

"Generator off" light illuminates if generator is not operating and Master Control switch is in "Generator On" or "Recirculate" position.

"Boom not extended" light illuminates if "Boom Extend" switch is actuated and boom is not fully extended.

"Flow" light illuminates when liquid is flowing from pump discharge line.

Precautionary circuitry interconnects:

Discharge valve can not be opened unless boom is extended.

Boom can not be retracted unless discharge valve is closed.

Recirculate valve is closed (if open) when trigger switch is depressed

Heaters:

Heater controls are actuated automatically, when the generator is on, by temperature sensing switches.

Filling and Decontaminating

Provisions for filling are illustrated schematically in figure 8. Connections from the filling pump are made to the flex line which goes into the recirculating system. As the tank is filled, it is vented through a flex line in the vent system to the return side of the filling system.

For decontamination of the store after use, the inner tank and plumbing may be flushed with a decontaminating liquid by pumping it through the recirculating, dissemination and vent systems. The aft compartments of the store containing the pump, actuator, valves, etc., may be decontaminated by access through doors in these compartments. The center compartment housing the agent tank is sealed off from the aft compartment so that agent or decontaminant in the aft compartment will not seep into the insulating material in the center section. The exterior of the store can be decontaminated by hosing with a decontaminating liquid.

REFERENCES

1. Report No. EM20948, Summary of Wind Tunnel Tests of the 20 Per Cent Scale External Store Model, Douglas Aircraft Company, El Segundo, California, dated 20 October, 1947

2. Report No. NA 55-1108, Summary of Aerodynamic Force Coefficients of MA-4 Unit in Free Flight and Installed on F-100 Airplane as Derived from Wind Tunnel Tests, North American Aviation, Los Angeles, dated 5 October 1955

3. Sandia Corp. Report No., SCTM 387-58-(51), 25 November 1958 (Confidential Restricted Data)

4. Report No. 4053, Wind Tunnel Investigation of Various Configurational Modifications of the Low Drag Bomb, NAVORD, US Naval Ordnance Laboratory, White Oak, Maryland, dated 22 July 1958, Confidential

5. Report No. 6661, Drag and Roll Coefficients at Subsonic to Supersonic Velocities of 1/7-Scale Free Flight Models of the 1000 Pound Low Drag Bomb (Mk-10), NAVORD, US Naval Ordnance Laboratory, White Oak, Maryland, dated 24 July 1959

6. Report No. NA 60-1403, Design Studies for an Airborne Line-Source Dissemination System for Liquid BW Agents, North American Aviation, Los Angeles, dated 4 November 1960. Secret

7. Report No. NA-59-632, Airborne Biological Warfare at Low Altitude, North American Aviation, Los Angeles, dated 16 June 1959, Secret

8. Report No. NA-60-1149, Proposal For Design, Manufacture and Installation of a Prototype Airborne Store for Dissemination of Liquid BW Agent, North American Aviation, Los Angeles, dated 16 September 1960. Confidential

9. Specification MIL-A-8591B(AS0), Military Specification Airborne Stores and Associated Suspension Equipment, General Design Criteria For, dated 26 May 1955.

10. Report NA-52-186, Airplane Loads for an Air Superiority Fighter-Day (Monoplace) AF Model F-100A, Vol IV, North American Aviation, Los Angeles, California, dated 3 May 1954.

DP-61-179

PREPARED BY R.S.N.

CHECKED BY

DATE FEB 23, 61

NORTH AMERICAN AVIATION, INC.

CONFIDENTIAL

PAGE 21 OF 32

REPORT NO NA-61-[illegible]

MODEL NO

GENERALIZED LIQUID AGENT STORE AERODYNAMIC DIMENSIONAL DATA

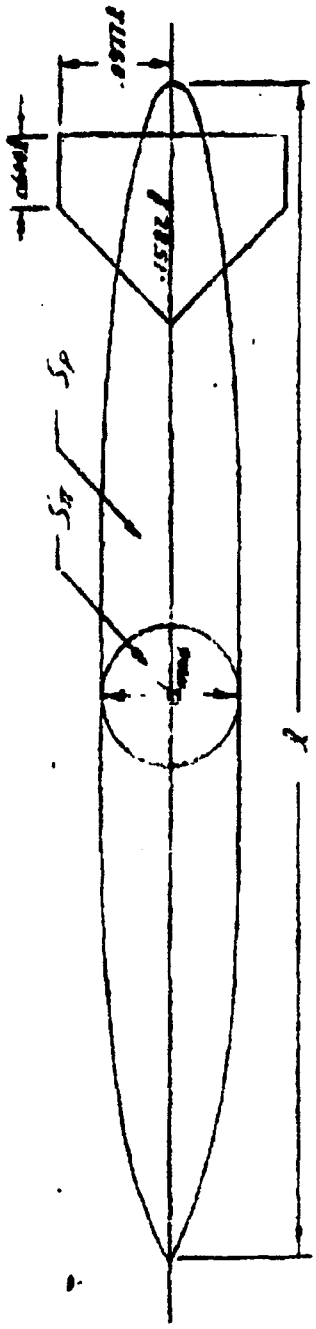

PLAN VIEW

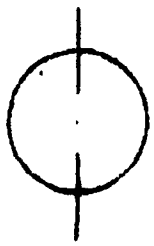

REAR VIEW

$\frac{S_P}{S_W} = 8.83$

$\frac{l}{d_{max}} = 8.5$

CONFIDENTIAL

DP-61-180

PREPARED BY RSN	NORTH AMERICAN AVIATION, INC.	REPORT NO NA-61-251-4
CHECKED BY		REPORT NO
DATE FEB. 17, 61		MODEL NO GO. 2533

GO 2533

ISOLATED STORE ESTIMATED AERODYNAMIC CHARACTERISTICS

LIFT, DRAG AND FLEXURE MOMENT

FINLESS CONFIGURATION

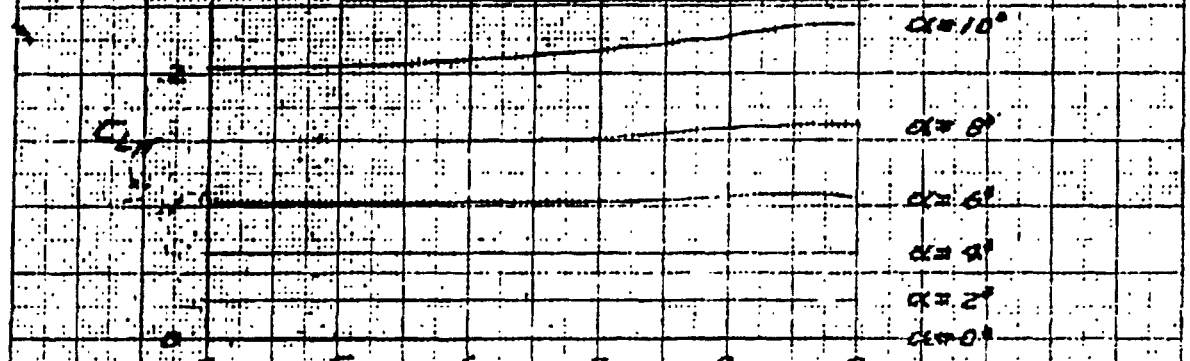

NOTE: DATA BASED ON MAXIMUM STORE CROSS-SECTIONAL AREA (SQ. FT.) & LENGTH (FT.)

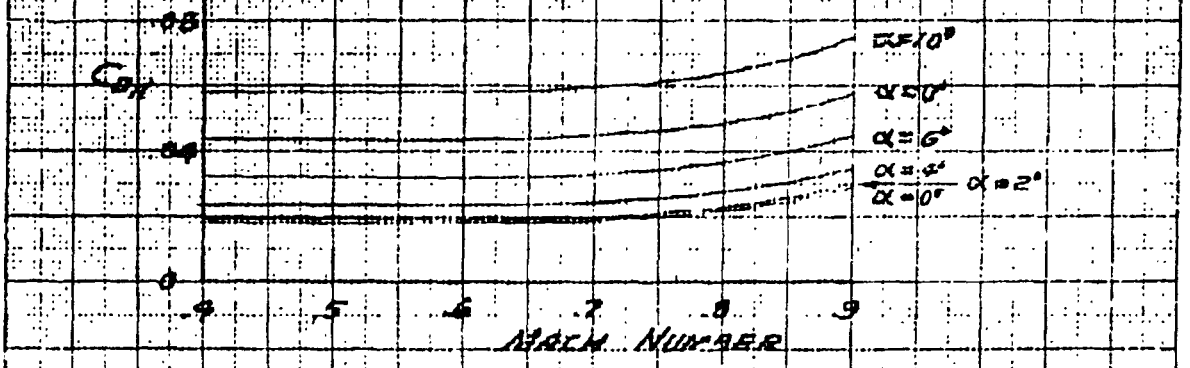

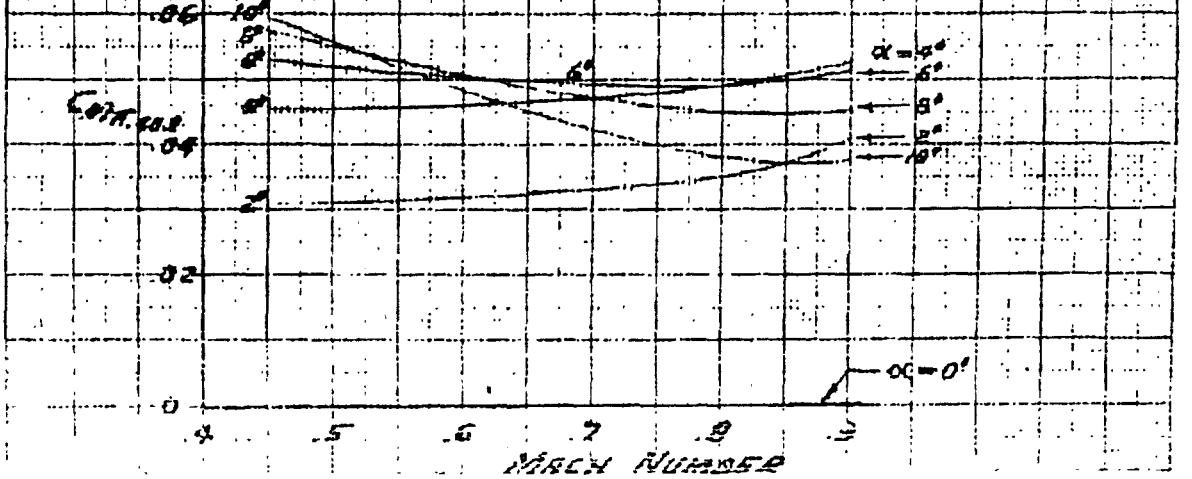

DP-61-181

NORTH AMERICAN AVIATION, INC.

23 FEB. 61

G.O. 2533

G.O. 2633 ISOLATED STORE

ESTIMATED AERODYNAMIC CHARACTERISTICS

DRAG COEFFICIENT

FINNED CONFIGURATION

NOTE: DATA BASED ON MAX. STORE CROSS-SECTIONAL AREA (SQ. FT.)

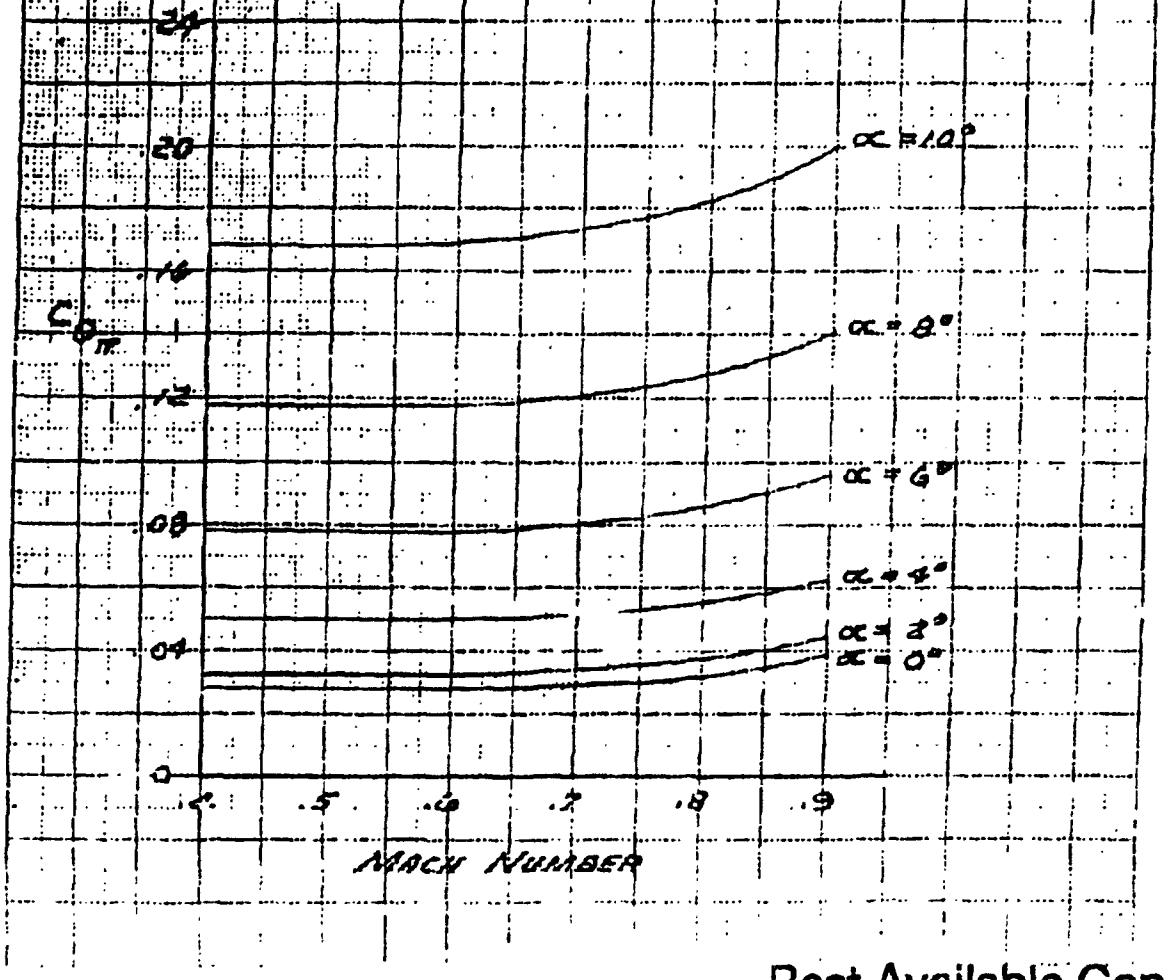

DP-61-182

NORTH AMERICAN AVIATION, INC.
CONFIDENTIAL

DATE 17 FEB. 61

G.O. 2833 ISOLATED STORE

ESTIMATED AERODYNAMIC CHARACTERISTICS

LIFT COEFFICIENT

FINNED CONFIGURATION

NOTE. DATA BASED ON MAX. STORE CROSS-SECTIONAL AREA (1.5 SQ. FT.)

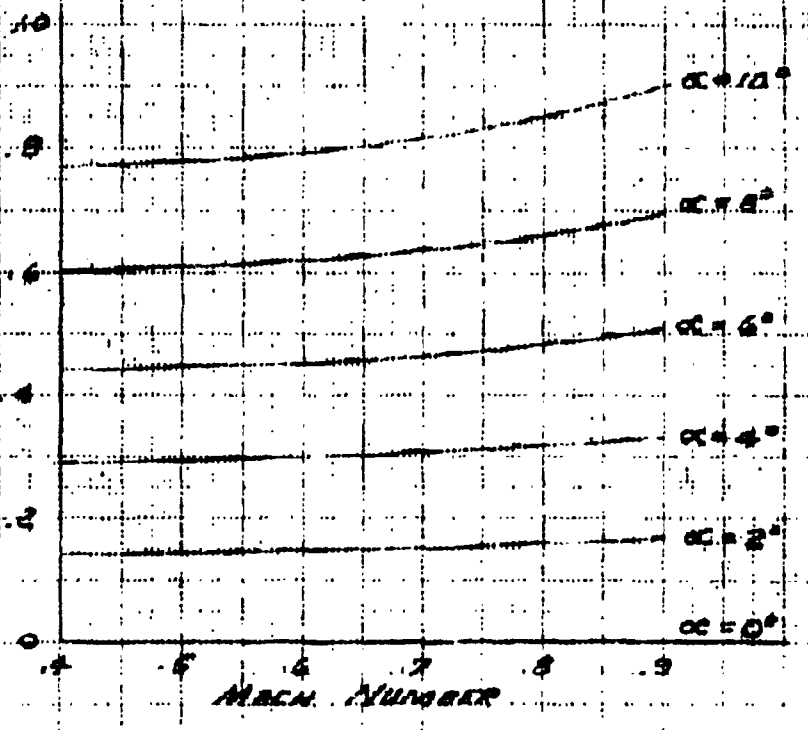

DP-61-183

NORTH AMERICAN AVIATION, INC

[redacted]

DATE 17 FEB 61

G.D. 2533 ISOLATED STORE

ESTIMATED AERODYNAMIC CHARACTERISTICS

PITCHING MOMENT COEFFICIENT

FINNED CONFIGURATION

NOTE: DATA BASED ON MAX STORE CROSS-SECTIONAL AREA (SQ. FT.) & LENGTH (FT.)

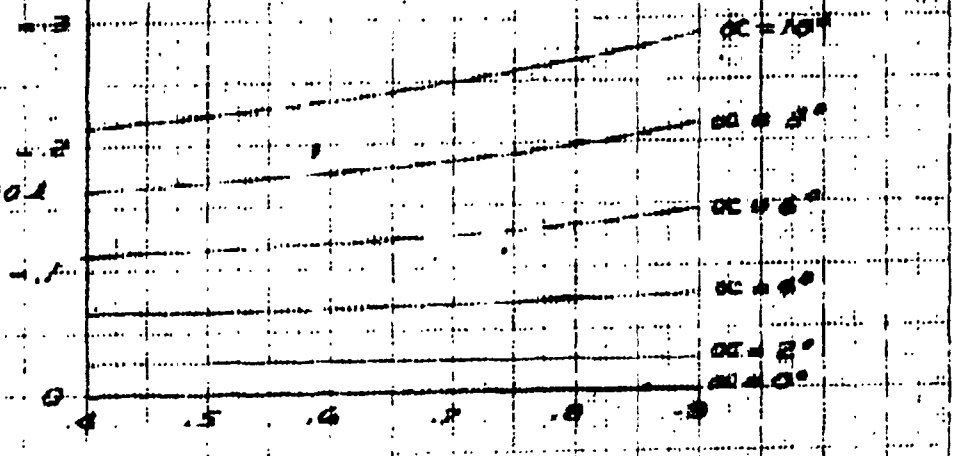

[redacted]

DP-61-184

NORTH AMERICAN AVIATION, INC.

H.J.

23 FEB. 61

G.O. 2533

G.O. 2533

ESTIMATED STORE NORMAL FORCE AND PITCHING MOMENT COEFFICIENTS AS MOUNTED AT INBD WING STA. OF F-100 AIRPLANE

NOTE: 1) DATA BASED ON STORE PLANVIEW AREA (SQ. FT) & LENGTH (FT) $\frac{S_P}{S_W} = 0.02$

2) DATA FOR LEFT WING STORE

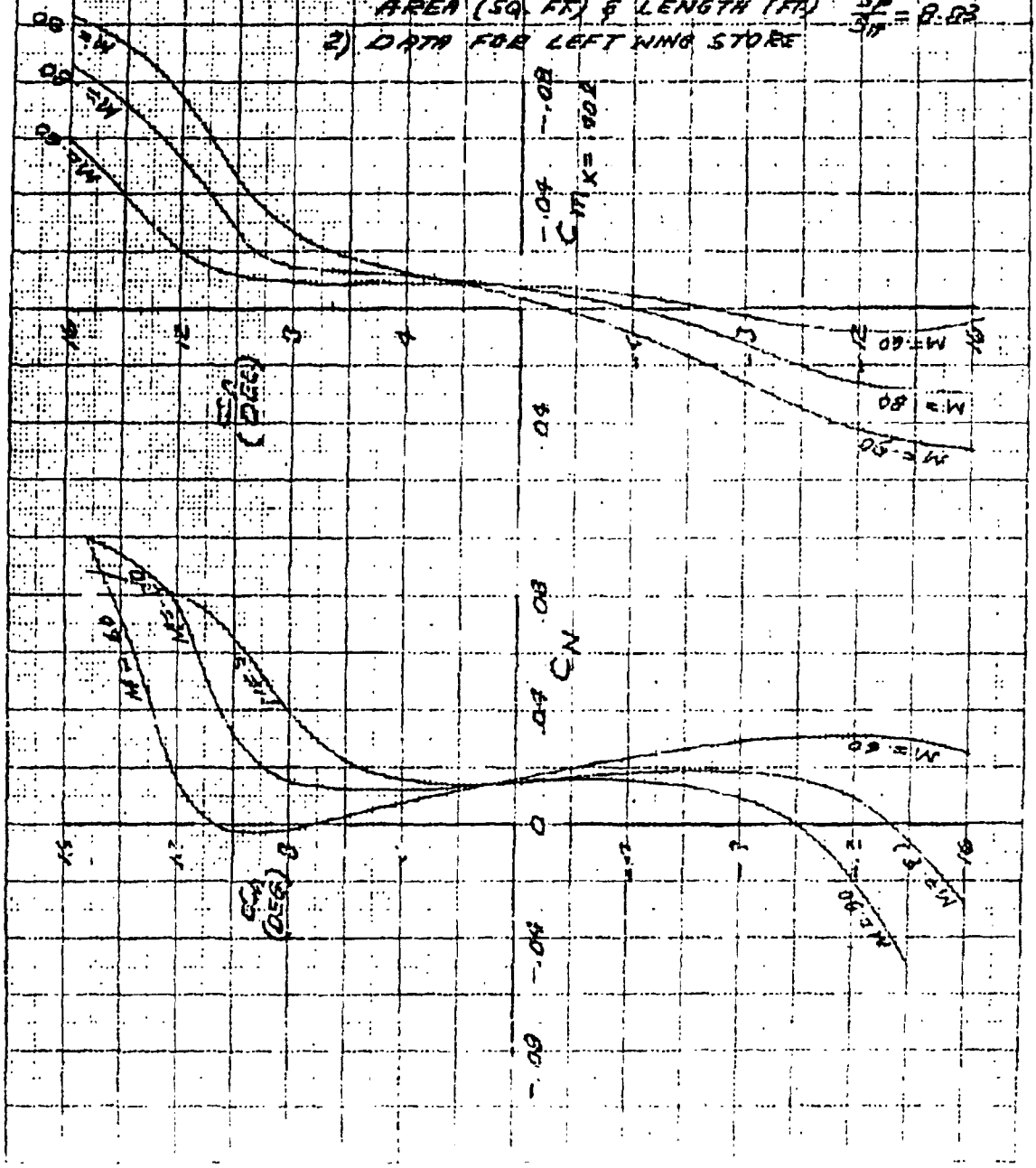

DP-61-185

PREPARED BY RSH	NORTH AMERICAN AVIATION, INC.	
DATE FEB. 23, 61		MODEL NO G.O. 2533

G.O. 2533

ESTIMATED STORE AXIAL FORCE COEFFICIENTS AS MOUNTED AT INBOARD WING STATION OF THE F-100 AIRPLANE

NOTES: DATA BASED ON STORE PLANVIEW AREA (SQ. FT.) & LENGTH (FT.)

$\frac{S_p}{S_{ft}} = 9.03$

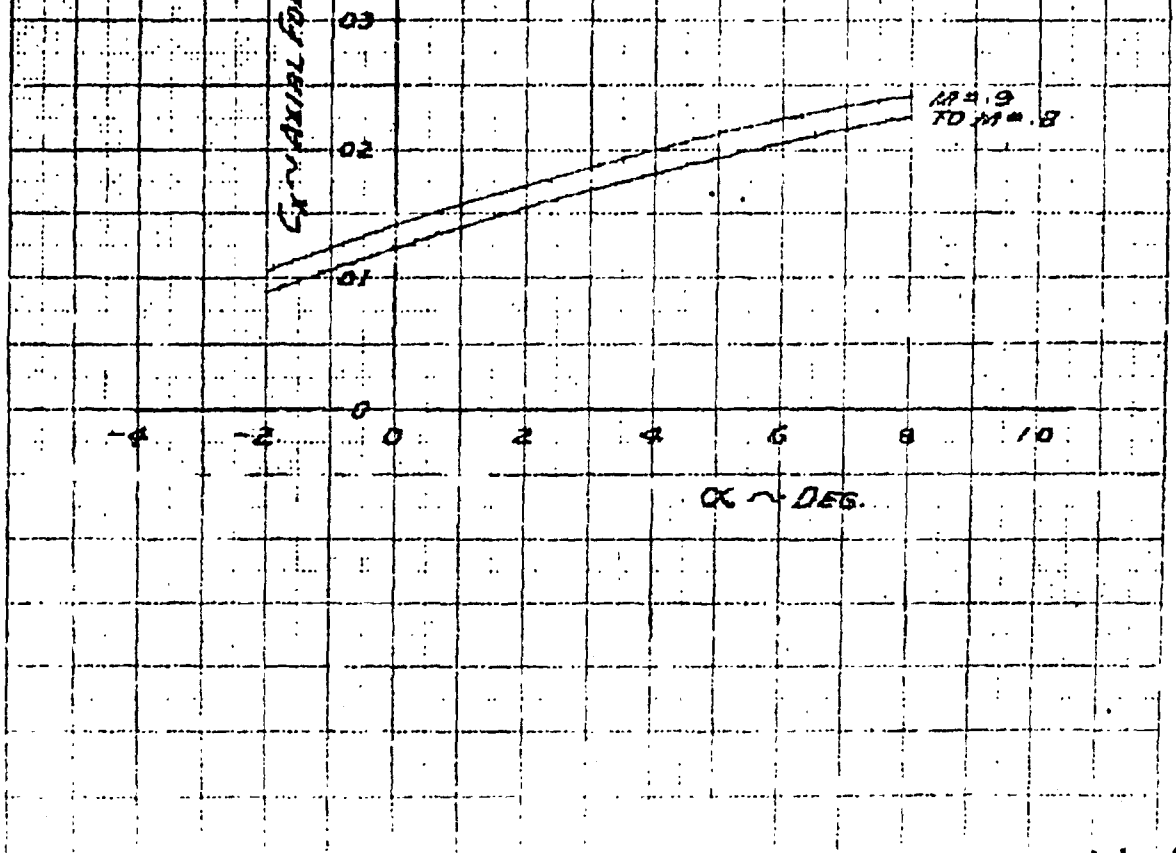

DP-61-186

PREPARED BY H.J.
CHECKED BY
DATE 23 FEB. 61

NORTH AMERICAN AVIATION, INC.

REPORT NO NA-61-221-15
MODEL NO G.O. 2533

G.O. 2533

ESTIMATED STORE YAWING MOMENT AND SIDE FORCE COEFFICIENTS AS MOUNTED AT INB'D WING STA. OF F-100 AIRPLANE

NOTE: 1) DATA BASED ON STORE PLANVIEW AREA (SQ. FT.) & LENGTH (FT.)

$\frac{S_P}{S_{ST}} = 8.83$

2) DATA FOR LEFT WING STORE

3) DATA INCLUDES EFFECTS OF VERTICAL FINS

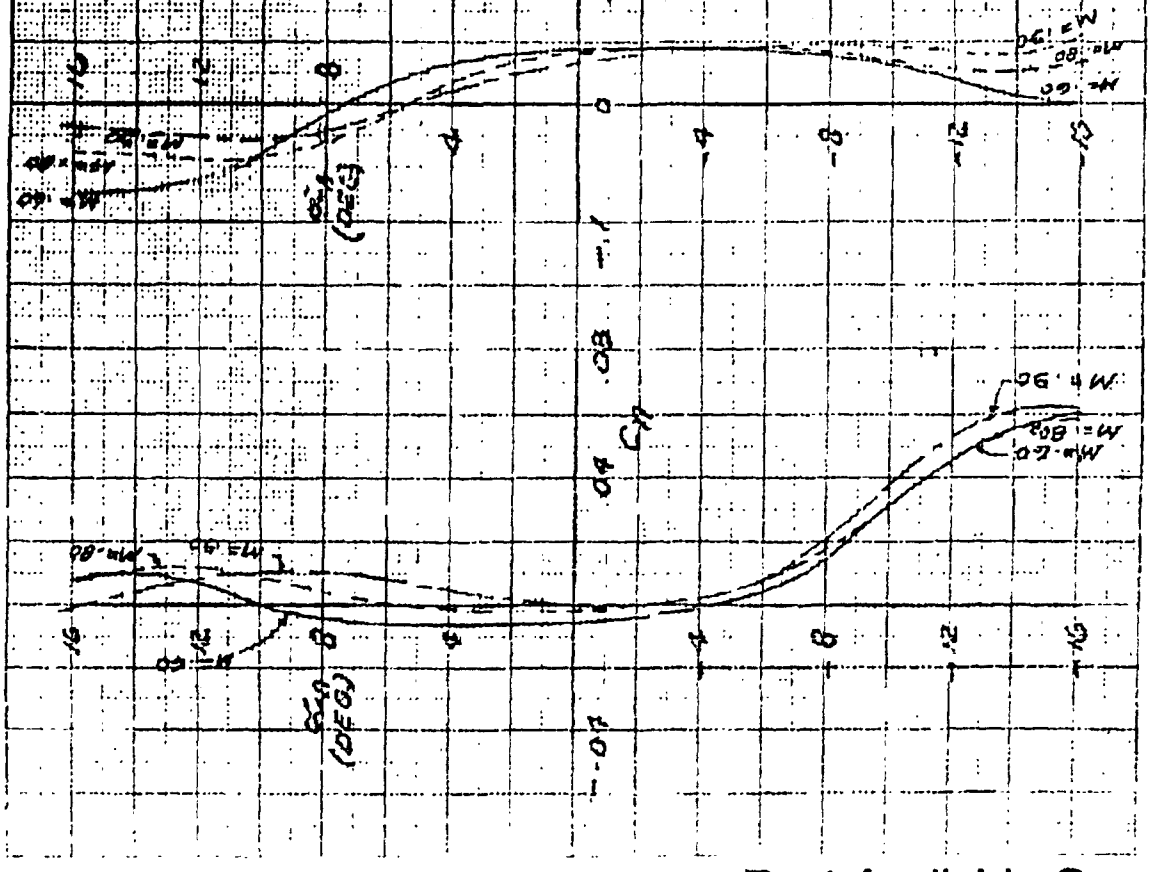

DP-61-187

PREPARED BY H.U.	NORTH AMERICAN AVIATION, INC.	TFD-61-251-11
CHECKED BY		REPORT NO
DATE 23 FEB. 61		MODEL NO G.O. 2533

G.O. 2533

INCREMENTAL NORMAL FORCE AND PITCHING MOMENT COEFFICIENTS DUE TO YAW ON THE STORE MOUNTED AT INBD WING STA. OF THE F-100 AIRPLANE FINNED CONFIGURATION

$0 \leq M \leq .90$

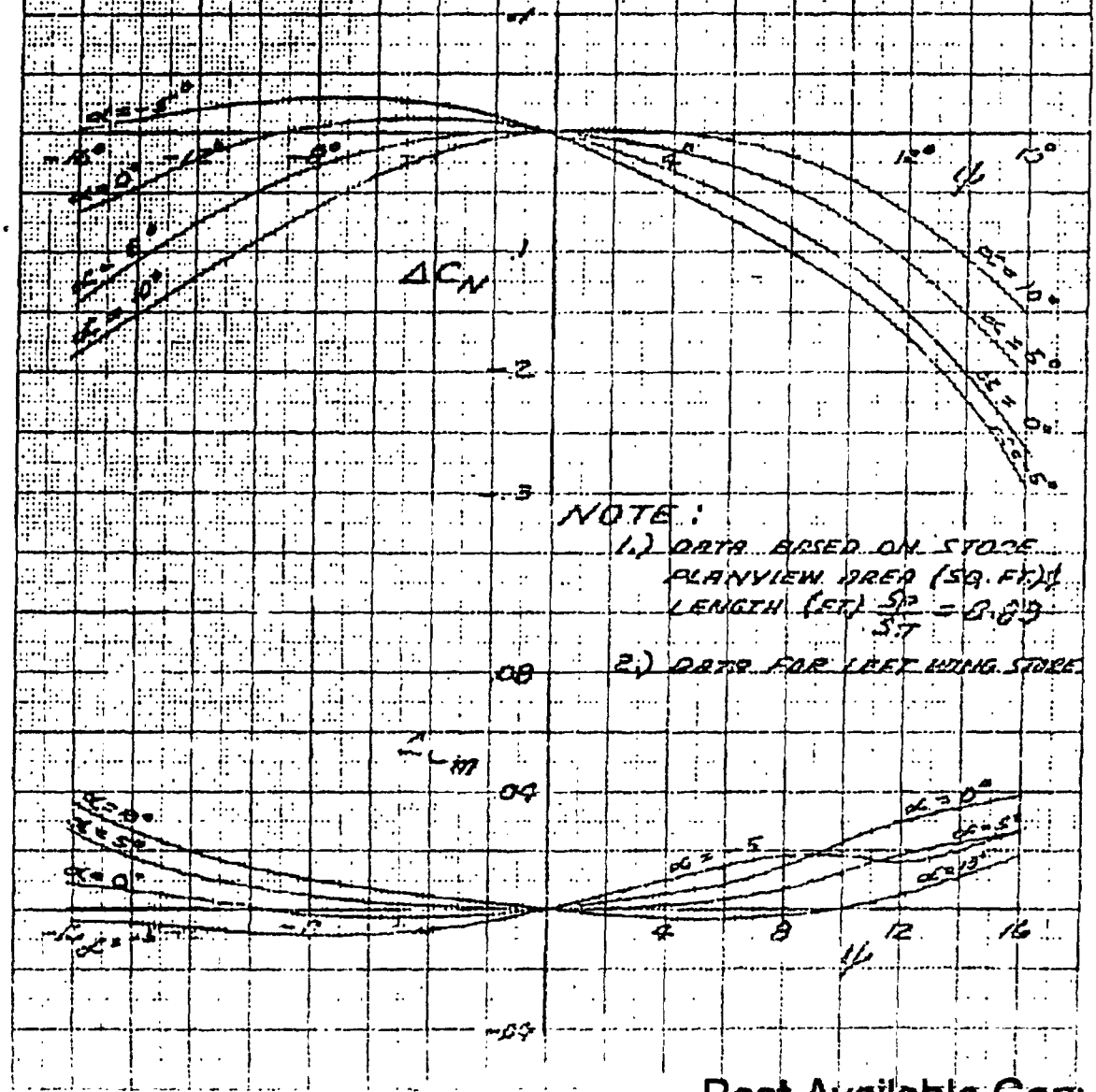

NOTE:

1.) DATA BASED ON STORE PLANVIEW AREA (SQ. FT) / LENGTH (FT) $\frac{S^2}{S \cdot T} = 0.09$

2.) DATA FOR LEFT WING STORE

DP-61-138

RSN	NORTH AMERICAN AVIATION, INC.	
DATE FEB 23, 61		GO 2533

GO 2533

INCREMENTAL SIDE FORCE AND YAWING MOMENT COEFFICIENTS DUE TO YAW ON THE STORE MOUNTED AT INBOARD WING STA. OF THE F-100 AIRPLANE FINNED CONFIGURATION

TO M = .80

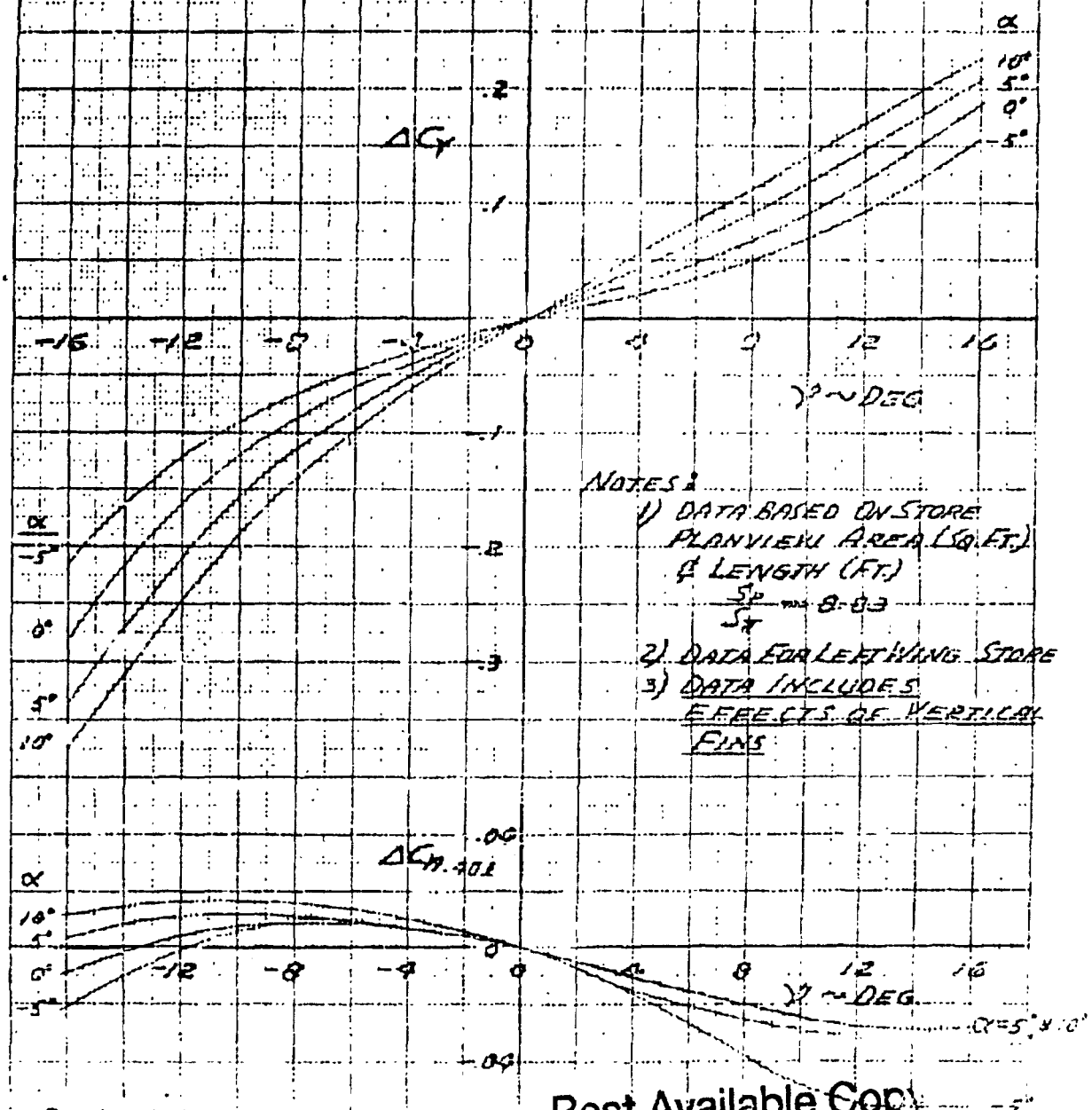

JP 61-184

NORTH AMERICAN AVIATION, INC.

CONFIDENTIAL

4

24 FEB. 61

G.O. 2533

WEIGHT & INERTIA CHARACTERISTICS OF A GENERALIZED LIQUID AGENT DISSEMINATING STORE

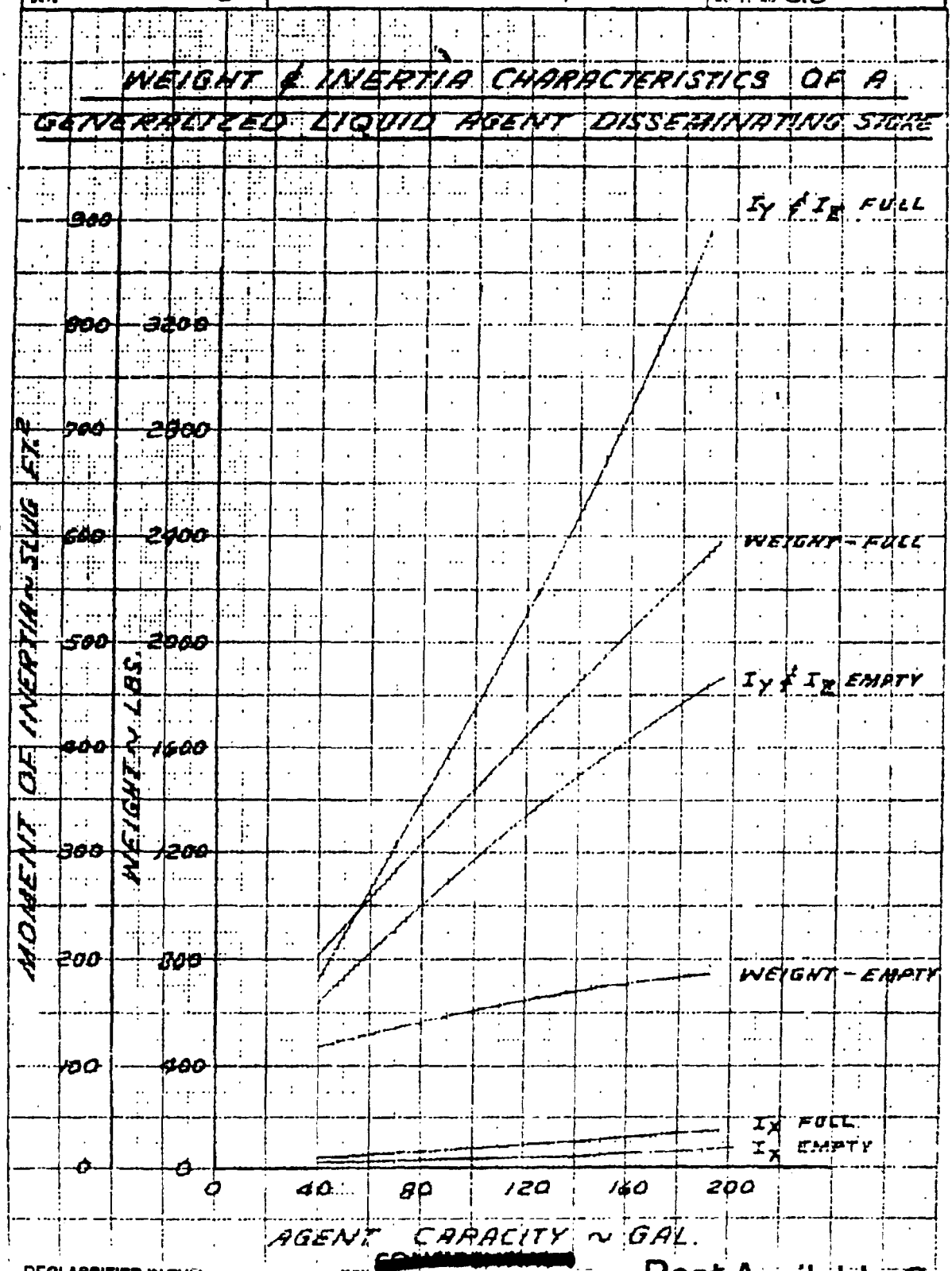

DP-61-190

NORTH AMERICAN AVIATION, INC.

[redacted]

DATE 24 FEB. 61

MODEL NO G.O. 2533

DIMENSIONAL CHARACTERISTICS OF A GENERALIZED LIQUID AGENT DISSEMINATING STORE

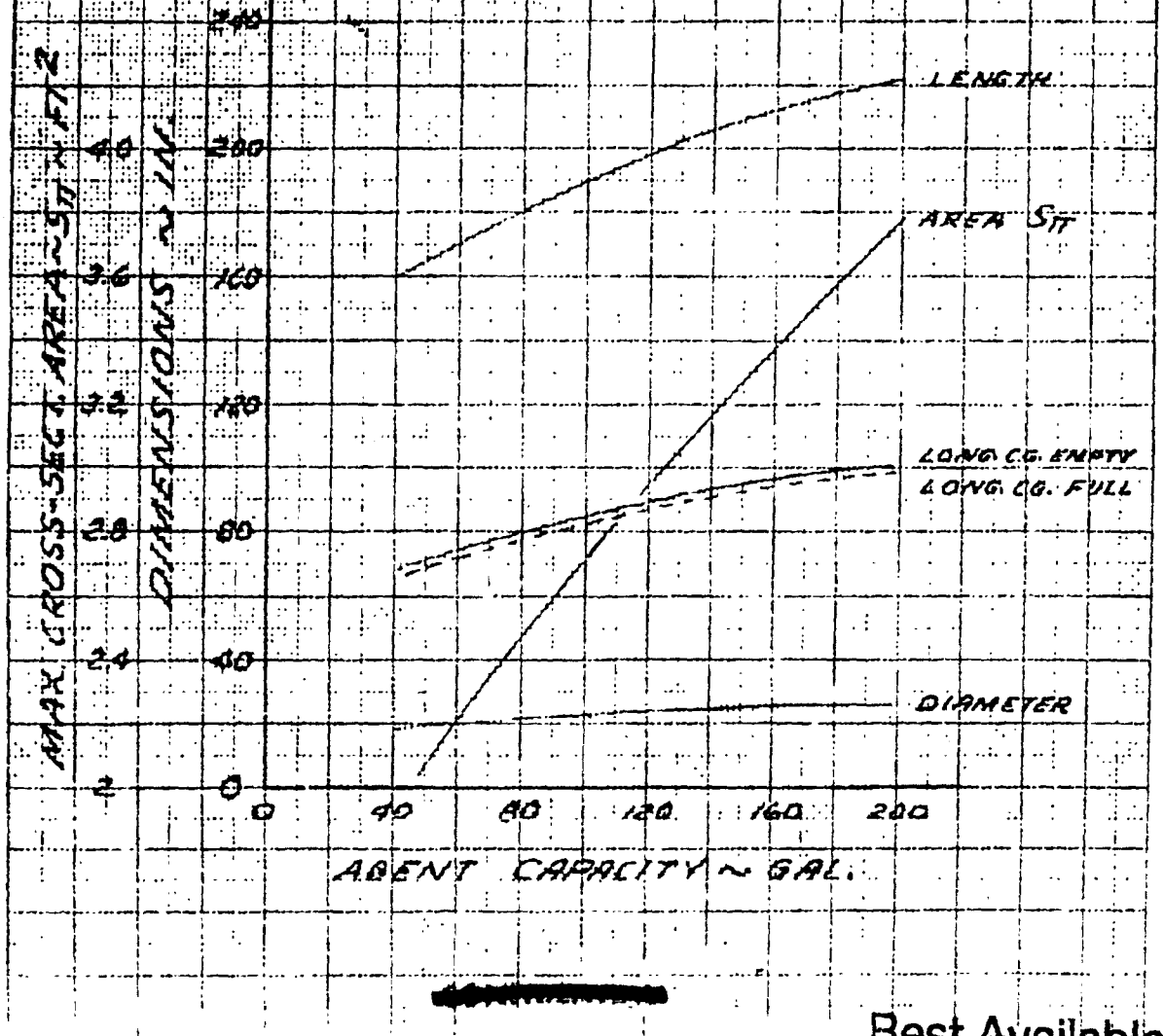

[redacted]

Best Available Co

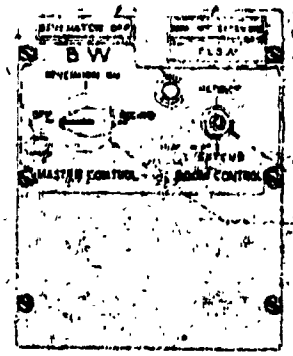

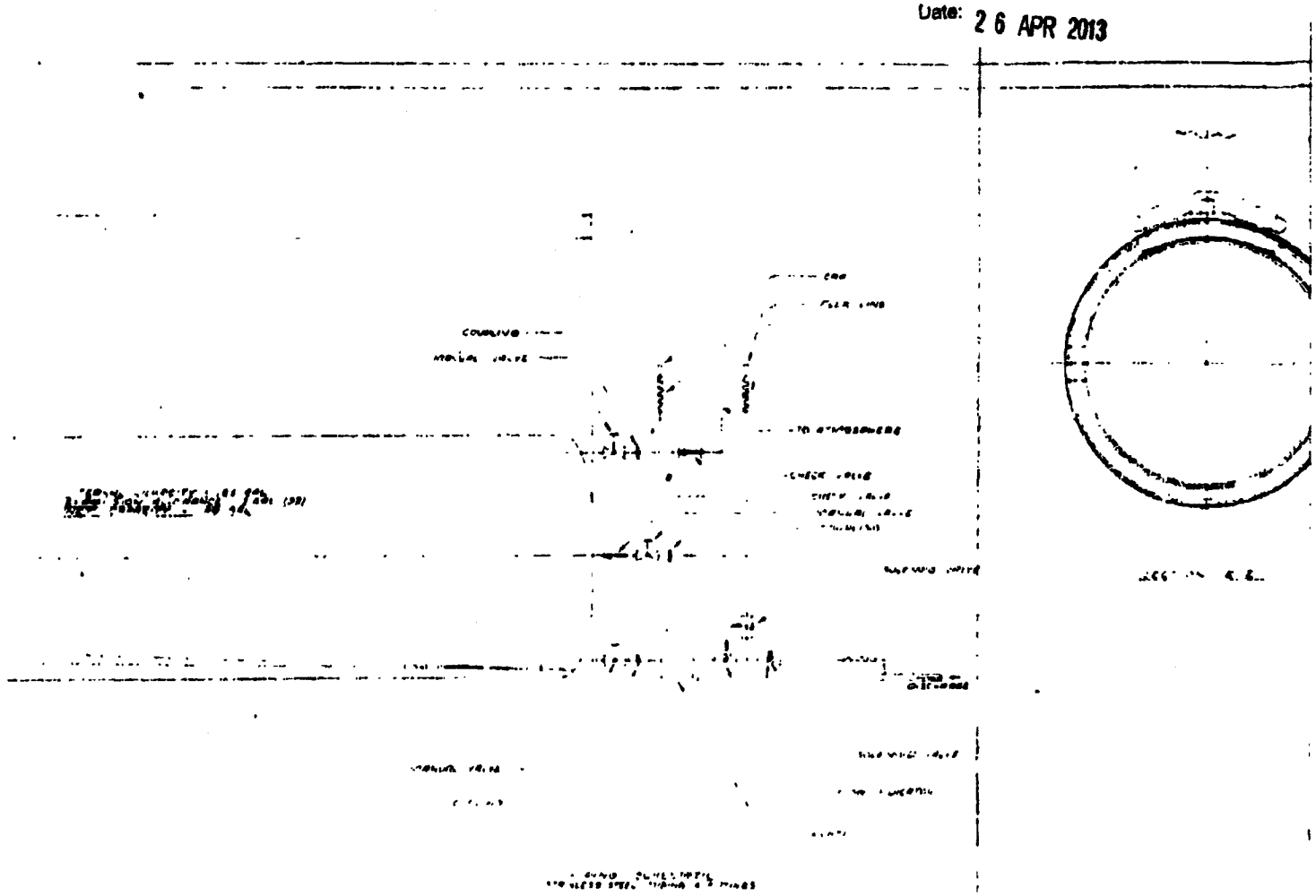

2

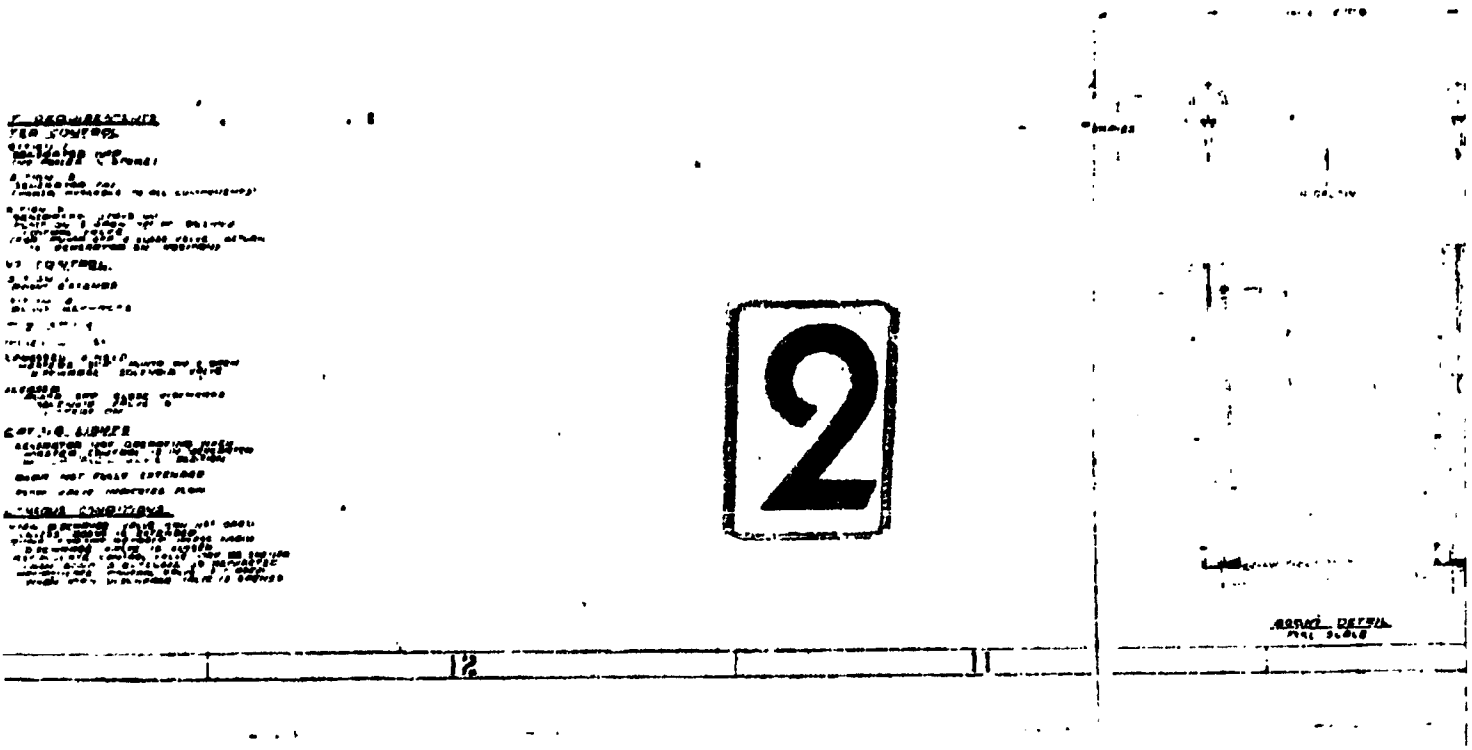

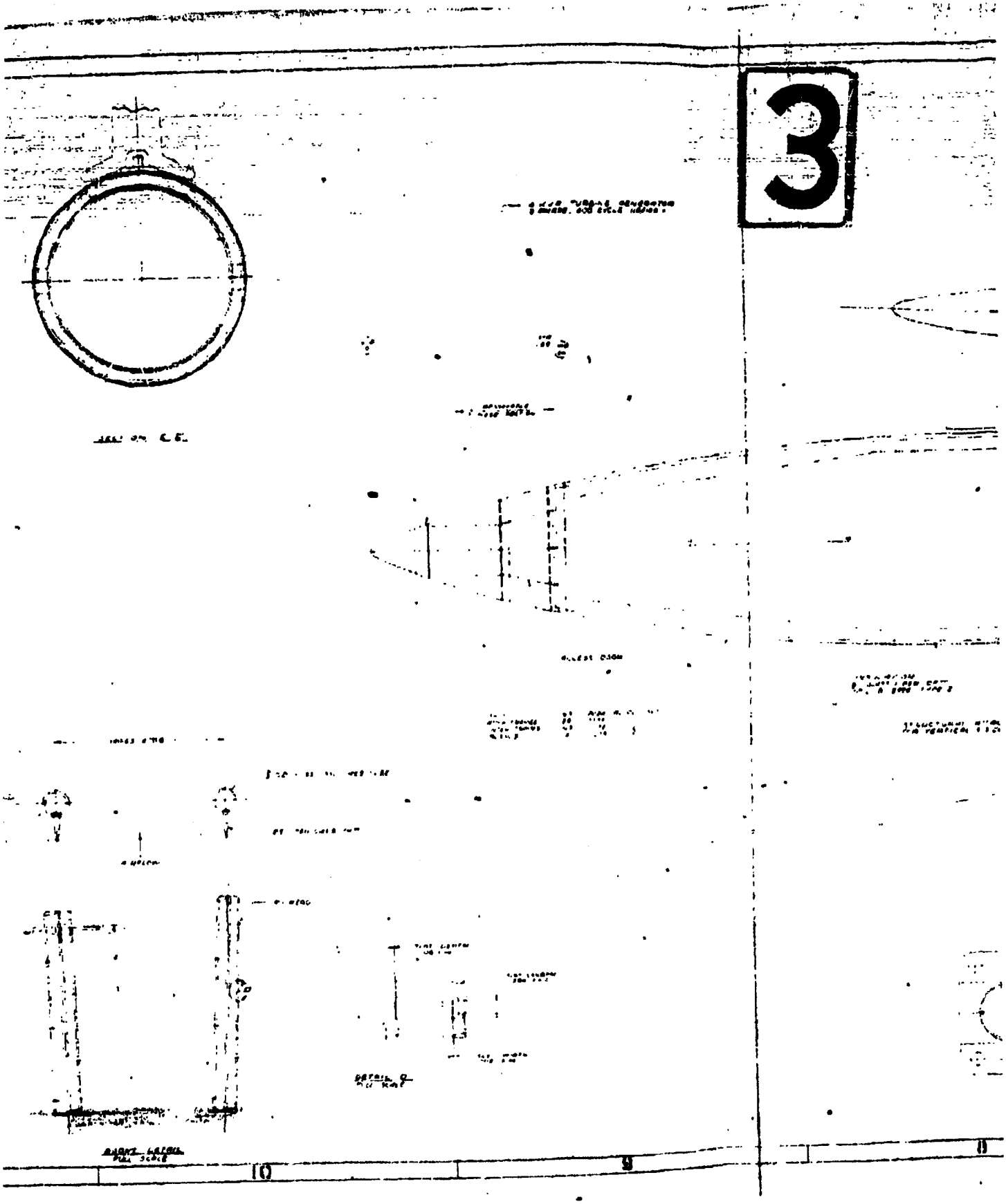

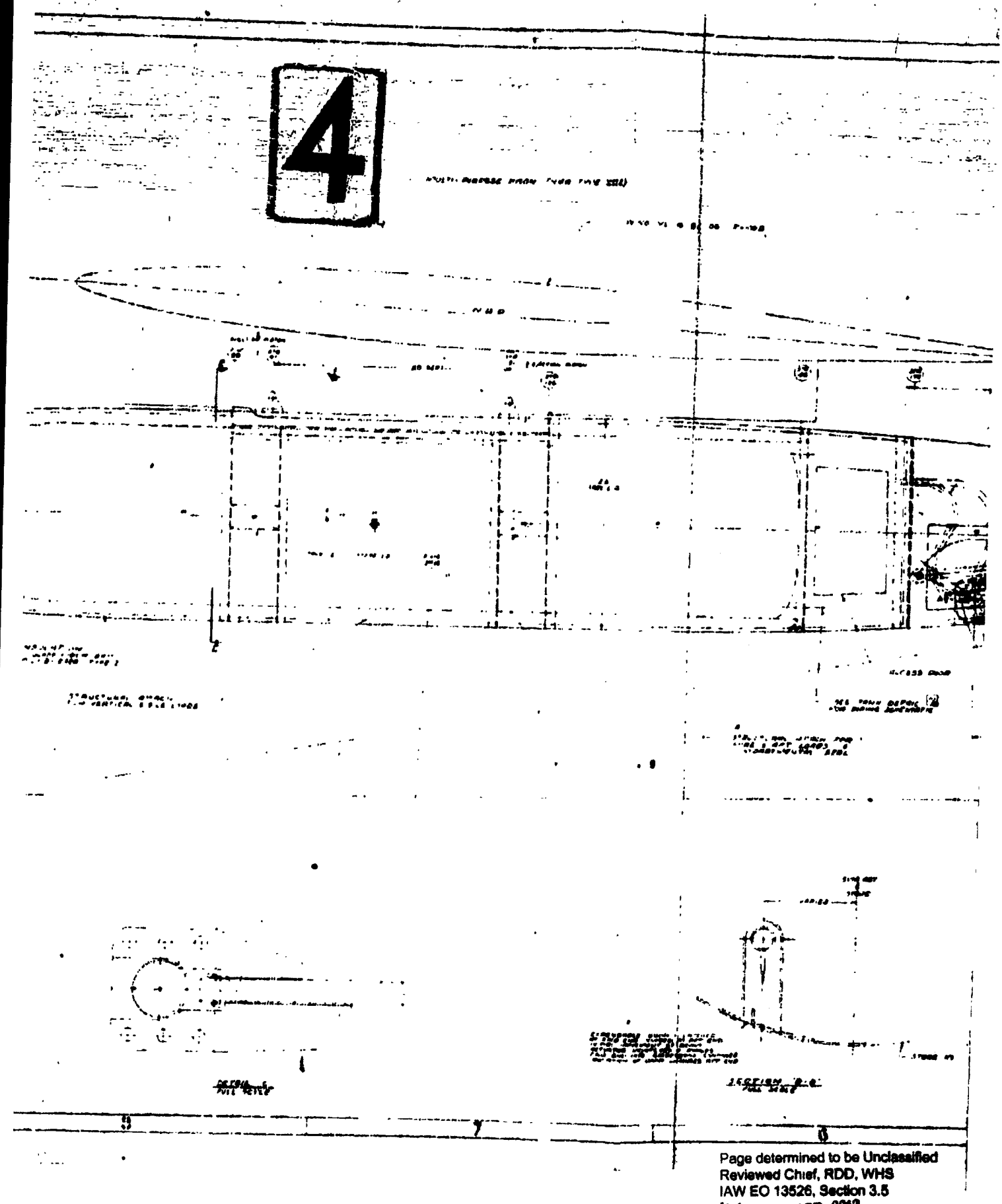

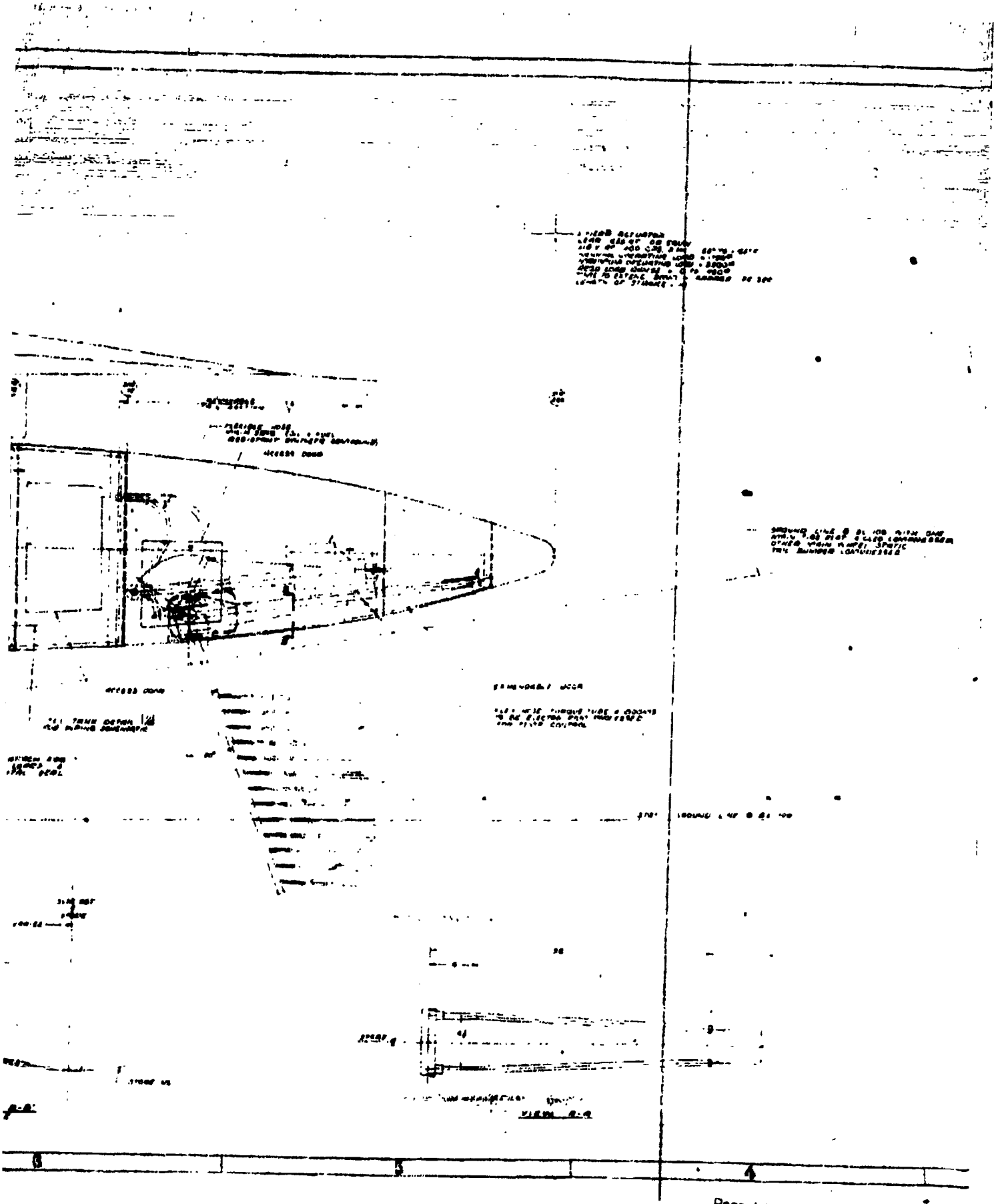

6

Figure 5.

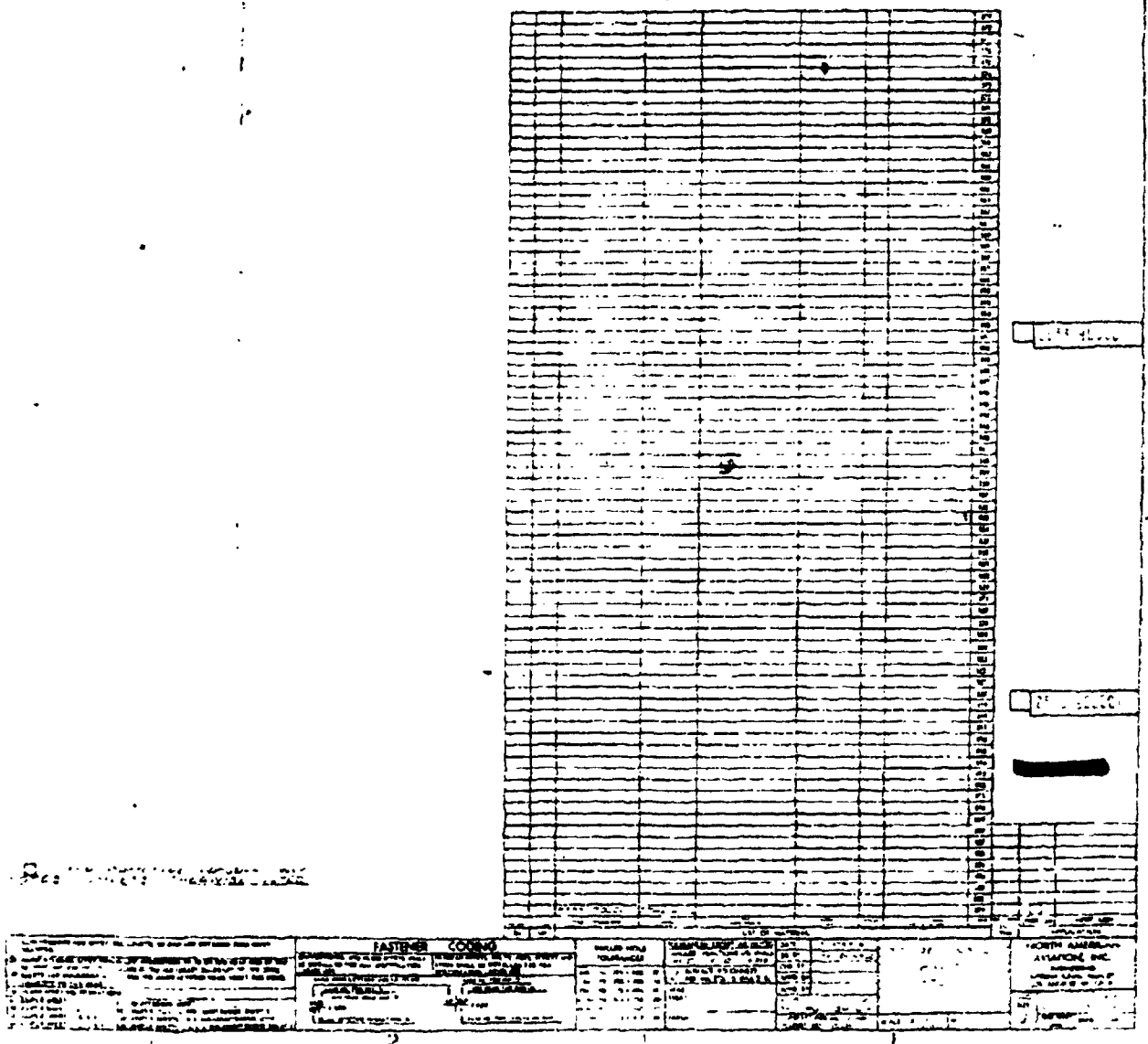

NORTH AMERICAN AVIATION, INC.

[redacted]

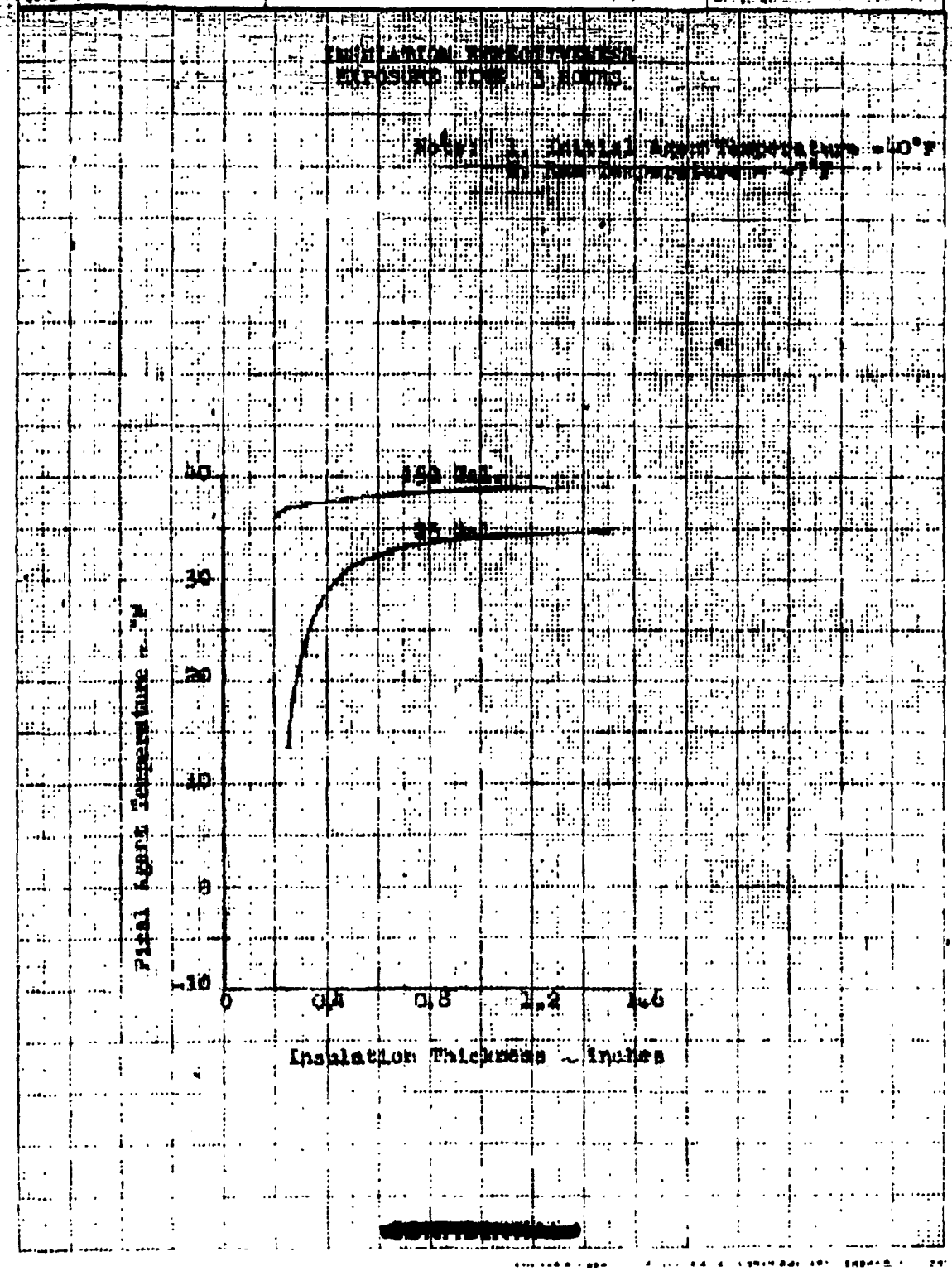

[redacted]

NORTH AMERICAN AVIATION, INC.

[redacted]

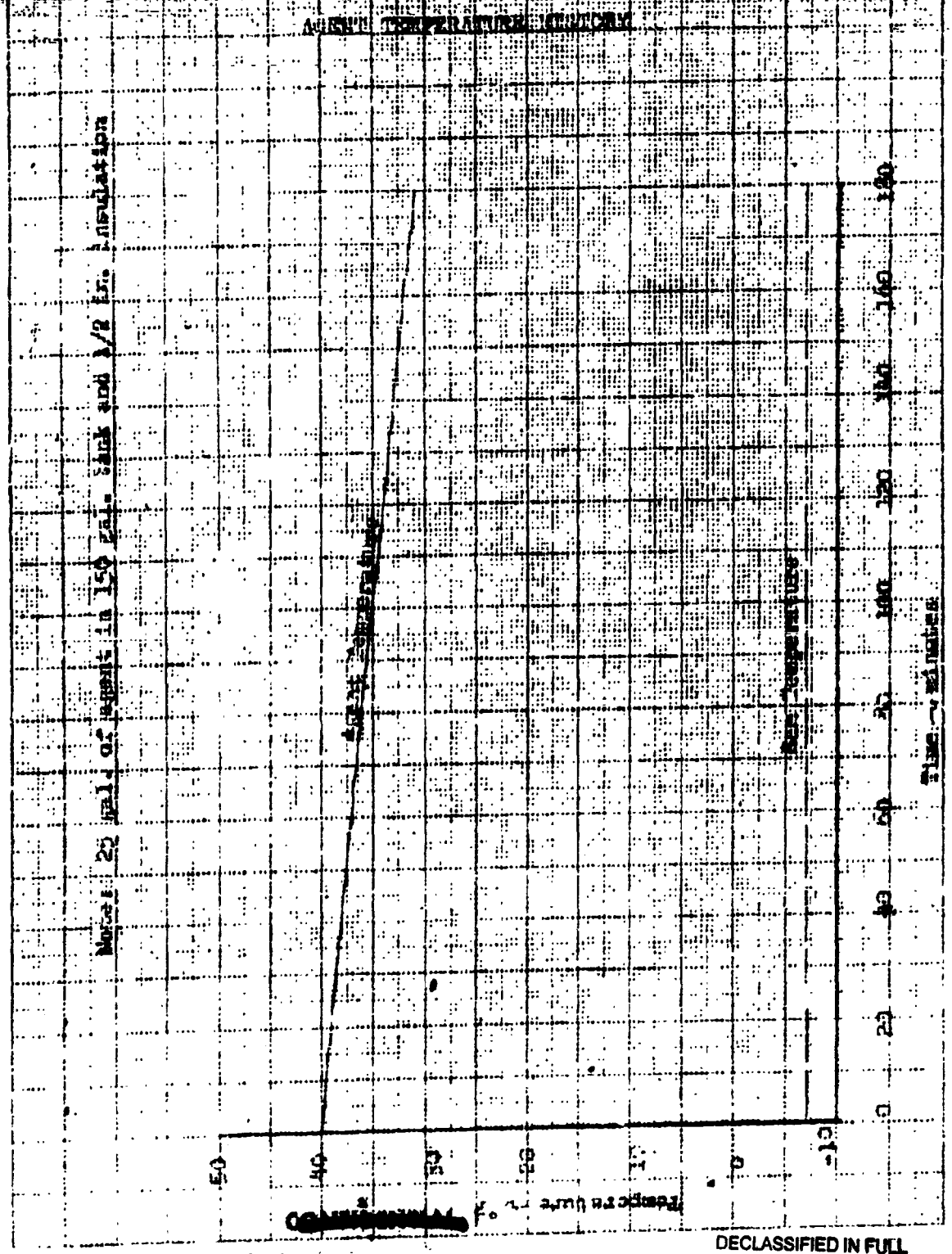

[redacted]

NORTH AMERICAN AVIATION, INC.

[redacted]

HEATING REQUIREMENTS FOR
DISSIPATION POWER
BOOM MOUNTED
SEA LEVEL

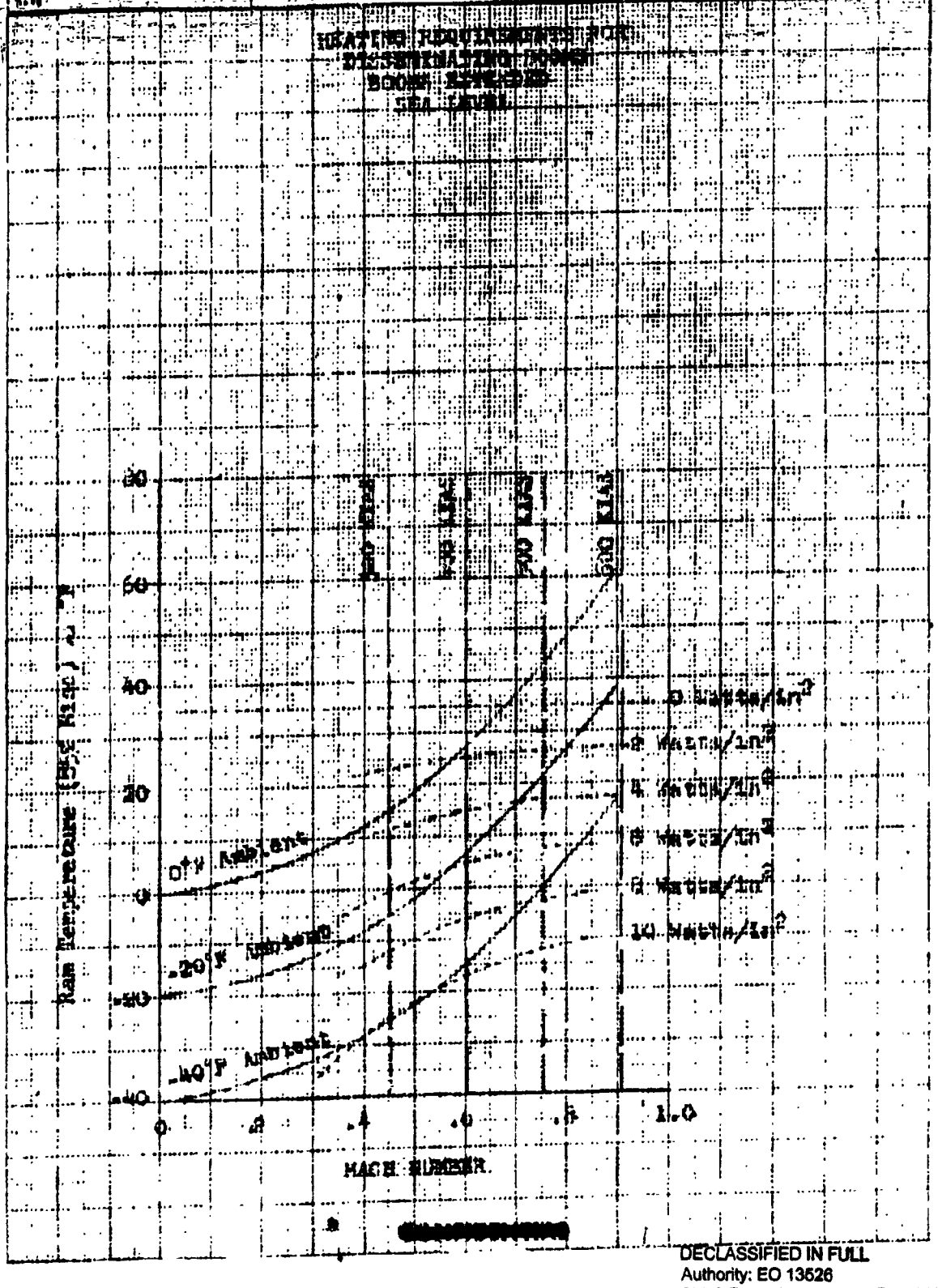

[redacted]

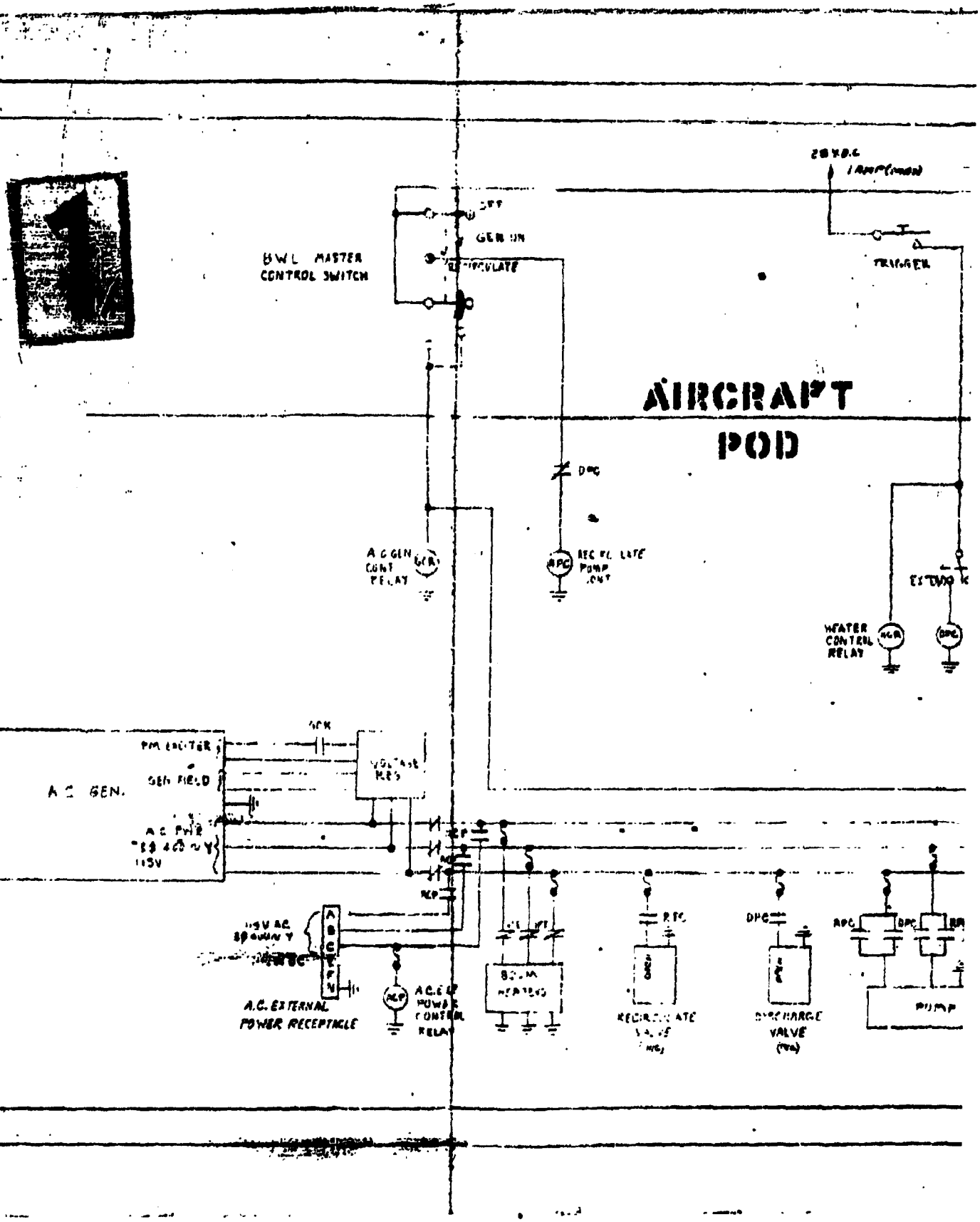

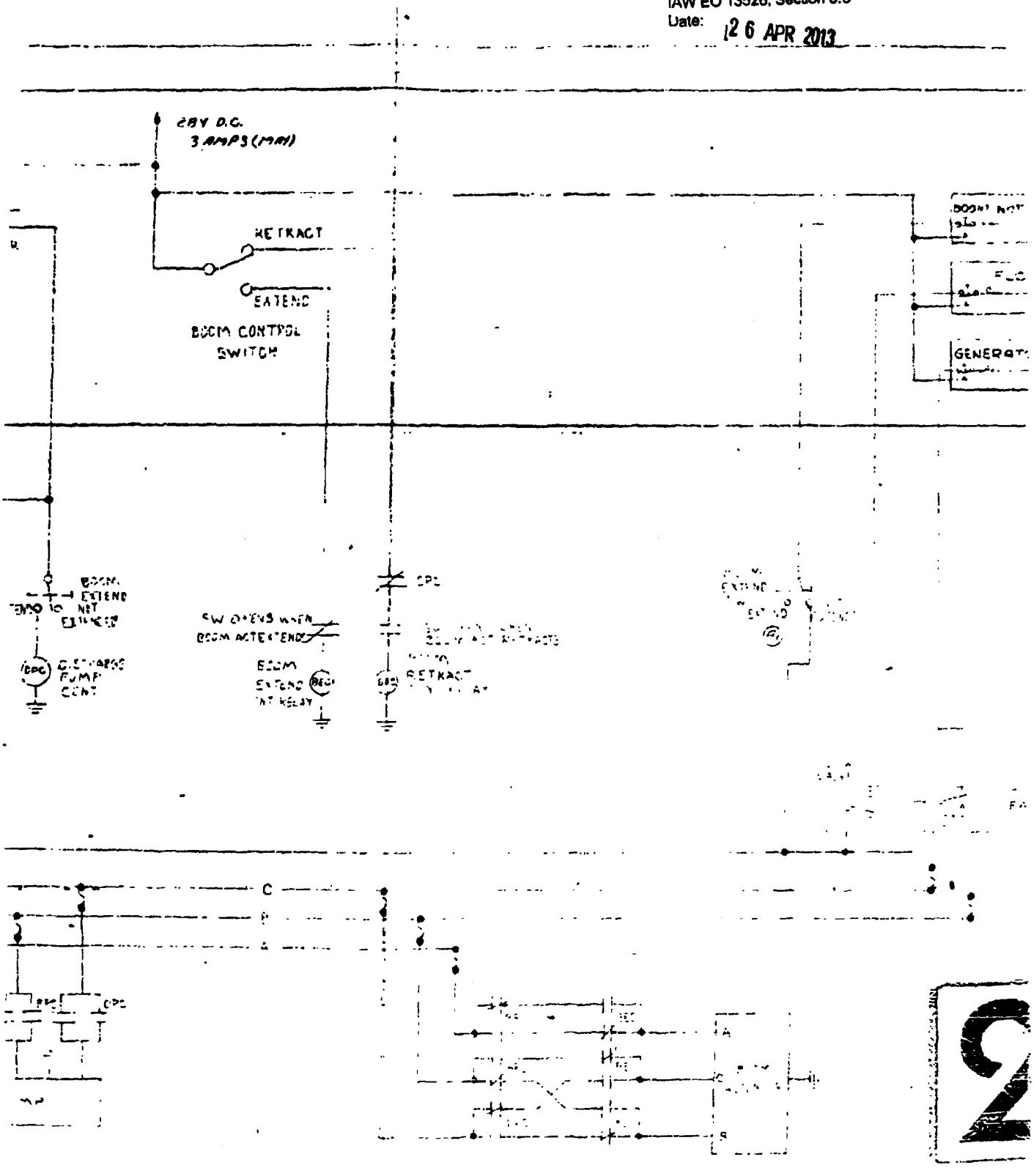

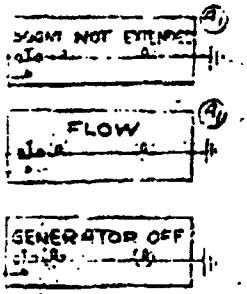

3

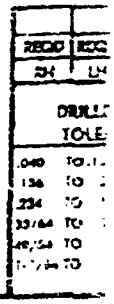

REVISIONS			
SYM	DESCRIPTION	DATE	SIGNATURE
A	1. REVISED 1 JUN 61		

NA-61-[illegible]
Page 32
Figure 12.

DECLASSIFIED IN FULL
Authority: EO 13526
Chief, Records & Declass Div, WHS
Date: 26 APR 2013

4

2533-900002

CONFIDENTIAL

REQD	REQD	PART NO.	DESC	MATERIAL	SIZE	ZONE	MATL SPEC
		LIST OF MATERIAL					

DRILLED HOLE TOLERANCES

TOLERANCES EXCEPT AS NOTED: ANGLES ±1° FRACTIONS ±1/32 DECIMALS ±.010

SURFACE ROUGHNESS PER MIL-STD-10

DATE: [illegible]
DR BY: [illegible]
CHK BY:
APPD BY:
APPD B.:

F100, F86 SP PROJ GROUP

ELECTRICAL SCHEMATIC—
(STUDY)

SCALE: NONE WT

USED ON / NEXT ASSY / APPLICATION

NORTH AMERICAN AVIATION, INC.
ENGINEERING
INTERNATIONAL AIRPORT
LOS ANGELES 45, CALIF.

DWG SIZE L 2533-900002

Best Available Copy